

Dissertation
submitted to the
Combined Faculties for the Natural Sciences and for Mathematics
of the Ruperto-Carola University of Heidelberg, Germany
for the degree of
Doctor of Natural Sciences

presented by

Maria Antonietta Tosches
born in Foggia, Italy
Oral-examination:

Development and function
of brain photoreceptors
in the annelid *Platynereis dumerilii*

Referees: Dr. Darren Gilmour
Prof. Dr. Jochen Wittbrodt

*“Quelli che s’innamoran di
pratica senza scienza son come
’l nocchier ch’entra in navilio
senza timone o bussola, che mai
ha certezza dove si vada.”*

Leonardo da Vinci

(Anyone who loves practice without
theory is like a sailor going aboard a
ship without rudder or compass and
having no idea where he is going.)

ACKNOWLEDGMENTS

This work was made possible by the contribution and the support of many people, and here I want to express all my gratitude for them.

First, I wish to thank Detlev Arendt, for giving me the opportunity to work in his lab, for the supervision and the support during this work, and for all our inspiring discussions, which contributed so much to my scientific maturation in these years.

I also want to thank my thesis advisory committee at EMBL, Prof. Jochen Wittbrodt, Dr. Darren Gilmour and Dr. Anne Ephrussi, for their comments and valuable advice during this work.

Moreover, I would like to thank Gaspar Jekely for his critical feedback, for very interesting discussions, for hosting the preparation of a neuropeptide antibody and for sharing unpublished data. Thanks also to Kristin Tessmar-Raible, for discussing data on the melatonin system, and for sending me her opsin antibody.

I am especially grateful to Nicola Kegel: we worked together on the Rx project - that she had initiated - during my first months in the lab, and she taught me all the secrets of Platynereis injections. Thanks also to Marianna Karageorgi and Nathalie Tisch, for helping me with special commitment and enthusiasm during their internships in the lab.

Here, I would like to thank the EMBL GeneCore and ALMF, for providing assistance and facilities for my experiments. Thanks also to the IT-Services, for rescuing my data more than once...

I feel very lucky because in these years I had the opportunity to work with many fantastic people, the past and present members of the Arendt lab. Thanks to Mette Handberg-Thorsager and Antonella Lauri for being great benchmates, and for working together on the development of new techniques for our unusual model system, with all the excitement and sometimes the frustration that this brings. I am indebted to Heather Marlow and Pavel Vopalensky: our

stimulating discussions on larval evolution and photoreceptors contributed significantly to the interpretation of my data. Thanks to Oleg Simakov and Tomas Larsson, for taking care of the Platynereis genomic and transcriptomic resources, which were so important for this work. I am grateful to Raju Tomer, who developed the PrImR resource, and assisted the generation of new average expression patterns. Thanks to Antje Fischer, who had always the patience to answer my naive questions on zoology and evolution. Moreover, I wish to thank Diana Hofmann for taking care so well of the animal cultures, and in particular the mutant worms, and Heidi Snyman for being a special “lab navigator” in these years. Thanks also to Fay Christodoulou, for being so much supportive, and for constantly spreading her enthusiasm and energy. Finally, I want to thank all the past and present members of the lab - the list would be so long here! - for the pleasant and stimulating working atmosphere. A special thanks to Silvia Rohr for translating the Summary of this thesis.

During these years in Heidelberg, I could count on the support of my “old” friends, especially those who by chance moved in the neighborhood, and of new friends here at EMBL. I want to thank them all for the support, and for having a great time together outside the lab.

My special gratitude belongs to Daniele. Thanks for tolerating my bad days and for enjoying with me the good ones. Thanks also to my parents, my sister and my brother. Despite the long distances, you have always been truly supporting and understanding. It's been a long way... and you have always been by my side.

TABLE OF CONTENTS

Summary	1
Zusammenfassung	3
I Introduction	5
1 Deciphering the evolution of nervous systems	7
1.1 Diversity of nervous systems in the animal kingdom	7
1.2 The annelid <i>Platynereis dumerilii</i> : a model system for studying brain evolution	10
1.2.1 Life cycle and early development of <i>P. dumerilii</i>	10
1.2.2 Advances of <i>P. dumerilii</i> as a model system	13
1.3 Homologies of brain regions and cell types in Bilateria	13
1.3.1 Conservation of brain regions along the anterior-posterior and the dorso-ventral axes	14
1.3.2 Conservation of cell types	15
1.3.3 The division of labour model for nervous system evolution	17
1.4 Studying marine larvae uncovers the earliest steps in brain evolution	20
2 Evolution of photoreceptor cell types and non-visual light detection	21
2.1 Ciliary and rhabdomeric photoreceptors	21
2.1.1 Phototransduction cascades	23
2.1.2 Opsin families	25
2.2 Non-visual light detection in animals	27
2.2.1 Illuminance detection and circadian rhythms in protostomes	28
2.2.2 Illuminance detection and circadian rhythms in vertebrates	30

2.3	The evolution of the vertebrate pineal and melatonin system	32
2.3.1	The pineal complex: luminance detection, melatonin release and shadow response	32
2.3.2	CSF contacting neurons and deep brain PRCs	36
2.3.3	Early evolution of pineal and retina	37
2.4	Roles of Rx in the development of ciliary photoreceptors	39
2.5	Aim of the thesis	41
II	Results	43
3	Development of <i>Platynereis</i> dorsal brain	45
3.1	Morphological landmarks in the dorsal brain	45
3.2	Timing of cell cycle exit and differentiation of the main cell types of the dorsal brain	48
3.3	Time-lapse imaging reveals the early steps of brain development . . .	51
3.3.1	First insights in <i>Platynereis</i> neurogenesis	55
3.4	Connecting lineages to early expression patterns and cell types in the developing episphere	60
3.4.1	The dorsal midline and the asymmetric serotonergic cell. . .	60
3.4.2	The lateral serotonergic cells and the adult eye region	63
3.4.3	The ciliary photoreceptors and the medial photoreceptive region	65
4	Establishment of techniques to study gene function in <i>Platynereis</i>	67
4.1	The genomic structure of the <i>rx</i> gene	68
4.2	The problem of single nucleotide polymorphisms (SNPs)	69
4.3	Validation of the knockdown efficiency of the <i>rxin1ex2</i> MO	69
4.4	Establishment of <i>rx</i> knock out lines with the zinc finger nucleases technology	73
4.4.1	Selection of an <i>rx</i> ZFN pair and validation of its mutagenicity	73
4.4.2	Establishment of <i>rx</i> knockout lines	75
5	Functions of Rx during the development of the dorsal brain	79
5.1	General considerations on the analysis of morphant phenotypes at 24hours post fertilization (hpf) and 48hpf	79
5.2	Rx is necessary to the differentiation of ciliary photoreceptors	80
5.3	Roles of Rx in the development of the brain serotonergic system . .	84

5.4	General effects of Rx loss of function on brain development	87
6	Role of the larval circadian system in the control of rhythmic behaviour	91
6.1	Circadian clock markers are expressed at early larval stages	91
6.2	The larval circadian system controls rhythmic locomotion	92
6.3	The clock cells are sensory and express different kinds of opsins . . .	95
6.3.1	The opsin repertoire of <i>Platynereis</i>	95
6.3.2	Expression of opsins in the <i>cry1</i> region	96
6.3.3	Imaging of neuronal activity shows the presence of light re- sponses in the dorsal brain	100
6.4	A CNG-dependent transduction cascade resets the locomotor rhythms	102
6.5	Melatonin is the molecular output of the larval circadian system, and modulates locomotor behaviour	105
6.5.1	The melatonin synthesis genes <i>hiomt</i> and <i>aanat</i> are present in a lophotrochozoan	106
6.5.2	Melatonin produced by the clock cells controls directly the cil- iary beating of the prototroch	107
6.5.3	In the juvenile, melatonin has a multiples roles in the nervous system	110
7	Molecular identity of the <i>hiomt+</i> cell types: a comparative analysis	113
7.1	The repertoire of <i>hiomt+</i> CNG+ cell types	113
7.2	Hierarchical clustering identifies two major subgroups of <i>hiomt+</i> cells	118
7.3	A comparison of molecular fingerprints of melatonin producing cells between annelids and vertebrates	125
III	Discussion	131
8	The ancestral function of melatonin as a modulator of locomotion	133
8.1	The effects of light on <i>Platynereis</i> locomotor behaviour	133
8.1.1	The photic control of melatonin synthesis	134
8.1.2	The role of the <i>c-ops1+</i> cells	134
8.2	Tracing the evolution of brain photoreceptors and circadian centers in Bilateria	138
8.3	Serotonergic photoreceptors in other invertebrates?	141
8.4	Ancient links between light receptors and indoleamines	143

8.5	The dawn of circadian clocks from an ecological perspective	145
9	From brain ciliary photoreceptors to complex vertebrate eyes	147
9.1	Conserved functions of melatonin in annelids and vertebrates	147
9.2	The origin of vertebrate photoreceptors: a view from serotonin and melatonin	148
9.3	Partial conservation of regulatory interaction explains the similarities between annelids and vertebrate cell types	151
9.4	Differences in the organization and development of annelid and vertebrate brains indicate how complex nervous systems evolved	155
9.5	Making the vertebrate eye from brain photoreceptors	156
9.6	Concluding remarks	158
9.7	Open questions and future outlook	159
IV	Materials and Methods	163
10	Materials	165
10.1	<i>Platynereis dumerilii</i> animal culture	165
10.2	Equipment	165
10.3	Reagents and solutions most commonly used for molecular biology and WMISH	166
10.4	Antibodies	167
10.5	Software	167
11	Cloning of genes and analysis of their expression	169
11.1	Immunostaining of <i>Platynereis</i> larvae	169
11.1.1	Fixation of <i>Platynereis</i> larvae for immunostaining	169
11.1.2	Immunostaining protocol	169
11.2	Clones of <i>Platynereis</i> genes	171
11.2.1	Extraction of RNA from <i>Platynereis</i> larvae	171
11.2.2	Preparation of cDNA libraries, and PCR	172
11.2.3	Preparation of RACE libraries, and RACE PCR	173
11.2.4	Cloning of PCR products	174
11.2.5	Sources of <i>Platynereis</i> clones used as template for probe synthesis	175
11.2.6	Phylogenetic analysis	178

11.3	Whole mount in situ hybridization	178
11.3.1	Fixation of <i>Platynereis</i> larvae for WMISH	178
11.3.2	Probe synthesis	179
11.3.3	Standard <i>Platynereis</i> WMISH protocol	180
11.3.4	Modified <i>Platynereis</i> WMISH protocol	182
11.4	EdU incorporation studies	183
11.4.1	Incubation of larvae with EdU	183
11.4.2	Detection of EdU after immunostaining and WMISH	183
11.5	Analysis of molecular fingerprints	184
11.5.1	Comparison of expression patterns with PrImR	184
11.5.2	Comparison of molecular fingerprints	187
12	Gene function studies and time lapse imaging	189
12.1	Analysis of <i>rx</i> gene structure and SNPs	189
12.1.1	Identification of <i>rx</i> introns with TAIL-PCR	189
12.1.2	SNP analysis	191
12.2	Injection of <i>Platynereis</i> zygotes	192
12.2.1	Preparation of injection solutions	192
12.2.2	<i>Platynereis</i> injection protocol	195
12.3	Analysis of morpholino and mRNA injected larvae	197
12.3.1	Analysis of splicing after <i>rxin1ex2</i> MO injection	197
12.4	Identification of mutations in ZFNs injected larvae	199
12.4.1	Extraction of genomic DNA	199
12.4.2	PCR, restriction analysis and sequencing	201
12.5	Time lapse movies of developing <i>Platynereis</i> embryos	203
12.5.1	Mounting and imaging	203
12.5.2	Analysis of the movies	203
13	Behavioural experiments	205
13.1	Imaging of calcium in <i>Platynereis</i> larvae	205
13.1.1	Preparation of the larvae, mounting and imaging	205
13.1.2	Analysis of the GCaMP3 movies	205
13.2	Measurements of ciliary beating frequency (CBF)	206
13.3	Phototaxis	207

V	Appendix	209
A	The apical organ cell types	211
B	Additional gene expression patterns	213
C	Phylogenetic trees	217
D	Vertebrate molecular fingerprint table	223
	References	227

LIST OF FIGURES

1.1	Simplified phylogenetic tree of Metazoa.	9
1.2	Life cycle and early development of <i>Platynereis dumerilii</i>	12
1.3	Conservation of brain regions along the AP and DV axes.	15
1.4	Examples of division of labour in nervous system evolution.	19
2.1	Ciliary and rhabdomeric photoreceptors, and their phototransduction cascades.	24
2.2	Opsin families in Bilateria.	26
2.3	Circadian organization in <i>Drosophila</i>	29
2.4	Circadian organization in vertebrates.	31
2.5	Melatonin synthesis pathway.	35
2.6	CSF-contacting neurons in the vertebrate brain.	38
3.1	The dorsal brain and the serotonergic system in <i>Platynereis trochopore</i> larvae.	46
3.2	The dorsal brain and the serotonergic system in <i>Platynereis neotochaete</i> larvae.	48
3.3	Incorporation of EdU during brain development	49
3.4	Birthdating of the ciliary photoreceptors region	50
3.5	<i>In vivo</i> imaging of membranes and nuclei	52
3.6	Clonal domains in developing <i>Platynereis</i> brain.	53
3.7	Cell lineages in developing <i>Platynereis</i> dorsal brain.	55
3.7	Migration of the head kidney cells through the episphere.	58
3.8	Division of a NSC.	59
3.9	Early expression of transcription factors in the dorsal midline domains.	61
3.10	Early expression of transcription factors in the dorso-lateral episphere.	64
3.11	Early expression of transcription factors in the dorso-medial episphere.	65

4.1	Genomic structure of the <i>rx</i> gene.	68
4.2	SNPs in the target sequences of Rx MOs.	70
4.3	Aberrant splicing of <i>rx</i> mRNA after <i>rxin1ex2</i> MO injection.	71
4.4	Survival rates of larvae injected with different morpholinos and mRNAs.	72
4.5	Design of Rx ZFNs.	74
4.6	Breeding scheme for the establishment of <i>rx</i> knockout lines.	75
4.7	Genotyping strategy for ZFN mutants.	77
4.8	ZFN-induced mutations in F0 worms and F1 lines.	78
5.1	Rx morpholino affects the differentiation of ciliary photoreceptors. . .	81
5.2	Knockdown of <i>rx</i> reduces <i>tll</i> expression in the ciliary photoreceptors. .	81
5.3	Knockdown of <i>rx</i> reduces the expression of <i>c-ops1</i>	82
5.4	Knockdown of <i>rx</i> reduces dorsal <i>pax6</i> expression.	85
5.5	Overexpression of <i>rx</i> promotes serotonergic differentiation.	85
5.6	Overexpression of <i>rx</i> expands the <i>otx</i> expression domain.	87
5.7	Knockdown of <i>rx</i> affects the expression of <i>tbx2/3</i>	88
5.8	Knockdown of <i>rx</i> reduces the expression of <i>ngn</i>	90
6.1	Expression of circadian markers at different developmental stages. . .	92
6.2	Circadian regulation of ciliary beating frequency.	93
6.3	Alignment and genomic structure of opsins.	96
6.4	Expression of opsins in the clock region.	99
6.5	Light-evoked Ca ²⁺ waves in the dorsal brain.	101
6.6	The CNG channel mediates light-dependent readjustment of the CBF. .	103
6.7	Conservation of intron positions in annelids and vertebrate <i>hiomt</i> genes. .	107
6.8	Melatonin is the molecular output of the larval circadian system. . . .	109
6.9	Effects of melatonin in nectochaete larvae.	111
7.1	Subdivision of the <i>hiomt</i> expression domain in minimal synexpression groups.	115
7.2	Repertoire of <i>hiomt</i> expressing cells.	119
7.3	Hierarchical clustering of <i>Platynereis hiomt</i> expressing cells.	120
7.4	MDS visualizes the relationships of the <i>Platynereis hiomt</i> expressing cells.	122
7.5	PCA of <i>hiomt</i> expressing cells.	124

7.6	Hierarchical clustering of <i>Platynereis</i> and vertebrate cell types involved in the melatonin system.	126
7.7	MDS of <i>Platynereis</i> and vertebrate cell types.	128
8.1	A model for the antagonism of serotonin and melatonin in <i>Platynereis</i>	135
8.2	The organization of <i>Platynereis</i> photic control of ciliary beating.	136
8.3	A model for the early evolution of metazoan serotonergic and melatonin systems.	144
9.1	Evolution of serotonin and melatonin photoreceptors in Bilateria.	150
12.1	<i>Platynereis</i> injection stage and needles.	196
A.1	The apical organ cell types.	212
C.1	Cryptochrome phylogenetic tree.	217
C.2	Aanat phylogenetic tree.	218
C.3	Hiomt phylogenetic tree.	219
C.4	Opsin phylogenetic tree.	220

LIST OF TABLES

5.1	Loss of ciliary photoreceptors after <i>rx</i> loss of function.	83
5.2	Role of Rx in the development of brain serotonergic cells.	86
5.3	Effects of Rx knockdown on the expression of brain markers.	89
6.1	Neurochemistry of the clock: candidates from the literature screened in <i>Platynereis</i>	108
7.1	Transcription factors of the vertebrate pineal, retina and SCN/anterior hypothalamus analysed in <i>Platynereis</i>	114

LIST OF ACRONYMS

5-HT	5-hydroxytryptamine
CBF	ciliary beating frequency
CSF	cerebrospinal fluid
CNG	cyclic nucleotide gated
CNS	central nervous system
cPRCs	ciliary photoreceptors
DDC	dorsal diencephalic conduction system
DVM	diel vertical migration
GECI	genetically encoded calcium indicator
GMC	ganglion mother cell
GPCRs	G-protein coupled receptors
GRNs	gene regulatory networks
hpf	hours post fertilization
INPs	intermediate neural progenitors
IPN	interpeduncular nucleus
ipRGCs	intrinsically photosensitive retinal ganglion cells
MDS	multidimensional scaling
NSCs	neural stem cells, or neuroblasts
NSW	natural sea water
PDF	pigment-dispersing factor
PrImR	<u>P</u> rofilin by <u>I</u> mage <u>R</u> egistration
PVO	paraventricular organ
RGRs	retinal G protein-coupled receptors
RPE	retinal pigmented epithelium
SCN	suprachiasmatic nucleus
TRP	transient receptor potential
WMISH	whole mount in situ hybridization
ZFNs	zinc finger nucleases

SUMMARY

The aim of this thesis was the molecular, developmental and functional characterization of brain photoreceptors in the annelid *Platynereis dumerilii*. These results shed new light on the evolution of photoreceptors and circadian centers within Bilateria.

Ciliary-type photoreceptors expressing *c-opsin1* and the circadian marker *bmal* were previously identified in the dorsal brain of *Platynereis* larvae (Arendt et al., 2004), indicating that these brain photoreceptors might be involved in the entrainment of the circadian clock.

To study their development, I used EdU incorporation analyses, together with time lapse imaging of embryos expressing fluorescent markers of histones and membranes. This showed that the brain circadian center (demarcated by the expression of *bmal* and *cry1*) is mostly formed by cells that belong to the same lineage. These cells are generated by asymmetric cell divisions of neural progenitors expressing the transcription factor *rx* (*retinal homeobox*), a crucial regulator of vertebrate pineal, retina and hypothalamus development.

Next, I established methods to study gene function in the developing *Platynereis* embryos (morpholino-mediated knockdown, overexpression of mRNA, knockout with zinc finger nucleases). I applied these methods to study the role of Rx in the development of the ciliary photoreceptor lineage. Rx knockdown resulted in the loss of ciliary photoreceptors and in extensive changes in brain development, consistent with a role of Rx in the maintenance and/or multipotency of neural progenitors.

The analysis of the molecular identity of these cells showed that they all express a *peropsin* gene, the melatonin synthesis marker *hiomt* and several markers of the pineal complex, the structure that in vertebrates releases the hormone melatonin. Among these cells, a new photoreceptor type was identified, which is an asymmetric serotonergic cell expressing *c-ops1* and several pineal markers. Hierarchical clustering of *Platynereis* and vertebrate cell types revealed that this serotonergic

cell and the “canonical” ciliary photoreceptors are the *Platynereis* cells more similar to the vertebrate pineal and retinal photoreceptors.

To understand the function of these brain *hiont* expressing cells, I investigated the expression of melatonin receptors. In the trochophore larva, the only site of expression of melatonin receptors was the prototroch, a belt of ciliated cells used for locomotion. Melatonin can specifically decrease the activity of the prototroch cells. Ciliary locomotion follows a circadian rhythm (with higher speed during daytime, and lower speed at night), which can be reset by phototransduction. This suggests that melatonin is the clock output mediating nighttime decrease of locomotor activity.

This study indicates that serotonergic and melatonin releasing ciliary photoreceptors existed at the base of Bilateria. These photoreceptors have a conserved regulatory signature (*rx*, *tbx2/3*, *lhx2/9*, *miR-7*) and their ancestral function was the direct control of ciliary locomotion.

ZUSAMMENFASSUNG

Das Ziel dieser Doktorarbeit war die molekulare, funktionelle und entwicklungsorientierte Charakterisierung der Photorezeptoren im Gehirn des Anneliden *Platynereis dumerilii*. Die gewonnenen Ergebnisse werfen ein neues Licht auf die Evolution von Photorezeptoren und zirkadianen Zentren in Bilaterien.

Im Vorfeld der Arbeit waren ziliäre Photorezeptoren, die Expression von *c-opsin1* und des zirkadianen Markierungsgens *bmal* zeigen, im dorsalen Gehirn von *Platynereis* identifiziert worden (Arendt et al., 2004). Die Expression dieser Gene wies auf eine mögliche Verknüpfung dieser Photorezeptoren mit der Justierung der inneren Uhr hin.

Um die Entwicklung dieser Zellen zu untersuchen, kombinierte ich die Aufnahme der Zellen von EdU zu verschiedenen Entwicklungszeitpunkten mit der Langzeitaufnahme lebender *Platynereis*-embryos, deren sämtliche Zellkerne und Zellmembranen mit fluoreszierenden Markern angefärbt waren. Diese Experimente zeigten, dass die meisten Zellen, die das zirkadiane Zentrum formen (abgegrenzt durch die Expression von *bmal* und *cry1*), dieselbe Abstammung haben. Die Zellen werden durch die asymmetrische Zellteilung neuraler Vorläuferzellen hervorgebracht, die ihrerseits den Transkriptionsfaktor *rx* (*retinal homeobox*) exprimieren, welcher ein entscheidender Regulator der Entwicklung des Pinealorgans, der Retina und des Hypothalamus in Wirbeltieren ist.

Darüber hinaus etablierte ich Methoden zur Untersuchung von Genfunktionen im sich entwickelnden *Platynereis*-embryo (Morpholino-Knockdown, mRNA Überexpression, Knockout mittels Zinkfinger-nukleasen) und verwendete diese, um die Rolle von *Rx* während der Entwicklung der ziliären Photorezeptoren zu untersuchen. Der Knockdown von *Rx* führte zum Verlust der ziliären Photorezeptoren, sowie zu erheblichen Veränderungen der Gehirnentwicklung. Dies ist im Einklang mit einer Funktion von *Rx* in der Erhaltung und/oder Multipotenz der neuralen

Vorläuferzellen.

Die Analyse der molekularen Identität dieser Zellen zeigte, dass alle die Expression eines *peropsin* Gens, des Melatoninsynthesemarkers *hiomt* und verschiedener weiterer Gene des Pinealorgans, welches in Wirbeltieren Melatonin ausschüttet, gemeinsam haben. In den von mir untersuchten Zellen wurde eine neue Photorezeptorart identifiziert: eine asymmetrische, serotonerge Zelle, die *c-opsin1* und mehrere Marker des Pinealorgans exprimiert. Hierarchisches Clustering von *Platynereis*- und Wirbeltierzelltypen zeigte, dass die asymmetrische serotonerge Zelle und die "kanonischen" ziliären Photorezeptoren die *Platynereis*-zellen sind, die den Wirbeltier Pinealorganzellen und Retinazellen am ähnlichsten sind.

Um die Funktion dieser *hiomt*-exprimierenden Zellen zu verstehen, untersuchte ich die Melatoninrezeptor-expression. Der einzige Ort an dem Melatoninrezeptoren in der Trochophoralarve exprimiert wurden, ist der Wimpernkranz (Prototroch), ein Ring aus Zellen mit jeweils mehreren Zilien, der der Lokomotion dient. Melatonin kann die Aktivität dieser Prototrochzellen herabsetzen. Die ziliäre Lokomotion folgt einem zirkadianen Rhythmus (höhere Schlaggeschwindigkeit tagsüber und langsames Schlagen in der Nacht), der durch Phototransduktion zurückgesetzt werden kann. Dies weist darauf hin, dass Melatonin der Zeitgeberoutput ist, der die Verringerung der Bewegungsaktivität in der Nacht vermittelt.

Diese Arbeit zeigt, dass serotonerge melatoninausschüttende ziliäre Photorezeptoren an der Basis der Bilaterien existierten. Diese Photorezeptoren exprimierten ein konserviertes Set einiger Transkriptionsfaktoren (*rx*, *tbx2/3*, *llx2/9*) und ihre ursprüngliche Funktion war die Kontrolle ziliärer Lokomotion.

INTRODUCTION

1.1. Diversity of nervous systems in the animal kingdom

The evolution of the central nervous system (CNS) remains one of the hardest questions to tackle in the fields of evolutionary developmental biology (EvoDevo) and comparative neuroscience. If the combination of comparative neuroanatomy and molecular markers can illuminate the major events of brain evolution within closely related species, there are still many controversies on how complex brains evolved in the first place.

The simplest forms of neural organization are found in animals that lack bilateral symmetry, like sea anemones and jellyfishes, which belong to the phylum Cnidaria (the outgroup of Bilateria). In these animals, the nervous system is organized as a diffuse nerve net, where the sensory information is elaborated locally to produce a locomotor output, with minimal integration of signals. Conversely, in the majority of Bilateria the nervous system is centralized, and organized for a more elaborated information processing, where different sensory inputs are integrated to generate coherent locomotor and neuroendocrine outputs. Hence the majority of the neurons are concentrated on one side of the body, and assembled into structures like nuclei, ganglia, neuropils, nerve tracts (Swanson, 2011).

It is evident that the question of the origin of nervous systems is intimately linked to the question of how was the body plan of the Urbilateria, the last common ancestor of Bilateria (animals with bilateral symmetry), and how was its life cycle (fig.1.1).

The existence of a common *Bauplan* in protostomes and deuterostomes was a matter of dispute already at the beginning of the 19th century, when Geoffroy St-Hilaire proposed that the ventral side of arthropods corresponds to the dorsal side of vertebrates, based on the relative arrangement of internal body structures (nervous system, heart, gut). This concept has been refined and expanded by Anton Dohrn at the end of the 19th century, who proposed that vertebrates evolved after dorso-ventral

inversion of an annelid-like ancestor (the so-called “annelid theory”, reviewed in Nübler-Jung and Arendt 1994).

More than one hundred years later, Dohrn’s ideas gained new support from molecular data: the molecules responsible of the dorso-ventral patterning in insects and vertebrates are homologous (Dpp and Sog in insects and BMP-4 and Chordin in vertebrates); the nervous system always develops from the non-Dpp side (Arendt and Nübler-Jung, 1994; Holley et al., 1995; Sasai et al., 1995). Consistently, the opposing gradients of dpp/BMP-4 and sog/chordin establish the same sequence of transcription factors in the developing nervous system (*vnd/nkx2* genes are expressed more medially, *msh/msx* genes more laterally, and so on).

Despite the new insights coming from molecular studies, the “annelid theory” and the bilaterian origin of the CNS are far from being established. The controversies are mostly linked to the lack of centralization at the base of deuterostomes (fig.1.1). In hemichordates, like the acorn worm *Saccoglossus kowalevskii*, neurons are organized in a nerve net, and brain patterning genes are expressed in rings over the entire ectoderm (Lowe et al., 2003). These data prompted several authors to propose that the ventral or the dorsal position of the nervous system in insects and vertebrates, respectively, resulted from independent condensation events from a diffuse nerve net, instead of dorso-ventral inversion (Holland, 2003; Lacalli, 2003). But, as a valid alternative explanation, hemichordates might have lost a centralized nervous system secondarily, because of their burrowing life style (Tautz, 2003). The more recent demonstration that *Saccoglossus* has some reduced form of centralization in adult stages further supports this interpretation (Nomaksteinsky et al., 2009).

A complete picture on brain evolution in metazoans can come only from molecular studies in several organisms, chosen in key positions of the tree of life (fig. 1.1). Organisms in slow-evolving lineages are going to be very insightful, since they more likely conserved aspects of nervous system organization already present in the last common ancestor of Bilateria. Unfortunately, “classic” invertebrate model organisms like *Drosophila* and *C.elegans* belong to fast evolving lineages, and for this reason they accumulated several changes from the ancestral urbilaterian characters.

A multi-level comparison of slow evolving animals, like the cnidarian *Nematostella*, the annelid *Platynereis* and the deuterostomes *amphioxus* and *Saccoglossus*, can help to solve the enigma of how the last common ancestor of Bilateria looked like.

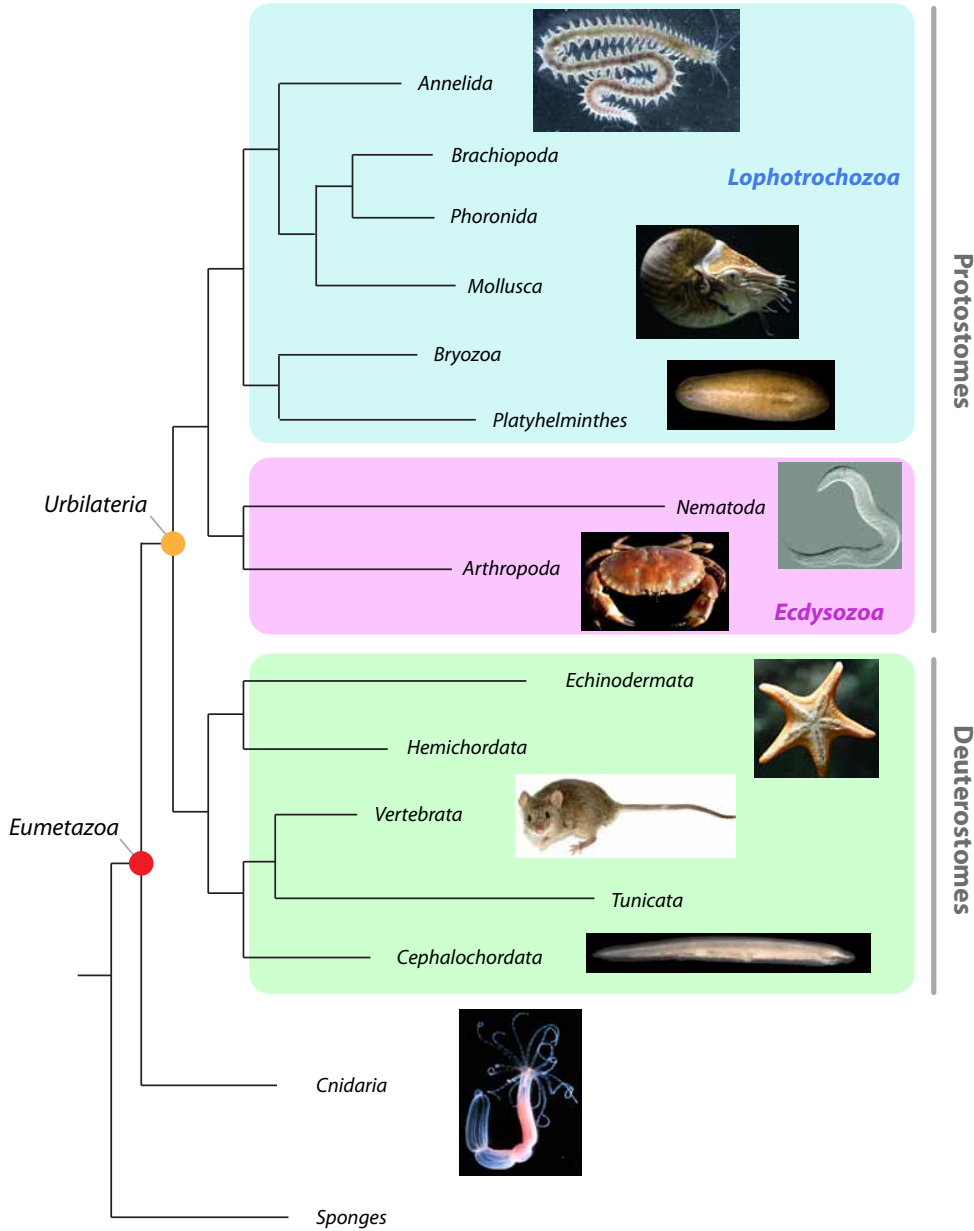


Figure 1.1: **Simplified phylogenetic tree of Metazoa.** The illustration, simplified from Hejnol et al. (2009), shows the phylogenetic position of the main metazoan groups. Sources of the images: Wikipedia and <http://genome.jgi-psf.org/>.

1.2. The annelid *Platynereis dumerilii*: a model system for studying brain evolution

Annelids occupy a very interesting phylogenetic position in the tree of life (fig. 1.1). They belong to the super-phylum of Lophotrochozoa, one of the two subdivisions of protostomes, which is poorly represented within “classical” developmental model organisms. Moreover, annelids have very few phylum-specific morphological characters, meaning that their body plan didn’t undergo extensive modifications after the emergence of the group (Tessmar-Raible and Arendt, 2003). Indeed, the cambrian fauna is populated by annelid trace fossils, including worms with segments, parapodia and chetae, resembling living polychaetes (Conway Morris, 2006; Conway Morris and Peel, 2008).

The new annelid phylogeny proposed recently by Struck et al. (2011) subdivides annelids in two major clades, Errantia and Sedentaria. The two names describe the prevalent lifestyle of the group members: Errantia show adaptations to a very motile, sometimes predatory lifestyle, while Sedentaria are burrowing worms, which live in a tube as filter-feeders. In both groups, morphological traits correlated with lifestyle adaptations have been identified (Struck et al., 2011).

Within annelids, *Platynereis dumerilii* (Annelida, Phyllodoceida, Nereididae) became recently a molecular model organism for evolution, development and neurobiology. *Platynereis* is a polychaete worm and belongs to the clade of Errantia, thus it has a broad repertoire of sensory structures and elaborated parapodial appendages for crawling. The analysis of gene structure and intron positions showed that *Platynereis* has a slow evolving genome (Raible et al., 2005). The possibility to keep *Platynereis* in the lab for its entire life cycle, and the delivery of offsprings in big numbers makes *Platynereis* amenable for developmental and molecular studies.

1.2.1. Life cycle and early development of *P. dumerilii*

The life cycle of *P. dumerilii* is subdivided in a pelagic and a benthic phase (fig. 1.2A, Fischer and Dorrestein 2004). The developmental stages have been recently described in great detail by Fischer et al. (2010). After fertilization, the embryo develops quickly into a *trochophora larva* (fig. 1.2B), characterized by an equatorial band of ciliated cells, called *prototroch*, an apical assembly of sensory and ciliated cells called *apical organ*, a through gut, a pair of larval protonephridia and a pair of larval eyes used for phototaxis (Jékely et al., 2008). The cells anterior to the

prototroch form the so called *episphere*, which includes the apical organ and the developing brain; posterior to the prototroch, the *hyposphere* will form the first three body segments. This phase of development is stereotypical and characterized by a fixed lineage; moreover, the larvae develop synchronously, making it possible to directly compare different individuals of the same stage.

In comparison with other annelids, *P. dumerilii* larvae are lecithotrophic and have a relatively short pelagic phase. After about three days of development, the larvae elongate posteriorly and develop the parapodia and become competent to settlement. This new larval stage, called *nectochaete larva*, lasts few days and is characterized by an higher developmental plasticity, probably as an adaptation to changing environmental conditions. The larvae start feeding and settle in the benthos only after the identification of an appropriate substrate. Afterwards, the *juvenile worm* grows new segments and undergoes the first metamorphosis (called cephalic metamorphosis), which consists in the transformation of the first chaetiferous segment into part of the head; this *atoke worm* builds himself a tube and lives in the benthos.

A second metamorphosis takes place few months later, immediately before the reproduction, and transforms the atoke worms in sexually mature *epitoke worms*. *P. dumerilii* is sexually dimorphic, and the sexes become recognizable at this stage, with yellow females and red-whitish males. Spawning is highly synchronized according to the moon phase; the epitoke mature worms become pelagic, find each other with pheromones, and after a nuptial dance they release their gametes in the water and die.

Nereidids development has been a subject of investigation since the end of the 19th century (Wilson, 1892). More recently, the early developmental stages of *P. dumerilii* have been described by Dorresteyn (1990); Fischer et al. (1996); Ackermann et al. (2005). Like other groups of lophotrochozoans, annelids have a spiralian cleavage (fig. 1.2C): during the first hours of development, the orientation of the mitotic spindles shifts at every subsequent cleavage; as a consequence, at the eight cells stage the four dorsal cells are not aligned to the four ventral cells. The first two cell divisions are unequal and define the four main embryonic quadrants, corresponding to the four blastomeres (A, B, C and D). These cells divide further generating the first set, or *quartet*, of micromeres (1a, 1b, 1c and 1d), located dorsally, and the first set of macromeres (1A, 1B, 1C and 1D), which retain most of the yolk content and have a ventral location. Other three sets of micromeres are generated by the subsequent three divisions of the macromeres; at this point, the spiralian phase terminates and

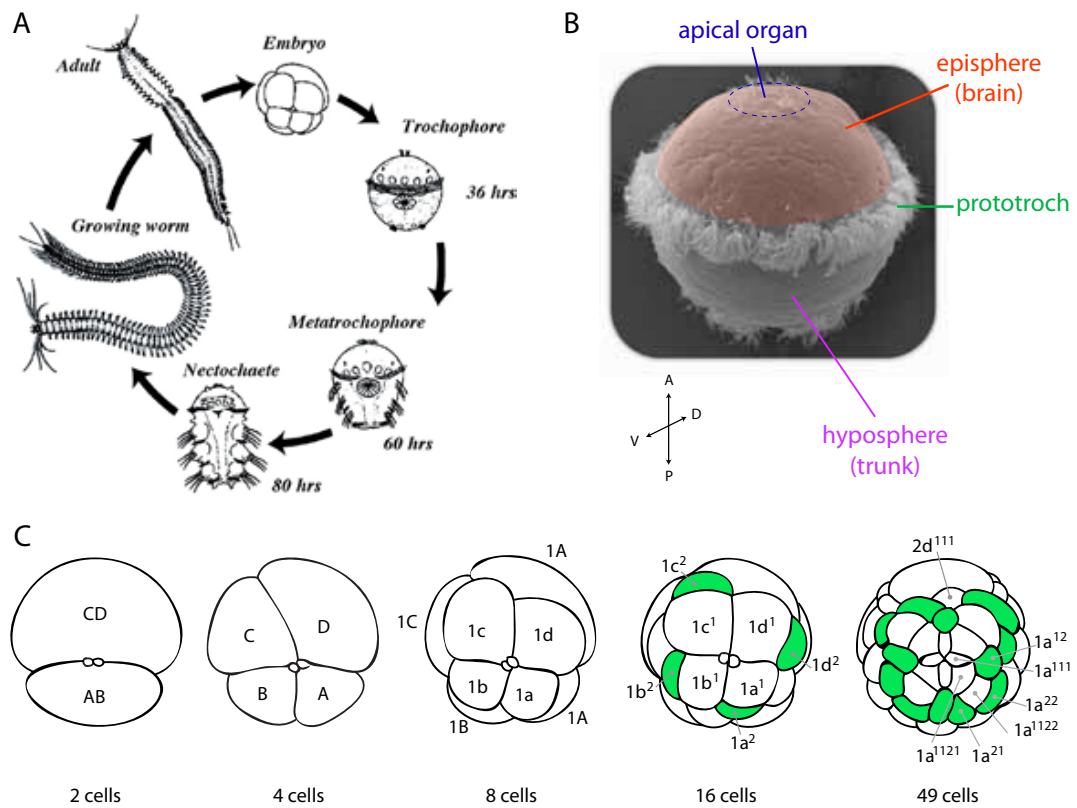


Figure 1.2: Life cycle and early development of *Platynereis dumerilii*. A. *P. dumerilii* life cycle (image courtesy of Dr. G. Belavoine). B. The *Platynereis* trochophore larva (SEM photo courtesy of Dr. H. Hausen). C. The early cleavages of *Platynereis* embryos. Green indicates the trochoblasts. Redrawn from Fischer and Dorresteyn (2004). For explanation, see text.

there is a transition to bilateral cleavage. The episphere develops (almost) entirely from the first set of micromeres. The cells of the apical organ (the so-called “apical rosette”) and the prototroch cells are produced during the very first divisions of the first quartet micromeres. At the 49-cell stage, the episphere is delimited by a ring of trochoblasts (which will divide to form the prototroch cells and accessory cells). In the middle, there are the four cells of the apical rosette (which will form the apical organ) and eight more cells (two from each quadrant: $1a^{1121-2} - 1d^{1121-2}$) that will give rise to the rest of the episphere. The dorsal part of the brain is a derivative of the C and D quadrants. Interestingly, the ring of trochoblasts is interrupted dorsally by the small $2d^{111}$ cell, a descendent of the second quartet micromeres.

1.2.2. Advances of *P. dumerilii* as a model system

The development of *P. dumerilii* is fast enough to make it amenable to developmental and molecular studies. The genome and the transcriptome have been sequenced recently (Arendt lab, unpublished). Single and double whole mount in situ hybridization (WMISH) allow the analysis of the expression domains of genes of interest during embryonic and larval stages (Tessmar-Raible et al., 2005); the expression patterns can be documented with a confocal microscope together with the tubulin staining of the axonal scaffold (reflection microscopy, Jékely and Arendt 2007). Since development is stereotypical and synchronized at larval stages, reflection microscopy has been used for image registration of expression patterns on a common reference axonal scaffold (Tomer et al., 2010). This technique, called Profiling by Image Registration (PrImR), allows to generate average expression patterns for a gene of interest; subsequently, the average expression patterns can be compared, since they are based on the same reference scaffold. This makes possible to determine *in silico* coexpression of multiple genes with a single cell resolution (Tomer et al., 2010).

Recently, techniques for the injection of zygotes have also been established (Kegel, 2008). This made possible, for the first time, to manipulate gene function by means of injection of synthetic mRNAs and morpholino antisense oligonucleotides, but also to establish knock out lines with the zinc finger nucleases (ZFNs) technology (described in par. 4.4). Similarly, transposon-mediated transgenesis has been established (Arendt lab and several other labs, unpublished).

1.3. Homologies of brain regions and cell types in Bilateria

The goal of comparative studies is to identify evolutionary relationships between the elements of interest, and to unravel their evolutionary origin. The question of homology can be addressed at different levels, depending on the choice of the units of comparison. The units to compare range different scales: entire organ systems (like eyes, hearts etc.), morphogenetic fields, molecular topographies (the spatial relationships of gene expression domains), neuronal architectures, cell types, cellular ultrastructures, signalling systems, protein sequences, differentiation cassettes... Over large phylogenetic distances, a more complete understanding of brain evolution can be clearly achieved only with the integration of all these different levels of comparison.

1.3.1. Conservation of brain regions along the anterior-posterior and the dorso-ventral axes

The analysis of gene expression patterns of key developmental genes revealed similarities in the relative arrangements of expression domains (“molecular topography”) along the anterior-posterior (AP) and dorso-ventral (DV) axes, after a similar activity of conserved signalling systems.

Conservation of the AP axis was suggested after the discovery of the *Hox* cluster in vertebrates and insects. An Hox code underlies the segmental organization of the *Drosophila* trunk and the vertebrate hindbrain-spinal cord. A clear segmental organization exists also in the insect brain. Similarly, the so-called “prosomeric model” for vertebrate brain suggests the existence of conserved brain compartments along the AP axis, delimited by morphogenetic boundaries (Rubenstein et al., 1994; Puelles and Rubenstein, 2003).

Some of these boundaries are conserved within Bilateria. In vertebrates, the most anterior part of the brain (forebrain) is demarcated by the expression of the transcription factor *six3*, followed posteriorly by *otx* expression. The investigation of *six3* and *otx* expression in *Platynereis* and in arthropods revealed that the same *six3-otx* AP sequence is present in the developing brains of protostomes (Steinmetz et al., 2010). The anterior *otx* expression domain is followed by *gbx* expression in vertebrates (midbrain-hindbrain boundary), insects, annelids and hemichordates (Wurst and Bally-Cuif, 2001; Lowe et al., 2003; Hirth, 2003; Steinmetz et al., 2011). Finally, it has been shown that the *fezf-irx* boundary is also conserved in Bilateria (Irimia et al., 2010). These findings support the hypothesis that the urbilaterian nervous system was patterned along the AP axis by a sequence of *six3-otx-gbx-hox* expression domains (fig. 1.3).

It is currently accepted that the vertebrate neural tube evolved from the folding of an ancestral, unfolded neuroepithelium. For this reason, the DV axis of the vertebrate neural tube corresponds to the medio-lateral axis of the developing protostome nervous system. The comparison of the annelid medio-lateral patterning with the vertebrate DV patterning showed impressive similarities in the sequence of transcription factors expressed along these axes in the developing ventral nerve cord (Denes et al., 2007). The same sequence is present in the developing *Drosophila* ventral nerve cord, making a clear case of conservation across Bilateria.

A similar comparison has been harder for the brain, where the different organization and sizes of brain nuclei underlies higher morphological variability. However,

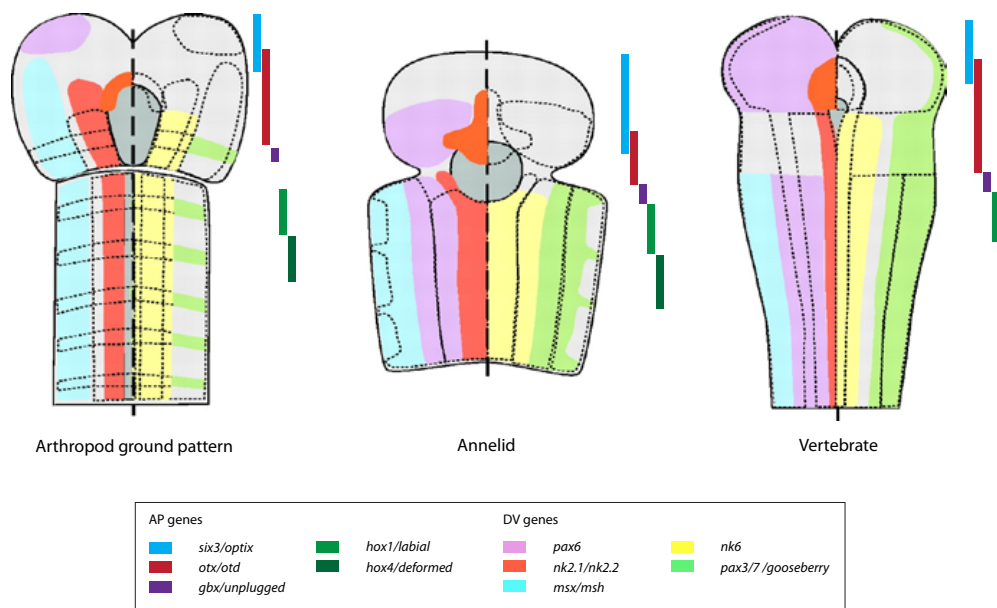


Figure 1.3: **Conservation of brain regions along the AP and DV axes.** Mediolateral neurogenic columns (drawings) and AP expression domains (lateral bars) of selected transcription factors, in annelids and arthropods (ventral views) and vertebrates (dorsal view with the open neural tube). Adapted from Arendt et al. (2008); see also Rubenstein et al. (1998); Steinmetz et al. (2010).

using annelids made possible to identify some instances of conservation of brain medio-lateral patterning. In both vertebrates and annelids, a medial *nk2.1/nkx2.1* expression domain is opposed to the lateral *pax6* expression (fig. 1.3, (Tessmar-Raible et al., 2007)). Moreover, lateral Wnt signalling is necessary to establish the same medio-lateral sequence of transcription factors that patterns the *Platynereis* brain and the vertebrate forebrain (Tomer et al., 2010). The emerging picture is that aspects of brain regionalization can be compared across long evolutionary distances, revealing a conserved *bauplan* for the bilaterian brain.

1.3.2. Conservation of cell types

Despite the conservation of brain patterning mechanisms within Bilateria, brain parts differ in many respects, like the number of cells, their connectivity, sometimes their function. Just as an example, eyes show remarkable differences in shapes and organization, which puzzled several scientists including Darwin; it is now accepted that eyes are not homologous in Metazoa. But then, why is brain regionalization so conserved?

One possible hypothesis is that brain regions were established in ancient times in relationship to the diversification of cell types. One example is the formation of eyes from *otx+* regions of the developing head of protostomes and deuterostomes (Steinmetz et al., 2010). In many cases, transcription factors with important roles in brain regionalization have been shown to control directly differentiation gene batteries in specific cell types (Manavathi et al., 2007; Ranade et al., 2008). An ancient role of regionalization genes in the specification of regionally-restricted cell types would explain the broad conservation of molecular topography in *Saccoglossus*, where the AP and only parts of the DV patterning are conserved, but morphologically distinct brain parts are not present (the nervous system is mostly a diffuse nerve net).

For these reasons, the comparison of cell types can reveal deep homologies in cases where the morphological evolution changed the body plan, sometimes drastically. A clear example has been shown in the sea urchin. Echinoderms like sea urchins are deuterostomes that evolved a pentameric symmetry, clearly a derived feature of the phylum. Morphologically distinct eyes, or even a brain, are not distinguishable in these organisms. However, photoreceptor cells homologous to the protostomes eye photoreceptors have been identified in the sea urchin tube feet (Ullrich-Lüter et al., 2011).

It is tempting to ask next why cell types are so conserved. One possible explanation might be related to the regulation of the cell type differentiation phenotype. Cell types are demarcated by structural and morphological features, which determine their function. This is especially true for sensory cells. These features depend on entire sets of differentiation genes, that need to be expressed all together. As an example, the dopaminergic phenotype of a neuron requires the presence of all the enzymes involved in dopamine synthesis and release. Intriguingly, it has been shown that gene regulatory networks (GRNs) for terminal differentiation are organized like “operons”, where one or few transcription factors, called “terminal selector genes”, activate directly the transcription of entire sets of interrelated differentiation genes, to produce defined cellular phenotypes (Hobert et al., 2010). Moreover, these terminal selector genes are conserved over large evolutionary distances (Flames and Hobert, 2009; Kratsios et al., 2011).

These considerations explain why a cell type needs to be defined by the combination of the *regulatory signature* (transcription factors) and the *differentiation signature* (differentiation markers, like structural proteins, neurotransmitters, receptors...), which together constitute the cell type *molecular fingerprint* (Arendt, 2005, 2008). If

the comparison of cell types across animals has been a focus of EM studies few decades ago, the analysis of molecular fingerprints expands tremendously the depth of investigation and the possibilities for comparisons.

The cell type approach proved to be successful in several cases: to demonstrate the surprising similarities in motorneuron specification between protostomes and deuterostomes (Thor and Thomas, 2002), the conservation of cranial motorneurons between ascidians and vertebrates (Dufour et al., 2006), the conservation of vasotocinergic neurosecretory cells in the annelid medial brain and the vertebrate hypothalamus (Tessmar-Raible et al., 2007), and to study the evolution of photoreceptor cell types (discussed later).

If a given cellular phenotype depends on certain differentiation gene batteries, controlled simultaneously by few transcription factors, it is hard to escape that the same gene batteries could be recruited in a completely new context. In these cases, the comparison of the brain regions where the cell types are found can help to distinguish between real conservation (similar cell types in similar contexts) or cooption (a cell type coopted in a completely different body region). If similar cell types exist within homologous brain regions, it is extremely likely that they come from the same common ancestor.

In conclusion, understanding brain evolution needs the integration of two different levels of comparison: regionalization genes and cell types. Both levels are highly conserved, due to different constraints. Most of the mechanisms involved in nervous system regionalization are the same ones that shape the animal body plan. Cell types are conserved because the cellular phenotype depends on the coordinated activation of differentiation genes, which determine the cellular function. It seems that evolution “played” in between these two levels, where brain diversity has been elaborated.

1.3.3. The division of labour model for nervous system evolution

If a cell type is defined by the expression of differentiation cassettes for specific cellular functions, this tightly links a cell type to its functions within the organism. But since new cell types evolve from preexisting ones, it is evident that the evolution of new cell types can happen only in two conditions: either by segregation of functions from a multifunctional cell type, or with the evolution of completely new functions (for example, together with the evolution of new genes).

Segregation of functions must have been the dominating mechanism in early

evolution of neuronal cell types, since the cell types of basal metazoans are multifunctional. The observation of myoepithelial cells (sensory and contractile cells) in cnidarians prompted Mackie (1970) to hypothesize that muscle cells and neurons evolved after functional segregation from a multifunctional cell type; the newly evolved cell types remained in contact, in order to perform the original function (fig. 1.4A). This “division of labour” model can be extended to other cell types, and can explain the evolution of simple neural circuits, starting from multifunctional sensory-motor cells (Arendt et al., 2008; Jékely, 2011).

A division of labour model has been proposed for the evolution of simple eyespots, like the *Platynereis* larval eyes (Arendt et al. 2009, fig. 1.4B). This hypothesis starts from the observation that cnidarian larvae have multifunctional cells, with a shading pigment, a rhabdom (for the packaging of opsin) and a locomotor cilium; the activity of the cilium depends on the directional light response from the same cell. In *Platynereis*, the three functions are subdivided between three cell types: a shading pigment cell and a photoreceptor cell, which form the larval eye, and a multiciliated prototroch cell. These three cells are functionally interconnected, since the larval eye innervates directly the prototroch cell, and in this way controls the ciliary beating of that cell (Jékely et al., 2008).

Mathematical modelling showed that division of labour processes are generally advantageous in biological systems (Gavrilets, 2010; Rueffler et al., 2011). It is not hard to imagine why this was advantageous also in the context of nervous system evolution. The segregation of functions between cell types allows each new cell type to specialize further on its new exclusive function. After the segregation of the sensory and the motor components, another immediate advantage was the possibility to integrate multiple sensory inputs for a finer control of the locomotor output. Moreover, division of labour can elegantly explain the evolution of interneurons, which do not exist in basal metazoans (Marlow et al., 2009; Galliot and Quiquand, 2011), and constitute the key acquisition of more complex, or “integrative” nervous systems. Finally, the rise in body plan complexity was accompanied by the specialization of tissue types, and the physical segregation of sense organs, brain, neuroendocrine organs and musculature.

The widespread occurrence of division of labour in the nervous system evolution must be taken in account whenever cell types are compared across distantly related taxa. In simple marine ciliated larvae, like the *Platynereis* trochophore, sensory cells innervate directly the ciliated cells responsible of locomotion, while in more complex

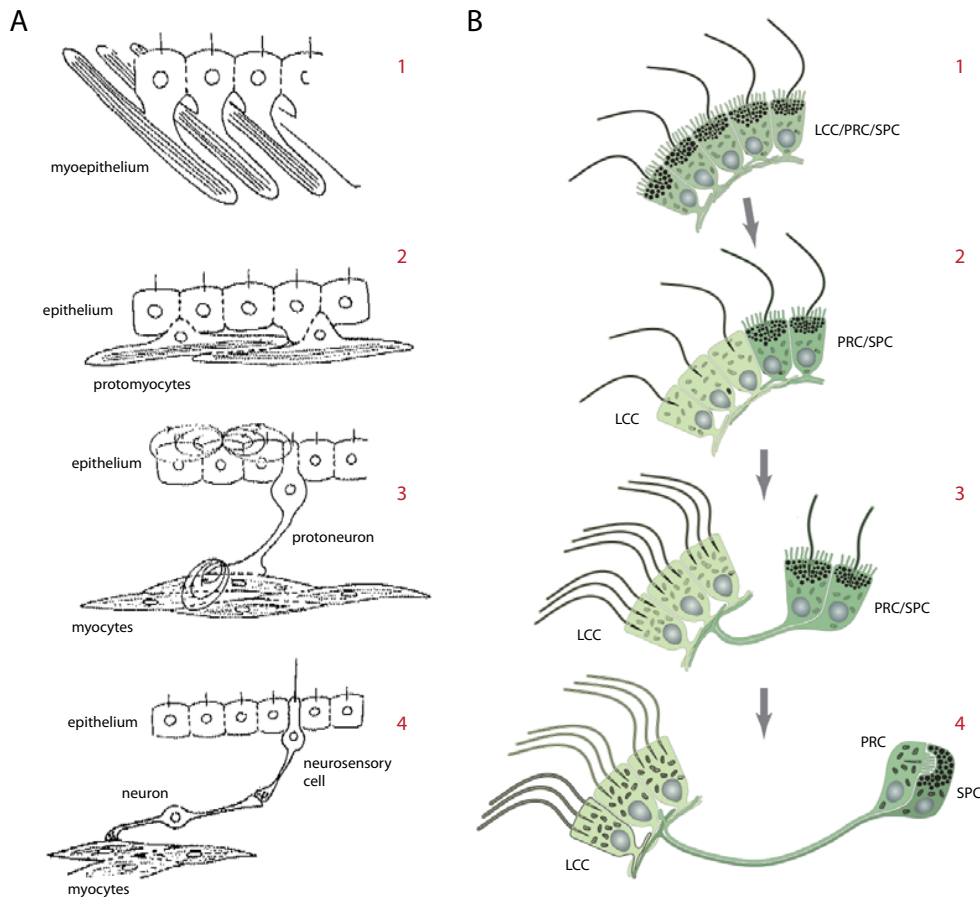


Figure 1.4: Examples of division of labour in nervous system evolution. A. Evolution of sensory-motor circuits from myoepithelial cells, according to Mackie (1970). Myoepithelial cells, like those existing in Cnidaria (1) start to sink internally (2). Protoneurons evolve, which sense environmental information externally and control myocyte contraction; the epithelial cells are electrically coupled (3). After another step of division of labour, specialized neurosensory cells and motoneurons evolve (4). They form a minimal circuit for the control of myocyte contraction. Image from Mackie (1970). B. The evolution of simple eyespots from an ancestral multifunctional cell. Multifunctional cells (1) are locomotor ciliated cells (LCC) that can sense light direction (PRC: photoreceptor; SPC: shading pigment cell). Some cells specialize in sensing light direction, while the others keep the original role in locomotion; a similar situation is present in some cnidarian larvae (2). The specialized PRC/SPC move away from the epithelium (3) and, after another step of division of labour, specialize in a PRC and a SPC (4). Image from Arendt et al. (2008).

organisms, sister cell types with the same sensory modality might control muscle-driven locomotion indirectly, through more complex neural circuits.

1.4. Studying marine larvae uncovers the earliest steps in brain evolution

Animal nervous systems have an astonishing diversity in forms, complexity and functions, yet they evolved from an obscure common ancestor.

In ancestral forms, locomotion was driven by cilia, like in extant marine larvae. Basal metazoans, like the Cnidaria, have non-centralized nervous systems consisting of simple nerve nets, made by bipolar sensory neurons, neurosecretory cells and ganglion cells, but not “true” interneurons (Marlow et al., 2009; Galliot and Quiquand, 2011). In these animals, the control of locomotion is exerted by multifunctional neurons, which are sensory cells and motorneurons at the same time. In Bilateria, this simple neuronal organization is elaborated further in circuits that integrate the sensory information, and produce a coherent motor output. The establishment of the first integrative systems to control locomotion was probably one of the first steps in nervous system centralization.

For these reasons, primary ciliated larvae, like the trochophore larvae of annelids, represent an ideal system to understand these early evolutionary events. First, they still move with cilia, which is the ancestral form of animal locomotion, since muscles evolved only later (Jékely, 2011). Second, they retain sensory-motor cells to control directly ciliary beating, like the larval eyes (Jékely et al., 2008) and several peptidergic neurons of the larval medial brain described in *Platynereis* (Conzelmann et al., 2011). But more importantly, most authors agree that primary ciliated larvae of protostomes and deuterostomes are homologous, as indicated by the conservation of morphological traits and molecular markers (Jägersten, 1972; Nielsen, 2005; Marlow et al., 2012; Santagata et al., 2012). Following these ideas, the life cycle of early bilaterians comprised a pelagic larval stage, thus studying extant primary ciliated larvae of marine invertebrates can give insights into how early nervous systems evolved.

2

EVOLUTION OF PHOTORECEPTOR CELL TYPES AND NON-VISUAL LIGHT DETECTION

2.1. Ciliary and rhabdomeric photoreceptors

The impressive diversity of animal eyes has been an evolutionary enigma since Darwin's times. The comparison of eyes or eye parts never brought to any conclusive scenario, until a cell type perspective was proposed. On the basis of ultrastructural studies, Eakin (1979) hypothesized the existence of two evolutionary lines of photoreceptors: a rhabdomeric line exclusive of protostomes, and a ciliary line in deuterostomes. Ciliary and rhabdomeric photoreceptors are distinguished by morphological characters: the presence of surface extensions associated to cilia (like in vertebrate rods and cones) or microvilli (like in *Drosophila* ommatidia), respectively (fig. 2.1A and C). However, the EM ultrastructural data were not really helpful to solve photoreceptor evolution: the discovery of several exceptions to Eakin's theory led Salvini-Plawen and Mayr to propose that photoreceptors with different morphologies evolved at least 40, if not 65 times independently (Eakin, 1979).

Molecular data seem to favor Eakin's views, since despite morphological variation within each class, ciliary and rhabdomeric photoreceptors are two distinct cell types, which were present in the last common ancestor of Bilateria, and were inherited differently in protostomes and deuterostomes (Arendt, 2003). The fundamental distinction between these two photoreceptor types is based on the second messenger system used in the phototransduction cascade (see below). The association of cellular morphology and phototransduction is so tight, that it might underlie a common and conserved regulatory logic, which is so far not understood.

Moreover, the comparison of molecular fingerprints revolutionized the old views on the phylogenetic distribution of ciliary and rhabdomeric photoreceptors (Arendt, 2003). Two pairs of ciliary photoreceptors (cPRCs) have been identified in the brain of *Platynereis* (Arendt et al., 2004). These cells have long, branched cilia, and express

an opsin (*c-opsin1*) ortholog to the opsins expressed in the vertebrate rods and cones. This finding was a surprise in the field, and refreshed the discussion on eye evolution (Nilsson, 2005). First, the presence of ciliary and rhabdomeric photoreceptors in a protostome indicates that the two cell types were already present in the urbilaterian ancestor. It was already known that some molluscs have photoreceptors with a ciliary morphology in their eyes, but these cells express other kinds of opsins; c-opsins were never identified outside vertebrates. Second, the annelid cPRCs, despite being related to vertebrate rods and cones, are located in the brain and not in the eyes. These cells are not used for vision, since they are not associated to pigments; they are rather involved in the entrainment of circadian rhythms, as indicated by the coexpression of the circadian marker *bmal* (Arendt et al., 2004).

It seems then that a switch of functions (visual and non-visual) happened at the transition between invertebrates (which have eyes based on rhabdomeric photoreceptors) and vertebrates (which have visual ciliary photoreceptors). If the annelid-like segregation of function was in place in the urbilaterian ancestor (rhabdomeric photoreceptors for vision, and ciliary photoreceptors for circadian entrainment), then any eye evolution scenario needs to explain why in vertebrates ciliary photoreceptors replaced rhabdomeric photoreceptors for vision. It was suggested that either the vertebrate ancestors were sessile, blind benthic animals (Nilsson, 2005), or that these ancestors conquered new ecological niches in deeper water, where the more sensitive c-opsins served visual functions better than r-opsins (Lamb, 2009). In any case, the new vertebrate eyes “evolved from the brain”; the morphogenetic movements taking place during vertebrate eye development (evagination of the optic vesicles) would then “recapitulate” what happened during evolution.

The power of molecular comparisons allowed also the discovery of new photoreceptors. Indeed, many photoreceptor cell types, and especially those with non-visual functions, do not have big surface extensions, so they cannot be recognized with EM, but only with the expression of markers. One example are the intrinsically photosensitive retinal ganglion cells (ipRGCs) of the vertebrate retina, which express melanopsin (the vertebrate ortholog of invertebrate rhabdomeric opsins, see below), have a typical rhabdomeric phototransduction cascade, but do not have any rhabdom. These cells do not participate to visual processes, but they are involved in the entrainment of the brain master clock (see later).

It has been argued that the increase of membrane extension is necessary to improve photosensitivity only in cells that are partially shielded by a pigment, hence in photoreceptors used for vision. According to this interpretation, photoreceptors

evolved at the very beginning for non-visual functions, and didn't have elaborated cilia or microvilli (Nilsson, 2009). It can be anticipated that the use of molecular tools will bring to the discovery of many more interesting photoreceptor types.

2.1.1. Phototransduction cascades

In both ciliary and rhabdomeric photoreceptor types, phototransduction starts with an opsin, G-protein coupled receptors (GPCRs) located in the ciliary membrane or in the rhabdom, respectively. Distinct types of opsins are associated to ciliary and rhabdomeric photoreceptors (referred to as ciliary and rhabdomeric opsins). Opsin activation by light triggers different G protein cascades in ciliary and rhabdomeric photoreceptors.

In rhabdomeric photoreceptors, light always activates a G protein with a G_q α subunit. The activated G_q activates a phospholipase C (PLC) protein, which produces phosphoinositides as second messengers (IP_3 and DAG). The final result is the opening of transient receptor potential (TRP) channels, which mediate the influx of positive ions and the depolarization of the cell membrane. Thus, the light response is always associated to cell depolarization; this is called "ON-response" (fig. 2.1B).

In ciliary photoreceptors, the α subunit of the G protein can be either a member of the G_i or G_o families, like the transducin of vertebrates (G_t), or a G_s protein, as found in cnidarians. These G proteins control the intracellular concentration of cyclic nucleotides (cAMP in cnidarians, cGMP in all the other animals), normally by changing the activity of a phosphodiesterase (PDE). The cyclic nucleotides control the opening of cyclic nucleotide gated (CNG) channels, hence the membrane resting potential. In vertebrate rods and cones, CNG channels are constitutively open at darkness, and the membrane potential is depolarized. Upon illumination, the G_t -dependent phototransduction cascade causes the decrease of cGMP concentration, and consequently the closure of CNG channels and the decrease of membrane potential. In other words, the vertebrate ciliary photoreceptors fire in the darkness; this is called "OFF-response" (fig. 2.1D).

In few examples, CNG channels have been shown to be involved in other kinds of photoresponses. In the lizard parietal eye and in the *C.elegans* photosensory cells, different G protein cascades increase the cGMP concentration and open the CNG channels; this response depolarizes the neuron in the presence of light, thus the cell is "ON-responding" (Finn et al., 1997; Ward et al., 2008; Liu et al., 2010). Addition-

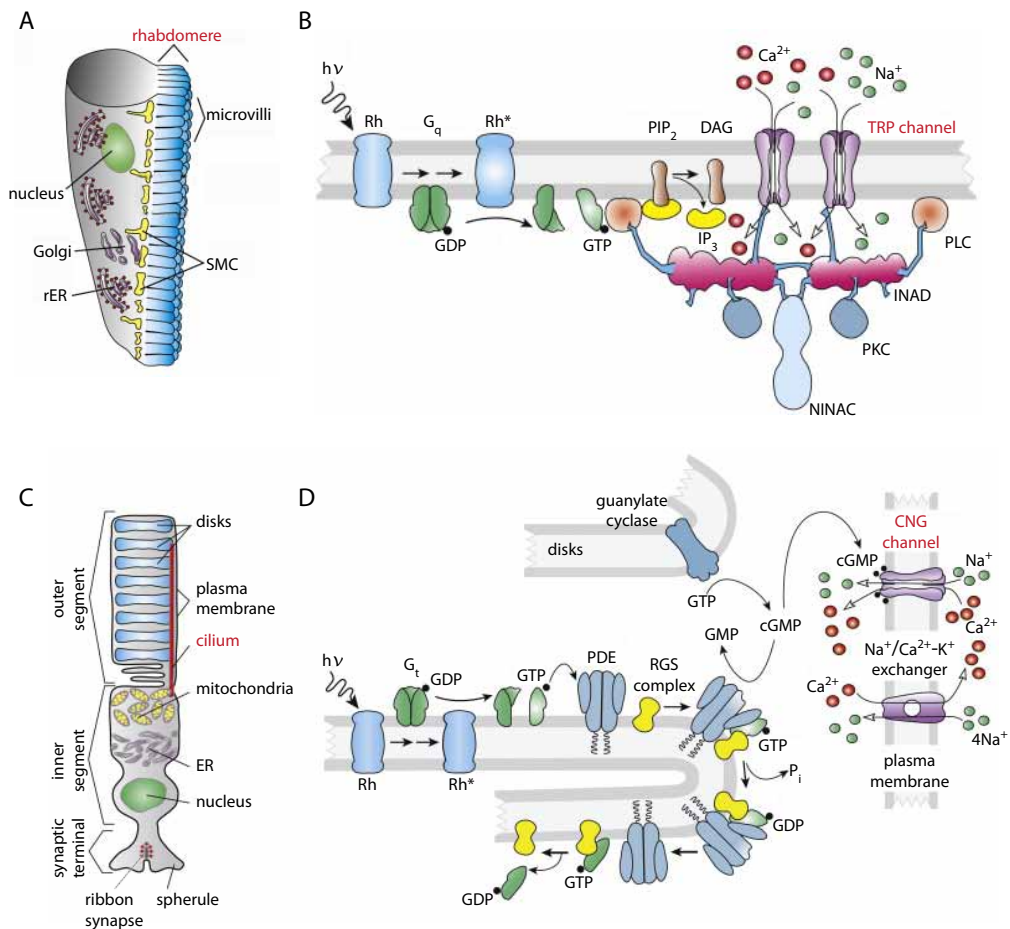


Figure 2.1: Ciliary and rhabdomeric photoreceptors, and their phototransduction cascades. A. Schematic representation of a rhabdomeric photoreceptor. B. Phototransduction cascade in a rhabdomeric photoreceptor. Light activates the rhabdomeric opsin (Rh); this triggers the exchange to GDP with GTP in the G_q protein. The activated G protein activates the phospholipase C (PLC) enzyme, which hydrolyzes the phosphatidylinositol 4,5-bisphosphate (PIP_2) into diacyl glycerol (DAG) and inositol 1,4,5-trisphosphate (IP_3). These products open the cationic TRP channel; the flux of Ca^{2+} and Na^+ ions in the intracellular space produces the depolarization of the cell (ON-response). The signalling complex includes structural proteins like INAD and NINAC. C. Schematic representation of a ciliary photoreceptor (the vertebrate rod). D. Phototransduction cascade in the vertebrate rod. Light activates the rhabdomeric opsin (Rh); this triggers the exchange to GDP with GTP in the G_t protein (transducin). The activated G protein activates the phosphodiesterase (PDE) enzyme, which hydrolyzes the cyclic GMP (cGMP) into GMP. cGMP is produced from GTP by the guanylate cyclase. In the dark, high levels of cGMP keep CNG channels open; this allows the influx of Ca^{2+} and Na^+ ions from the extracellular space. A $Na^+/Ca^{2+}-K^+$ exchanger maintains steady levels of Ca^{2+} . The decrease of cGMP concentration upon illumination causes the closure of CNG channels, the decrease of cationic influx in the cell, and the hyperpolarization of the cell (OFF-response). RGS complex: a protein complex that accelerates GTP hydrolysis by the transducin. Adapted from Fain et al. (2010).

ally, CNG channels mediate the depolarization of olfactory sensory neurons, but in this case the second messenger used is cAMP, which is produced in the olfactory neuron with the activation of the adenylate cyclase (AC; Bradley et al. 2005).

It is currently unknown if all the invertebrate ciliary photoreceptors have an OFF-response. This is the case for the ciliary photoreceptors of the scallop eye, which use a G_o cascade for hyperpolarization; however, the opsin mediating this process is not homologous to the opsins expressed in the vertebrate eye (see below). It remains to be shown if invertebrate c-opsins (orthologs of the rods and cones opsins) trigger OFF-responses, despite the G_t evolved only in vertebrates.

2.1.2. Opsin families

Opsins are GPCRs covalently bound to a chromophore, the vitamin A derivative retinal. The isomerization of retinal upon light absorption triggers conformational changes which start the phototransduction cascade. In the vertebrate retina, the 11-*cis*-retinal is converted in all-*trans*-retinal. The *cis* isomer is then reconstituted in the retinal pigmented epithelium (RPE) or in the cells of the Müller glia after a complex set of reactions, known as the visual cycle.

Opsins probably evolved in the last common ancestor of Cnidaria and Bilateria (the eumetazoan ancestor), since they have not been found in more basal metazoan groups. According to their phylogeny and their genomic structure, they can be classified in three big families (fig. 2.2).

Rhabdomeric opsins (r-opsins) are expressed in rhabdomeric photoreceptors, and exclusively use the rhabdomeric cascade. Vision in invertebrates is generally associated to these opsins. The vertebrate ortholog, melanopsin, is expressed in the ipRGCs, and triggers also a typical rhabdomeric transduction.

Ciliary opsins (c-opsins) are expressed in the rods and cones of vertebrate retina, in the annelid brain photoreceptors, and in insect brains (pteropsins, Velarde et al. 2005). They are always expressed either in cells without surface extension, or in photoreceptors with ciliary morphology. The phylogeny of c-opsins confirms that the vertebrate visual c-opsins evolved from non-visual opsins. The most basal vertebrate c-opsins, like the encephalopsin, the VA- and VAL-opsin, are all expressed in extra-retinal tissues. In the cases investigated, these opsins are bistable, which means that the retinal remains covalently bound to the opsin and is regenerated upon the absorption of a second photon (Sato et al., 2011; Sakai et al., 2012). Since the visual cycle for retinal regeneration evolved only in vertebrates (Albalat, 2011),

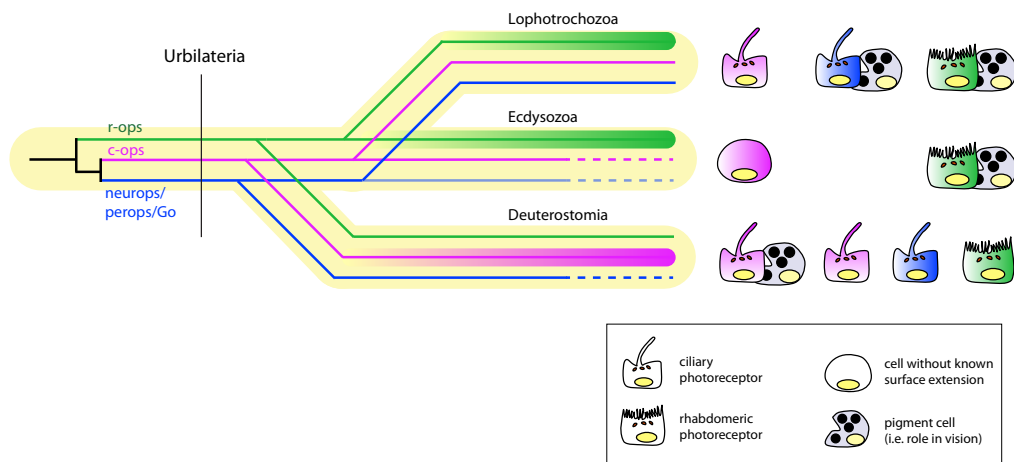


Figure 2.2: **Opsin families in Bilateria.** Schematic representation of the relationships and the distribution of the three main bilaterian opsin families. Thick lines represent the involvement of the opsin family in vision. Dashed lines indicate the loss of the opsin family in the most commonly studied organisms of the group (i.e. loss of c-opsins in *Drosophila*). The schematic cartoons show the dominant situation in Lophotrochozoa, Ecdysozoa and Deuterostomia; the visual function of a photoreceptor is indicated by its coupling with a pigment cell. The schematic is likely to be incomplete, due to the paucity of data from protostomes non-model organisms.

it is extremely likely that the ancestral c-opsins were bistable as well.

There is also a third group of opsins, supported by phylogeny and by the analysis of the genomic structure (conservation of intron positions; see par. 6.3 and Albalat 2011). This group comprises three poorly studied gene families: the G_o -opsins, the peropsins/RGRs and the neuropsins (or *opn5* family).

G_o -opsins have been found exclusively in cnidarians, lophotrochozoa and amphioxus; the name comes from the discovery of G_o coupling in the ciliary photoreceptors of the scallop eye, where they trigger OFF-responses.

The peropsins and retinal G protein-coupled receptors (RGRs) -opsins are putative photoisomerases, because they are expressed in the RPE and they are homologous to the squid retinochrome, an opsin that convert the retinal from the all-*trans* to the 11-*cis* isomer. However, while in RGRs and retinochromes critical residues for signalling have been lost, the peropsins still retained all the protein residues for signal transduction. A signalling function for peropsins has also been proposed by Nagata et al. (2010), where the presence and the expression of peropsins in invertebrates was shown for the first time.

The neuropsin family is even more enigmatic. These opsins are expressed very broadly in the brain of vertebrates (Tarttelin et al., 2003); they exist also in proto-

stomes, where their expression patterns have not been documented yet (see par. 6.3 and Kaller 2011). Very recent studies provided some indications on the function of this neglected gene family. Chick and quail *Opn5* are UV sensitive, couple to G_i and are expressed in deep brain photoreceptors of the hypothalamus (Nakane et al., 2010; Yamashita et al., 2010; Kojima et al., 2011; Ohuchi et al., 2012). It is likely that these photoreceptors in the hypothalamus participate to the photic regulation of neuroendocrine activity (Nakane and Yoshimura, 2010).

The functional characterization of these opsins in invertebrates, and especially in lophotrochozoans, is going to be very interesting, to understand how different routes to photoreception are employed by these animals in the regulation of physiology and behaviour.

2.2. Non-visual light detection in animals

Light is a rich source of information for animals. The spectral composition of light in the sea is an indication of the depth, since short-wavelength light penetrates deeper than long-wavelength light. Day-night transitions are marked by fast changes of light intensity and spectral composition (twilight). The length of daytime is indicative of the season at non-tropical latitudes. And finally, moonlight signals quasi-monthly cycles. All this relevant information can be extracted from the environment using simple irradiance detectors, not associated with vision.

In animals, physiology and behaviour are regulated according to daily, monthly and seasonal rhythms. These rhythms are organized by neuronal networks subdivided into three components: core internal clocks, constituted by internal oscillators; input pathways, to synchronize the clock to the environment; and output signals. Light is the main input to the clocks, since environmental illuminance is the most robust and “reliable” source of time information.

At any level of the tree of life, light cycles regulates several physiological processes, like metabolism, growth, metamorphosis, reproduction and even cell cycle (Schultz and Kay, 2003; Kohsaka and Bass, 2006; Bradshaw and Holzapfel, 2007; Hunt and Sassone-Corsi, 2007). In many instances, this is achieved by coupling circadian rhythms, photoreception or both to hormonal release (Morgan and Hazlerigg, 2008; Nakane and Yoshimura, 2010). Metabolic networks and circadian rhythms are intimately interlocked: genes with a direct role in metabolic control belong to circadian oscillators, while food itself contributes to the entrainment of central and peripheral clocks. These mechanisms are probably very important for adaptation

and optimal energy storage and utilization (Kohsaka and Bass, 2006; Yang et al., 2006).

Behavioural rhythmicity is also widespread in the animal kingdom. The existence of sleep-like behaviours has been documented in vertebrates and protostomes (Allada and Siegel, 2008). In many cases, rhythmic behaviour is directly associated to metabolic cycles and energy balance (Green et al., 2008).

The fundamental importance of rhythmic processes explains why mechanisms for illuminance detection and circadian rhythms are present in most animals, and probably why photoreception evolved in the first place (Nilsson, 2009).

2.2.1. Illuminance detection and circadian rhythms in protostomes

The genetics of circadian clocks has been dissected in *Drosophila*. The core circadian oscillator is constituted by transcriptional feedback loops and rhythmic phosphorylation of the two DNA-binding heterodimers Clock/Cycle (Clk/Cyc), mostly active during the late day, and Period/Timeless (Per/Tim), mostly active at night (fig. 2.3A; for details, see Allada and Chung 2010; Peschel and Helfrich-Förster 2011). These genes are expressed in about 150 neurons of the adult *Drosophila* brain; some of these neurons are located in the accessory medulla, which is considered the true circadian pacemaker of insects (Helfrich-Förster, 2004), while others are found in the insect neurosecretory centers, the pars intercerebralis (PI) and the pars lateralis (PL). The most important output of the circadian system is the neuropeptide pigment-dispersing factor (PDF), expressed in several clock neurons including the accessory medulla; other transmitter systems, like serotonin, acetylcholine, histamine, GABA and several neuropeptides, have also been implicated downstream the clock (Yuan et al., 2005; Johard et al., 2009; Peschel and Helfrich-Förster, 2011).

Multiple pathways participate to the light entrainment, to ensure a sophisticated temporal fine-tuning of behaviour. The blue-light receptor *cryptochrome* (*dCRY*) is expressed in a subset of clock neurons, and when activated by light it triggers the degradation of the tim protein. Moreover, subsets of the *Drosophila* clock neurons are directly innervated by the visual system (Helfrich-Förster et al., 2001; Collins and Blau, 2007; Dubruille and Emery, 2008). At larval stages, the cholinergic larval eye called Bolwig organ innervates some *pdf+* *bsh*¹ cells in the prospective accessory medulla (Jones and McGinnis, 1993). After metamorphosis, the Bolwig organ transforms in a new photoreceptive structure, called Hofbauer-Buchner (HB) eyelet, but

¹The *Drosophila bsh* gene is the homolog of the vertebrate *bsx*.

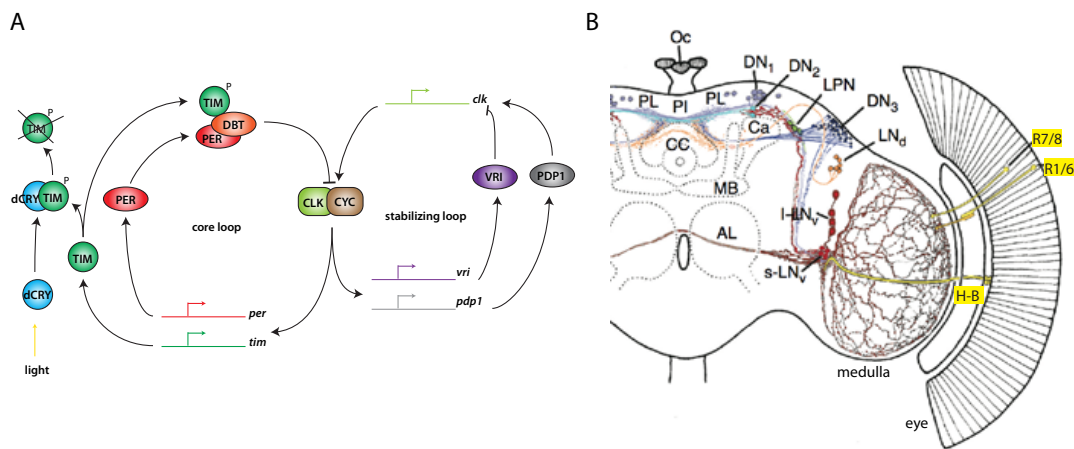


Figure 2.3: **Circadian organization in *Drosophila***. A. The molecular oscillators of the *Drosophila* clock. Redrawn from Gallego and Virshup (2007). B. The organization of the adult *Drosophila* circadian circuits. Clock neurons are distributed in the accessory medulla, and in the pars intercerebralis (PI) and pars lateralis (PL). The clock neurons receive photic input from the eye rhabdomeric photoreceptors (R7/8, R1/6) and from the Hofbauer-Buchner eyelet (H-B). DN: dorsal neurons, LN: lateral neurons, AL: antennal lobe, MB: mushroom body, Ca: calix, CC: central complex, Oc: ocelli. Adapted from Helfrich-Förster (2005).

still makes contacts with the *pdf*⁺ neurons of the accessory medulla (Helfrich-Förster et al., 2002; Malpel et al., 2002). In the adult, the HB eyelet, the ocelli and the eyes are all necessary, together with dCRY, to clock entrainment (fig. 2.3B, Helfrich-Förster et al. 2001).

A comparable system is in place in crustaceans (Strauss and Dirksen, 2010). The presumed crustacean pacemaker is located in the eyestalk, thus close to the optic lobes, like in insects. Behaviour and neurosecretion are regulated by clock neurons through different kinds of outputs, like PDH (the homolog of the insect PDF), several other neuropeptides, and serotonin. The entrainment requires cryptochromes, eyes and extraretinal photoreceptors.

The presence of *c-ops1*⁺ *bmal*⁺ cells in the brain of annelids and some arthropods suggests that the *c*-opsin-dependent input to the circadian clock might have been present in the last common ancestor of Ecdysozoa, but lost in *Drosophila* (Arendt et al., 2004; Velarde et al., 2005).

The role of PDF as a clock output might be a conserved feature of protostomes, since *pdf* orthologs have been found in lophotrochozoans, but not in cnidarians and deuterostomes (Anctil, 2009; Veenstra, 2010, 2011). Clock genes have been cloned

and analyzed in several protostomes, but nothing is known about the neurobiology of clocks outside the few established model systems. It is likely that the *Drosophila* situation is partially derived, after several instances of gene loss (discussed later).

2.2.2. Illuminance detection and circadian rhythms in vertebrates

The vertebrate circadian system has been dissected in great detail for the mouse. The circadian oscillator is based on a transcriptional-translational feedback loop, which involves the DNA-binding heterodimers Clock/Bmal (*bmal* is the ortholog of the *Drosophila cycle*) and Per/Cry (fig. 2.4A).

The main circadian oscillator of the mouse brain is the suprachiasmatic nucleus (SCN), located in the hypothalamus. The SCN receives photic information from the ipRGCs, and innervates several brain nuclei (mostly in the hypothalamus) to control hormonal release and locomotor rhythmic activity, like sleep-wake cycles (fig. 2.4B).

Besides the SCN, the olfactory bulb and the retina have self-sustained independent oscillators. Several other brain nuclei are semiautonomous and slave oscillators (circadian oscillator that are synchronized by the master clock), meaning that most of the brain activity follows circadian rhythms (fig. 2.4D, Dibner et al. 2010). Finally, peripheral circadian oscillators exist in other tissues outside the CNS, like the liver. These oscillators are not entrained by light directly, but are synchronized to the master clock through neuroendocrine pathways (Dibner et al., 2010).

The hormone melatonin is the main systemic output of the vertebrate circadian system. Melatonin is produced in several tissues, but only the pineal gland releases melatonin in the circulation. The activity of the pineal gland is controlled by the SCN through a multisynaptic pathway, involving the autonomic nervous system (fig. 2.4B).

The structure of the circadian system in anamniotes is different, because more self-sustained oscillators exist in the brain, and the role of the SCN has a less dominant role in circadian organization.

In anamniotes, the pineal organ is formed by photoreceptors and projection neurons; the photoreceptors have a autonomous clock, thus the melatonin release is controlled locally by the circadian rhythm and the direct photic input. Moreover, the pineal projects to several nuclei of the hypothalamus and the preoptic area, including the SCN, and participates to the entrainment of the clock (fig. 2.4C).

The organization of the mammalian and the insect circadian systems have been compared at several levels. Despite the neuronal structure of the central pacemakers

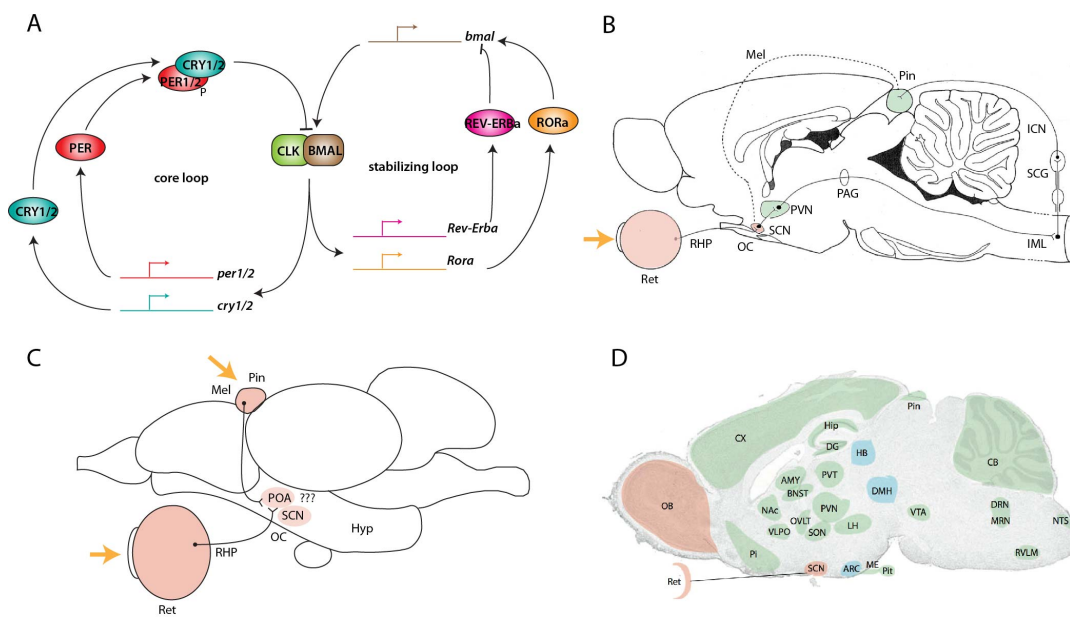


Figure 2.4: Circadian organization in vertebrates. A. The molecular oscillators of the mammalian clock. Redrawn from Gallego and Virshup (2007). B. Circadian organization in mammals. The ipRGCs of the retina (Ret) send photic information through the retino-hypothalamic tract (RHT) to entrain the SCN. The SCN projects to several hypothalamic nuclei to regulate circadian processes. One of these nuclei is the paraventricular nucleus (PVN), that projects to the intermediolateral nuclei (IML) of the spinal cord through the mesencephalic periaqueductal grey (PAG). The IML innervates the superior cervical ganglia (SCG) that projects to the pineal gland (Pin) via the internal carotid nerve (ICN). The pineal releases melatonin in the circulation, which acts as the systemic signal for darkness. The presence of self-sustained circadian oscillators is indicated in pink, slave oscillators in green. Yellow arrow: light input to the clock. Adapted from Klein et al. (2010); C. Circadian organization in the teleost fish. Retinal ganglion cells and pineal projection neurons send projections to the hypothalamus, like to the SCN and the preoptic area (POA). The pineal has photoreceptors with a self-sustained circadian oscillator (pink). So the rhythm of melatonin release is regulated in the pineal directly, without any input from the hypothalamus. More semiautonomous and slave oscillators exist in the fish brain (not shown). Yellow arrows: light inputs to the clock. D. Circadian oscillators in the mammalian brain. As above, the presence of self-sustained circadian oscillators is indicated in pink, semiautonomous oscillators in blue and slave oscillators in green. AMY, amygdala; ARC, arcuate nucleus; BNST, bed nucleus of the stria terminalis; CB, cerebellum; CX, cortex; DG, dentate gyrus; DMH, dorsomedial hypothalamus; DRN, dorsal raphe nucleus; HB, habenula; Hip, hippocampus; LH, lateral hypothalamus; ME, median eminence; MRN, median raphe nucleus; NAc, nucleus accumbens; NTS, nucleus of the solitary tract; OB, olfactory bulb; OVLT, vascular organ of the lamina terminalis; Pi, piriform cortex; Pin, pineal gland; Pit, pituitary gland; PVN, paraventricular nucleus of the hypothalamus; PVT, paraventricular nucleus of the thalamus; Ret, retina; RVLm, rostral ventrolateral medulla; SCN, suprachiasmatic nuclei; SON, supraoptic nucleus; VLPO, ventrolateral preoptic area; VTA, ventral tegmental area. Image from Dibner et al. (2010).

(SCN and accessory medulla) are similar (Helfrich-Förster, 2004), the main output systems used are different (melatonin and PDF, respectively). In any case, the entrainment of the clock involves both cryptochromes and opsins; however, mammals (but not all the other vertebrates!) apparently lost both the cryptochrome and the ciliary photoreceptor input, while *Drosophila* lost the ciliary photoreceptor component.

Looking at the circadian organization in a slow evolving lophotrochozoan, like *Platynereis*, will help to reconstruct the ancestral state at the base of Bilateria. The *bmal*-expressing ciliary photoreceptors of *Platynereis* brain, probably involved in annelid circadian entrainment, need to be compared to the ciliary photoreceptors involved in entrainment of the vertebrate clock. For this reason, here I will describe in more detail the non-visual ciliary photoreceptors of vertebrates.

2.3. The evolution of the vertebrate pineal and melatonin system

In vertebrates, ciliary photoreceptors are present in several diencephalic derivatives. Besides the rods and cones of the retina, related photoreceptors are present in the pineal complex, as indicated by similarities in morphology and expression profile (Mano and Fukada, 2007; Bailey et al., 2009). The term “pineal complex” defines two unpaired structures located at the roof of the diencephalon: the pineal proper, and the parapineal (called frontal eye in reptiles). In mammals, the photoreceptive component has been lost, and the pineal kept only a neuroendocrine function (melatonin synthesis). Finally, ciliary photoreceptors are present in the hypothalamus, along the lining of the third ventricle. While the retina specialized for vision, pineal and deep brain photoreceptors are involved in photic control of physiology and behaviour. It has been suggested that all these vertebrate ciliary photoreceptor types are evolutionarily related (Vigh et al., 2002). Thus, understanding the evolution of the ciliary photoreceptor line in Bilateria requires the comparison of invertebrate ciliary photoreceptors, like the annelid ones, with all these populations of vertebrate photoreceptors.

2.3.1. The pineal complex: luminance detection, melatonin release and shadow response

The pineal complex of vertebrates is able to measure environmental illuminance. This was demonstrated with electrophysiological recordings from pineal photoreceptor cells, which showed that the changes in membrane potential are linearly cor-

related with light intensity (Kusmic et al., 1992; Meissl and Yànez, 1994). Moreover, convergence of photoreceptors on ganglion cells is almost absent (in contrast to the retina), meaning that each projection neuron receives inputs from one, or sometimes only few photoreceptors.

The pineal complex has a dual output. The most famous, the hormonal output, consists in the release of melatonin during darkness. A second output is purely neural, it is also implicated in circadian entrainment and locomotor behaviour, but has been less intensely studied.

The humoral output: melatonin release.

Melatonin is an indoleamine synthesized in two steps from serotonin or 5-hydroxytryptamine (5-HT). Briefly, serotonin is produced from tryptophan directly in the pinealocyte by an enzymatic cascade, which involves the specific enzyme Tryptophan Hydroxylase (Tph). Serotonin is then acetylated by the enzyme Arylalkylamine N-Acetyltransferase (Aanat); the resulting product, N-acetylserotonin, is converted to melatonin with a methylation reaction catalyzed by the enzyme Hydroxyindole O-Methyltransferase (Hiomt), also called Asmt). While Anaat can acetylate many different substrates, Hiomt instead is very specific of the melatonin pathway.

Melatonin synthesis is directly coupled to darkness. In mammals, pineal activity is controlled by the SCN. In contrast, in anamniotes, melatonin synthesis is regulated by an endogenous circadian clock (Cahill and Besharse, 1993), and can also be suppressed directly by illumination during the dark phase. The circadian clock in the pineal photoreceptors controls the transcription of Anaat and/or Hiomt, while light suppression involves the post-transcriptional control of the stability and/or the enzymatic activity of these enzymes (Ribelayga et al., 1999; Falcón et al., 2010a). In zebrafish, the light spectrum able to induce melatonin suppression is broad, indicating that light suppression is triggered by multiple photopigments (Ziv et al., 2007). Although the details haven't been elucidated, the acute effects of light on melatonin suppression are likely to involve the full phototransduction cascade, since they are correlated with the decrease of intracellular Ca^{2+} concentration, which is controlled by voltage-gated L-type Ca^{2+} channels (Bégay et al., 1994; Meissl et al., 1996; Kroeber et al., 2000).

Being directly coupled to darkness, melatonin is a perfect signal for daily but also seasonal rhythms (Reiter, 1993). Indeed, pineal melatonin has been implicated in a range of processes, like seasonal control of sexual maturation, induction of sleep,

regulation of pigmentation, metabolism and hypothalamic activity (Pandi-Perumal et al., 2006; Falcón et al., 2007, 2010b; Zhdanova et al., 2001; Appelbaum et al., 2009; Morgan and Hazlerigg, 2008; Ekström and Meissl, 1997; Burgess and Granato, 2007; Zhdanova et al., 2001).

This pleiotropic role as a modulator of physiology and nervous system activity is also indicated by the distribution of melatonin receptors, which are expressed in several parts of the brain, including the SCN, and areas involved in sensory processing (like the optic tectum, but also the retina itself) and in neurosecretion (like the pituitary). Thus, it has been proposed that three functions - systemic signalling of darkness, modulation of visual processing and control of neuroendocrine secretion - were associated with melatonin signalling at the beginning of vertebrate evolution.

Unfortunately, there are not so many studies of melatonin function in fishes or lampreys, which would be more telling on the ancestral functions of melatonin. Moreover, many investigators analyzed pineal function used pinealectomy, which doesn't distinguish between humoral and neural outputs.

The pineal and parapineal neural outputs.

The analysis of the pineal efferent projections suggests that the photic input from the pineal has a broad impact on brain activity. The pineal projections of anamniotes overlap considerably with the projections coming from the retinal ganglion cells. The most conserved projection sites are the optic tectum, the SCN/preoptic area and the mesencephalic tegmentum, with variations between different species (Pombal et al., 1999; Mandado et al., 2001; Yáñez et al., 2009). The innervation of pre-motor areas from the pineal indicates that the photic input from this organ can modulate the overall activity patterns and behavioural state. But as discussed before, the relative contribution of humoral and neural outputs is not clear.

The shadow response is the best characterized function of the pineal efferent pathways. In this respect, the pineal is more correctly described as a "semivisual" organ (Vígh et al., 2002); indeed, the presence of pigment cells provides some discrimination of light directionality.

The shadow response has been well studied in *Xenopus* tadpoles, where light dimming induces upward swimming; this behaviour depends on the OFF-response of the pineal organ. A pineal-dependent response to light dimming has been reported also in surface fishes and cavefish (Foster and Roberts, 1982; Yoshizawa and Jeffery, 2008; Wales, 1975). In *Xenopus*, this response is mediated by a direct neuronal pathway from the pineal to diencephalic-mesencephalic interneurons, and then the

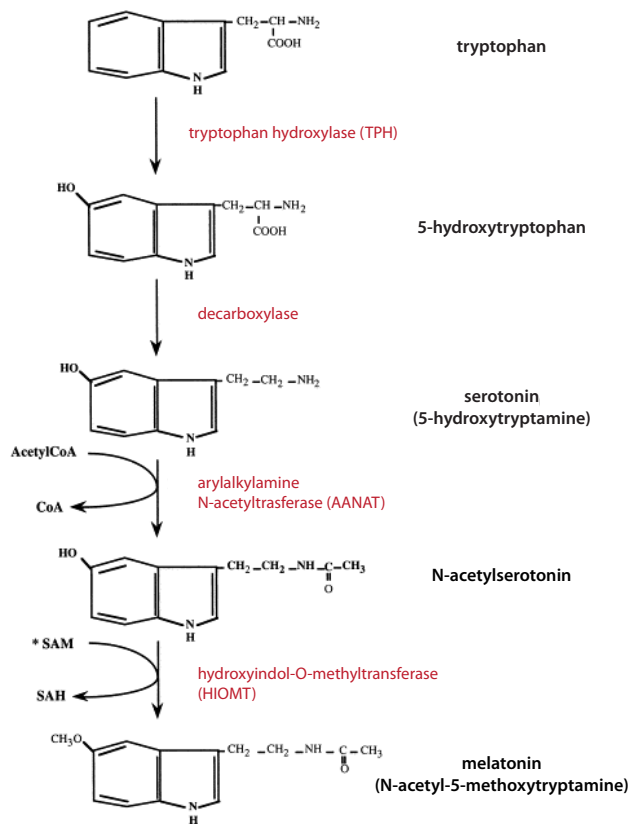


Figure 2.5: **The melatonin synthesis pathway.** Serotonin is produced from tryptophan with two enzymatic reactions. Then, serotonin is converted in melatonin after one acetylation step, catalyzed by Aanat, and an hydroxylation reaction, catalyzed by Hiomt.

hindbrain (Jamieson and Roberts, 1999, 2000).

The function and the connectivity of the parapineal are quite different. The fish parapineal and its homolog in lizard, the parietal eye, have also been implicated in the shadow response, but also in sun-compass navigation. The parapineal contributes to the so called dorsal diencephalic conduction system (DDC), a very conserved pathway in the vertebrate brain, that integrates sensory information to modulate locomotion (Bianco and Wilson, 2009; Hikosaka, 2010). The DDC is formed by the habenulae, dorsal epithalamic nuclei that project to different locomotor control centers in the brainstem; projections from the habenula reach the serotonergic raphe nuclei either directly or via the interpeduncular nucleus (IPN) of the hindbrain (Stephenson-Jones et al., 2011; Lorente-Cánovas et al., 2012). Neurons of the parapineal were found to project to the lateral habenula and to the IPN directly, meaning

that photic information controls directly the locomotor centers, as also shown by behavioural studies.

2.3.2. CSF contacting neurons and deep brain PRCs

The ependymal surface of the brain, especially in the third ventricle, contains many neuronal types that have a sensory morphology and extend ciliated endings into the cerebrospinal fluid (CSF); these cells are called CSF-contacting neurons. Because of these structural features, reminiscent of neurons of the amphioxus nervous system, they are considered “protoneurons” (Vigh and Vigh-Teichmann, 1998; Vigh et al., 2002; Joly et al., 2007).

Some CSF-contacting neurons of the hypothalamus are deep brain photoreceptors, as shown by their morphology and cross-reactivity with opsin and arrestin antibodies. The exact function of these cells has remained enigmatic for a long time. The involvement of deep brain photoreceptors in the regulation of growth and sexual maturation was suggested, after studies on the effects of illumination on blind, pinealectomized animals (Vigh et al., 2002).

Recently, it has been shown in birds that the serotonergic CSF-contacting neurons of the hypothalamic paraventricular organ (PVO) express *neuropsin* (*opn5*) and respond to UV light (Nakane et al., 2010; Yamashita et al., 2010). The PVO neurons control seasonal reproduction: they project to the median eminence of the hypothalamus, adjacent to the pars tuberalis of the pituitary gland, where they control an hormonal cascade which terminates with the control of gonadotropins (Nakane and Yoshimura, 2010).

Several lines of evidence suggest that melatonin synthesis takes place in other deep brain photoreceptors of the hypothalamus, and contributes to this cascade. First, the expression of *hiomt* and *aanat*, and the presence of melatonin in the hypothalamus have been documented in several species (Kang et al., 2007; El Halawani et al., 2009). Moreover, melatonin has effects on the release of sex hormones in birds, while pinealectomy doesn't affect sexual maturation (Chowdhury et al., 2010). Finally, in several species melatonin receptors are strongly expressed in the pars tuberalis of the pituitary gland, indicating strong conservation of a melatonin-dependent regulation of neurosecretion. In the turkey preamillary nucleus, melatonin release from photoreceptors expressing melanopsin and clock genes has been shown (Kang et al., 2007; El Halawani et al., 2009; Kang et al., 2010; Leclerc et al., 2010). However, the widespread occurrence of opsins from all the three major opsin groups in the hy-

pothalamus indicates the existence of more, and yet uncharacterized hypothalamic photoreceptor cell types.

2.3.3. Early evolution of pineal and retina

The affiliation of the pineal complex to deep brain photoreceptors is indicated by the presence of CSF-contacting neurons in the pineal and parapineal organs. Indeed, in lampreys these organs are proper vesicles, with a lumen in continuity with the third ventricle (Víggh et al., 2002; Joly et al., 2007). Interestingly, in the pineal and parapineal the CSF-contacting neurons are not only the photoreceptors themselves (which in many cases have surface extensions like retinal rods and cones), but also the photoreceptors' postsynaptic neurons, that send projections to the brain.

Transient CSF-contacting neurons are well known in the retina as well. The topology of the retina, which is also a diverticle of the third ventricle, shows that the outer nuclear layer (i.e. the photoreceptor layer) is the former CSF-contacting surface. During development, the bipolar cells (photoreceptors' postsynaptic neurons) send CSF-contacting dendrites to the apical surface of the neuroepithelium; these transient structures are called Landolt's clubs, and are the first CSF-contacting neurons ever described (fig. 2.6, Víggh et al. 2002).

Several lines of reasoning support the evolutionary relatedness of retina and pineal. As mentioned before, pineal and retinal photoreceptors have very similar ultrastructural features. Moreover, on the histological level the pineal is a simple retina, with only the photoreceptor and the ganglion cell layers, and pigment cells. Gene expression profiles of retina and pineal are also extremely similar (Bailey et al. 2009, and discussed later). Finally, there is extensive overlap between the pineal and the retinal projections (Yáñez et al., 2009), suggesting that these structures evolved after duplication of a common ancestor (Mano and Fukada, 2007).

Most likely, at the base of vertebrates four photoreceptive structures were already present: the lateral eyes, and two more "eyes" at the roof of the diencephalon (corresponding to the pineal and parapineal, Concha and Wilson 2001). This is indicated by fossils of ostracoderm fishes (bony fishes), which have two foramina in their skull. Moreover, lampreys (sister group of ostracoderm fishes, Gess et al. 2006; Janvier 2006) have also well developed pineal and parapineal organs.

In contrast, hagfishes have only a pair of lateral eyes, but these eyes are simple luminance detectors and have only photoreceptors and ganglion cells. The hagfish situation is hard to interpret, since the phylogenetic position of this group is not

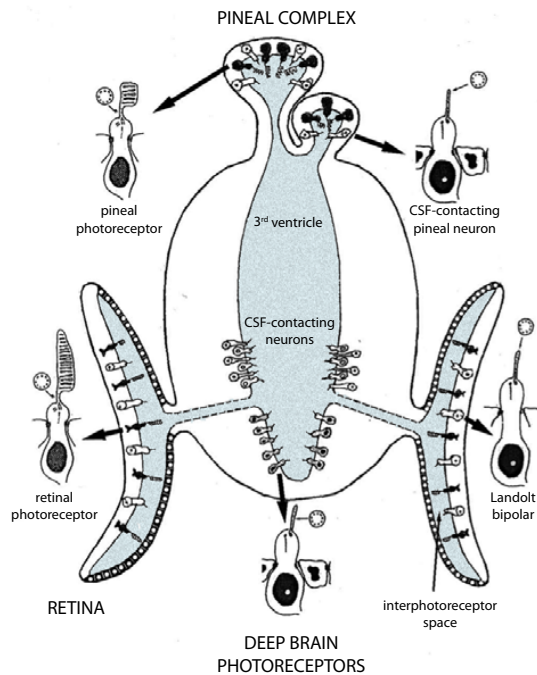


Figure 2.6: **CSF-contacting neurons in the vertebrate brain.** The drawing shows a coronal section of the 3rd ventricle, and the distribution of CSF-contacting neurons and photoreceptors in the retina, pineal and deep brain. Modified from Vigh et al. (2002).

settled. If hagfishes and lampreys are monophyletic, then the hagfish would have lost the pineal complex (Lamb et al., 2007). Viceversa, if hagfishes evolved before lampreys, then the hagfish eyes could represent the situation at the base of craniates (hagfishes, lampreys and vertebrates), with a pair of simple illuminance detectors.

The situation at the base of chordates is less clear. In amphioxus, an unpaired frontal eye is formed by shading pigment cells and ciliary photoreceptors that contact the external space, fulfilling Vigh's "protoneuron" definition. Based on morphological grounds, the frontal eye has been compared to the vertebrate retina (Lacalli, 1996). If this comparison will hold true after molecular investigations, then a similar structure with "CSF-contacting" ciliary photoreceptors and pigment cells might have existed at the base of chordates, being the forerunner of vertebrate retina and pineal.

To summarize, there is indirect evidence that retina and pineal evolved from CSF-contacting ciliary photoreceptors in the brain. For these reasons studying the annelid brain ciliary photoreceptors can disclose commonalities not only to vertebrate brain, but also pineal and retina photoreceptors.

2.4. Roles of Rx in the development of ciliary photoreceptors

Ultrastructural and functional arguments indicate that the three main population of vertebrate ciliary photoreceptors - deep brain, pineal and retinal photoreceptors - are evolutionarily related. In principle, this hypothesis could be tested looking at the molecular fingerprint of these cells types.

Unfortunately, there has not been a detailed molecular characterization of deep brain photoreceptors. One of the few transcription factors known so far for being present in all these cell types is the paired-class homeobox gene *retinal homeobox* (*rx*, called *rax* in mammals; Furukawa et al. 1997; Mathers et al. 1997; Casarosa et al. 1997; Deschet et al. 1999; Chuang et al. 1999; Ohuchi et al. 1999; Loosli et al. 2001; Asbreuk et al. 2002), although some species-specific differences exist (like the lack of *rx* expression in the fish pineal).

In the tunicate *Ciona intestinalis*, *Ci-rx* is expressed in the ciliary photoreceptors of the larval ocellus. Knockdown of *Ci-rx* suppresses ocellus development and consequently the shadow response (D'Aniello et al., 2006; Yoshida and Saiga, 2011).

The expression of *rx* has been investigated in another deuterostome, the sea urchin *Strongylocentrotus purpuratus*. In this species morphologically distinguishable ciliary photoreceptors do not exist, but *rx* is expressed in the serotonergic cells of the apical pole (Wei et al., 2009).

In vertebrates, Rx function has been characterized in more detail in the context of retinal development, where this gene has a dual role. First, a functional Rx protein is necessary to sustain proliferation of the retinal progenitors, during the expansion of the optic vesicles (Zhang et al., 2000; Loosli et al., 2001; Andreazzoli et al., 2003); moreover, in the fish Rx3 is necessary to the evagination of the optic vesicles (Rembold et al., 2006). For these reasons, *rx* loss of function produces eyeless animals (Mathers et al., 1997; Loosli et al., 2001, 2003). Later, in the retinal neuroepithelium, *rx* expression is restricted to the undifferentiated retinal progenitors of the ciliary marginal zone (CMZ). Consistently, a role of Rx in the maintenance of multipotency of retinal progenitors has been proposed (Casarosa et al., 2003; Nelson et al., 2009; Martinez-De Luna et al., 2011). During photoreceptor differentiation, *rx* genes are turned on again, where they control directly the transcription of opsins and other phototransduction genes (Kimura et al., 2000; Wang et al., 2004; Pan et al., 2006; Wu et al., 2009; Pan et al., 2010). Moreover, a role for Rx in the control of differentiation genes in the mammalian pineal has been proposed (Asbreuk et al., 2002; Rohde et al., 2011).

The function of Rx in the developing hypothalamus is significantly different. In mammals, *rx* is expressed transiently in all the hypothalamic precursors at stage E10.5, and then is downregulated very quickly (Furukawa et al., 1997; VanDunk et al., 2011). Here, the transient expression of *rx* might be associated to its role in the repression of the telencephalic fate (Chuang and Raymond, 2001; Stigloher et al., 2006). In the adult brain, *rx* expression persists only in the lining of the third ventricle, in the pineal and in the posterior pituitary (or neurohypophysis; Asbreuk et al. 2002; Medina-Martinez et al. 2009).

Despite *rx* expression has been shown in the developing pineal (Casarosa et al., 1997; Asbreuk et al., 2002), the function of Rx in pineal development has never been investigated. The pineal complex of vertebrates develops from a dorsal *anlage*, where the anterior cells become the parapineal. This unpaired medial *anlage* forms after neurulation, from the fusion of two domains at the edge of the neural plate.

At early stages, the pineal *anlage* expresses several genes that label also the eye field, like *rx*, *otx* genes and *tbx2/3* (Gamse et al., 2002; Snelson et al., 2008a). Indeed, fate map studies in *Xenopus* at the neurula stage showed that the pineal precursors lie in continuity with the more medial eye field (Eagleson and Harris, 1990; Rubenstein et al., 1998). So it is possible that the same patterning mechanisms establish very early the diencephalic domain that gives rise to photoreceptive structures.

The pineal *anlage* is distinct from the surrounding tissues by the expression of the transcription factor *not*, which is never present in the eye, and plays an important role in the maintenance and proliferation of the pineal (but not parapineal) progenitors (Masai et al., 1997; Snelson et al., 2008a). Later, other pineal-specific genes, like *bsx* and *foxD3*, are found in the differentiating pineal cells (Gilmour et al., 2002; D'Autilia et al., 2010). Additionally, the transcription factor *gfi-1/sens* is expressed specifically in the zebrafish parapineal neurons, which lose *not* expression after migrating away from the midline (Dufourcq et al., 2004; Snelson et al., 2008a).

Taken together, the published developmental data indicate that the hypothalamus, the pineal and the retina develop from the same early anterior diencephalic field, demarcated by *rx* expression. Later, these structures acquire distinct fates according to their medio-lateral (and later dorso-ventral) arrangement. Reflecting this, specific combinations of transcription factors are activated in the hypothalamus (like *otp*, *nk2.1* and *bsx*), in the retina (*otx* genes) and in the pineal (*not*, *foxD3*, *bsx* and *otx* genes). After morphogenesis and differentiation, *rx* genes are expressed again in ciliary photoreceptors.

As discussed above, reconstructing the evolution of bilaterian ciliary photoreceptors needs to take in account two levels of comparison: the cell type molecular fingerprint, but also the position of the cell within a comparable scheme of brain regions. It is currently unclear where and how diversity has been shaped in between these two levels, through the rewiring and modification of GRNs. However, at the dawn of metazoan evolution, sensory cells and developmental genes were already present, despite the lack of a sophisticated body plan. For these reasons, it has been postulated that regulation of differentiation batteries evolved first, and subsequently the same transcription factors were employed to establish the brain regions where those cell types were located (Erwin and Davidson, 2002).

In the case of ciliary photoreceptors, it is clear that *rx* might have been one of the earliest ciliary-photoreceptors specifiers, given its dual function in vertebrate development. The presence of *rx* in the annelid ciliary photoreceptors region is highly suggestive of the evolutionary relatedness of annelid and vertebrate ciliary photoreceptor cell types (Arendt et al., 2004). Thus the investigation of Rx function in *Platynereis* has the potential of providing some insights on how this photoreceptor line evolved.

2.5. Aim of the thesis

The aim of this thesis was the molecular, developmental and functional characterization of brain photoreceptors in the annelid *Platynereis dumerilii*. These different levels of investigation were essential to solve open questions on the evolution of the ciliary photoreceptor line in Bilateria.

First, which was the repertoire of ciliary photoreceptors in the urbilaterian ancestor? Previous work from Arendt et al. (2004) and Tessmar-Raible et al. (2007) had shown that different *c-ops1+* cells exist in *Platynereis* brain; these cells were compared to the vertebrate ciliary photoreceptors, located in the hypothalamus, pineal and retina. However, there were other *c-ops1+* not yet described, and more non-visual opsins existed in the *Platynereis* genome. How do all these different *c-ops1+* cells compare to the vertebrate hypothalamic, pineal and retinal photoreceptors? Are there molecular signatures that identify subtypes, for instance *Platynereis* cells more similar to the pineal photoreceptors? Or this diversity is the result of independent diversification processes in the annelid and vertebrate evolutionary lines? A deep molecular characterization of *Platynereis* brain photoreceptors was necessary to answer these questions.

Second, does conservation of expression of a transcription factor equal conservation of its developmental function? How do we account for morphological evolution? The vertebrate Rx genes are essential for eye development and morphogenesis, but also for the maintenance of the photoreceptor cell identity. In *Platynereis*, *rx* is expressed in the ciliary photoreceptors region, but obviously vertebrate-like eyes do not form in protostomes. My aim here was to investigate the role of Rx in the context of ciliary photoreceptors development. For this purpose, it was necessary to trace the developmental lineage where the ciliary photoreceptors come from, and to establish techniques to interfere with gene function during embryonic development.

Finally, the differentiation signature of a cell type defines its function. If a cell type is conserved throughout evolution, it is tempting to ask how the function of that cell type is conserved within a changing brain organization. Was this conserved function the determinant for positive selection over large evolutionary distances? For this purpose, I used a combination of expression data and behavioural assays to investigate the function of brain photoreceptors in the *Platynereis* trochophora larva.

RESULTS

3

DEVELOPMENT OF *Platynereis* DORSAL BRAIN

The experimental work described in this thesis is focused on the dorsal brain of *Platynereis*. This area harbours the annelid circadian center, including cell types conserved between annelids and vertebrates, like the previously described ciliary photoreceptors. From early developmental stages onwards, the dorsal brain expresses the transcription factor *retinal homeobox (rx)*, a key developmental regulator of vertebrate structures involved in the circadian control. Finally, this is the area that releases melatonin, an hormone with a conserved function as the output of the circadian system.

The investigation of the *Platynereis* circadian system from the development of its components to the function in the larval behavior allows a complete multiscale comparison with the circadian system of other species.

3.1. Morphological landmarks in the dorsal brain

With the term “dorsal brain” I refer here to the cells that occupy the dorsal half of the episphere of *Platynereis* trochophore larvae. These cells are mostly sensory cells, while the sensory-associative structures (like the mushroom bodies), which constitute the brain *sensu stricto*, are located in the ventral episphere (Tomer et al., 2010). Since most of these dorsal sensory cells are primary sensory neurons, we still refer to the dorsal episphere as “brain”.

In this region, different cell types and structures have been described previously (Fischer et al., 2010). These structures are very useful morphological landmarks, thus here I summarize and integrate previous findings and my own observations.

The first differentiated structures that appear in the episphere are the prototroch, the larval eyes (Jékely et al., 2008) and the *apical organ*. The apical organ is located in the center of the episphere, or the anterior tip of the animal (fig. 3.1A). It is composed by different kinds of sensory cells, some of them multiciliated. A de-

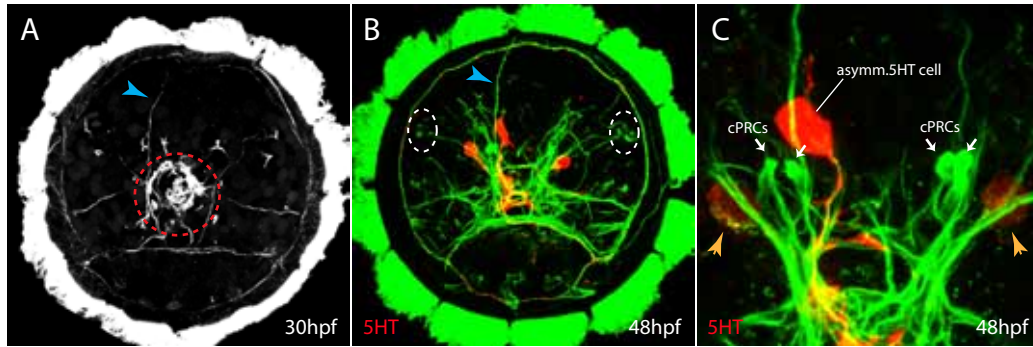


Figure 3.1: **The dorsal brain and the serotonergic system in *Platynereis* trochophore larvae.** A. Z-projection of an acetylated tubulin staining, showing the axonal scaffold at 30hpf, apical view. The cells of the apical organ (red dashed line) and the dorsal unpaired axon (arrowhead) can be recognized. B. Acetylated tubulin (green) and serotonin (5HT, red) immunostaining of a 48hpf larva, apical view. The apical organ is not included in the Z-projection. The ciliated cells of the nuchal organ start to be visible (white dashed line). C. Magnification of the cPRCs region of a 48hpf larva. The cilia bundles (white arrows) of the four cPRCs can be distinguished, very close to the lateral serotonergic neurons (orange arrowheads) and the asymmetric serotonergic cell (note the cilium extending apically).

tailed morphological and molecular description of the *Platynereis* apical organ is in Appendix A and in Marlow et al. (2012).

The first sign of morphological differentiation in the dorsal brain is a *dorsal unpaired axon* that starts from a cell located at the level of the prototroch, very close to the midline, and reaches the developing neuropile at the center of the episphere (fig. 3.1A). This is one of the multiple asymmetric structures that exist along the dorsal midline: at 30 hpf, an *asymmetric serotonergic cell* becomes visible on the left side of the brain (apical view) with an anti-serotonin immunostaining (fig. 3.1B-C). This cell is a sensory cell, as it develops a typical sensory cilium that reaches the surface of the animal and branches into multiple small motile cilia. The axon of the asymmetric serotonergic cell joins the brain serotonergic plexus, which starts with a serotonergic interneuron of the apical organ. Few hours later, two *lateral serotonergic cells* join the serotonergic neuropil. These cells have a deep position and do not show apical cilia or dendrites, thus they likely function as interneurons. They are still present in later juvenile stages, but they disappear later after the metamorphosis of the first cephalic segment (Dr. Antje Fischer, personal communication). Around 36hpf, the deep brain *ciliary photoreceptors* (cPRCs) become visible immediately adjacent to the lateral serotonergic cells (fig. 3.1C). The cPRCs are two pairs of photoreceptor cells located in a deep medial position. They have huge membrane extensions supported by long branching cilia, which can be easily recognized after

immunostaining with an anti-acetylated tubulin antibody. The cPRCs are thought to be responsible to the entrainment of the larval circadian system, as they are not associated to pigmented cells but they are embedded into a *bmal+* expression domain (Arendt et al., 2004).

In a more lateral position, the cilia of the *nuchal organs* become visible at around 48hpf (fig. 3.1B). The nuchal organs are sensory organs specific of annelids, formed by sensory ciliated cells and multiciliated support cells; because of their morphology, they are considered chemosensory.

Few hours later, the *adult eyes* start with two rhabdomeric photoreceptor cells and two pigmented cells on each side (Rhode, 1992; Arendt et al., 2002). The first pigments are recognizable from 51hpf, and the size of the eyes grows constantly during development. The adult eyes send projections to the medial brain and participate to the phototaxis of nectochaete larvae.

During the late nectochaete stage (5dpf) the massive growth of the foregut and the ventral brain induces the “rotation” of the whole prostomium, and the dorsal brain acquires a posterior position (fig. 3.2B). All the structures described above can be identified before settlement. The serotonergic plexus grows as more serotonergic neurons develop between the cPRCs and the adult eyes (fig. 3.2A-A’). These serotonergic neurons form a prominent *dorsal unpaired neuropil*, and innervate most of the brain, including the antennae, the mushroom bodies and the palpa (fig. 3.2C-C’). Unpaired midline neuropils are amongst the most distinctive features of arthropod and annelid brain neuroanatomy (Heuer et al., 2010). The cell bodies of the posterior brain, including the nuchal organs, send axons anteriorly to the medial brain. This whole area has been defined “posterior brain lobes” (Gehirnloben) in the classical literature (Müller, 1973). Along the posterior midline, a new sensory structure, previously called “dorsal sensory organ”, can be recognized from the presence of small cilia, which surround one opening that reaches the coelom (not shown).

To summarize, the dorsal part of the larval episphere develops into the posterior part of the brain of the juvenile worm. This area has been classically described as the neurosecretory center (Baskin, 1976). It also harbours many sensory structures, including adult eyes and ciliary photoreceptors, suggesting that the neurosecretory activity is under circadian control.

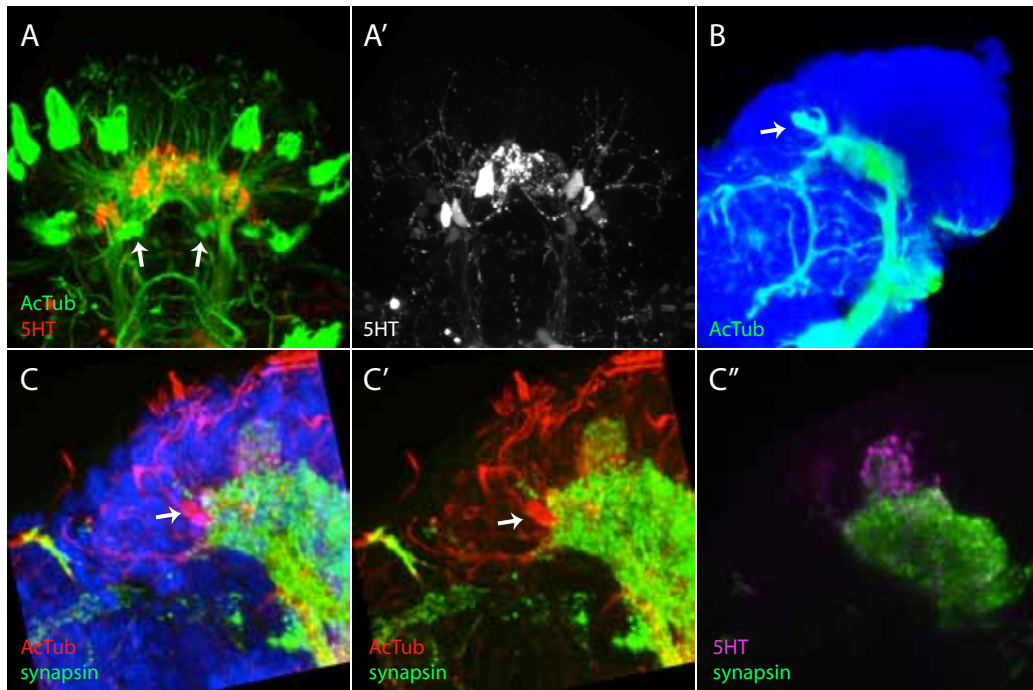


Figure 3.2: **The dorsal brain and the serotonergic system in *Platynereis nectochaete* larvae.** A. Dorsal view of a 5dpf brain, stained with anti-acetylated tubulin (green) and anti-serotonin (5HT, red) antibodies. The arrows indicate the cPRCs A'. Serotonin immunostaining of the larva showed in A. B. Lateral view of a 5dpf larva, anti-acetylated tubulin (green) and dapi (blue) staining. Anterior is on the left. The white arrow points to the cPRCs. C-C''. Higher magnification of the posterior brain of 5dpf larvae, the images are Z-projections from the medial brain, lateral views. The larva is stained with anti-acetylated tubulin (red), anti-synapsin (green), anti-serotonin (5HT, magenta) antibodies, and DAPI (blue). Arrows: cPRCs. C'' shows clearly the unpaired serotonergic neuropil.

3.2. Timing of cell cycle exit and differentiation of the main cell types of the dorsal brain

The appearance of morphological characters in the dorsal brain gives an estimate of the timing of cell birth and differentiation. However, these data are not enough to reconstruct the development of this region in detail, which is a crucial prerequisite to interpret the results obtained from functional studies like gene perturbations.

To understand when the cell types of interest become postmitotic, I performed cell proliferation studies using EdU, an analog of BrdU. Some of these experiments were performed by Marianna Karegeorgi, during her internship in our lab. Between 18 and 30hpf, the incorporation of EdU (2-hours incubations) confirms that the first postmitotic cells of the episphere are the prototroch cells, the apical organ and the larval eyes (fig. 3.3A-D'). As development proceeds, more postmitotic cells

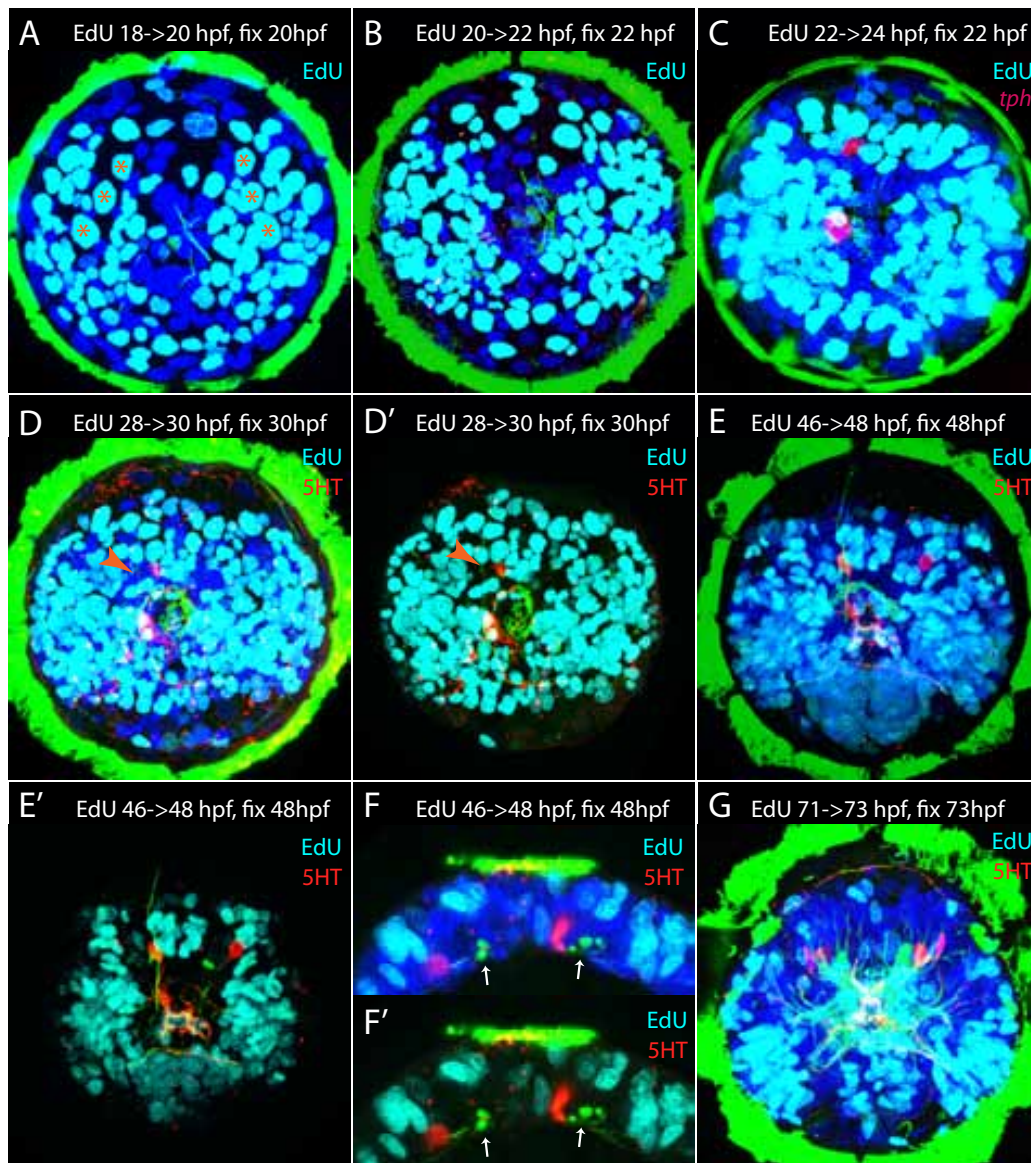


Figure 3.3: **Incorporation of EdU during brain development.** A. Episphere of a 20hpf larva, apical view. The larva was incubated in EdU two hours before fixation. Asterisks: big NSCs. B. 20hpf larva, apical view. EdU incubation two hours before fixation. C. 24hpf larva, apical view. EdU incubation two hours before fixation. WMISH for the *tryptophan hydroxylase* (*tph*) gene (red). D. 30hpf larva, apical view. EdU incubation two hours before fixation. Some EdU negative cells can be recognized close to the serotonergic cells (arrowheads). D'. Same as in D., showing a 15 μ m Z-projection in the cPRCs region. E. 48hpf larva, apical view. EdU incubation two hours before fixation. E'. Same as in E., showing a 25 μ m Z-projection in the cPRCs region. F-F'. Dorsal view of a 48hpf larva, fixed after 2 hours of EdU incubation. 10 μ m Z-projection around the cPRCs (arrows). Anterior is up. G. 73hpf larva, apical view. EdU incubation two hours before fixation. In all the panels, 5HT staining in red, DAPI staining in blue, EdU staining in cyan and tubulin staining in green unless otherwise specified.

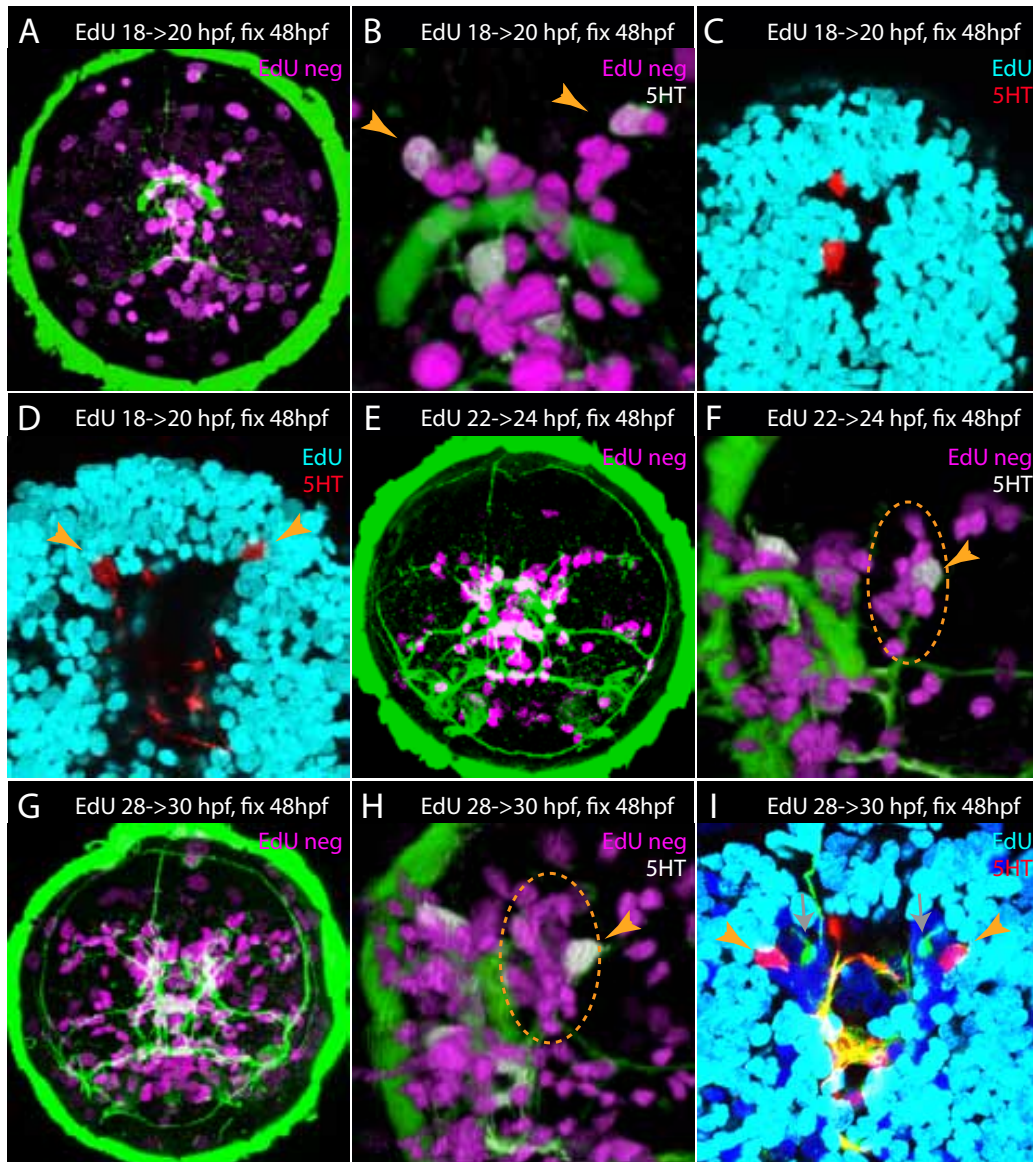


Figure 3.4: **Birthdating of the ciliary photoreceptors region.** A. EdU negative cells between 18 and 20hpf (magenta), larva fixed at 48hpf. B. Same larva as in A., 3D view of the apical region. Serotonin staining in white, the two lateral serotonergic cells are indicated by arrowheads. C. 6- μ m Z-projection showing the asymmetric and the apical organ serotonergic cells (red) in a larva incubated with EdU (cyan) between 18 and 20hpf, and fixed at 48hpf. The two serotonergic cells are EdU negative, meaning that they were postmitotic already at 18hpf. D. Same as in C, showing the two lateral serotonergic cells. E. EdU negative cells between 22 and 24hpf (magenta), larva fixed at 48hpf. F. Same larva as in E., 3D lateral view of the cPRCs region (dashed circle). Arrowhead: lateral serotonergic cell. G. EdU negative cells between 28 and 30hpf (magenta), larva fixed at 48hpf. H. Same larva as in E., 3D lateral view of the cPRCs region (dashed circle). Arrowhead: lateral serotonergic cell. I. 2 μ m slice showing the cPRCs (grey arrows) and the lateral serotonergic cells (orange arrowheads) in a larva incubated in EdU (cyan) from 28 to 30hpf, and fixed at 48hpf. The cPRCs and some surrounding cells are EdU negative. In all the panels, 5HT staining in red or white, DAPI staining in blue, EdU staining in cyan and tubulin staining in green. The EdU negative cells (magenta) were obtained subtracting the EdU channel from the DAPI channel.

are added dorsally, close to the midline. Interestingly, three giant EdU positive cells are clearly distinguishable into two rows going from dorso-medial to ventro-lateral position (fig. 3.3A). At 30hpf, two patches of 10-15 postmitotic cells can be recognized as two “wings” in the dorsal brain. These cells have the position of the cPRCs and the neighboring cells (including the serotonergic cells).

To confirm that the post-mitotic cells observed at 30hpf correspond to cPRCs and serotonergic neurons, we performed “birthdating” experiments. In these experiments, *Platynereis* larvae were incubated with EdU for two hours at different time points during development, then the EdU was washed away and larvae were raised until 48hpf, the stage when cPRCs and serotonergic neurons are clearly distinguishable after immunostaining. In larvae incubated with EdU from 18 to 20hpf and fixed at 48hpf, all the four serotonergic cells of the brain were EdU negative, indicating that these cells are already postmitotic at 18hpf (fig. 3.4A-D). Unfortunately, it was not possible to perform birthdating experiments at earlier stages, as this leads to toxicity and misdevelopment of the animals. Most of the cells of the cPRCs area become postmitotic by 30hpf; this is the case for the cPRCs as well (fig. 3.4).

The dorsal midline and the adult eye territory differentiate only later: at 48hpf, EdU positive cells can still be identified in these regions, while at 72hpf most of the cells of the dorsal brain are postmitotic¹ (fig. 3.3G).

In conclusion, these experiments revealed that the cell types of interest in the dorsal brain are amongst the first postmitotic cells of the larval brain. Thus the complete reconstruction of their development requires the investigation of cell lineages and gene expression at these early stages.

3.3. Time-lapse imaging reveals the early steps of brain development

Previous studies in *Nereis* and *Platynereis dumerilii* described the earliest steps of embryonic development in Nereididae (Wilson, 1892; Dorresteijn, 1990; Ackermann et al., 2005).

Unfortunately, these earlier lineage studies were limited to the analysis of the first cleavages and did not describe later brain development and morphogenesis. A first attempt to establish the complete cell lineage of *Platynereis* brain was done in the lab by Dr. Antje Fischer (Fischer, 2010). The approach used, called 4D microscopy, was

¹It has to be specified that with this approach it might be possible to miss slowly dividing cells, like stem cells, as the EdU incubations were performed for only 2 hours.

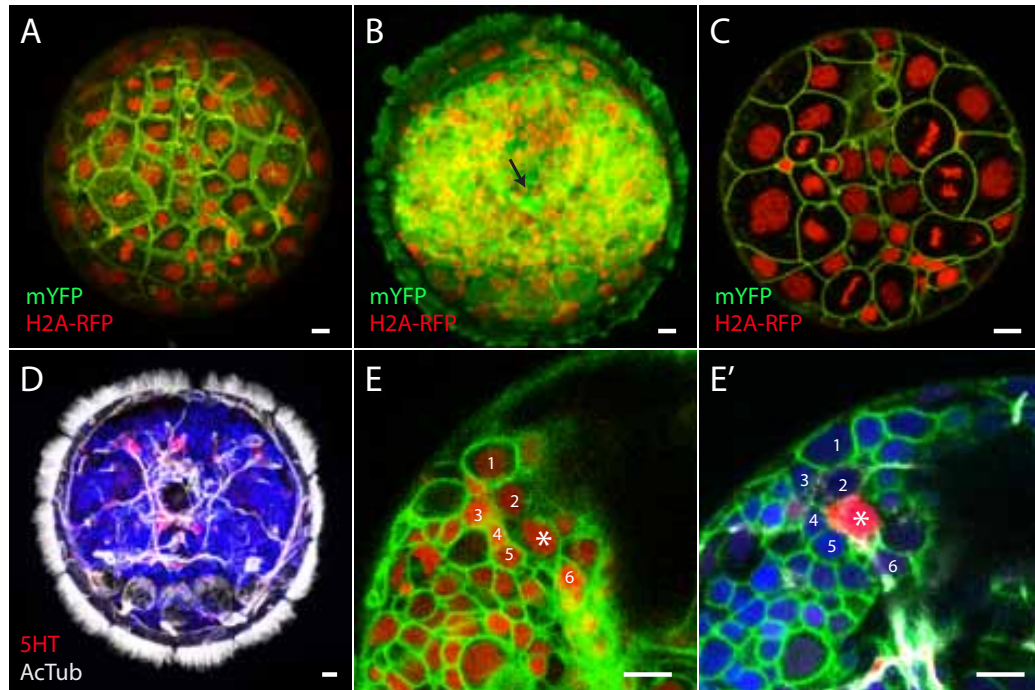


Figure 3.5: *In vivo* imaging of membranes and nuclei. A. Fluorescence in a larva injected with H2A-RFP (red) and mYFP (green) mRNAs. Z-projection of a $67.5\mu\text{m}$ stack of the episphere at 12hpf ($t=1$). B. Same larva as in A., at the end of the recording (about 31hpf). The mYFP labels the main axonal tracts (arrow). C. One focal plane of the same movie as in A and B, showing cells at different stages of mitosis. D. The same larva as in A-C, fixed immediately after the time-lapse, and stained with anti-acetylated tubulin (white) and serotonin (red) antibodies, plus DAPI (blue). E-E'. The area surrounding the right lateral serotonergic cell (asterisk) in the time lapse (E) and after immunostaining (E'). Corresponding cells (numbers) can be identified from their shape, size and relative positions. Scale bar= $10\mu\text{m}$.

based on high-resolution DIC stacks acquired over time. This method is efficient for the very early developmental stages, when the brain is mainly composed by big dividing cells. However, as the development proceeds and smaller differentiating cells are produced, the risk of missing them with DIC images is quite high.

In order to get more insights on the dynamics of brain development during the formation of the circadian center, I used time-lapse movies of developing *Platynereis* larvae. For this purpose, I took advantage of the established injection technique for *Platynereis* zygotes, and I overexpressed the messenger RNAs for the H2A-RFP fusion protein and a membrane-bound YFP². The H2A-RFP localizes to the chromatin, and allows to follow the cell divisions and to track the positions of individual nuclei.

²This approach to follow embryonic development has been established in the lab by Dr. Mette Handberg-Thorsager, who kindly provided the mRNA.

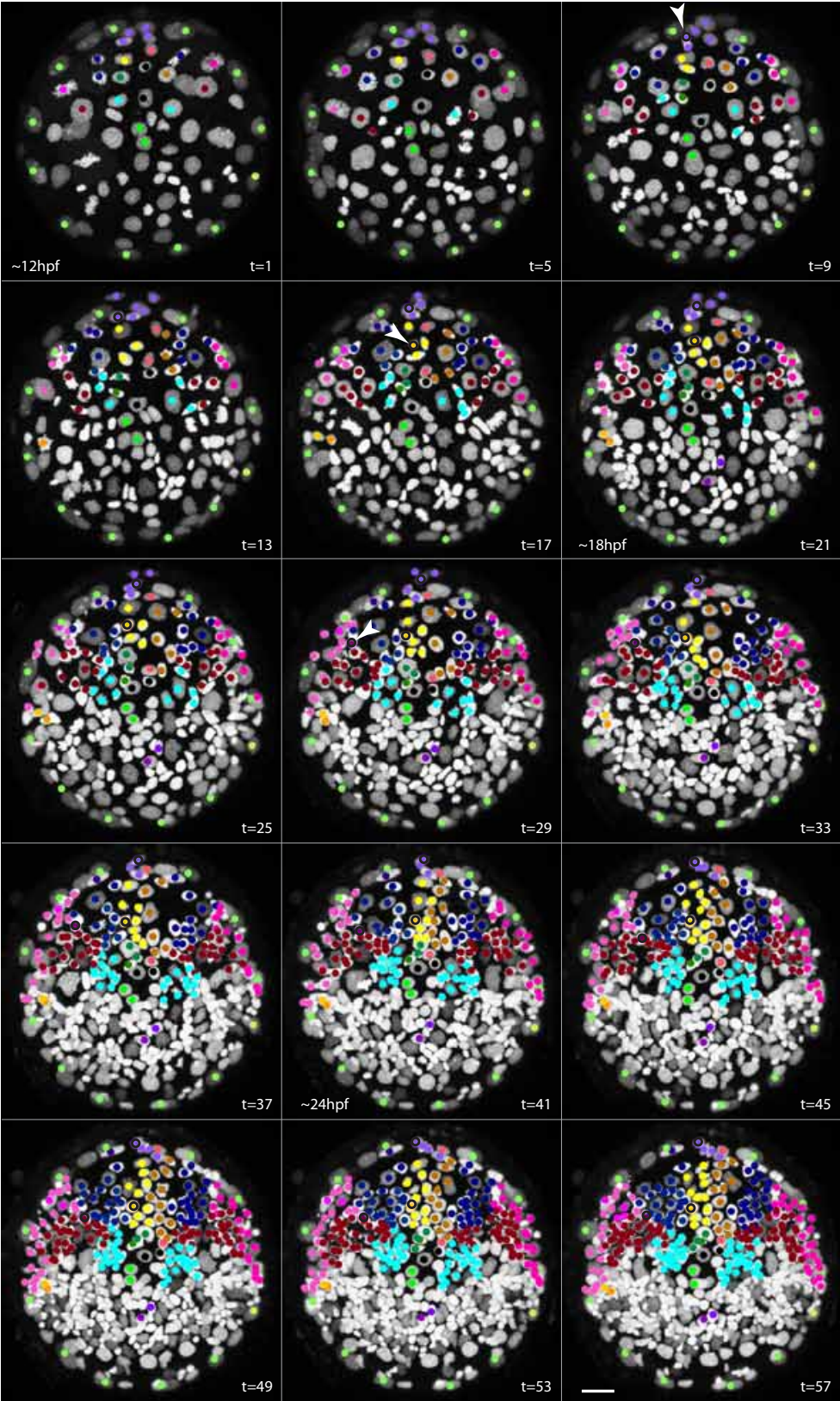
The mYFP labels the cell membranes, and this is not only useful for cell tracking, but it also provides additional landmarks to connect the lineage with differentiated structures: the developing axonal scaffold and the ciliated cells are enriched of mYFP, making them very easy to identify (fig. 3.5A-C). The injected embryos were imaged with confocal microscopy, and the individual cells were tracked manually using the MTrackJ plugin of ImageJ (see chapter 12). All the movies were taken from well-developing embryos, and after the time lapse all the animals showed normal morphology and behavior. The movies were all showing comparable patterns of cell divisions.

In the best movie I was able to record embryonic development from 12hpf to approximately 30hpf in a perfect apical view (since the temperature of the room during the time lapse was slightly higher than 18 °C, the developmental stage was estimated by comparing the number of nuclei in the movie with the number of nuclei in properly staged, fixed specimens). At this stage, the episphere was formed by 72 cells; thus, it was not possible to connect these cells to the earlier descriptions from Dorresteijn (1990). However, it was already possible to recognize the prototroch cells and the ampullary cells of the apical organ. Immediately after imaging, this larva was fixed and immunostained with anti-acetylated tubulin and anti-serotonin antibodies, to identify the cell types of interest (fig. 3.5D-F).

The analysis of the time-lapse movies from 12hpf revealed the distribution of the main clonal domains forming the dorsal brain, all derivatives of the blastomeres C and D. The tracking of cells and the clonal domains are shown in fig.3.6. Fig.3.7 shows the cell divisions of two larvae: the overall patterns of cell division are the same, supporting the reproducibility of these observations.

Most of the brain is generated by cells that divide asymmetrically, and form clones of cells which do not migrate, but remain all close to each other. The identity of these clones, in relationship with gene expression patterns and cell types, is discussed in

Figure 3.6 (on the next page): **Clonal domains in developing *Platynereis* dorsal brain.** The panel shows Z-projections of the episphere of one larva (dorsal is up); the larva was injected with H2A-RFP and mYFP (not shown) and imaged from 12hpf onwards. Stacks were acquired every 12:30 min; *t* indicates the frame number of the movie. The colored dots correspond to the clones tracked from the cells labelled in *t* = 1. The light green dots represent the prototroch cells and the ampullary cells of the apical organ (the two cells in the center). The arrowheads indicate specific cell types at the moment of their "birth": the cell projecting the dorsal unpaired axon (*t*=9), the asymmetric serotonergic cell (*t*=17) and the lateral serotonergic cell (*t*=29). Scale bar=20µm.



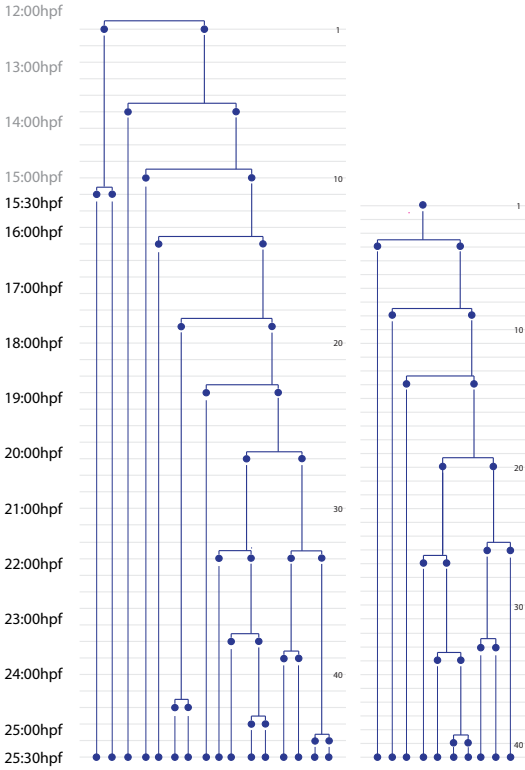
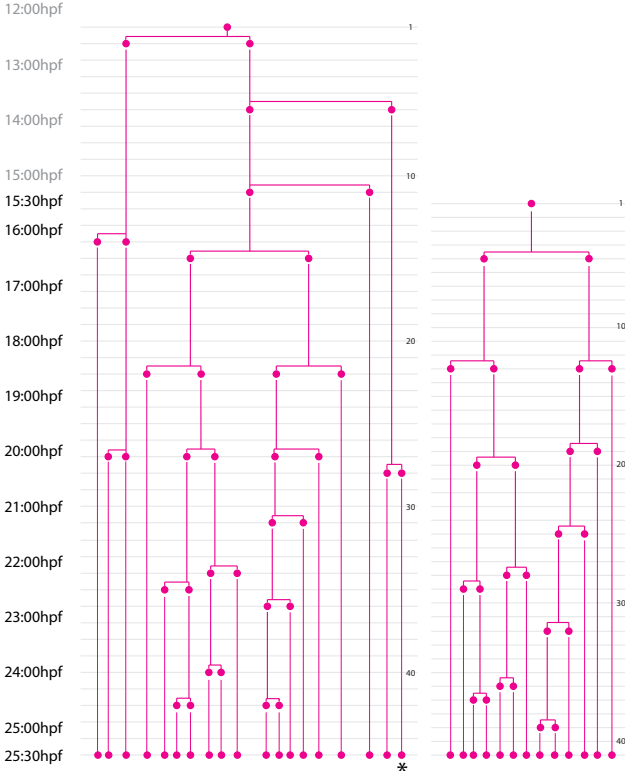
the following section. Here, I describe briefly the two instances of cell migration that were observed in the time-lapse movies. The first case of cell migration, already reported by Fischer (2010), involves two large cells located in a deeper position in the episphere (fig. 3.7A). These cells can be recognized from 10hpf onwards (Fischer, 2010), they move very quickly between the superficial epithelium and the yolk, from a medial to a lateral position, and finally they disappear below the prototroch cells (fig. 3.7AB). Their position, morphology and migratory behaviour corresponds exactly to the description that Wilson (1892) gave of the nephroblasts, the precursors of the head kidney cells, the first protonephridia of early annelid larvae (Hasse et al., 2010).

Other migrating cells are present at the dorsal edge of the episphere. Here, two streams of migration can be distinguished. A first, small group of cells moves ventrally, and reach a final position close to the ampullary cells of the apical organ (“black” and “light red” cells in fig. 3.6), although it is not very clear if it is a case of active migration or if the cells are displaced by the proliferation of neighboring cells. A second group of cells (“violet” cells in fig. 3.6) starts more or less in the same position, but undergoes several rounds of proliferation and migrates to the dorsal trunk, passing through the two most dorsal prototroch cells. These cells might correspond to the progeny of $2d^{111}$, which interrupts the prototroch cells dorsally at the 49 cells stage; indeed, according to Ackermann et al. (2005), $2d^{111}$ gives rise to the “dorsomedian trunk epidermis” (see also par. 1.2.1). Few of them remain in the episphere, like the cell generating the dorsal asymmetric axon, which could be identified after the time-lapse recording, with immunostaining of the same larva.

3.3.1. First insights in *Platynereis* neurogenesis

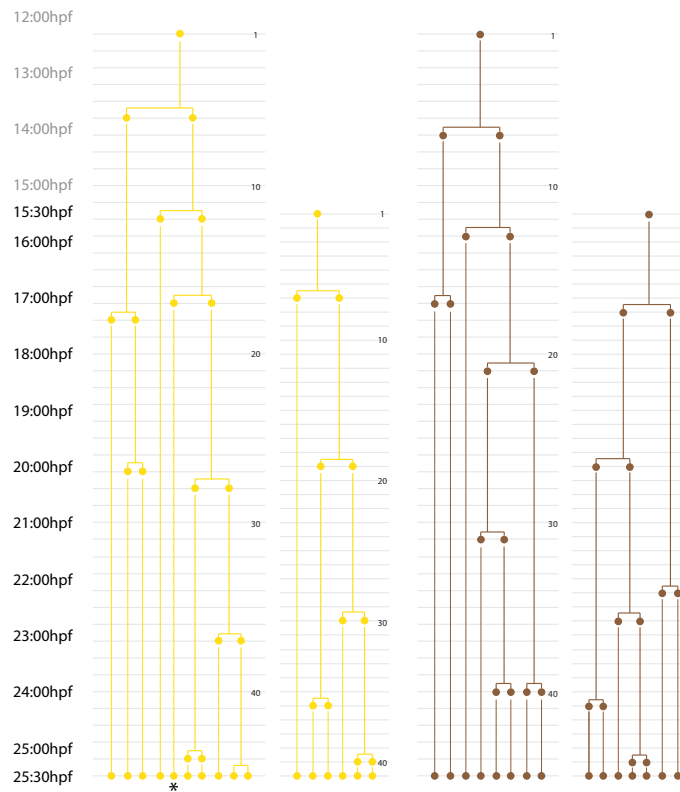
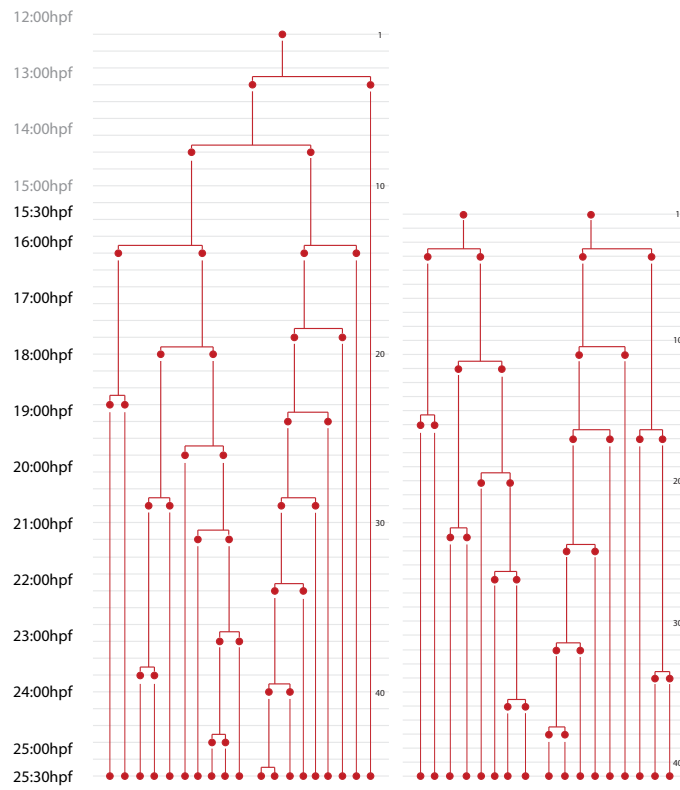
The analysis of these time-lapse movies provided some insights on *Platynereis* brain neurogenesis. The episphere starts as a monostratified epithelium (compare fig. 3.7) and becomes a pseudostratified epithelium, where the dividing cells are

Figure 3.7 (on the next page): **Cell lineages in developing *Platynereis* dorsal brain.** The plot shows the cell divisions of main clonal domains identified from time-lapse movies of two larvae. Only the cells of the left side (D quadrant derivatives) are shown. The second larva was imaged for a shorter time (from 15:30hpf to 25:30 hpf). The colors correspond to the color-code of fig.3.6. The cell divisions are plotted according to the frame number of the movie (gray horizontal lines). The asterisks indicate the lateral and the asymmetric serotonergic cells, which were identified after immunostaining of the first larva (fig.3.5D-F).



(a) Part I

3. Development of *Platynereis* dorsal brain | 57



(b) Part II

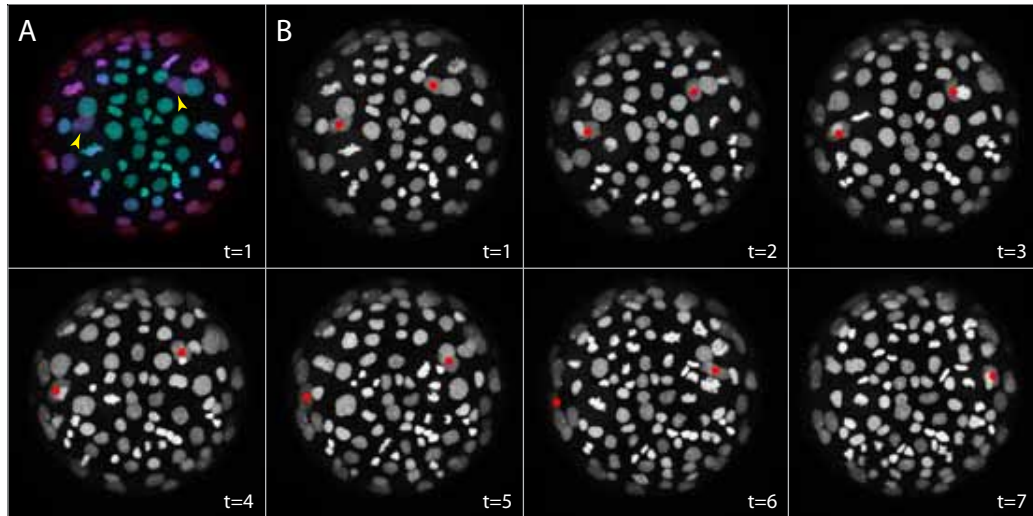


Figure 3.7: **Migration of the head kidney cells through the episphere.** A. Depth-coded Z-projection of the first time point of the movie (12hpf) showing that the head kidney cells (arrowheads) are deeper than the surrounding cells (green is superficial, red is deep). B. Time points in the movie showing the position of the head kidney cells (red dots).

located on the surface (fig. 3.3H-H'). A series of NSCs can be recognized from the big size and the intense mitotic activity (compare also fig. 3.3A). During the stages analyzed, the NSCs keep contacts with the basal and the apical membranes of the pseudostratified epithelium: in other words, the NSCs do not undergo ingression, in contrast to what has been described for arthropods and for another annelid, *Capitella teleta* (Meyer and Seaver, 2009). A prototypical cell division is illustrated in fig. 3.8: at the moment of mitosis, the NSC “rounds up” and apparently loses contact with the basal membrane (although the presence of tiny basal processes cannot be excluded), while the nucleus moves apically. After the cytokinesis, the daughter cells re-establish the contact with the basal membrane, and their nuclei migrate more basally. This might be an instance of interkinetic nuclear migration, recently proposed to be a conserved feature of pseudostratified epithelia within Bilateria (Meyer et al., 2011).

In arthropods, two modalities of neurogenesis have been described (Boyan and Reichert, 2011). In the type-I lineages, the NSCs divide asymmetrically to produce another NSCs and a neural precursor. This neural precursor, called ganglion mother cell (GMC), will divide again symmetrically, to produce two neurons (or a neuron and a glial cell). In the type-II lineages, the NSC produces a series of intermediate neural progenitors (INPs), which are self-renewing progenitor able to generate a se-

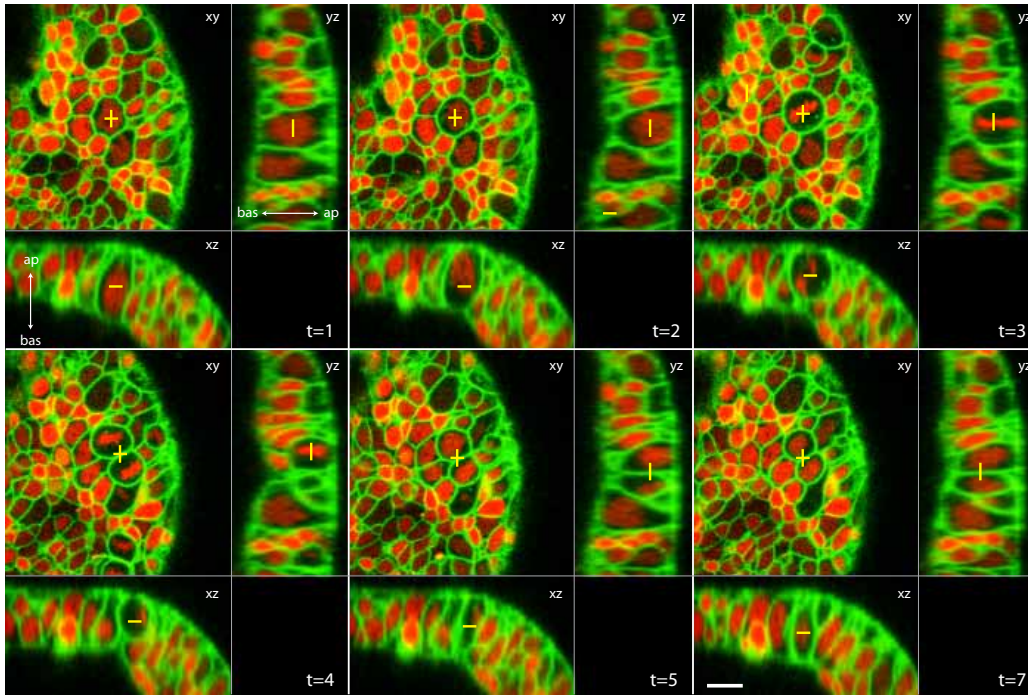


Figure 3.8: **Division of a NSC.** The image shows orthogonal views from consecutive frames of a time-lapse movie, with H2A-RFP labelling in red and mYFP labelling in green. Images were acquired every 12min30sec. The yellow lines demarcate a NSC which undergoes cell division. The nucleus shifts apically (t=2), the chromosomes align at metaphase while the cell “rounds up” apically (t=3). After cytokinesis (t=4), the cell membranes and the nuclei shift basally again (t=5 and t=7). “ap” and “bas” indicate the apical and basal side, respectively. The difference between consecutive time points t is 12 min 30 sec. Scale bar=10 μ m.

ries of GMCs. This dichotomy of neuronal lineages was not evident in *Platynereis*. Looking at the lineages in fig. 3.7, it is possible to recognize alternative mechanisms. In some cases, differentiated neurons are generated directly after one asymmetric cell division of a NSC, as in the case of the asymmetric serotonergic cell (demarcated by the asterisk in fig. 3.7, “yellow” lineage). In other cases, a NSC produces indeed a cell that remains small, and then divides again after a very long time, similarly to a GMC; this is the case for the lineage of the lateral serotonergic cell (demarcated by the asterisk in fig. 3.7, “purple” lineage). Finally, a peculiarity of *Platynereis* NSCs is that they sometimes stop the asymmetric division, and undergo one round of symmetric division, which generates two new NSCs (this can be observed for the “purple”, the “blue” and the “brown” lineages in fig. 3.7). We can speculate that in *Platynereis* these multiple modalities of cell division provide the basis for a more complex brain morphogenesis, and/or for the generation of big-

ger numbers of cells. The simultaneous generation of early differentiating neurons and proliferating progenitors in the same lineage could be a strategy for developing first a simple larval nervous system, and later a more complex adult nervous systems, without drastic metamorphic changes and in continuity with the preexisting structures.

3.4. Connecting lineages to early expression patterns and cell types in the developing episphere

Animals with a deterministic mode of development and a fixed lineage, like spiralian or ascidians, provide the unique opportunity to study gene regulation and GRNs within lineages and at the single cell level. For *Platynereis*, this is especially tempting, since the early trochophore larva has a limited number of cells, which can be distinguished even by eye, based on their position, shape and neighbours.

Thus, I combined information from the time-lapse movies of early development and in situ expression data to gain indications on which transcription factors are involved in the development of the dorsal brain. The choice of genes was guided from the cell type analysis described in Chapter 7, which provided specific markers for the cells of interest.

During the developmental stages documented by the time-lapse movies (between 12 and 24hpf) the major events that establish the main *Platynereis* brain regions take place. Most of the cells of the episphere undergo massive proliferation, with the exception of the cells of the apical organ, which exit the cell cycle around these stages. As a consequence, the expression patterns of transcription factors are extremely dynamic, and change very quickly with time. Here I describe the main lineages that contribute to the cell types analyzed in this thesis, and how these lineages are demarcated by the expression of distinct transcription factors.

3.4.1. The dorsal midline and the asymmetric serotonergic cell.

Intriguingly, the dorsal midline has a dual clonal origin. The NSCs that produce the two halves are heterogenous, as the NSC on the right side (the C quadrant; from apical view, “brown” cells in fig.3.6) would correspond by position and early cell division patterns to a cell that stops dividing after few mitoses, and produces the crescent cell of the apical organ (“dark green” cells in fig. 3.6; see Appendix A). The NSC on the left side (the D quadrant; “yellow” cells in fig. 3.6) does not have

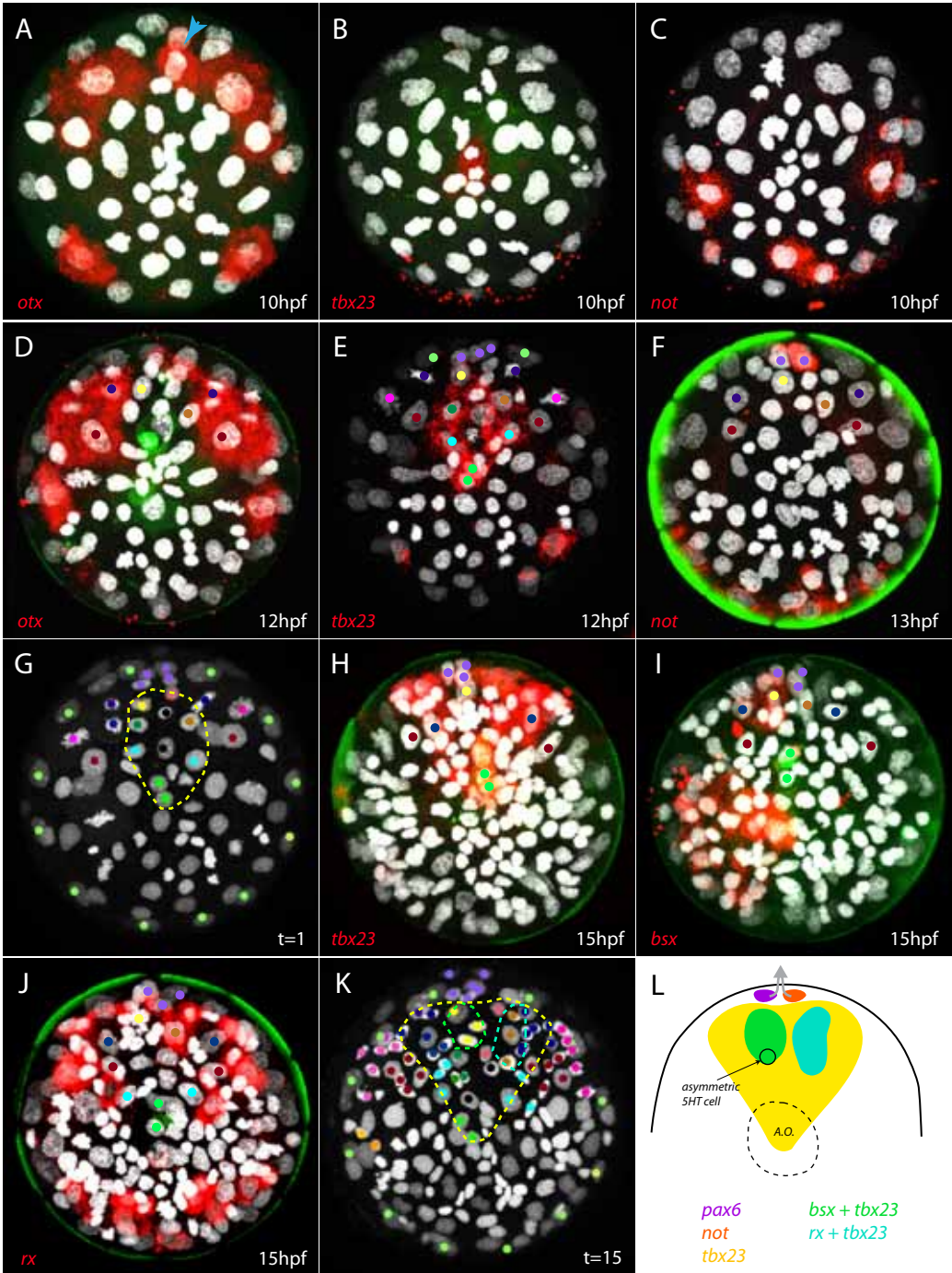
any counterpart on the other side of the episphere. This latter progenitor generates the asymmetric serotonergic neuron, which arises at about 16hpf, consistent with what has been found previously with the EdU incorporation studies.

The cells of the dorsal midline have a distinct molecular identity, compared to the cells in the vicinity. The most specific marker is the T-box transcription factor *tbx2/3*, which at 10hpf is expressed only in the ampullary cells of the apical organ, and two hours later its expression extends to about 10 cells along the dorsal midline. The comparison of these cells with the time-lapse movies clearly shows that they correspond to the two asymmetrical dorsal midline clones described previously (indicated by the colors “yellow” and “brown”). *tbx2/3* remains expressed in these cells after they become postmitotic and differentiate. A second marker for the midline cells is the transcription factor *bsx* (*brain specific homeobox*, the homolog of the *Drosophila bsh*). *bsx* expression is restricted to a subpopulation of the *tbx2/3+*, which probably correspond to the “yellow” clone. As a peculiarity, *bsx* is asymmetric and dynamic: at 24hpf this gene is still expressed in the dorsal midline, and in a cell that might correspond to the asymmetric serotonergic cell, while at 48hpf the dorsal midline expression disappears, and *bsx* expression dominates the most anterior tip of the episphere (Appendix B).

The diversity of the two clonal domains that populate the dorsal midline is demarcated also by *rx* expression. The earliest *rx* expression pattern could be documented for the 16hpf stage, although qPCR shows the presence of *rx* transcripts from 12hpf (Fischer, 2010). The dorsal asymmetry of *rx* expression could be followed until 36hpf, although the number of *rx+* cells in this region changes during development.

Similarly to *rx*, the expression of *otx* is asymmetric in the dorsal edge of the episphere. *otx* can be detected already at 10hpf in five cells of the dorsal brain, where one of them is unpaired and located on the right side. Between 20 and 24hpf, two

Figure 3.9 (on the next page): **Early expression of transcription factors in the dorsal midline domains.** A-C: Expression of *otx* (A), *tbx2/3* (B) and *not* (C) at 10hpf. *otx* has a dorsal asymmetric spot of expression (arrowhead). D-F: Expression of *otx* (D), *tbx2/3* (E) and *not* (F) at 12-13hpf. The dots represent corresponding cells in the first frame (t=1) of the time lapse movie (G). The dashed yellow line in G represent the presumed *tbx2/3* expression domain. H-K: Expression of *tbx2/3* (H), *bsx* (I), *rx* (J) and *pax6* (K) at 15-16hpf. The dots represent corresponding cells in the frame 15 (t=15) of the time lapse movie (L). The dashed yellow, green and cyan lines in L represent respectively the expression domains of *tbx2/3*, *bsx* and *rx*. L. Schematic drawing showing the expression of *bsx*, *rx*, *tbx2/3*, *not* and *pax6* at 15-16hpf. In A-F and H-J, DAPI staining in white, gene expression in red and tyrosinated tubulin in green.



paired dorso-medial domains of *otx* arise from the division and subsequent proliferation of one *otx*+ cell. The timing and later onset of *otx* expression in the dorsal midline exclude its direct involvement in the specification of the asymmetric serotonergic cell.

Other two genes show asymmetric expression in one or few cells at the dorsal edge of the episphere. The transcription factor *not* (called *flh* in zebrafish) is transiently expressed from 13 to 18hpf in one cell. By position, it corresponds to one of the “violet” cells (fig. 3.6) that migrate to the dorsal trunk; consistently, in WMISH at 16hpf the dorsal *not*+ cell is closer to the prototroch. After 18hpf the dorsal *not* staining disappears, and indeed, in the movie this cell migrates to the trunk and then divides at about 18hpf. Similarly, at 16hpf *pax6* shows a transient expression in one cell which, by position, is one of the cells migrating to the dorsal trunk. Although the cell projecting the dorsal asymmetric axon belongs to this migrating cell population, it does not seem to correspond to the *not* or the *pax6* cells. Live imaging with reporter constructs driving the expression of one of these genes will allow to investigate in more detail the dynamics of this peculiar cell population.

The lineages generated by the two midline NSCs are organized according to a “temporal topology”, where the earliest-born neurons are located more distally in the episphere (i.e. more ventrally). These NSCs continue to divide for a long time: at 48hpf, a “rosette” of EdU+ cells can still be recognized in this position (compare fig.3.3F). This rosette will later originate the dorsal tube of connective tissue penetrating the brain (Heuer and Loesel, 2008); it is not clear yet if it is equally contributed by the two midline lineages, or just one of them. Thus, at 48hpf stage, the earliest-born neurons occupy a medial position, in between the cPRCs cells. Intriguingly, the cells in this position have the most pronounced asymmetries in gene expression profiles (neuropeptides, GPCRs, some transcription factors): it is clear now that these asymmetries are encoded in the different clonal origins of the left and right midline.

3.4.2. The lateral serotonergic cells and the adult eye region

The lateral clonal domains are formed by symmetric and asymmetric cell divisions of NSCs located bilaterally, just anterior to the prototroch cells (“purple” cells in fig. 3.6). In this lineage, most of the mitotic spindles are perpendicular to the prototroch; this allows the extension of this clone to the ventral halves of the episphere, very close to the larval eyes (indicated by the “orange” cells). Thus, the majority of the

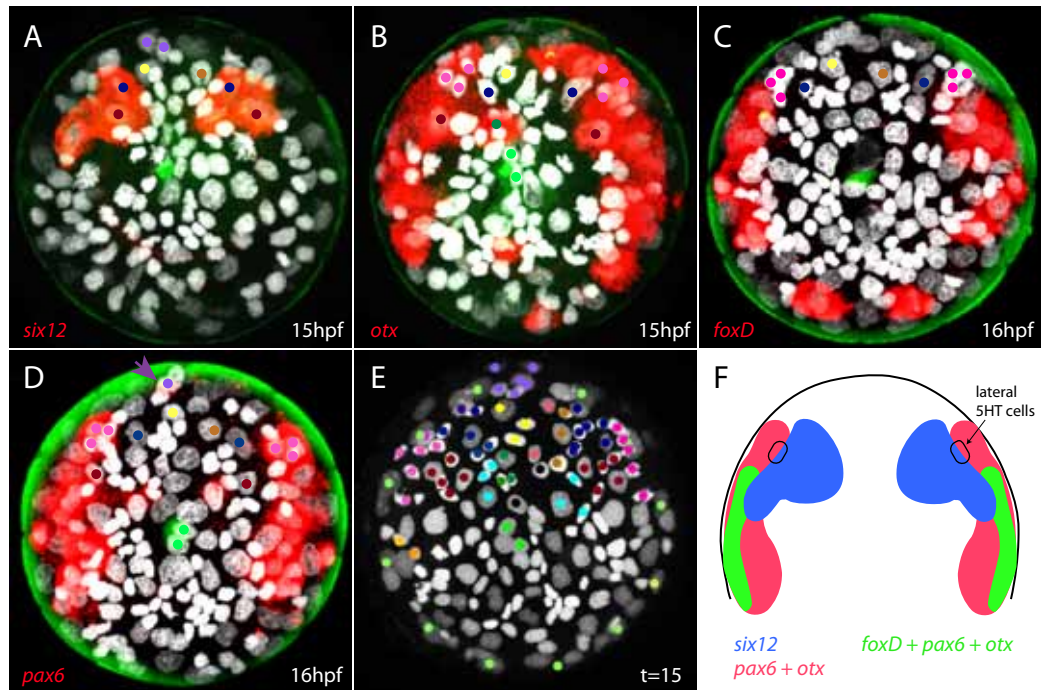


Figure 3.10: **Early expression of transcription factors in the dorso-lateral episphere.** A-D: Expression of *six1/2* (A), *otx* (B), *foxD* (C) and *pax6* (D) at 15-16hpf. *Pax6* has a dorsal asymmetric spot of expression (arrowhead). The dots represent corresponding identifiable cells in the time-lapse (t=15, panel E). F. Schematic drawing showing the expression of *six1/2*, *pax6*, *otx* and *foxD* at 15-16hpf. In A-D, DAPI staining in white, gene expression in red and tyrosinated tubulin in green.

cells of this domain remain located at the periphery of the episphere, where they will probably give rise to sensory cells. Only few cells extend medially: the two serotonergic interneurons, located next to the cPRCs, indeed correspond to the most medial cells of these lateral clones.

A second cell population can be recognized just more medially (“dark red” cells in fig. 3.6). This cell population produces a large part of the cells of the episphere. The NSC of this lineage can still be recognized from its size at 20hpf (fig. 3.3). The fate of these cells is not easy to establish, since most of them are not differentiated at the stages investigated.

Most likely, the adult eyes are one derivative of these lateral clones. This is strongly indicated by the early expression of two adult eye markers, the transcription factors *otx* and *six1/2*. The patterns of these genes are not identical, but they overlap in the most lateral edges of the episphere, where the lateral serotonergic cells will form. Indeed, these cells keep the expression of *otx* and *six1/2* also after differentiation.

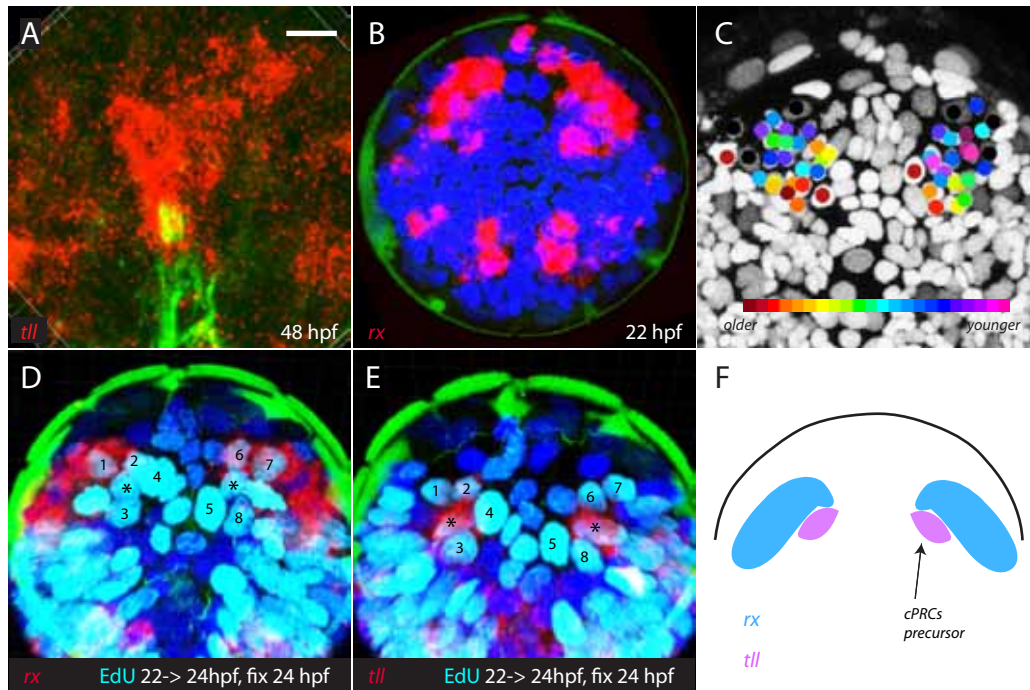


Figure 3.11: **Early expression of transcription factors in the dorso-medial episphere.** A. Specific expression of *tll* in the cells of the cPRCs complex at 48hpf. Scale bar=20 μ m. B. Expression of *rx* in the dorsal NSCs. C. “Temporal topology” in the medio-dorsal clonal domains (“blue” cells in fig. 3.6). Color-code indicates the birthdate, according to the tracking of the time lapse movie. The NSCs are in black. D-E. Expression of *rx* (D) and *tll* (E) in adjacent proliferating cells of the dorsal episphere. The larvae were incubated with EdU from 22 to 24hpf, and fixed immediately after the incubation. Corresponding cells are labelled by numbers; the asterisks (*) indicate the cPRCs precursors. F. Schematic drawing showing the expression of *rx* and *tll* at 24hpf. The images in A, D and E are Imaris projections. In A-E, DAPI staining in blue, gene expression in red, EdU in cyan and tyrosinated tubulin in green.

At 16hpf, three *pax6*⁺ cells can be identified on each side at the most dorsal edge of the “purple” domain. As above, two of them are the lateral serotonergic neurons; the fate of the remaining *pax6*⁺ dorsal population is still unknown.

3.4.3. The ciliary photoreceptors and the medial photoreceptive region

The two medio-dorsal clonal domains arise from symmetric and asymmetric cell divisions of a NSC, located between the lateral and the midline domains (“blue” cells in fig.3.6). This domain gives rise to the majority of the cells in the cPRCs region. Here, gene expression is very dynamic, and it is more difficult to sort out the cells expressing *otx*, *pax6*, *tbx2/3* and *six1/2*. Similarly, *rx* expression is also associated with this lineage, but it changes quickly throughout development.

The NSCs of this lineage produce a clone of neurons with a “temporal topology”, where the earliest-born cells are in a more ventro-medial position; these cells are close to the asymmetric and lateral serotonergic cells, where the first projections to the central neuropil will develop.

A first attempt to identify the developing cPRCs can be made comparing these data with the cell birthdating data, which indicate that the cPRCs become postmitotic after 24hpf (fig.3.4), and the expression of *tll*. This transcription factor has a very dynamic expression in neural progenitors, but it keeps its expression site in the cPRCs after differentiation. At 24hpf, *tll* is expressed in two EdU+ cells laying just ventrally to a larger domain of *rx*+ cells; all these cells belong to the “blue” lineage. In the movie, the putative *tll*+ cells divide only once more, so they behave as putative GMCs. At 20hpf, *rx* expression labels dividing cells in the dorsal part of the “blue” clone. From these data, the hypothesis is that *rx* is dynamically expressed in NSCs generating the cPRCs territory, and that in the GMC originating the cPRCs, *rx* expression is downregulated, while *tll* is turned on. Further experiments, using transgenic reporters, will be required to test this hypothesis.

4

ESTABLISHMENT OF TECHNIQUES TO STUDY GENE FUNCTION IN *Platynereis*

The gene *rx* is a critical regulator of the development of photoreceptors and circadian structures of vertebrate brain (par. 2.4). As shown before, in *Platynereis* *rx* is expressed in the NSCs of the lineage forming the entire larval circadian center (par. 3.4.3). This suggests that Rx might have an important role in the development of the circadian structures of annelids. In order to test this hypothesis, gene perturbation studies and identification of target genes are required. The recent development of techniques for injection of *Platynereis* zygotes made all this possible for the first time (Kegel, 2008). The focus of my work was the analysis of Rx function with a combination of techniques. Morpholino antisense oligonucleotides (MOs) were chosen for the knock-down of *rx*; MOs are synthetic modified oligonucleotides that are able to inhibit transcription after binding to the 5'UTR (translation-blocking MOs), or to interfere with splicing after binding to a splice junction (splice-interfering MOs) (Angerer and Angerer, 2004; Morcos, 2007; Eisen and Smith, 2008).

Despite MOs are a powerful tool currently employed in several species to investigate gene function, they present two significant disadvantages: the “dilution” of the effects during development, associated with the lack of a complete loss of function of the gene, and the presence of toxic side effects which require tight controls (Robu et al., 2007). For this reasons, I used a parallel approach to interfere with Rx function, establishing Rx knock out lines by means of zinc finger nucleases (ZFNs). ZFNs are recombinant proteins engineered to bind to specific sequences in the genome, and to produce double-strand DNA breaks. This site-specific DNA damage induces cell repair responses and ultimately the introduction of mutations (Porteus and Carroll 2005; detailed in par. 4.4).

Finally, the overexpression of *rx* mRNA was used as a complementary approach to investigate the effects of gene gain-of-function.

The design of MOs and ZFNs requires a detailed knowledge of the genomic

structure of the gene of interest, and of the eventual presence of single nucleotide polymorphisms (SNPs). Since the current *Platynereis* transcriptome and genome resources were not available yet at the time when this study was started, these data were obtained with classical approaches, as described below. Part of this work, together with the testing of the first *rx* MOs, was done by Nicola Kegel, a diploma student in the lab (Kegel, 2008).

4.1. The genomic structure of the *rx* gene

The genomic structure of *rx* was obtained with a TAIL PCR approach. Briefly, multiple sequence alignment of Rx protein sequences in different species, together with genomic information, were used to identify putative conserved exon-exon boundaries. One candidate exon-exon boundary was located in the homeodomain. Then, to identify the genomic sequences flanking these exon-exon boundaries, a tail-PCR approach was chosen. With this technique, gene-specific primers are used in combination with degenerate genomic primers in three rounds of nested PCRs (for details, see par. 12.1.1). A first series of tail-PCRs allowed the confirmation of the conserved exon-exon boundary in the homeodomain. A second set of tail-PCRs going towards the 5' end of the gene led to the identification of a second exon-exon boundary. All these sequence information were subsequently confirmed by the data coming from the *Platynereis* genome assembly. In conclusion, the *Platynereis rx* gene has three exons, with the start codon in the first exon, and the stop codon in the last one, and the homeodomain spanning exons two and three (fig. 4.1).

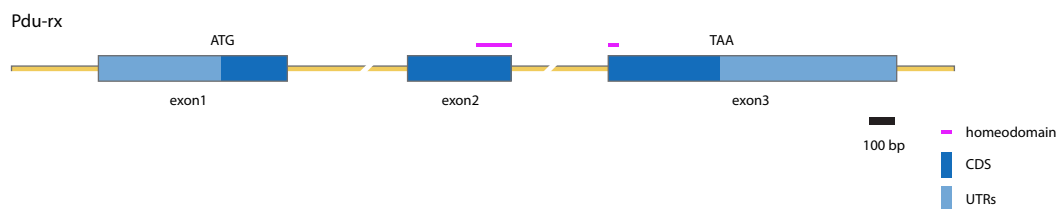


Figure 4.1: Genomic structure of the *rx* gene.

4.2. The problem of single nucleotide polymorphisms (SNPs)

The first *rx* MOs were designed to target the exon2-intron2 and intron2-exon3 boundaries. Injection of these morpholinos at different concentrations led to inconsistent results, where some embryonic batches showed strong phenotypes, while others were not affected at all by morpholino injection. This prompted us to check for the presence of SNPs in the MOs binding sites. It is known that the presence of SNPs reduces the affinity of MOs to their binding sites, thus reducing dramatically the efficiency of knock-down (Eisen and Smith, 2008; Coffman et al., 2004). Indeed, PCR amplification and sequencing of exon2-intron2 and intron2-exon3 boundaries from different individuals showed the presence of two SNPs in each MO binding site (fig. 4.2). A SNP analysis for the entire *rx* gene was then performed, screening genomic DNA amplicons from ten different individuals. The frequency of SNPs was higher in the UTRs and in the introns of the gene. A project developed later in the lab by Oleg Simakov produced deep sequencing transcriptomic data from different *Platynereis* strains, with the aim of studying the distribution of SNPs in the genome. The comparison of my data with this new dataset revealed that the SNPs identified by “classical” approaches correspond to the most frequent ones in the deep sequencing dataset. Moreover, the *rx* gene has the special feature of being enriched in SNPs compared to the average SNP frequency for other coding sequences.

4.3. Validation of the knockdown efficiency of the *rxin1ex2* MO

The mapping of SNPs made possible to design new morpholinos targeting sequences without polymorphisms. For this purpose, I chose to use a splice-interfering MO against the intron1-exon2 splice site. In the case of the *rx* gene, the advantages of splice MOs over translation-blocking MOs are several. First, the efficiency of splice MOs is more easy to control, as this can be assayed via PCR. Unfortunately a good *Rx* antibody is not available yet, although this would be the perfect system to check the efficiency of MOs. Moreover, the *rx* 5'UTR is very polymorphic, making it almost impossible to identify a suitable MO target sequence.

A morpholino against the intron1-exon2 splice site, called *rxin1ex2* MO, was injected at different concentrations in *Platynereis* zygotes. As a control, the *stctrl* MO provided by GeneTools (the company producing MOs) was injected at the same concentrations in sibling zygotes. To assess the effect of the *rxin1ex2* MO on RNA splicing, total RNA was extracted from injected larvae and this was used to pro-

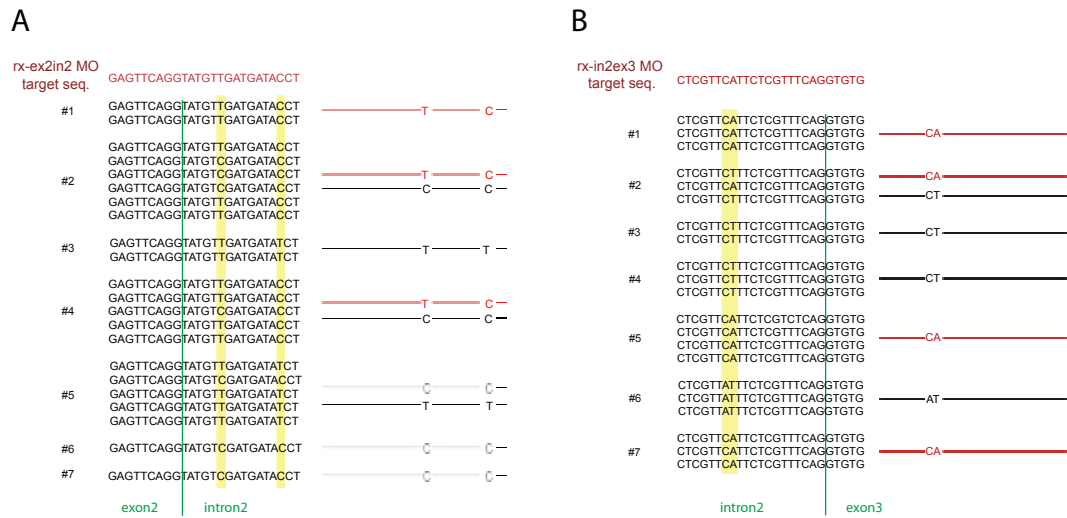


Figure 4.2: SNPs in the target sequences of Rx MOs. A. and B. show the distribution of SNPs in the target sequences of the first Rx MOs tested, *rx-ex2in2* MO and *rx-in2ex3* mo respectively. The alleles were identified after amplification and sequencing of several clones from different individuals (#1-7).

duce cDNA and then to amplify the *rx* gene (par. 12.3). From the *rx* gene structure and the position of the MO, the *rxin1ex2* MO was expected to produce the retention of intron1 in the mature mRNA. Instead, I found that the *rxin1ex2* MO produces the skipping of exon2 (fig. 4.3A-B). The consequence of this is the production of a shorter mRNA with a frameshift mutation and a premature stop codon; only a small part of the homeodomain is retained in this aberrant transcript.

The efficiency of knock down could be quantified with a qPCR assay (fig. 4.3C and par. 12.3). I used qPCR primers spanning the exon1-exon2 junction; these primers are designed to amplify specifically the normal transcript. Moreover, the total amount of *rx* transcript was measured with primer pairs in exon3 (present in both the normal and the aberrant mRNAs). In 48hpf injected larvae, there was up to a 75% downregulation of the normal *rx* mRNA. The efficiency of knock down was variable between injected batches, as a consequence of variability of injection volumes between different injection sessions.

In order to make different injection sessions more comparable, the injection protocol was improved with the addition of TRITC-Dextran as injection tracer, and with the optimization of the injection needles, to deliver more consistent amounts of in-

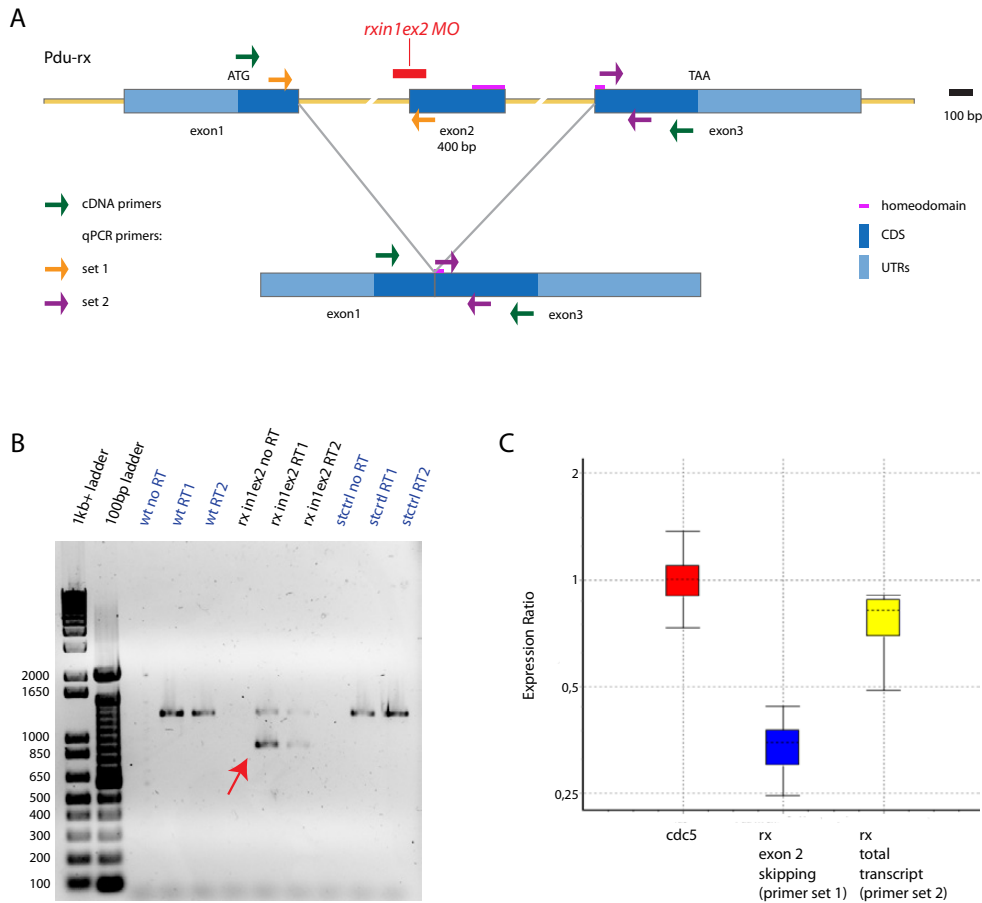


Figure 4.3: **Aberrant splicing of *rx* mRNA after *rxin1ex2* MO injection.** A. Schematic drawing showing the position of *rxin1ex2* MO, the aberrant splice product produced after *rxin1ex2* MO injection, and the primer pairs used to analyze *rx* mRNA splicing. B. Gel picture of *rx* RT-PCR products, using a primer pair that amplifies the entire *rx* coding region. The *rxin1ex2* MO injected larvae (48hpf) have two isoforms; the shorter one (arrow) lacks exon2 (407bp). C. Quantification of aberrant mRNA splicing with qPCR. In 48hpf injected larvae, the total amount of *rx* transcripts is not different between *rxin1ex2* MO larvae and *stctrl* MO larvae (primer set 2, exon3). However, in the morphant larvae there is a significant reduction of the normal *rx* transcripts, recognized by a primer pair spanning the exon1-exon2 boundary.

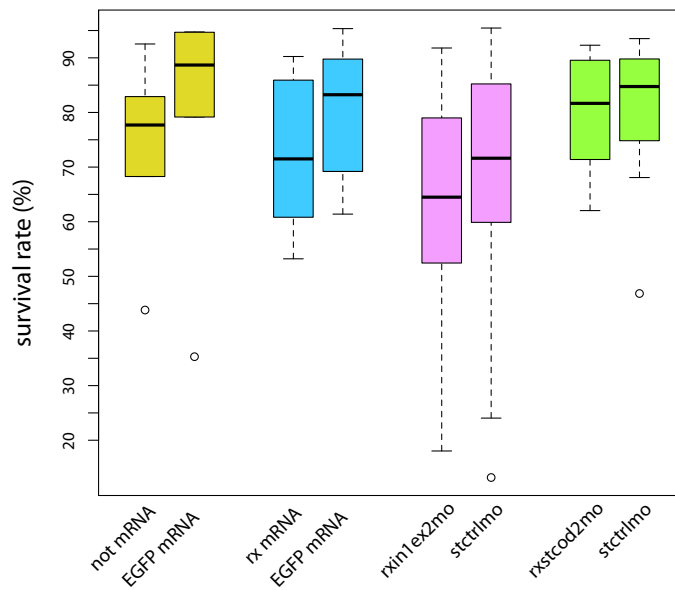


Figure 4.4: **Survival rates of larvae injected with different morpholinos and mRNAs.** The differences between each experimental treatment and the controls are not statistically significant (t -test). *not* mRNA injections (100-200 ng/ μ l): 6 experiments, 957 larvae, $p=0.59$; *rx* mRNA injections (312.5 ng/ μ l): 12 experiments, 2352 larvae, $p=0.21$; *rxin1ex2* MO injections (800 μ M): 43 experiments, 9144 larvae, $p=0.21$; *rxstcod2* MO injections (500 μ M): 11 experiments, 2155 larvae, $p=0.89$.

jection solution¹.

In different series of experiments, I injected the mRNAs for *not* and *rx* and two different *rx* MOs (*rxin1ex2* MO and *rxstcod2*, a MO targeting the 5'UTR). After each injection session, the embryos that failed the early cleavages were discarded. The embryos were also inspected for TRITC fluorescence, and the non injected embryos were eliminated. At the moment of fixation (usually 24 or 48hpf), I counted the number of surviving larvae in the experimental and in the control groups (the controls were always injected either with *stctrl* MO or with the EGFP mRNA). The statistics are shown in fig. 4.4. For each treatment, the survival rate of control group was not significantly different from the survival rate of the experimental group. The survival rate was correlated with the quality of the embryonic batch used for injection. Injected larvae where the survival rate was lower than 50% were non considered for further analysis.

¹Eppendorf Femtotips II were previously used, which break more easily; this caused higher variability in the injection volumes. Glass needles were tested and optimized with Dr. Mette Handberg-Thorsager. See also par. 12.2.2

This comparison indicates that none of the morpholinos or the mRNAs increased mortality, compared to their controls. In all the experiments, the larvae of the control groups developed normally. Then, it can be assumed that the phenotypes observed in the experimental groups were specific and not caused by injection artifacts.

4.4. Establishment of *rx* knock out lines with the zinc finger nucleases technology

The ZFNs technology emerged recently as a powerful tool for targeting specific genomic loci (Porteus and Carroll, 2005). ZFNs are recombinant proteins composed by 3-4 zinc finger DNA-binding domains and a domain of the *FokI* endonuclease. The binding of two ZFNs proteins to DNA sequences separated by a 5-6 nt spacer brings together the two *FokI* domains between the two ZFNs binding sites. The *FokI* endonuclease then produces a double-strand break, which triggers cell repair responses like the non-homologous end joining (NHEJ) or the homologous recombination (HR).

ZFNs have been used in several model and non-conventional organisms to produce custom changes in specific DNA sequences (Lloyd et al., 2005; Morton et al., 2006; Meng et al., 2008; Doyon et al., 2008; Ochiai et al., 2010; Mashimo et al., 2010). The NHEJ pathway can introduce repair errors, which result in mutations. On the other end, providing a template for HR allows the custom modification of the genomic locus, like the introduction of a reporter gene or the "editing" of the gene of interest (Cui et al., 2011).

The site-specificity of ZFNs is encoded in the zinc finger DNA binding domain. The zinc finger transcription factors are the most abundant and diverse in animal genomes, since the zinc finger DNA binding domain is modular: each "finger" recognizes three base pairs, and the specificity depends on the identity of the three aminoacid residues at the edge of each finger. Thus combinations of different "fingers" allow the recognition of different DNA sequences.

4.4.1. Selection of an *rx* ZFN pair and validation of its mutagenicity

I applied the ZFNs technology to the *Platynereis rx* locus. For this purpose, I used ZFNs designed and produced by Sigma. The commercial ZFNs use a patented method for the design and the selection of the most specific and efficient ZFNs targeting a locus of interest. The SNP analysis described previously (see par. 4.2)

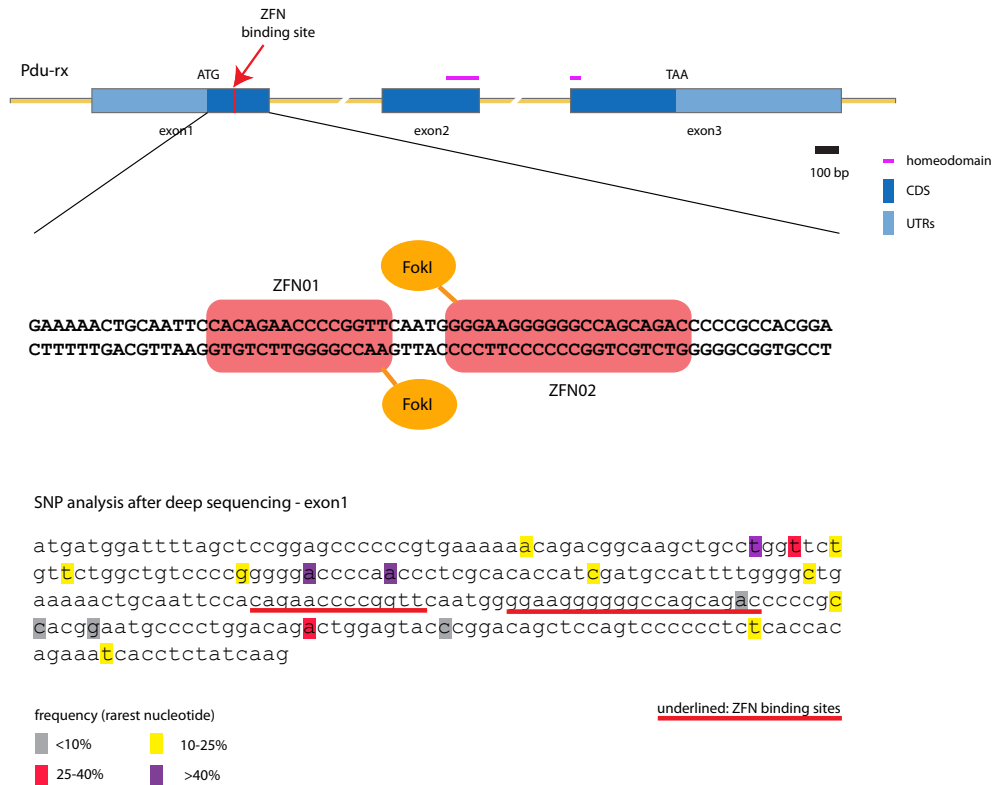


Figure 4.5: **Design of Rx ZFNs.** The Rx ZFNs were designed to target the first exon, before the homeodomain. The ZFN pair binds to opposite DNA strands, and brings together the two subunits of the FokI endonuclease in between the ZFNs binding sites. The entire first exon was analyzed for the presence of SNPs, using deep sequencing data (generated by Oleg Simakov); the ZFNs target a sequence with only few low frequency SNPs (underlined).

was critical to select ZFNs targeting non-polymorphic sites.

A pair of ZFNs was designed to target the *rx* coding sequence in the first exon (fig. 4.5). The mRNAs encoding the two ZFNs subunits were injected at different concentration, to test toxicity effects. A final concentration of 320 ng/ μ l was used to inject large numbers of zygotes, used to test the ZFNs efficiency and to raise the mutant lines.

To check the mutagenicity of the ZFNs, genomic DNA was extracted from pools of 50 zygotes, injected with different concentrations and raised to the 48hpf stage. A genomic fragment of 996bp flanking the ZFNs cutting site was amplified from the genomic DNA and analyzed with gel electrophoresis. This revealed the presence of shorter amplicons, possibly generated by large deletions occurring after the double-

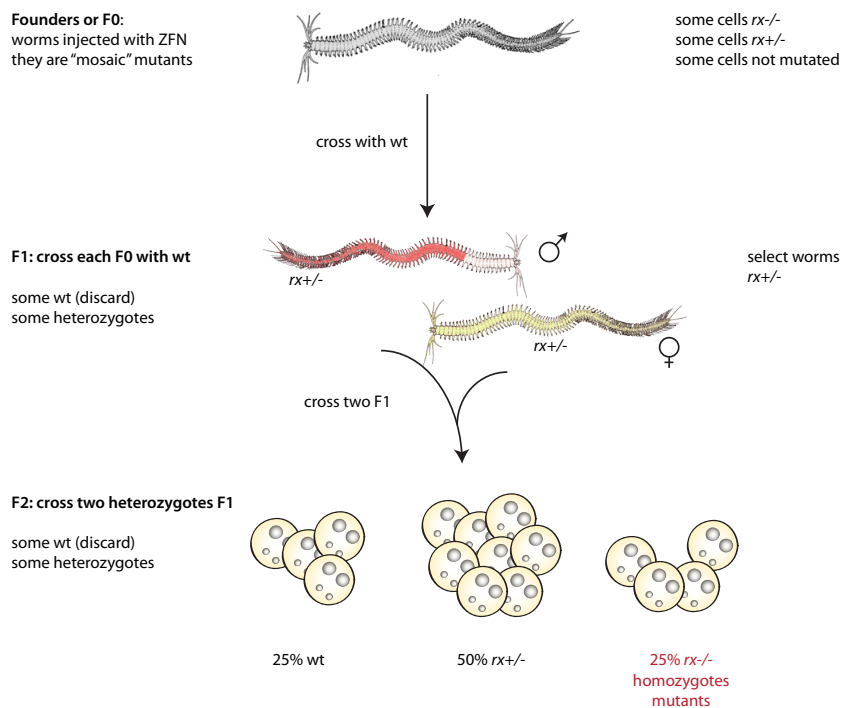


Figure 4.6: Breeding scheme for the establishment of rx knockout lines.

strand break. To confirm this hypothesis, the different fragments were cloned after gel extraction and sequenced. Indeed, the shorter amplicons were corresponding to the rx locus, but with large deletions starting exactly from the ZFNs cutting site. These first results were very encouraging, confirming that the ZFNs were effectively inducing mutations in the rx locus. Using a complementary approach, injected larvae raised to 48hpf were immunostained with anti-acetylated tubulin and anti-serotonin antibodies. A fraction of ZFNs injected larvae showed malformations of the axonal scaffold. The frequency of these loss of function phenotypes was extremely low (around 5%), as expected considering the low likelihood of a loss of function mutation in both chromosomes.

4.4.2. Establishment of rx knockout lines

After the assessment of ZFNs efficiency, I injected many zygotes to screen for founders harbouring loss of function mutations in the germline. A total of 13 injection sessions were partially dedicated to this purpose, and about 750 worms at 5 dpf stage were destined to culture; of these, less than 10% survived to adulthood. These

worms represent the F0 ("F zero") generation of putative founders. At sexual maturation, they were all out-crossed to wild type worms, producing the F1 generation. After crossing, the F0s were kept at -80°C for the subsequent extraction of genomic DNA.

The F0 worms are not all necessarily "interesting", hence the need of a screening of the worms themselves and their progeny. Because the ZFNs were introduced in the zygotes as mRNAs, the F0 worms are necessarily genetic mosaics, with some cellular clones harbouring the wild type alleles, other clones with a mutation in heterozygosity, and (possibly) cellular clones with homozygote mutations. For this reason, some of the F0s might not be able to transmit the mutation(s) through the germline, if the cell lineage producing the germ cells was not affected by the ZFNs. On the other end, each founder can have different mutations, as a result of independent ZFNs cutting events.

Once the real founders have been identified, a further screening is necessary to distinguish between the loss of function mutations and all the other mutations which do not affect protein function, like deletions of three nucleotides or synonymous substitutions.

The breeding scheme planned for the establishment of knockout lines is shown in fig. 4.6. The outcross of F0s with wild type animals produces a progeny that includes some heterozygote worms, if the F0 harboured mutation in the germline. The cross of $rx^{+/-}$ F1 worms will then produce an F2 progeny, where the mutant alleles are distributed according to a mendelian ratio. Currently, several strains of $rx^{+/-}$ F1 worms have been isolated, and at the sexual maturation they will be crossed to obtain F2 mutant homozygotes.

The screening of rx mutants involved Heidi Snyman, the former lab technician, and Nathalie Tisch, a lab trainee (methods described in par. 12.4).

First, the F0 worms were screened for mutations after spawning. This turned out to be extremely useful, since the detection of mutations in the founders correlated with the frequency of mutant F1 worms in its progeny.

The rx locus was amplified with two PCRs, and then digested with the restriction enzyme *AgsI*, which has a recognition site overlapping with the ZFNs cutting site. The absence of *AgsI* digestion products indicates modifications of the ZFNs cutting site, produced by NHEJ after the ZFNs activity (fig. 4.7A). Although this assay is prone to false-negatives, it was effective to identify the F0 worms with mutations of the rx locus, as confirmed with sequencing. 43% of the F0 worms screened has a

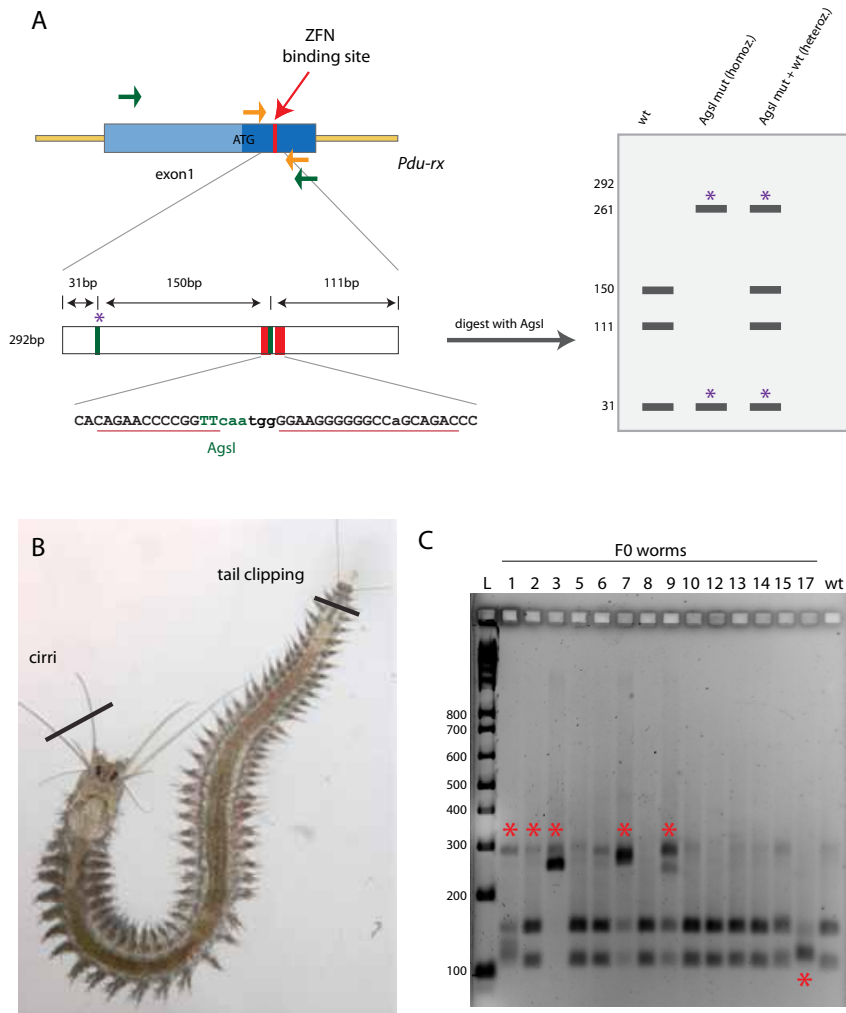


Figure 4.7: **Genotyping strategy for ZFN mutants.** A. The scheme shows the position of the primer pairs used to amplify 292bp flanking the ZFN binding site. The AgsI restriction site overlaps partially with the spacer between the two ZFNs binding sites; digestion of the 31bp wild type amplicon with AgsI produces fragments of 31, 111 and 150bp. A mutation of the second AgsI cutting site produces only two fragment, of 31 and 261bp. Since the first AgsI cutting site is polymorphic (asterisk), in some cases the absence of the second AgsI site produces a fragment of 292bp (undigested amplicon). B. Clipping of cirri or of the tail for the genotyping of F1 worms. Photo courtesy of Antje Fischer. C. Representative gel picture, showing the screening of different F0 worms. The 31bp digestion product ran out of the gel. The red asterisks indicate mutant F0 worms. In the number 17, the mutation was a large deletion of the *rx* locus, that's why the normal restriction fragments are not produced.

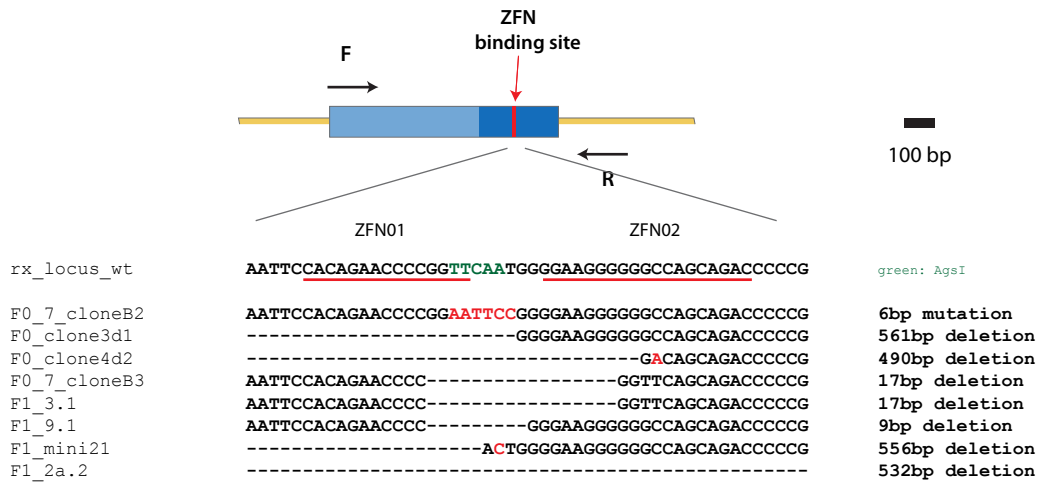


Figure 4.8: **ZFN-induced mutations in F0 worms and F1 lines.** The image shows representative mutant alleles identified after sequencing of F0 and F1 worms. Deletions were very frequent; insertions were never observed, while the NHEJ without insertions and deletions occurred only ones (F0_7_cloneB2). In the lines with large deletions (F0_clone3d1, F1_mini21) the deletion includes the start codon.

mutant AgsI site (example in fig. 4.7B).

The progeny of the founder worms (F1 generation) was screened further using a tail-clipping protocol, specifically developed for *Platynereis* (fig. 4.7B; see also par. 12.4). This showed that the F0 worms with an higher percentage of mutant alleles (as estimated by the restriction analysis) were those with an higher transmission rate to the germline. This is could be explained by the lineage relationships of the germline and most of the trunk of the adult worm, all coming from the D blastomere (Dorresteijn, 1990). An early mutation of the D lineage would then affect the majority of the cells in the body, and also all the germline.

Currently, 5 independent lines of heterozygotes worms are being raised in the lab. These lines were selected from 28 AgsI mutants, identified with the screening of about 150 F1 worms (from six different F0 founders). One of these lines has a deletion of 556bp, which eliminates the start codon (more examples of mutations are shown in fig. 4.8). The *rx*^{+/-} worms develop normally, are viable and will be crossed to produce mutant homozygotes offspring according to mendelian ratios.

5

FUNCTIONS OF RX DURING THE DEVELOPMENT OF THE DORSAL BRAIN

In vertebrates, Rx has a dual role: before differentiation, it sustains the proliferation of neural precursors both in the hypothalamus and in the eye field (VanDunk et al., 2011; Loosli et al., 2001, 2003; Andreazzoli et al., 2003; Casarosa et al., 2003); later, it is expressed in differentiated retinal photoreceptors, where it is necessary to maintain the expression of opsins (Pan et al., 2010; Wu et al., 2009; Kimura et al., 2000; Wang et al., 2004; Pan et al., 2006), but also in the pineal gland, where it is expressed rhythmically (Asbreuk et al., 2002; Rohde et al., 2011), in the pituitary (Medina-Martinez et al., 2009) and in deep brain photoreceptors (Deschet et al., 1999; Asbreuk et al., 2002).

In *Platynereis*, *rx* is expressed in neural precursors that give rise to the ciliary photoreceptors and to the lateral serotonergic cells (as shown in par. 3.4). Using the developmental knowledge from birthdating and lineage studies, my goal was to understand the contribution of Rx to the specification and differentiation of individual cell types in the dorsal brain region.

5.1. General considerations on the analysis of morphant phenotypes at 24hpf and 48hpf

In all the morpholino experiments, larvae were selected with stringent criteria before subsequent analysis. Embryos with defects in early development were easily excluded based on morphological landmarks, like the number of lipid droplets (in normal development, 4 lipid droplets are present from 8hpf onwards, so proper lipid droplet formation occurs before the onset of *rx* expression). Generally, at 24hpf *rxin1ex2* MO injected larvae were swimming slower than the *stctrl* MO larvae. These differences were attenuated or even not recognizable at 48hpf, when two subgroups of larvae could be identified: larvae with normal swimming, and larvae that were more stationary, in the bottom of the dish, despite they could still move (the pro-

totroch was intact). Consistently, after immunostaining and WMISH the phenotypes at 24hpf were more homogeneous, without huge differences between the individuals injected with the *rxin1ex2* MO. Viceversa, at 48hpf two phenotypic groups could be recognized after immunostaining of the axonal scaffold with an anti-acetylated tubulin antibody. Some larvae has mild defects in the axonal scaffold, but the general layout was still in place. Some other larvae instead had a severe phenotype, with a completely disorganized scaffold, where it was very hard to recognize the normal commissures and the main axonal tracts. Larvae with similar characteristics were never found in *stctrl* MO injected siblings, and in other independent injection experiments. Considering that *rx* is expressed very broadly in the brain before neural differentiation, and taking in account that is not very easy to inject constant volumes in *Platynereis* zygotes, the most plausible explanation is that the mild and severe phenotypes at 48hpf are cause by Rx loss of function, but they are produced by different amounts of morpholino. In the mild case, the axonal scaffold could develop almost normally (although other phenotypes at the level of gene expression can be identified). In the severe case, the animals did not recover after loss of Rx, but accumulated non-specific effects on top of the specific problems caused by Rx loss of function. This explains why the phenotypes at 24hpf are more homogeneous, and in principle argues against analyzing any phenotype at later stages. However, analysis at 48hpf was still used to pinpoint effects on the development of selected cell types, which cannot be recognized earlier.

5.2. Rx is necessary to the differentiation of ciliary photoreceptors

The role of *rx* in the differentiation of the deep brain ciliary photoreceptors was investigated with injection of *rxin1ex2* MO and immunostaining at 48hpf. The cPRCs can be easily visualized at 48hpf after immunostaining with an anti-acetylated tubulin antibody, which stains the huge cilia of these cells; since the cilia are not fully formed before 48hpf, scoring the larvae at earlier stages requires different methods. The injection of *rxin1ex2* MO produced a consistent decrease of the number of cPRCs compared to the larvae injected with *stctrl* MO (fig. 5.1); this result was reproducible in independent experiments, although the penetrance of the phenotype was different between different injection sessions (table 5.3). As an internal control, the development of the ventral nerve cord was analyzed, since *rx* is almost not expressed in the trunk. In most of the cases, the ventral nerve cord was developing normally; sometimes a slight retardation could be observed (shown in fig. 5.1A",B");

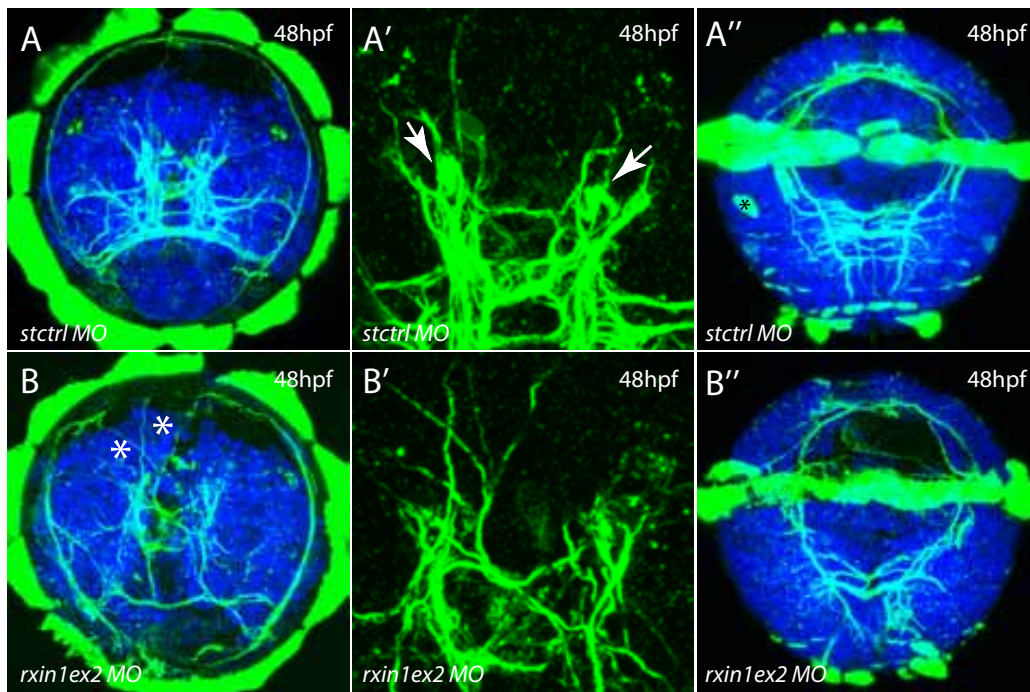


Figure 5.1: **Rx morpholino affects the differentiation of ciliary photoreceptors.** A. Axonal scaffold of a 48hpf larva injected with *stctrl* MO, apical view. A'. Magnification of the cPRCs region from the larva in A. (20 μ m Z-projection). The arrows point to the cilia of the cPRCs. A''. Ventral view of the larva shown in A. (The asterisk shows some unspecific tubulin staining). B. Axonal scaffold of a 48hpf larva injected with *rxin1ex2* MO, apical view. The asterisks indicate additional dorsal axons that connect to the prototroch nerve ring. B'. Magnification of the cPRCs region from the larva in B. The cilia of the cPRCs are not visible (15 μ m Z-projection). B''. Ventral view of the larva shown in B. The main connectives of the ventral nerve cord are present, although some defects can be observed in the commissure, probably because of a slight retardation.

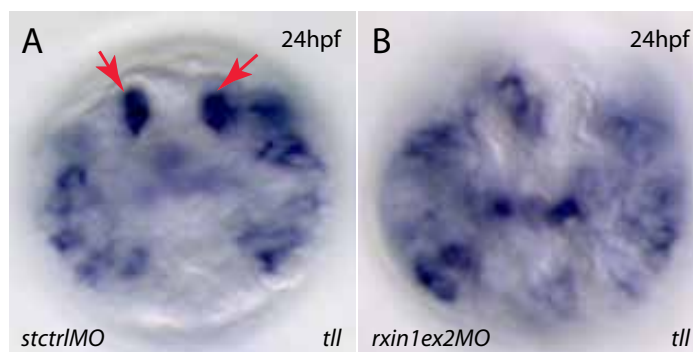


Figure 5.2: **Knockdown of rx reduces *tll* expression in the ciliary photoreceptors.** A. *tll* expression in a *stctrl* MO-injected 24hpf larva, apical view. The arrows point to the differentiating cPRCs. B. *tll* expression in a *rxin1ex2* MO-injected 24hpf larva, apical view. The large *tll* expression domains in the dorsal brain, corresponding to the developing cPRCs, are not visible.

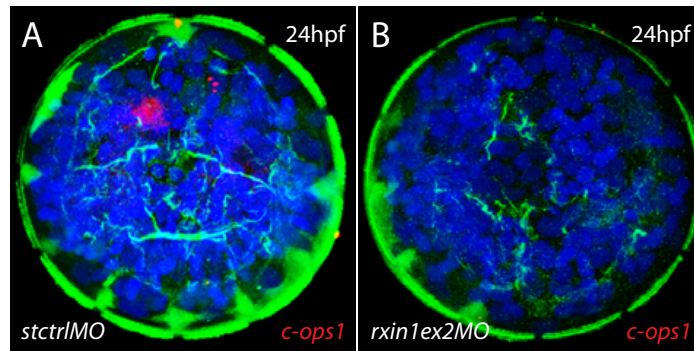


Figure 5.3: **Knockdown of *rx* reduces the expression of *c-ops1*.** A. *c-ops1* expression in a 24hpf larva injected with *stctrl* MO, apical view. B. *c-ops1* expression in a 24hpf larva injected with *rxin1ex2* MO, apical view. No *c-ops1*+ cell is present.

absence or severe retardation of the ventral nerve cord were considered signs of misdevelopment; those larvae were excluded from further analysis (par. 5.1).

To further investigate this phenotype, I analyzed the expression of the transcription factor *tll*. This gene has several expression domains in the brain, including the cPRCs precursors, which are distinguishable at 24hpf as two strong medio-dorsal spots of expression. The comparison of early expression patterns and developmental lineages suggests that *rx*-expressing NSCs produce *tll*+ intermediate progenitors, which then will produce the cPRCs (par. 3.4.3). Later, *tll* remains expressed in the cPRCs until the nectochaete stage (not shown). In *rxin1ex2* MO injected larvae, the expression of *tll* was severely affected compared to controls (fig. 5.2, table 5.3). Generally, the cPRCs expression domain was lost. In some cases, this was the only phenotype observed in morphants; more often, other expression domains were affected as well, and *tll* expression was reduced and/or disorganized (table 5.3). These phenotypes were never observed in *stctrl* MO injected larvae, so they are probably the consequence of Rx loss of function in other regions of the brain.

Finally, I checked *c-ops1* expression in *rx* morphants at 24hpf. At this stage, *c-ops1* is expressed in a cell on the left side of the episphere; this cell is the asymmetrical serotonergic cell (as described later in 6 and figure 6.4). Rx knockdown produced a significant loss of *c-ops1* expression, with an high penetrance, while control larvae showed normal *c-ops1* expression (fig. 5.3 and table 5.3). These phenotypes would indicate a role of Rx in the development of the asymmetric serotonergic cell. However, the lineage studies indicated that *rx* is never expressed in the lineage leading to the asymmetric serotonergic cell, but in adjacent cells of the dorsal brain (compare

Table 5.1: Loss of ciliary photoreceptors after *rx* loss of function.

exp. ID	stage	phenotype	<i>rxin1ex2</i> MO	<i>stctrl</i> MO	<i>p-value</i>
n1, AcTub ihc	48hpf	<4 cPRCs	33.3%, n=4	0	0.09638
		4 cPRCs (not affected)	66.7%, n=8	100%, n=10	
n2, AcTub ihc	48hpf	<4 cPRCs	50%, n=5	0	0.04412
		4 cPRCs (not affected)	50%, n=5	100%, n=7	
41.18, AcTub ihc	48hpf	<4 cPRCs	54.8%, n=17	5.3%, n=1	0.0005671
		4 cPRCs (not affected)	45.2%, n=14	94.7%, n=18	
		misdevelopers	n=7		
43.18, AcTub ihc	48hpf	<4 cPRCs	25%, n=2	0	0.183
		4 cPRCs (not affected)	75%, n=6	100%, n=10	
		misdevelopers	n=1		
exp. ID	stage	phenotype	<i>rxstcod2</i> MO	<i>stctrl</i> MO	<i>p-value</i>
12.18, AcTub ihc	48hpf	<4 cPRCs	55.6%, n=10	0	0.09638
		4 cPRCs (not affected)	44.4%, n=8	100%, n=4	
		misdevelopers		n=9	
exp. ID	stage	phenotype	<i>rxin1ex2</i> MO	<i>stctrl</i> MO	<i>p-value</i>
25.4, <i>tll</i> ish	24hpf	cPRCs domain missing	26.7%, n=4	10%, n=1	3.12e-05
		brain expr affected	66.7%, n=10	0	
		normal <i>tll</i> expression	6.7%, n=1	90%, n=9	
		misdevelopers	n=3		
54.18, <i>tll</i> ish	24hpf	cPRCs domain missing	23.1%, n=3	0	3.632e-06
		brain expr affected	61.5%, n=8		
		normal <i>tll</i> expression	15.4%, n=2	100%, n=15	
		misdevelopers	n=2		
53.18, <i>c-ops1</i> ish	24hpf	asymm. <i>c-ops1</i> cell absent	62.5%, n=25	3.6%, n=1	4.487e-07
		normal <i>c-ops1</i> expr.	37.5%, n=15	96.4%, n=27	
54.18, <i>c-ops1</i> ish	24hpf	asymm. <i>c-ops1</i> cell absent	72.3%, n=43	7.4%, n=2	1.413e-09
		normal <i>c-ops1</i> expr.	27.7%, n=13	92.6%, n=25	
48.18, <i>c-ops1</i> ish	24hpf	asymm. <i>c-ops1</i> cell absent	70.3%, n=26	11.1%, n=2	3.999e-05
		normal <i>c-ops1</i> expr.	29.7%, n=11	88.9%, n=16	

The table shows the analysis of phenotypes in different biological replicas. The number in “exp. ID” is a code for each injection session. The *p-value* is calculated after Fischer’s exact test. Misdevelopers are included for completeness, but not considered for the statistical test. For the scoring of the *tll* ish, “cPRCs domain missing” refers to the larvae where the dorsal *tll*-expression domains are missing, but the remaining *tll* expression sites in the brain are not affected; “brain expr affected” refers to larvae where the whole *tll* expression is affected (reduced and disorganized). ish= in situ hybridization, ihc= immunohistochemistry.

fig. 3.9). So it remains to be elucidated if the necessity of Rx for 24hpf *c-ops1* expression is cell-autonomous, or if it is indirect (i.e. if loss of Rx changes a signalling system necessary to specify the asymmetric serotonergic cell).

5.3. Roles of Rx in the development of the brain serotonergic system

The lineage analysis indicates that *rx* is expressed in the developing lateral serotonergic cells (par. 3.4). This is consistent with the later expression of *rx* in the same cells after differentiation. The same cells express also *pax6* and *otx* (see Chapter 7). For these reasons, I used serotonin immunostainings to investigate the effect of Rx loss of function on the development of the serotonergic system. The lateral serotonergic cells show serotonin immunoreactivity only after 34hpf, thus I analyzed their presence in *rx* morphants at 48hpf. With this experiment, I could observe occasionally the absence of one lateral serotonergic cell, and this was always concomitant to the loss of the neighboring cPRCs. However, the penetrance of this phenotype in morpholino experiments was very low, and these results were not easily reproducible (table 5.2). In this analysis, the severely affected larvae (par. 5.1) were always excluded; in the majority of these larvae, the lateral serotonergic cells were not present.

For these reasons, I investigated an alternative marker of the lateral serotonergic cells, which could more reliably show the eventual loss of the lateral serotonergic cells at earlier stages. The previous analysis (par. 3.4) indicated that the best marker is *pax6*, expressed at 24hpf in an isolated small group of cells of the dorsal episphere. Injection of *rxin1ex2* MO affected the expression of *pax6* in the brain (fig. 5.4, table 5.2). In the majority of the larvae, the lateral patches of *pax6* expression were disorganized, and the smaller dorsal expression domains were lost.

These results suggest that *rx* is involved in the development of the lateral serotonergic cells, consistent with the expression of this gene in this cell type throughout development and after differentiation. However, more experiments are needed to further substantiate this conclusion.

This hypothesis was tested further using overexpression experiments. The mRNA for *rx* was injected in zygotes, and sibling larvae were injected with *EGFP* mRNA as a control. The injection of *rx* mRNA (312.5ng/ul) did not have any obvious effect on the morphology and the behaviour of 48hpf larvae. These larvae had 4 lipid droplets, developed ciliary bands and did not show signs of misdevelopment or

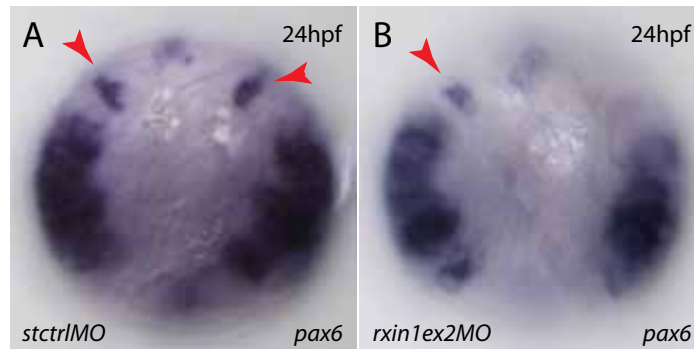


Figure 5.4: **Knockdown of *rx* reduces dorsal *pax6* expression.** A. *pax6* expression in a 24hpf larva injected with *stctrl* MO, apical view. The lateral dorsal domains giving rise to the lateral serotonergic cells are indicated by the red arrowheads. B. *pax6* expression in a 24hpf larva injected with *rxin1ex2* MO, apical view. Only one of the two lateral dorsal domains is present (arrowhead).

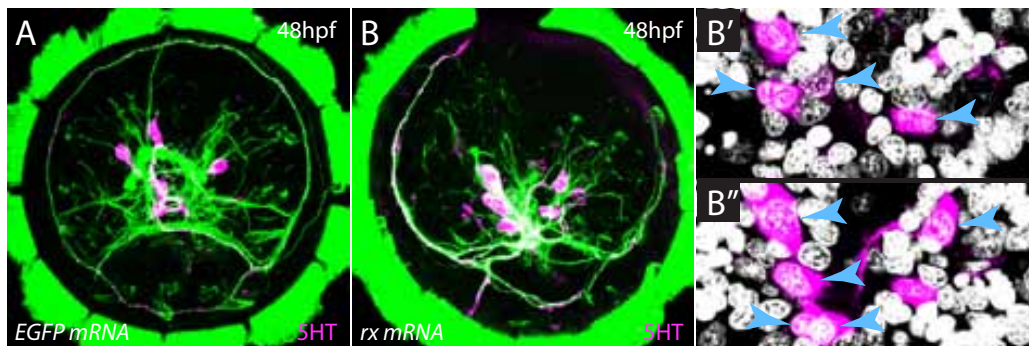


Figure 5.5: **Overexpression of *rx* promotes serotonergic differentiation.** A. Serotonin (magenta) and anti-acetylated tubulin (green) immunostaining of a 48hpf larva injected with *EGFP* mRNA, apical view. The larva has a normal axonal scaffold and four brain serotonergic cells, as in wild types. B. Serotonin (magenta) and anti-acetylated tubulin (green) immunostaining of a 48hpf larva injected with *rx* mRNA, apical view. This larva has a moderately-affected axonal scaffold, with all the neuronal processes concentrated in the ventral half of the brain. Nine brain serotonergic cells are present, most of them organized in lateral pairs. B' and B''. Magnification of the larva in B, showing the serotonin immunostaining together with DAPI (white). B' and B'' are two optical slices separated by 10 μ m. Different overlapping serotonergic cells are indicated by arrowheads.

Table 5.2: Role of Rx in the development of brain serotonergic cells.

exp. ID	stage	phenotype	<i>rxin1ex2</i> MO	<i>stctrl</i> MO	<i>p-value</i>
41.18, 5HT ihc	48hpf	<4 5HT cells	32.3%, n=10	5.3%, n=1	0.03893
		4 5HT cells (normal)	64.5%, n=20	89%, n=17	
		>4 5HT cells	3.23%, n=1	5.3%, n=1	
		misdevelopers	n=7		
43.18, 5HT ihc	48hpf	<4 5HT cells	12.5%, n=1	10%, n=1	1
		4 5HT cells (normal)	87.5%, n=7	90%, n=9	
		>4 5HT cells			
		misdevelopers	n=1		
28.4, <i>pax6</i> ish	24hpf	<i>pax6</i> expr. affected	58.3%, n=7	0	0.004577
		normal <i>pax6</i> expr.	41.7%, n=5	100%, n=12	
		>4 5HT cells			
		misdevelopers	n=6		
exp. ID	stage	phenotype	<i>rx</i> mRNA	<i>egfp</i> mRNA	<i>p-value</i>
24.18, 5HT ihc	48hpf	<4 5HT cells	21.1%, n=4	6.7%, n=1	0.01034
		4 5HT cells (normal)	36.8%, n=7	87%, n=13	
		>4 5HT cells	42.1%, n=8	6.7%, n=1	
		misdevelopers			
44.18, 5HT ihc	48hpf	<4 5HT cells	29.2%, n=7	0	0.08436
		4 5HT cells (normal)	50%, n=12	100%, n=7	
		>4 5HT cells	20.8%, n=5	0	
		misdevelopers			

The table shows the analysis of phenotypes in different biological replicas. The number in “exp. ID” is a code for each injection session. The *p-value* is calculated after Fischer’s exact test. Misdevelopers are included for completeness, but not considered for the statistical test. ihc=immunohistochemistry; ish=in situ hybridization.

toxicity. They were fixed at 48hpf and stained with anti-acetylated tubulin and anti-serotonin antibodies. Immunostaining at 48hpf revealed consistent differences in the axonal scaffold of *rx* mRNA injected larvae, compared to controls. The scaffold was disorganized, and neurites and nerve tracts were usually more concentrated in the ventral brain. Moreover, the number of brain serotonergic cells was significantly higher (fig. 5.5A-B and table 5.2). These additional serotonergic cells were organized in lateral “grapes”, in the position of the lateral serotonergic cells, and were connected to the rest of the nervous system (fig. 5.5B’-B”). Occasionally, ectopic serotonergic cells were observed at the level of the prototroch, but the significance of these phenotypes requires further investigations. These results indicate that *rx* can favor the serotonergic phenotype specifically in the lateral domains of the dorsal brain, in those lineages where it is expressed.

The expansion of the serotonergic cell population after upregulation of *rx* might involve the *otx* transcription factor. Indeed, *rx* and *otx* expression domains overlap

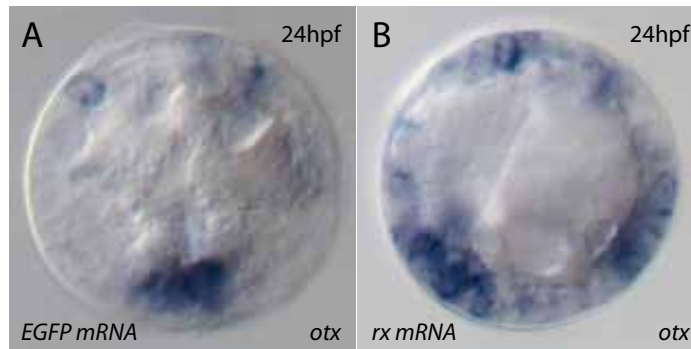


Figure 5.6: **Overexpression of *rx* expands the *otx* expression domain.** A. *otx* expression of a 24hpf larva injected with *EGFP* mRNA, apical view. The photo is focused at the level of the prototroch. B. *otx* expression of a 24hpf larva injected with *rx* mRNA, apical view. The photo is focused at the level of the prototroch, where *otx* expression is expanded compared to controls.

in the lateral episphere, where the lateral serotonergic cells will develop, and *otx* expression is maintained later in these cells after terminal differentiation. Then I tested the effects of *rx* overexpression on *otx* expression at 24hpf. Consistently, *rx* mRNA injection induced a strong upregulation of *otx*, specifically in the lateral episphere (fig. 5.6).

Next, I asked if *otx* expression is affected by Rx downregulation. This was not the case: larvae injected with *rxin1ex2* MO showed no significant change in *otx* expression pattern compared to control larvae. These results are consistent with the developmental data (par. 3.4), which show that *otx* expression precedes the onset of *rx* expression. Probably, Rx can reinforce *otx* expression, but it is not primarily involved in establishing its expression.

5.4. General effects of Rx loss of function on brain development

The immunostainings with anti-acetylated tubulin antibody at 48hpf showed additional defects in brain morphogenesis. The most significant phenotypes could be identified in the dorsal brain, where the asymmetric axon was either not connected properly to the prototroch nerve ring, or was “duplicated” (fig. 5.1). Thus, to reveal additional effects of *rx* on brain development, I investigated the expression of genes preferentially expressed in the dorsal episphere.

One of the genes chosen is the transcription factor *tbx2/3*; this gene has a peculiar expression domain, since it appears in the apical organ and in the most dorsal cell populations, including the midline, at about 15hpf, where it partially overlaps with

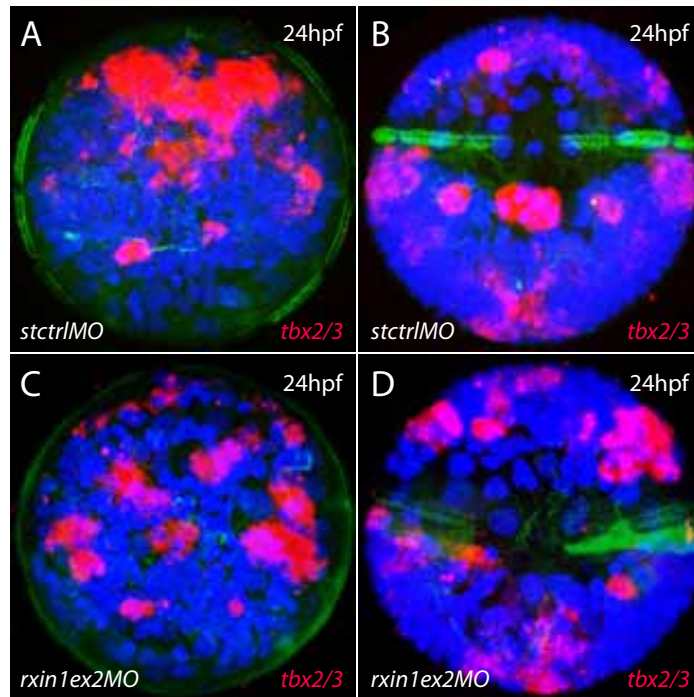


Figure 5.7: **Knockdown of *rx* affects the expression of *tbx2/3*.** A. *tbx2/3* expression of a 24hpf larva injected with *stctrl* MO, apical view. B. *tbx2/3* expression of a 24hpf larva injected with *stctrl* MO, ventral view of the larva in A. C. *tbx2/3* expression of a 24hpf larva injected with *rxin1ex2* MO, apical view. The dorsal expression of *tbx2/3* is severely reduced. The apical organ expression is not affected. Moreover, *tbx2/3* expression is expanded in the lateral brain. D. *tbx2/3* expression of a 24hpf larva injected with *rxin1ex2* MO, ventral view of the larva in C. The ventral expression of *tbx2/3* is mostly the same as in the control larva, with the exception of the expression in the stomodeum.

rx expression (cfr. par.3.4). Interestingly, in *rxin1ex2* MO injected larvae at 24hpf the expression of *tbx2/3* was reduced in the dorsal brain, but not in the apical organ, while the expression was expanded in lateral-ventral domains (fig. 5.7A,C). The specificity of this phenotype was evaluated using the trunk expression of *tbx2/3* as an internal control: in this way, it was possible to estimate the number of misdevelopers or severe retardation events, and exclude these embryos from the analysis (fig. 5.7B, D). Moreover, showing that only a fraction of the injected larvae had no specific phenotypes, this estimate gave confidence on other phenotypes described previously, where the genes analyzed (like *c-ops1*) are restricted to the brain or even to few cells of the brain.

The *tbx2/3* phenotypes were characterized by a general decrease of the total cell number in the brain. This raised the question whether Rx activity in the brain during early development is required to keep the proliferative state of neural progenitors.

A similar hypothesis could also explain the increase of the number of serotonergic and *otx* expressing cells after Rx gain of function. To test this hypothesis, I checked the expression of the proneural transcription factor *neurogenin* (*ngn*) at 24hpf. In control larvae, *ngn* expression is enriched in the lateral dorsal episphere, where there is still sustained proliferation at 24hpf (as shown by live imaging and EdU experiments, cfr. Chapter 3). In *rxin1ex2* MO injected larvae, the expression of *ngn* was generally disorganized, and severely reduced, especially in the lateral dorsal domains. This further suggests that Rx has a role in maintaining the proliferative state of neural progenitors, and it is consistent with its extremely dynamic expression pattern throughout development.

Table 5.3: Effects of Rx knockdown on the expression of brain markers.

exp. ID	stage	phenotype	<i>rxin1ex2</i> MO	<i>stctrl</i> MO	<i>p-value</i>
25.4, <i>tbx2/3</i> ish	24hpf	brain expr. affected	64.7%, n=11	0	5.353e-06
		normal <i>tbx2/3</i> expr.	35.3%, n=6	100%, n=23	
		misdevelopers	n=13	0	
54.18, <i>tbx2/3</i> ish	24hpf	brain expr. affected	28.6%, n=8	0	0.006385
		normal <i>tbx2/3</i> expr.	71.4%, n=20	100%, n=22	
		misdevelopers	n=4	0	
6.4, <i>ngn</i> ish	24hpf	brain and trunk affected	25%, n=1	0	0.0007326
		brain affected, trunk normal	75%, n=3	0	
		normal <i>ngn</i> expr.	0	100%, n=11	
		misdevelopers	n=1	0	
58.18, <i>ngn</i> ish	24hpf	brain and trunk affected	32.4%, n=11	0	8.975e-10
		brain affected, trunk normal	52.9%, n=18	12.1%, n=4	
		normal <i>ngn</i> expr.	14.7%, n=5	87.9%, n=29	
		misdevelopers	n=2	0	

The table shows the analysis of phenotypes in different biological replicas. The number in “exp. ID” is a code for each injection session. The *p-value* is calculated after Fischer’s exact test. Misdevelopers are included for completeness, but not considered for the statistical test. ish=in situ hybridization.

The experiments discussed above are the first gene functional experiments ever attempted in *Platynereis*. These experiments could establish some roles of Rx in the development of ciliary photoreceptors and serotonergic cells, cell types that belong to the larval circadian system. A similar role for Rx has been shown in vertebrates, where this transcription factor is essential for eye development, but also important for the correct development and functioning of the hypothalamus and the pineal. However, further experiments in *Platynereis* are needed to understand more precisely

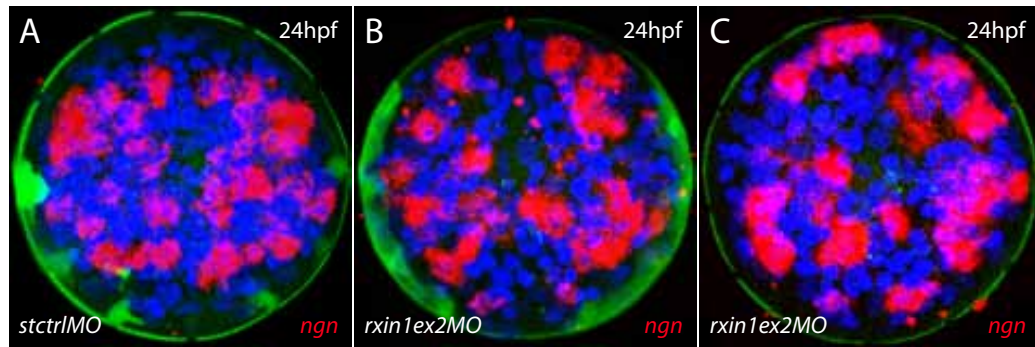


Figure 5.8: **Knockdown of *rx* reduces the expression of *ngn*.** A. *ngn* expression in a 24hpf larva, injected with *stctrl* MO, apical view. B. and C. *ngn* expression in a 24hpf larvae, injected with *rxin1ex2* MO, apical view. The pattern of *ngn* expression is disorganized and overall reduced compared to controls.

the developmental roles of Rx. Indeed, the use of morpholinos to knock down gene expression has very well known issues about specificity, which are aggravated by using them in a new model system, where functional studies were never performed so far. For this reason, this description of Rx function is very conservative and does not include (numerous) other phenotypes that were observed after WMISH on morphant larvae. The development of mutant lines with the ZFN technology will allow to achieve a more complete description of Rx loss of function phenotypes, and together will offer the opportunity to test Rx function with complementary techniques (like RNA-seq and CHIP-seq), which require larger numbers of larvae.

6

ROLE OF THE LARVAL CIRCADIAN SYSTEM IN THE CONTROL OF RHYTHMIC BEHAVIOUR

6.1. Circadian clock markers are expressed at early larval stages

The EdU and time lapse analysis described in chapter 3 shows that the cells of the clock region in the dorsal brain are among the first ones to develop in *Platynereis* larval brain. Most of them belong to the same neuronal lineage (the “blue” lineage in ch. 3) and are postmitotic at 30hpf. Thus the larval circadian system is established and functional in trochophore larvae. To further confirm this hypothesis, I analyzed the expression of circadian marker genes at several larval stages (24hpf, 34hpf and 48hpf).

The only indication for an association of the dorsal brain with the circadian clock was the expression of *bmal* in this region at 48hpf (Arendt et al., 2004). Thus I reinvestigated the expression of *bmal* at earlier stages and, as expected from the birthdating data, I found *bmal*+ cells in the cPRCs region already at 34hpf, and few *bmal*+ cells at 24hpf (fig.6.1A-B).

To extend these findings, I searched other circadian markers in the *Platynereis* genome and transcriptome. In this way, I identified a new member of the *cryptochrome* gene family, called (*cry1*) for its similarity to the *Drosophila dCRY* gene (compare fig. C.1 in Appendix C). Like *bmal*, *cry1*+ cells are present in the dorsal brain at 34hpf (fig.6.1D); later, *cry1* expression is robustly associated to the cPRCs region (fig.6.1E). At 5dpf, *cry1* expression expands to include the so-called “posterior brain lobes”, which probably correspond to the cell bodies of the nuchal organs (fig.6.1F).

Moreover, I could identify the *Platynereis* homolog of *period* (*per*), a key transcription factor of the molecular oscillator, both in *Drosophila* and in vertebrates (see par. 2.2 and Cermakian and Sassone-Corsi 2000). Unfortunately, its spatial distribution was hard to document with WMISH at early stages. However, *per* expression pattern at 5dpf is very similar to *cry1* (fig.6.1C).

Taken together, these results show that differentiated neurons of the larval circa-

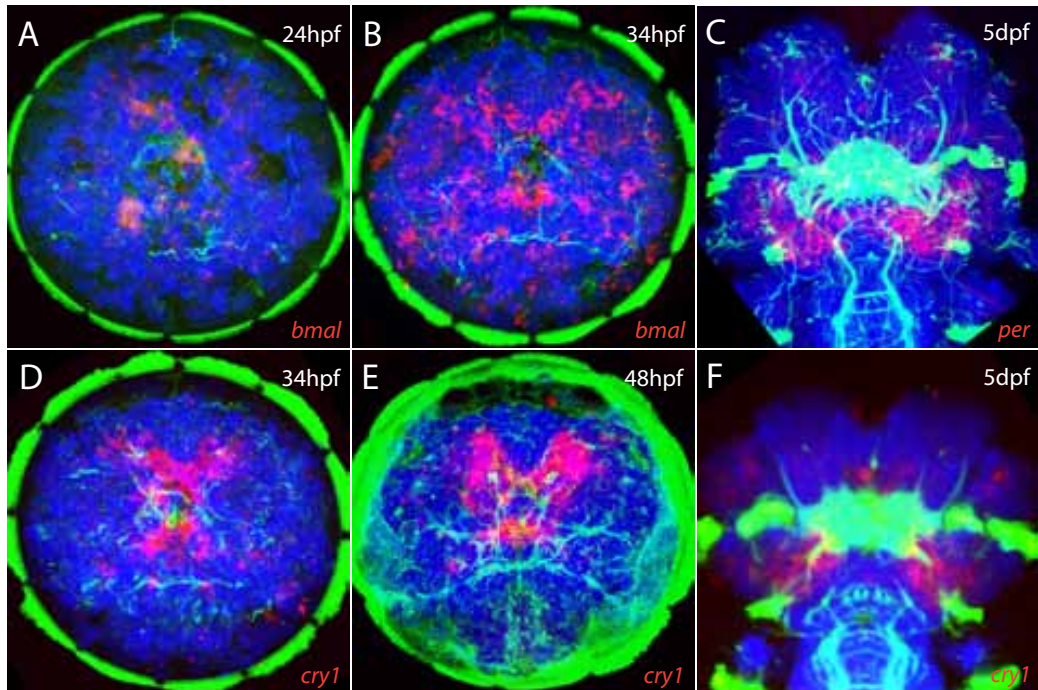


Figure 6.1: **Expression of circadian markers at different developmental stages.** A. Expression of *bmal* in the brain at 24hpf, apical view. B. Expression of *bmal* in the brain at 34hpf, apical view. C. Expression of *per* in the posterior brain at 5dpf, dorsal view. D. Expression of *cry1* in the brain at 34hpf, apical view. E. Expression of *cry1* in the brain at 48hpf, apical view. F. Expression of *cry1* in the posterior brain at 5dpf, dorsal view. In all the images, red is gene expression, blue is DAPI and green is acetylated or tyrosinated tubulin staining.

dian clock exist at early larval stages (certainly at 34hpf, few neurons even at 24hpf). The analysis of these new markers extends the observations in Arendt et al. (2004), and confirms further that the medio-dorsal brain of *Platynereis* larvae is the site of the central clock (peripheral clocks might exist or develop later). Although there aren't yet studies addressing the molecular mechanism of *Platynereis* clock machinery, preliminary qPCR data indicate that the transcript levels of *per*, *cry1* and *bmal* truly oscillate during the light-dark cycle, and with different phases (not shown), suggesting that the annelid circadian clock is based on a transcriptional oscillator, as documented in other species (par. 2.2 and Young and Kay 2001).

6.2. The larval circadian system controls rhythmic locomotion

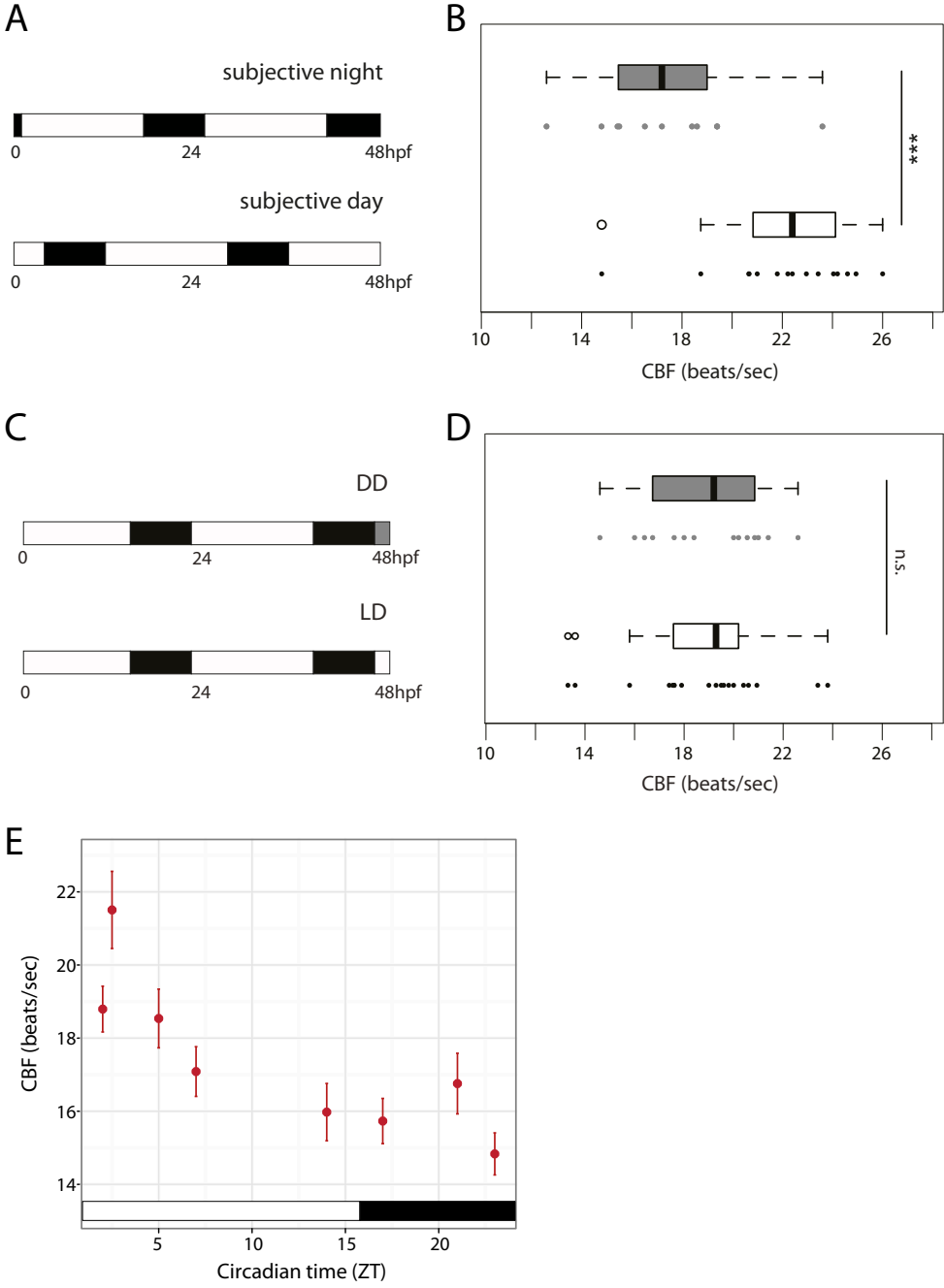
The expression of circadian markers in the dorsal brain from early stages indicates that the larval circadian system is established and functional in trochophore

larvae. During this stage, *Platynereis* larvae swim in the water column and are positively phototactic (Jékely et al., 2008). They might also respond already to other sensory cues like chemicals and gravity, as suggested by the presence of different kinds of sensory neurons and the effect of neuropeptides released by these neurons on swimming depth (Conzelmann et al., 2011). Moreover, it is known that marine larvae adjust their position in the water column according to day-night rhythms (Rhode et al., 2001; Hansson et al., 2007b); this daily rhythm of zooplankton, called diel vertical migration, has been suggested to be the first manifestation of circadian clocks in animal history (Pittendrigh, 1993). This points to a role of the larval circadian system in the regulation of locomotor activity, through a direct control of the locomotor system or an indirect modulation of the activity of sensory neurons.

In *Platynereis* trochophore larvae, locomotion is entirely based on the activity of the prototroch cells, and the beating of the prototroch's cilia propels the larvae forward. The swimming depth is modulated via changes in the ciliary beating frequency (CBF): the increase of CBF corresponds to upward swimming in the water column, while decrease of CBF or arrest of cilia activity lead to the sinking of the larvae (Conzelmann et al., 2011).

Thus, to assess the functionality of the circadian system, I used the CBF as the behavioral assay. The CBF can be measured with high-resolution recordings of larvae mounted between a slide and a coverslip (see Chapter 13 for details). First, I tested if there is a circadian rhythm in CBF. For this purpose, I raised sibling larvae in two op-

Figure 6.2 (on the next page): **Circadian regulation of ciliary beating frequency.** A. Experimental design to test the difference of CBF between subjective day and subjective night. Sibling larvae were subdivided into two groups after fertilization, and raised in opposite light-dark cycles (16L:8D). Larvae were assayed at 48hpf, during the subjective day (ZT12) or the subjective night (ZT23), according to the experimental group. B. CBF (beats/second) of 48hpf larvae from the two experimental groups in A. The larvae in subjective night (gray bar, n=11) have a CBF significantly lower than the larvae in subjective day (white bar, n=15). (p -value= 0.0003299, unpaired t test). C. Experimental design to test the circadian dependence of CBF. Sibling larvae were raised in the same light-dark cycle (16L:8D, fertilization at ZT2). The experimental group was kept in constant darkness (DD) after the second night, while the control remained in the normal light-dark (LD) cycle. D. CBF (beats/second) of 48hpf larvae from the two experimental groups in C. The larvae in DD (gray bar, n=14) and the controls in LD (white bar, n=19) do not have significantly different CBFs (p -value= 0.9247, unpaired t test). E. CBF (beats/second) at different circadian time points (ZT). The plot represents mean \pm SEM of the CBF measured in 48hpf larvae from different batches (total number of larvae = 117). The results were not compared directly because of batch-to-batch variability in CBF, however this plot shows how generally the CBF is always lower in the subjective night compared to subjective day.



posite light-dark regimes and assayed their CBF at the early metatrochophore stage (48hpf, fig. 6.2A). The CBF was significantly lower during the subjective night compared to subjective day (fig. 6.2B). This experiment showed that there are significant (and measurable) differences in CBF between day and night, meaning that the larval locomotor activity changes in the light-dark cycle. Independent measurements of CBF, in 48hpf larvae from different batches and at different circadian points, confirms that CBF is normally lower in the subjective night compared to daytime (fig. 6.2E).

Next, I tested if these differences in CBF were purely light dependent or controlled by a circadian clock. In case of a circadian control of CBF, after the initial entrainment larvae kept in constant darkness should keep the circadian rhythm of CBF, as if they were in the normal light-dark cycle. To check this, I compared the CBF of sibling larvae, where a group was kept in the normal light-dark cycle and a second group was transferred to constant darkness after one day of entrainment (fig. 6.2C). Larvae kept in constant darkness (DD) after entrainment showed no significant difference in CBF compared to larvae kept under a normal light-dark cycle (LD, fig. 6.2D). This clearly indicates that the modulation of CBF is under circadian control, thus the larval circadian system controls the activity of the prototroch cells.

6.3. The clock cells are sensory and express different kinds of opsins

The existence of a larval clock entrained by light raises the question of how the photic input reaches the molecular clock for entrainment. A first candidate is Cry1, which is homologous to the insect light-sensitive cryptochromes (fig. C.1). As shown in *Drosophila*, it is possible that a light-responsive Cry1 interacts directly with the components of the molecular oscillator (par. 2.2).

A second input to the clock might be provided by opsins. *c-ops1* is expressed in the cPRCs and few other cells of the clock region (Arendt et al., 2004). I investigated further the presence and the expression of opsins in *Platynereis* larvae, in order to obtain a complete picture on the possible photic inputs to the clock.

6.3.1. The opsin repertoire of *Platynereis*

In order to identify additional opsins involved in the entrainment of the larval clock, I investigated the expression of all the opsins present in the *Platynereis* transcriptome and genome (in collaboration with Dr. Pavel Vopalensky, who characterized the rhabdomeric opsins).

As reviewed in the Introduction, the bilaterian opsins can be subdivided into three major groups: the ciliary opsins, the rhabdomeric opsins, and the neuropsin/peropsin/ G_o group (par. 2.1.2). There are two c-opsins in *Platynereis* genome; they both have a genomic structure typical of the ciliary opsin group, with intron positions shared with vertebrate c-opsins (not shown). Moreover, additional non-rhabdomeric and non-ciliary opsins were identified in the genome. Phylogenetic analysis of these new opsins from *Platynereis* and other lophotrochozoans (the annelids *Capitella teleta* and *Helobdella robusta*, and the mollusc *Lottia gigantea*) show unambiguously that distinct neuropsins, peropsins and G_o -opsins exist in lophotrochozoans (Appendix C and Dr. G. Jekely, personal communication). Moreover, the conservation of intron positions in *Platynereis* neuropsin, peropsin and G_o -opsin confirms that these opsins belong to the same clade, as also suggested by a recent analysis of amphioxus opsins (fig. 6.3, and Albalat 2011). The conservation of key residues for G-protein binding and signal transduction indicate that all these opsins might potentially signal the presence of light.

This analysis indicates that distinct neuropsins, peropsins and G_o -opsins were present in the urbilaterian ancestor (neuropsins were previously considered vertebrate-specific opsins).

6.3.2. Expression of opsins in the *cry1* region

The presence of a circadian behavior at 48hpf proves that the circadian system is functional at this stage, and entrained by light. In the circadian experiment described previously (fig. 6.2C-D), the animals underwent a light-dark transition at 14hpf, a dark-light transition at 22hpf, and a last light-dark transition at 38hpf. This indicates

Figure 6.3 (on the next page): **Alignment and genomic structure of opsins.** Alignment of the protein sequences of representative lophotrochozoan and human opsins. The alignment is colored based on the percentage of identity. Exon-exon boundaries are indicated by vertical red bars. The green box highlights the D/ERY motif, generally conserved in opsins. The yellow box indicates the conserved lysine (K) covalently linked to the 11-*cis*-retina. The red box surrounds the conserved NPxxY(x)_{5,6}F motif. The yellow asterisks indicate conserved cysteine (C) residues. The green arrowhead shows a conserved tyrosine (Y), that provides the negative counterion. The red arrowhead shows the conserved glutamate (E). See ? for details. The alignment includes the following opsins: neuropsins (*Lottia gigantea*, jgi id: 103802; *Homo sapiens* EAX04324.1); peropsins (*Lottia gigantea*, jgi id: 154374; *Homo sapiens* NP_006574.1); human RGR (NP_001012738.1) and the *Platynereis* neuropsin, peropsin and G_o -opsin. The lack of an exon in *Pdu-neurops* is probably the consequence of alternative splicing (currently under investigation).

6. Role of the larval circadian system in the control of rhythmic behaviour | 97

NEUR_Lottia_gigantea/1-371	1 - M E S F N D I - - - - - H C I S S H T F T L N V F I F S V C T S I L 29
NEUR_Platynereis_dumerilii/1-296	1 - - - - - G P D S R D P V - - - - - T Q L G V L S I L 17
RGR1_Homo_sapiens/1-291	1 - M A E T S A L P T G - - - - - F G E L E V L A V G M V L L V E A L S G L S 32
C-OPS2_Platynereis_dumerilii/1-352	1 - M D D L G F L G N S S V N Y T V P L L Q E D P L L R I L Y F G P T S Y V I T A I N L C I V G V I G T L 52
PER1_Homo_sapiens/1-337	1 - M L R N N L G N S S D S K N E D G S V - - - - - F S Q T E H N I V A T Y L I M A G M I S I I 41
PER_Platynereis_dumerilii/1-313	1 - M E N H S Y H N T T I M P H S D N T S Y Q - - - - - H D F L F H S I T G I G Y L I I G I L G I 43
NEUR_Lottia_gigantea/1-298	1 - - - - - M T A A E - - - - - F S S F E H S I V G I T Y M V I G I S G T L 27
NEUR1_Homo_sapiens/1-353	1 M A L N H T A L P Q D E R L P H Y L R D G D P F A S K - - - - - L S W E A D L V A G F Y L T I I G I L S T F 49
GoOPS_Platynereis_dumerilii/1-412	1 M E F N H T T E D S Y N S T F D F I T Y G T H V E I Y K R P D I Q P R V Y M V I G V Y L T I A G I I S T V 53
NEUR_Lottia_gigantea/1-371	30 M N S L I L F V L Y Q H R - S R L M F T D Y F I V S L A I T D L G S P L F A Y P M A C T S Y S H K W L Y 81
NEUR_Platynereis_dumerilii/1-296	18 L N V L V I L T V L C R R - R S V S P L E I Y V I N M A V V D L C P T V L A Y P S T T A S A F N H G W I L 69
RGR1_Homo_sapiens/1-291	33 L N T L T I F S F C K T P - E L R T P C H L L V L S L A L A D S G I S L N A L - V A A T S L L R R W P Y 83
C-OPS2_Platynereis_dumerilii/1-352	53 S N G V I M Y L Y F K D K - S L R S P M N L L F V N L A M S D F T V A F F G A M F Q G L T C T R K Y M S 104
PER1_Homo_sapiens/1-337	42 S N I I V L G I F I K Y K - E L R T P T N A I I I N L A V T D I G V S S I G Y P M S A A S D L Y G S W K F 93
PER_Platynereis_dumerilii/1-313	44 G H V T L A A L F S R E N - L V S R G S A A V H V A M A I S N A G V - L A G F P F T A S A F A G R W L F 94
NEUR_Lottia_gigantea/1-298	28 L S L L V A L T F I R E K G L F K Y G R A W L H I S L A I A N V G V - V G A F P F S G S S F S G R W L F 79
NEUR1_Homo_sapiens/1-353	50 G N G Y V L Y M S S R R K - K K L R P A E I M T I N L A V C D L G I S V V G K P F T I I S C F C H R W V F 101
GoOPS_Platynereis_dumerilii/1-412	54 G N S V V I G V V V K N E L R K Q G H N I L L L N L A I C D L G F T F V G Y P L T A S S A F A Q R W L F 106
NEUR_Lottia_gigantea/1-371	82 - K D I E C Q I N G E L G F Y F G I C G M E T L A V M S F V R Y I K I C H R R Y A A R L N D C W - T Y F M 132
NEUR_Platynereis_dumerilii/1-296	70 - G D T - - - - - D M V N R R F - V L L T 83
RGR1_Homo_sapiens/1-291	84 - G S D G C Q A H G F O G F V T A L A S I C S S A A I A W G R Y H H Y C T R S Q L A W N S - - - - - A V S L 131
C-OPS2_Platynereis_dumerilii/1-352	105 P G M A L C D F Y G E I T F L G S L A S E M N L F I I S V E R Y L A V V R P F D V G N L T N R R - V I A G 156
PER1_Homo_sapiens/1-337	94 - G Y A G C Q V Y A G L N I F F G M A S I G L L T V V A V D R Y L T I C L P D V G R R M T T N T - Y I G L 144
PER_Platynereis_dumerilii/1-313	95 - G E A G C Q F Y A F E G M F F G I S S I L L G V L S V D R F I N I H W P Q Y Y G D L Y L R P - Y W L A 145
NEUR_Lottia_gigantea/1-298	80 - G S G M C T F Y G E I G M F F G I A A I G N V F A L C V E R Y L V S K K K D S V D K V S N Q F - Y W M I 130
NEUR1_Homo_sapiens/1-353	102 - G W I G C R W Y G W A G F F F G C G S L I T M T A V S L D R Y L K I C Y L S Y G V W L K R K H - A Y I C 152
GoOPS_Platynereis_dumerilii/1-412	107 - G H L G C V I Y G E C C T V L A L T D I N I L M A L S I Y R Y I V I C K P H I R H I L H R R T V A A M 158
NEUR_Lottia_gigantea/1-371	133 I I A I Y V S C A I I A G C P F F S W G E Y D L E I F G T S C S V V W - - R K R D L G Y I T F I M - - - I 180
NEUR_Platynereis_dumerilii/1-296	84 L I P Y Y G N A L I W C F T P L V G W G R Y G P E S S G I S C A L E W - - - - - H H L P L S Y V I K I F V 131
RGR1_Homo_sapiens/1-291	132 V L F W L S S A F W A A L P L L G W G H Y D E P L G T C C T L D Y - - - S K G D R N F T S F L F T M S F 182
C-OPS2_Platynereis_dumerilii/1-352	157 G V F W W L Y S L V F A G G P L V G W S S Y R P E G L G T W C S I S W - - Q D R S M N T S Y V T A F V L 207
PER1_Homo_sapiens/1-337	145 I L G A W I N G L F W A L M P I I G W A S Y A P D P T G A T C T I N W - - R K N D R S F V S Y T M T V I A 195
PER_Platynereis_dumerilii/1-313	146 I L V C Y L T A A F W S T V P I V G W A R Y A L D K T H V A C V D W - - A N P T S S Y K S Y I F A I T M 196
NEUR_Lottia_gigantea/1-298	131 T A L V W I N A F F W G I M P A L G W T S W D I E P S G T S C T I K W - - Q N Y D S G Y S F M A M S L 181
NEUR1_Homo_sapiens/1-353	153 L A A I W A Y A S F W T T M L V G L G D V P E P P F G T S C T L D W W L A Q A S V G G Q V F I L N I L F 205
GoOPS_Platynereis_dumerilii/1-412	159 V T S C W V Y S L L W G V A A L V G W N R Y T N E A F G T S C S I D W - - T A R G A S D L S Y T I L M I F 209
NEUR_Lottia_gigantea/1-371	181 T C L V I P F F V M C A S Y I G I V R V T R - - - - - C Y A K A S R S K H S A I L T R V Y V L Y 223
NEUR_Platynereis_dumerilii/1-296	132 T G F L M P V A I M I F C Y G C I I R E V - - - - - Y I T Q K G T Q M I R K R - M D I Y M - 170
RGR1_Homo_sapiens/1-291	183 F N F A M P L F I T I T S Y S L M - - - - - E Q K L G K S G - - - - - H L - 209
C-OPS2_Platynereis_dumerilii/1-352	208 G C Y F F P V S I I I F C Y F N V W R K V K - - - - - E A A D A Q G G A G T A G K A E K S I - - 248
PER1_Homo_sapiens/1-337	196 I N F I V P L T V M F Y C Y Y H V T L S I K H H - - - - - T T S D C T E S L N R D W S D Q I D V - 238
PER_Platynereis_dumerilii/1-313	197 S C F M L P Y A L M A I G F I R T - - - - - C L G R K A T S T N V E K L S D R D H - 232
NEUR_Lottia_gigantea/1-298	182 T C F L I P L P V A L I C L I L S G - - - - - T D K I T E D K E E K T Y F R E D Q L - 218
NEUR1_Homo_sapiens/1-353	206 F C L L P T A V I V F S Y V K I I A K V K S S S K - - - - - E V A H F D S R I H S H V L E M K L - 250
GoOPS_Platynereis_dumerilii/1-412	210 F C Y I S H I I V M T F C Y Y K I K Q R S S L M L S R L R N H H K F S A E D A V L I N N I R N E K R L - 260
NEUR_Lottia_gigantea/1-371	224 F Q T T L F M C I A F V S A W M P Y A V I S M L S V L Y D R E V V T E D I S I V P H L V A K S S H L L N P 276
NEUR_Platynereis_dumerilii/1-296	171 I K M T I M T L C F L V A W T P Y A V A F L A T E P W S Q E I S V T L S V A S S F L A K S S F Y N P 223
RGR1_Homo_sapiens/1-291	210 Q V N T T L P A R T L L L G W G P Y A I L Y L Y A V I A D V T S I S P K L Q M V P A L I A K M V P T I N A 262
C-OPS2_Platynereis_dumerilii/1-352	249 F R M S V I M V T C Y L T A W T P Y A I V C L I A S Y G P P N G L P I Y A E V L R S L F A K S S Q V Y N P 301
PER1_Homo_sapiens/1-337	239 T K M S V I M I C M F L V A W S P Y S I V C L W A S F G D P K K I P P M A I I A P L F A K S S T F Y N P 291
PER_Platynereis_dumerilii/1-313	233 D L I V R S L S I V S M V T W T P F A L L C L Q F L V R D P Y D T S I T M A A M P A L I C K A V T A G V P 285
NEUR_Lottia_gigantea/1-298	219 R S T C T F L L I L A L I G W G P Y C F I C I W A L F A D T T Q V S M L A A V I P P L A A K T M V L L Y P 271
NEUR1_Homo_sapiens/1-353	251 T K V A M L I C A G F L I A W I P Y A V V S V W S A F G R P D S I P I Q L S V V P T L L A K S A A M Y N P 303
GoOPS_Platynereis_dumerilii/1-412	261 T V M T M V M V G G F I L V W S P Y A W V A W K I V V - P D G V P D W L T T F P T M F A K A T P M L N P 312
NEUR_Lottia_gigantea/1-371	277 V V Y F F M N N K Y Q R Y V V G M V R R M C N C K K E P T E E T R M T S G G E L V S S N K Q R E K D V E M 329
NEUR_Platynereis_dumerilii/1-296	224 I V Y V F T V K R F R R E V I E V - - - - - L R C S V T K D T N A T M A T - - - - - 255
RGR1_Homo_sapiens/1-291	263 I N Y A L G N E M V C R G I - - - - - W Q C L S P Q K R E K D R T K - - - - - 291
C-OPS2_Platynereis_dumerilii/1-352	302 I I Y V L M N K P Y R S A L V S L - - - - - V C R G R N P F D E A G G T A G - - - - - 334
PER1_Homo_sapiens/1-337	292 C I Y V V A N K K F R R A M L A M - - - - - F K Q T H Q T M P V T S I L - - - - - 323
PER_Platynereis_dumerilii/1-313	286 L V Y A V C S A E I R Y S I K H M - - - - - F S T T C P E R K R T - - - - - 313
NEUR_Lottia_gigantea/1-298	272 V A Y C Q G N K R F K N A F L G M - - - - - F I F N E S P K Q Q - - - - - 298
NEUR1_Homo_sapiens/1-353	304 I I Y Q V I D Y K F - - - - - A C C Q T G G L K A T K K K S - - - - - 328
GoOPS_Platynereis_dumerilii/1-412	313 L I Y V S T N R K F R R E A R G M L R R W C C F S A K V D D I V A S A I R N R Q A S P K E K R V Y F V N 365
NEUR_Lottia_gigantea/1-371	330 E K I N Y K K V P K Q D I G N E V E L E S S S D D S S D P K D N E K N E Q E N T V L - - - - - 371
NEUR_Platynereis_dumerilii/1-296	256 - - - - - N F N L N E V K R P L D N Q K E S E F L L S D I H N K S R S E P S T D V R G S K E - - - - - 296
RGR1_Homo_sapiens/1-291	335 - - - - - G T T A K D E T L G K G N K V A A A - - - - - 352
C-OPS2_Platynereis_dumerilii/1-352	324 - - - - - P M D V S Q N P L A S G R I - - - - - 337
PER1_Homo_sapiens/1-337	329 - - - - - L E G F R L H T V T T V R K S S A V L E I H E E V - - - - - 353
PER_Platynereis_dumerilii/1-313	366 M T K E G I Y T G K R R V S A N H R N Y L L V L T I R P Y A N A V D S Q Y I H R I I T S A S A 412

that the cells able to entrain the clock are already photosensitive and active at those stages, i.e. latest at 38hpf, assuming that one light transition is sufficient to set the clock.

At 34hpf, the rhabdomeric larval eyes, which express *r-opsin1*, are already differentiated, and their function is to mediate phototaxis (Arendt et al., 2002; Jékely et al., 2008). Among all the other opsins present in the *Platynereis* genome, only the *perops* and the *c-ops1* are expressed in the larval brain at early stages (fig. 6.4). The *perops* pattern starts with several cells in the cPRCs and apical organ region at 24hpf, and it becomes broader at later developmental stages (fig. 6.4A-C and Marlow et al. 2012). The expression of *c-ops1* is restricted to fewer cells (fig. 6.4E-F). The first *c-ops1*+ cell appears at around 20hpf in a big dorsal cell, located on the left side of the episphere (apical view, arrowhead in fig. 6.4E). By morphology, position and birthdating, this cell reminds very closely the dorsal asymmetrical serotonergic cell (arrowhead in fig. 6.4D). Indeed, coexpression analysis with PrImR (Tomer et al., 2010) shows that *c-ops1* and the serotonergic marker *tph* are expressed in the same cell (fig. 6.4G). Thus, the asymmetric serotonergic cell is a newly identified ciliary photoreceptor, and the first ciliary photoreceptor which develops in *Platynereis* brain, early enough to be involved in the entrainment of the CBF rhythm.

The analysis with PrImR at 48hpf revealed that all the *c-ops1*+ cells (asymmetric serotonergic cell, cPRCs and few others) coexpress the clock marker *cry1* (fig. 6.4H), meaning that the same cells running the clock can be entrained directly by light. Remarkably, the *c-ops1*+ cells represent a subset of the *cry1* domain. Unfortunately, it was not possible to include *perops* in the PrImR analysis. However, in the dorsal brain the *perops* pattern is very similar to the *cry1* pattern, suggesting that the *cry1*+ *c-ops1*- cells are also light-sensitive. One possibility is that the two opsins respond differently to light (different wavelengths, different kinetics of response...) and thus provide different inputs to the clock.

Finally, the expression of *c-ops1* and *perops* compared to the clock markers indicates that all the clock cells are sensory neurons. The sensory specializations of the ciliary photoreceptors and the serotonergic cells have been discussed in chapter 3. The other cells of the region bear apical sensory dendrites, which reach the surface of the episphere and contact the external environment (fig. 6.4I). These sensory endings do not resemble the “typical” apical specialization of photoreceptor cells (like “ciliary” or “rhabdomeric”, Arendt (2003)), and in principle they might serve other sensory modalities, like chemo- or mechanosensation.

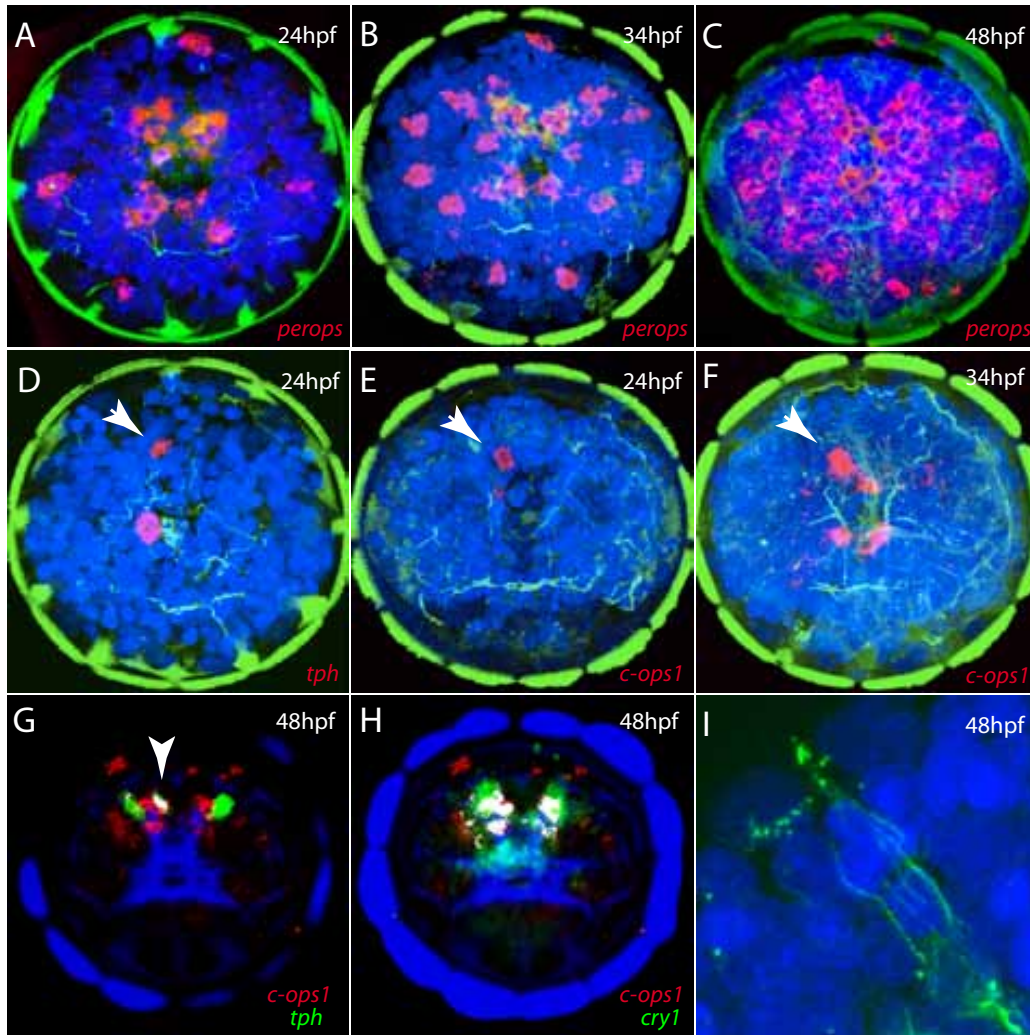


Figure 6.4: Expression of opsins in the clock region. A-C. Expression of *perops* in the brain at 24hpf (A), 34hpf (B) and 48hpf (C), apical views. D. Expression of *tph* in the brain at 24hpf. E-F. Expression of *c-ops1* at 24hpf (E) and 34hpf (F). G. Colocalization of *c-ops1* (red) and *tph* (green) at 48hpf, according to PrImR. H. Colocalization of *c-ops1* (red) and *cry1* (green) at 48hpf, according to PrImR (arrowhead). I. Sensory dendrites extending from cells in the clock region to the surface. In A-F and I, gene expression in red, DAPI in blue and tyrosinated tubulin in green.

6.3.3. Imaging of neuronal activity shows the presence of light responses in the dorsal brain

The presence of two opsins - *c-ops1* and *perops* - in the same cells raises questions on the physiology of these photoreceptor cells. Are the *c-ops1*+ cells OFF-responding, like their vertebrate counterparts? Is the Peropsin really involved in light sensitivity, or is “just” a photoisomerase? Or rather, is the presence of two opsins in the same cell the basis of a chromatic response, like in the lizard parietal eye (Su et al., 2008)?

In order to get some insights on the physiology of brain photoreceptors, I used the genetically encoded calcium indicator (GECI) GCaMP3 to visualize Ca^{2+} dynamics in the brain. GECIs are becoming very popular optogenetic tools to study neuronal activity in animals, without invasive methods (Hires et al., 2008; Tian et al., 2009). GCaMPs are fusion proteins of GFP and calmodulin, where the GFP brightness increases upon Ca^{2+} binding to the calmodulin moiety. Monitoring the Ca^{2+} dynamics is a very good indicator of neuronal activity, since increase of Ca^{2+} concentration is triggered after sensory transduction (ON-response), depolarization and synaptic release.

I injected the mRNAs of GCaMP3 and H2A-RFP (as an injection tracer) in *Platynereis* zygotes, and then I analyzed Ca^{2+} dynamics in metatrochophore larvae (48hpf). To assay light responses, it was necessary to use a two-photon setup, which allows to excite the GCaMP3 fluorophore using infrared light, without stimulating the photoreceptors (which are not sensitive to infrared illumination; see Chapter 13 for details). Unfortunately this series of experiments is not complete yet, but the first results are already providing some interesting information on the light responsiveness of the brain cells.

First of all, injection of GCaMP3 mRNA was sufficient to express this indicator in the cytoplasm of all the cells at 48hpf and at 5dpf (not shown), and to observe changes of fluorescence indicative of neuronal activity. Ca^{2+} waves were observed in the prototroch cells (not shown), consistent with the notion that Ca^{2+} controls the beating frequency of cilia. Moreover, changes of Ca^{2+} concentration were concomitant to muscular twitching (not shown). This indicates that the changes of GCaMP3 brightness reflect real physiological changes of Ca^{2+} concentration.

In the brain, recordings in darkness conditions showed some spontaneous activity in isolated brain cells and axons. To test the presence of light responses in the dorsal brain, I imaged Ca^{2+} fluctuations under constant illumination. One example

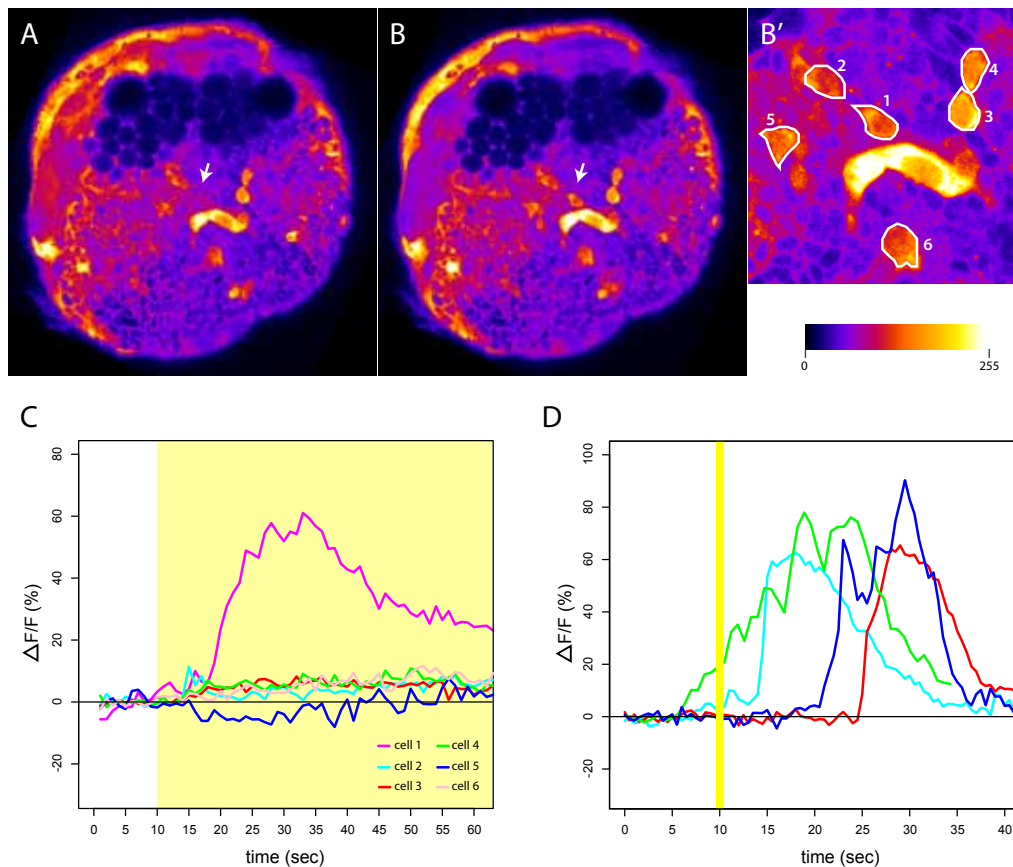


Figure 6.5: **Light-evoked Ca^{2+} waves in the dorsal brain.** A. GCaMP3 signal in the episphere of a metatrochopore larva, integrated over 10 sec before light stimulation. B. GCaMP3 signal in the episphere of a metatrochopore larva, integrated over 10 sec after light stimulation. The arrow in A. and B. indicates a cell that reacts to light stimulation. B'. Magnification of the cells in the medial brain shown in B. C. Quantification of the response of the cells outlined in B'. The light response is expressed as % of $\Delta F/F$, where F is the GCaMP3 fluorescence. The presence of light is indicated by the yellow block. D. Quantification of responses from different cells imaged from different metatrochopore larvae. In this case, the stimulus was a 150ms light flash (yellow bar). The light response is expressed as % $\delta F/F$, where F is the GCaMP3 fluorescence.

is shown in figs.6.5A-C, where light (a combination of 488nm and 561nm lasers) is turned on after 10 sec. There are very few cells that react to light in these conditions; one of them is shown in figs. 6.5A-B (arrows), and is located dorsal to the crescent cell (the bright half-moon shaped cell), where some *c-ops1* expression is present. Quantification of the changes of GCaMP3 brightness shows that this cell has an ON response to light stimulation; other cells in the surroundings show minimal or not significant responses (fig. 6.5C). The slow kinetics of response are consistent with the production of graded potentials, as documented for other invertebrate sensory neurons (Tian et al., 2009).

Next, I asked if a light flash alone (about 150ms) can trigger similar responses. This was indeed the case in several larvae tested (representative traces in fig. 6.5D). In all the examples, the cells responding to light were located in the dorsal brain. Unfortunately, the position of the cell alone is not enough to assign an identity. However, it is very likely that the *c-ops1+* cells are the ON responding cells. This conclusion is based on two arguments: first, the cells showing response to light are always in the dorsal brain; second, the responding cells must express an opsin, and in the dorsal brain the *c-ops1+* cells are very few, while the *perops* domain is more broad.

Future experiments will need to prove more precisely that the *c-ops1+* cells are ON responding. This can be achieved using a cell-specific promoter to label the cells of interest, or to drive GCaMP3 expression only in those cells. Moreover, blocking phototransduction with pharmacological treatments should suppress the light-evoked Ca^{2+} fluctuations. Finally, a closer investigation of the *perops+* cells is needed to understand if and how these cells respond to light.

6.4. A CNG-dependent transduction cascade resets the locomotor rhythms

The presence of *c-ops1* and *perops* expressing cells in the clock does not exclude the involvement of other photoreceptor cells types - like the larval eyes - in the entrainment of the clock. In other species, rhabdomeric and non-rhabdomeric photoreceptors employ distinct phototransduction cascades; in particular, photoreceptors expressing *c-opsins*, *peropsins* and *G_o-opsins* use a cascade based on cyclic nucleotides and CNG cationic channels (par. 2.1.1 and Matulef and Zagotta 2003; Ward et al. 2008; Su et al. 2008). Thus, I investigated the expression of a *CNGa* channel subunit in *Platynereis* brain. Interestingly, *CNGa* is expressed from 24hpf onwards in the dorsal clock region (fig. 6.6A-C), including the ciliary photoreceptors, the asymmet-

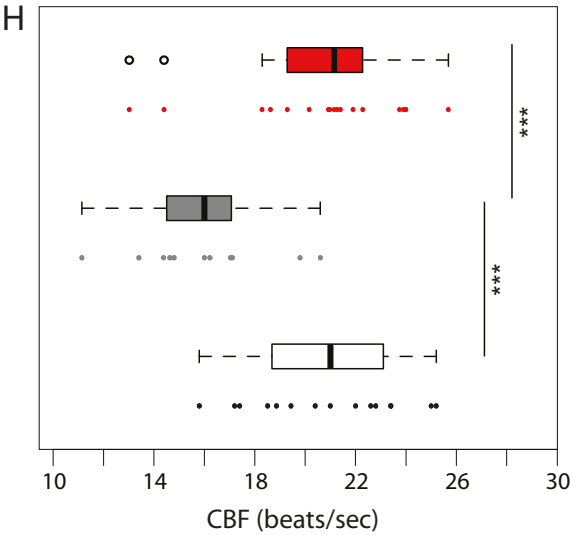
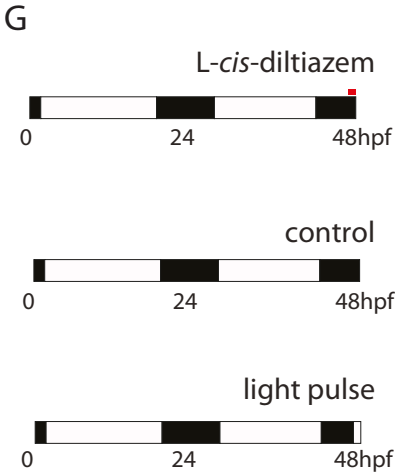
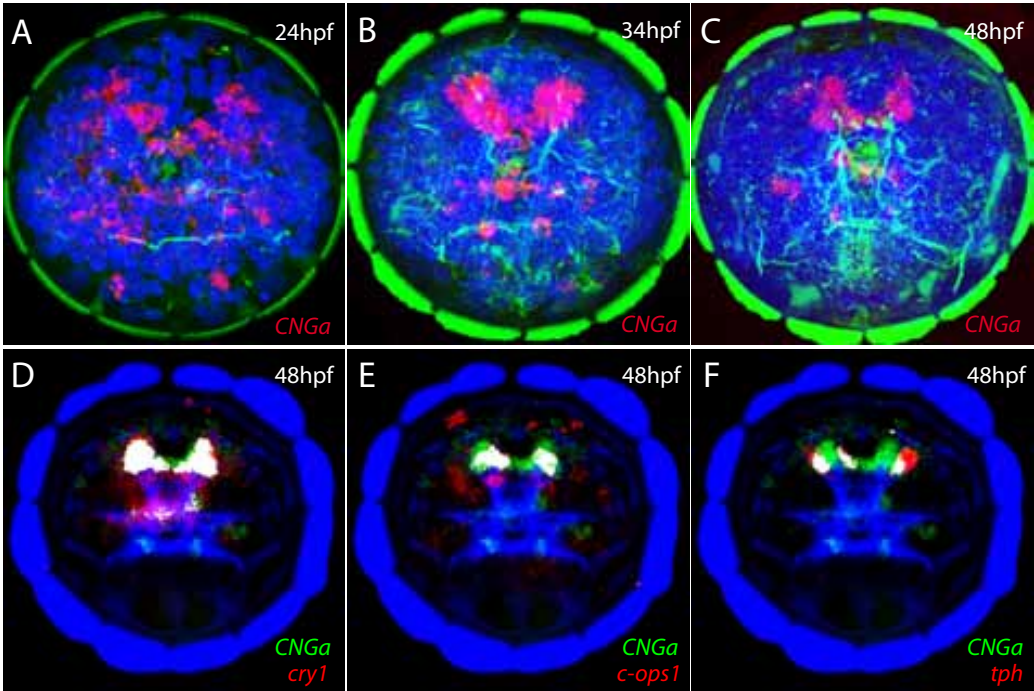
ric serotonergic cell and the *cry1-perops* expressing cells (fig. 6.6D-F). Notably, no *CNGa* expression was found in the larval and adult eyes.

The involvement of CNG channels in phototransduction has been characterized in detail for the vertebrate rods and cones. In these photoreceptors, phototransduction ends with the closure of CNG Ca^{2+} - Na^{+} channels, which are normally open at darkness, and sustain the depolarization of the membrane potential (the so-called dark current). The closure of CNG channels leads to an hyperpolarization of the membrane potential, because the flux of positive ions in the cells is interrupted; this mechanism is called OFF-response (par. 2.1.1 and Matulef and Zagotta 2003; Zhang and Cote 2005) and is a defining feature of ciliary photoreceptors. In the scallop eye, CNG K^{+} channels are present in *G_o-opsins*-expressing ciliary photoreceptors. In these cells, light also induces cell hyperpolarization, but through the opening (instead of closing) of CNG K^{+} channels (Gomez and Nasi, 2005).

The specific expression of CNG in brain photoreceptors provides the opportunity to target them with a CNG channel inhibitor, and thus to test if these photoreceptors are sufficient to set the clock. Under the hypothesis that the CNG channels mediate an OFF-response also in *Platynereis*, the inhibition of these channels would mimic the response to light exposure.

Thus, I designed an assay to determine if a CNG-dependent cascade can override the clock (fig. 6.6G). For this purpose, first I tested if the CBF circadian rhythm is readjusted after light exposure during the night phase. Indeed, a 60 min light exposure during the subjective night is sufficient to increase the CBF, compared to

Figure 6.6 (on the next page): **The CNG channel mediates light-dependent readjustment of the CBF.** A-C. Expression of the *CNGa* subunit of CNG channel in the brain of 24hpf (A), 34hpf (B) and 48hpf (C) larvae, apical views. D. Coexpression of *CNGa* (green) and *cry1* (red) at 48hpf, obtained with PrImR. E. Coexpression of *CNGa* (green) and *c-ops1* (red) at 48hpf, obtained with PrImR. F. Coexpression of *CNGa* (green) and *tph* (red) at 48hpf, obtained with PrImR. G. Experimental design to test the changes of CBF after a light pulse or *L-cis*-diltiazem treatment during the subjective night. Sibling larvae were raised in the same light-dark cycle (16L:8D, fertilization at ZT22.5). One hour before the assay, some larvae were exposed to the light (light pulse group), while others were kept in the dark and incubated with $100\mu\text{M}$ *L-cis*-diltiazem. H. CBF (beats/second) of 48hpf larvae from the three experimental groups described in G. The light pulse (white bar, n=15) caused a significant increase of CBF compared to controls (gray bar, n= 11; p -value= 0.0001987, unpaired t test). Treatment with *L-cis*-diltiazem (red bar, n= 17) also caused a significant increase of CBF compared to controls (p -value= 0.0004984, unpaired t test). Moreover, the CBF of larvae exposed to the light pulse, and of larvae treated with *L-cis*-diltiazem, are not significantly different (p -value= 0.8431, unpaired t test).



controls (fig. 6.6H). Next, I treated sibling larvae with the CNG channel inhibitor *L-cis*-diltiazem. This inhibitor has been used in several vertebrate and invertebrate species to close CNG channels (Haynes, 1992; Ward et al., 2008). CNG channel closure in the darkness also increases significantly the CBF, similarly to what happens after light exposure (fig. 6.6H). Moreover, there is no significant difference between the larvae exposed to light and the larvae treated with *L-cis*-diltiazem, indicating that closing the CNG channels is sufficient to mimic the effects of light exposure.

These results indicate that light can adjust the CBF through an opsin phototransduction cascade (CNG channels are not involved in *Cry1* light responses). Moreover, CNG channels expressed in non-rhabdomeric photoreceptors mediate an OFF-response to light, because closing the CNG channels mimics the effects of light exposure. This OFF-response causes the increase of CBF, either by suppressing a CBF-decreasing signal, or by activating a CBF-increasing signal. The expression patterns and the preliminary GCaMP3 data suggest that the Peropsin, rather than the *c-Opsin1*, is the OFF-responding opsin.

In summary, the *Platynereis* larval clock neurons are directly entrained by light, because they express three light sensitive molecules: *cry1*, *perops* and *c-ops1*. The CBF circadian rhythm can be overridden by an opsin-dependent OFF-response to light, probably via Peropsin. *Cry1* might still participate to the entrainment of the clock, acting directly on the transcription and/or stability of clock genes. Moreover, the presence of three distinct light sensitive molecules suggests that the *Platynereis* larval clock might sense different wavelengths, and use this information for a more sophisticated entrainment of circadian rhythms.

6.5. Melatonin is the molecular output of the larval circadian system, and modulates locomotor behaviour

Finally, I aimed to understand how the circadian system is organized and how the larval clock controls the ciliary beating of the prototroch. Looking at the morphology of the cells in the clock region, it was clear that most of them are sensory neurons of different kinds, consistent with the expression of the CNG channel and other sensory markers (see Chapter 7). One possibility is that the circadian system has a hierarchical organization, i.e. the inputs from these sensory cells are integrated in another structure, and then this intermediate “relay station” controls the prototroch cells. Another option is that all these sensory cells participate directly and in parallel

to the control of ciliary beating, via the direct innervation of the prototroch. This hypothesis is supported by the observation that most of the differentiated cells of the larval brain project directly to the prototroch, as shown by Conzelmann et al. (2011) with immunohistochemistry for several neuropeptides.

To answer these questions, it is necessary to identify the molecular output (i.e. neurotransmitters, neuropeptides, hormones) of the circadian system, and to understand how these molecules affect the larval locomotor activity (for example, testing the expression of specific neurotransmitter receptors in the prototroch cells).

6.5.1. The melatonin synthesis genes *hiomt* and *aanat* are present in a lophotrochozoan

Studies in other protostomes and in vertebrates have identified several neurotransmitters released as the output of the circadian clock. In *Drosophila*, the clock neurons of the brain release the neuropeptide PDF, which works as the main output of the system. Vertebrates do not have PDF, but the activity of the central clock is translated in the photoperiodic release of the hormone melatonin by the pineal gland (reviewed in par. 2.2). Melatonin receptors expressed in other brain region and in peripheral tissues mediate the adjustment of physiology and behaviour to photoperiod (Reiter, 1993).

Despite its key role in vertebrate chronobiology, the evolutionary history of melatonin signalling is not clear. The absence of clear orthologs of the melatonin synthesis genes *hiomt* and *aanat* in ecdysozoan representatives suggested the hypothesis that melatonin signalling is a vertebrate innovation (Klein, 2004; Iyer et al., 2004). However, melatonin presence and its effects on behaviour and physiology have been reported in several invertebrate species, including cnidarians, suggesting that melatonin signalling might have been present in the urbilaterian ancestor (Vivien-Roels and Pévet, 1993).

A search in the new *Platynereis* genomic and transcriptomic resources yielded sequence fragments with high homology to *hiomt* and *aanat*. These fragments were extended by RACE PCR, and the full length clones were compared to published sequences from other species. The orthologs of *hiomt* and *aanat* were also identified in the genomes of other two annelids, *Capitella teleta* and *Helobdella robusta*, and in the mollusc *Lottia gigantea*. The phylogenetic analysis (Appendix C) and the conservation of intron-exon boundaries (fig. 6.7) clearly indicate that the lophotrochozoan *hiomt* and *aanat* genes are the homologs of the correlative vertebrate genes.

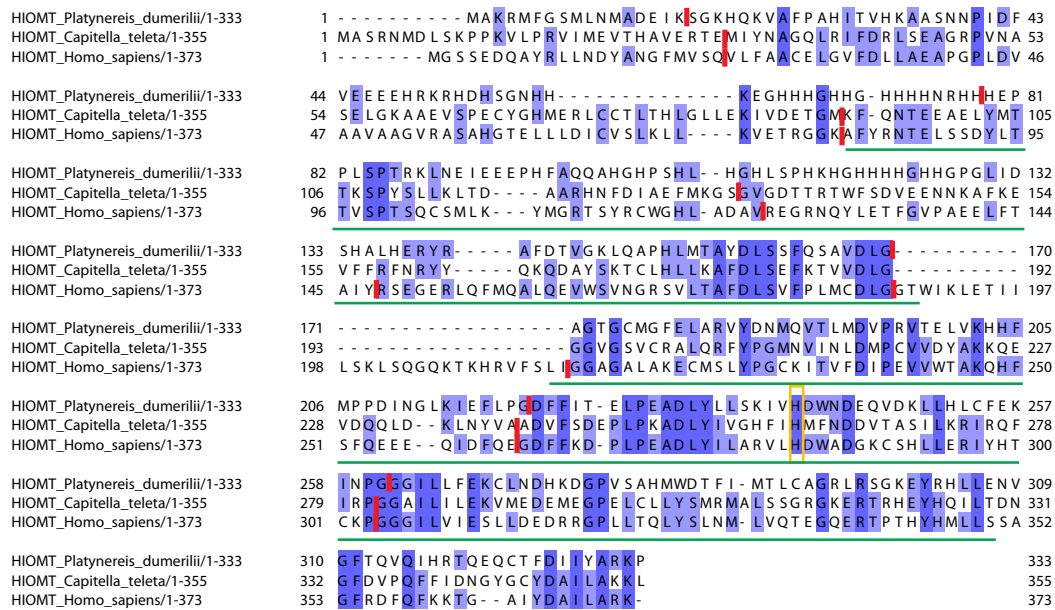


Figure 6.7: Conservation of intron positions in annelids and vertebrate *hiomt* genes. Alignment of human, *Platynereis* and *Capitella* *Hiomt* sequences. The alignment is colored based on the percentage of identity. The vertical red bars represent the exon-exon boundaries, determined from Ensembl, JGI and the *Platynereis* genome, respectively. The O-methyltransferase domain is underlined (green). The yellow box highlights the conserved H residues, important for the catalytic activity.

Moreover, several *hiomt* orthologs have been recently identified in the cnidarian *Nematostella vectensis* (Ancil, 2009). This analysis indicates that the genes involved in melatonin synthesis were present in the urbilaterian ancestor, and possibly in the eumetazoan ancestor (the presence of *aanat* in cnidarians remains to be shown).

6.5.2. Melatonin produced by the clock cells controls directly the ciliary beating of the prototroch

To reveal the sites of melatonin synthesis, the expression of *hiomt* was investigated with WMISH. The expression of *aanat* is less indicative, since this gene is involved in more enzymatic pathways other than melatonin synthesis. Unfortunately, it was not possible to determine the expression pattern of *aanat* with WMISH, although *aanat* transcripts are detectable at larval stages with RT-PCR.

Few *hiomt* expressing cells were present in the medial brain at 34hpf, while at 48hpf *hiomt* expression encompassed the entire *CNG-cry1-perops* synexpression group, as confirmed by co-expression analysis with PrImR (fig. 6.8A-B, D,F). No-

Table 6.1: Neurochemistry of the clock: candidates from the literature screened in *Platynereis*.

name	marker gene	species	presence of the gene in <i>Platynereis</i>	48hpf expression in <i>Platynereis</i> CNG+ <i>cry1+</i> domain
acetylcholine	<i>ChAT</i>	<i>Drosophila</i>	yes	yes (cPRCs)
GABA	<i>GAD</i>	mouse, <i>Drosophila</i>	yes	no
glutamate	<i>VGLuT</i>	mouse, <i>Drosophila</i>	yes	yes (subset of cells)
histamine	<i>hdc</i>	<i>Drosophila</i>	yes	no
IPNamide, MTYamide	NPLP1	<i>Drosophila</i>	no	
melatonin	<i>hiomt</i>	vertebrates*	yes	yes
NPF	NPF	<i>Drosophila</i>	no	
PDF	PDF	<i>Drosophila</i>	yes	no
serotonin	<i>tph</i>	mouse, <i>Drosophila</i>	yes	yes (5HT cells)
VIP/PACAP	VIP/PACAP	mouse	no	

The table lists neurotransmitters and neuropeptides with a known function in the mammalian and the insect clock, and their presence in *Platynereis*. Main references: Vivien-Roels and Pévet (1993); Cardoso et al. (2007); Nitabach and Taghert (2008). Abbreviations: 5HT=5-hydroxytryptamine (serotonin), *ChAT*=choline acetyltransferase, cPRCs=ciliary photoreceptors, as described by Arendt et al. (2004), *GAD*=glutamate decarboxylase, *hdc*=histidine decarboxylase, *tph*=tryptophan hydroxylase, *VGLuT*=vesicular glutamate transporter.

*=There are examples of invertebrates where a role of melatonin in circadian processes has been shown, but for those animals a clear ortholog of *hiomt* does not exist.

tably, *hiomt* is expressed in ciliary photoreceptors and in the lateral and dorsal asymmetric serotonergic cells (fig. 6.8E).

The expression of *hiomt* in the clock region does not necessarily imply neither that melatonin is the molecular output of the circadian system, nor that other molecules are not involved. Thus I analyzed the presence and the expression of other candidates coming from the literature. The results of this analysis are summarized in table 6.1. Notably, *hiomt* is the only marker with an expression pattern covering the entire CNG-*cry1*-*perops* synexpression group. Other candidate markers were either not expressed at all in this territory, or expressed in just a subset of the clock cells.

Next, I searched¹ the melatonin receptors in *Platynereis* genome and transcriptome, in order to define the sites of action of melatonin. We identified three different melatonin receptors, but only one of them, the *melatonin receptor A*, showed expression at the trochophora larva stages (34 and 48hpf). Surprisingly, this melatonin receptor was expressed exclusively in the multiciliated locomotory cells of the animal (the prototroch and the telotroch). This result indicates that the *hiomt*+ sensory

¹In collaboration with Dr. Tomas Larsson.

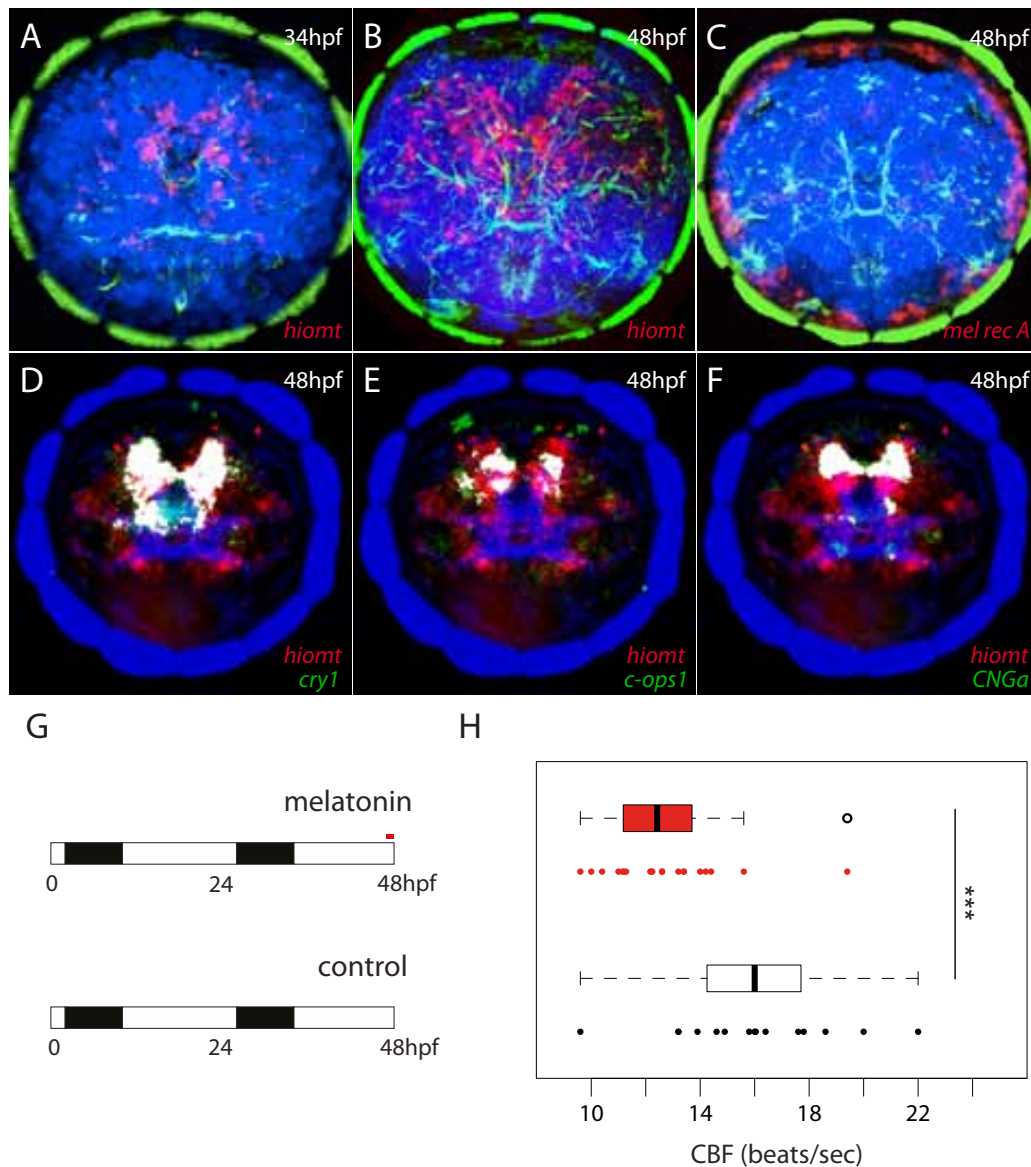


Figure 6.8: **Melatonin is the molecular output of the larval circadian system.** A-B. Expression of *hiomt* in the brain of 34hpf (A) and 48hpf (B) larvae, apical views. C. Expression of *melatonin receptor A* in the prototroch cells of 48hpf larvae, apical view. D. Coexpression of *hiomt* (red) and *cry1* (green) in the 48hpf brain, according to PrImR. E. Coexpression of *hiomt* (red) and *c-ops1* (green) in the 48hpf brain, according to PrImR. F. Coexpression of *hiomt* (red) and *CNGa* (green) in the 48hpf brain, according to PrImR. G. Experimental design to test the effect of melatonin on CBF. Sibling larvae were raised in the same light-dark cycle (16L:8D, fertilization at ZT14). A group of larvae was incubated with 1 mM melatonin one hour before the assay (red bar). H. CBF (beats/second) of 48hpf larvae from the two experimental groups described in G. The larvae treated with melatonin (red bar, n=20) have a CBF significantly lower than control larvae (white bar, n=15; p -value= 0.0008067, unpaired t test).

cells of the circadian center signal directly and in parallel to the prototroch, using melatonin as a common molecular output.

These data suggest a model where the *CNG+ cry1+ hiomt+* clock neurons can directly sense light and release melatonin during a precise phase of the light-dark cycle. In vertebrates, melatonin is released by the pineal gland during the night. To understand how this system works in *Platynereis*, a melatonin quantification is necessary. A complementary study in the lab of Dr. Kristin Tessmar-Raible (Vienna) demonstrated that the melatonin levels in *Platynereis* increase during the night and decrease at daytime (Dr. K. Tessmar-Raible, personal communication). Thus, if melatonin is indeed the output of the circadian clock released during the night, melatonin treatment during the subjective day should reduce the CBF. According to this model, melatonin would be a CBF-decreasing signal inhibited by the CNG-dependent OFF-response to light (par. 6.4). To test this hypothesis, I compared CBF during the subjective day in larvae incubated for one hour with 1 mM melatonin, and in untreated sibling larvae (fig. 6.8G). In this experiments, the melatonin treatment induced a significant decrease of CBF compared to controls (fig. 6.8H). This shows that melatonin produced by the clock cells controls directly the activity of the prototroch cells, thus this “hormone of darkness” has a conserved role in reducing locomotor activity in vertebrates and annelids.

6.5.3. In the juvenile, melatonin has a multiples roles in the nervous system

The transition from the early larval stages (trochophore larvae) to later larval stages and juvenile worms involves changes in the locomotor behaviour, and a gradual transition from ciliary-driven to muscle-driven locomotion. Nectochaete larvae elongate posteriorly, and start to use their muscles to change the direction of swimming. This transition is paralleled by structural and gene expression changes in the brain.

To get an idea of the function of melatonin at later larval stages, I investigated the expression of melatonin receptors at 5dpf. While the *melatonin receptor A* maintains its expression in the ciliary bands, a second melatonin receptor, absent in trochophore larvae, is expressed broadly in the medial brain and in the ventral nerve cord, with stronger expression in the first segment (fig. 6.9A-B).

Nectochaete larvae change also their phototactic behaviour, from positive to negative phototaxis. In the phototaxis assay (Jékely et al., 2008), larvae incubated with melatonin were completely insensitive to light, while sibling larvae were swimming

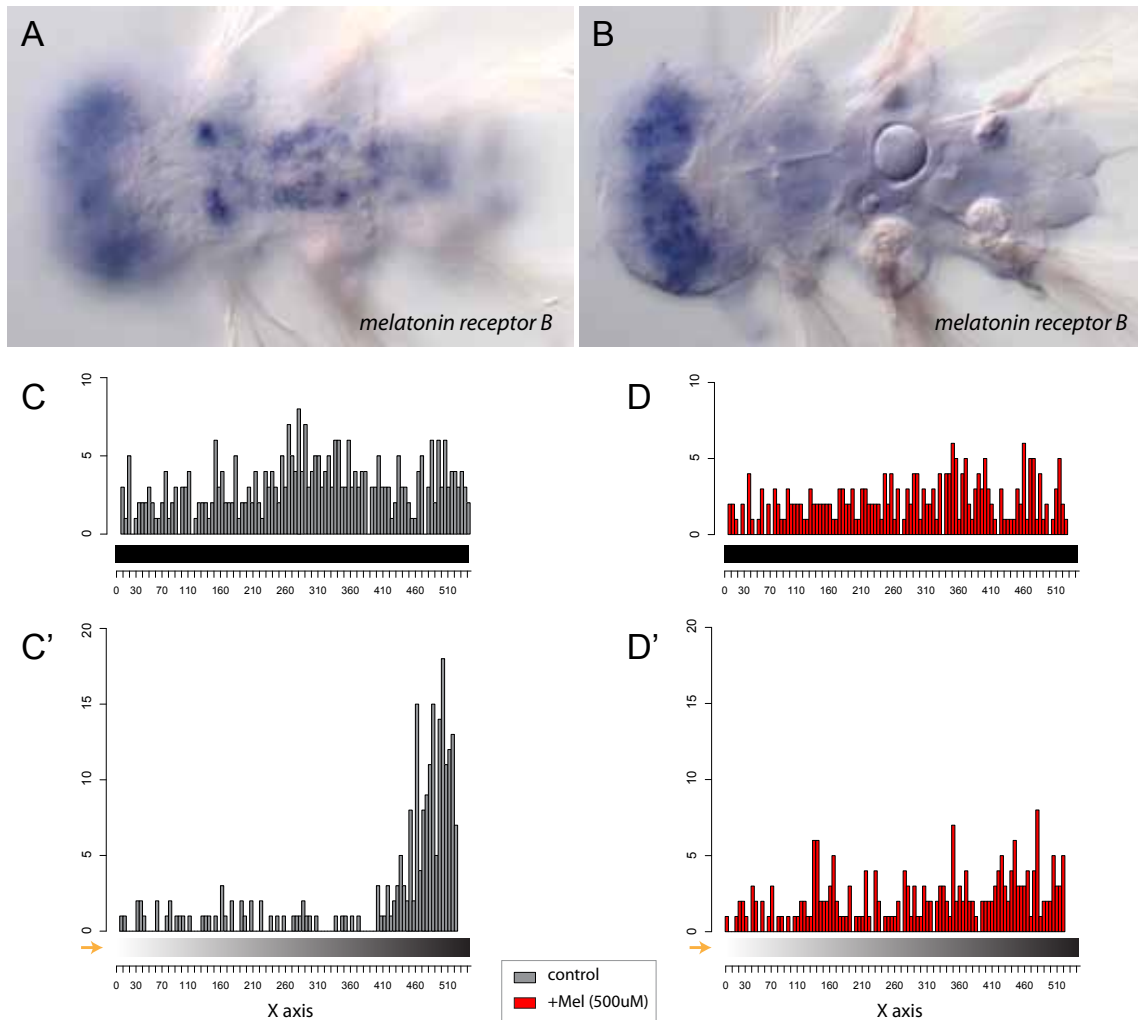


Figure 6.9: **Effects of melatonin in nectochaete larvae.** A-B. Expression of the *melatonin receptor B* in 5dpf larvae. The photos are ventral views, from a more superficial (A) and a deeper (B) level. C-C'. Distribution of control 6dpf larvae in the phototaxis chamber before (C) and after (C') illumination of the phototaxis chamber from one side (indicated by the yellow arrow). The nectochaete larvae respond to illumination by swimming away from the light source. D-D'. Distribution of 6dpf larvae, previously treated for 30 min with melatonin (500 μ M), in the phototaxis chamber before (D) and after (D') illumination from one side (indicated by the yellow arrow). The treated larvae do not respond to illumination, but remain evenly distributed in the phototaxis chamber.

away from the light source in few seconds (fig. 6.9C-D'). Melatonin did not affect the speed of phototaxis, since the treated larvae never moved away from the light source, even after prolonged observation. This effect was specific of nectochaete larvae, since in similar experiments with trocophore larvae phototaxis was not affected by melatonin incubation (not shown).

Thus the effect of melatonin on phototactic behaviour is highly correlated with the appearance of *melatonin receptor B* expression in the brain and the ventral nerve cord. This effect cannot be explained with the reduction of responsiveness of the eyes, since the eyes do not express any melatonin receptor. The effect must be related to the processing of light information, at the level of the interneurons and/or the motorneurons of the circuit that mediates negative phototaxis.

In summary, *Platynereis* larvae can use light cues to entrain a circadian rhythm of locomotion. The light input is transduced by a CNG-dependent cascade in cells that also express all the molecules of a functional circadian clock. These cells are heterogeneous and multifunctional, but they share a unique output, melatonin, which can affect specifically the prototroch cells. Remarkably, some of these cells have the same differentiation signature of ciliary photoreceptors of the vertebrate pineal organ. These cell types share not only the differentiation signature but also functions like the modulation of locomotor activity; however, the neuronal organization underlying these functions is very different, as it belongs to nervous systems of different levels of complexity.

7

MOLECULAR IDENTITY OF THE *hiomt+* CELL TYPES: A COMPARATIVE ANALYSIS

The results presented in the previous chapters show the existence of photoreceptors of the ciliary type, which run a circadian clock and produce melatonin, in *Platynereis dumerilii*, a lophotrochozoan. A similar cell type is highly reminiscent of the vertebrate pineal photoreceptors, and has never been identified in other non-vertebrate species. This raises new questions about the evolution of eyes and photoreceptors in general, and the relationships between the evolution of the melatonin signalling and the emergence of a pineal organ. I used a cell type molecular fingerprint approach (Arendt, 2008) to deepen the comparisons between annelids and vertebrates.

7.1. The repertoire of *hiomt+* *CNG+* cell types

The *CNGa*-expressing clock neurons that have been functionally characterized represent a subset of the *cry1* and *hiomt* expression domains. As shown in fig.6.6D and fig.6.8D,F, these genes form nested expression domains, where *hiomt*>*cry1*>*CNGa*. Moreover, only a subset of the *CNGa* expressing cells is constituted by cells expressing *c-ops1* (like the “canonical” cPRCs and the asymmetric serotonergic cell, compare fig.6.4). This implies that the clock region includes several cell types, with different specializations.

The availability of PrImR for the 48hpf stage (Tomer et al., 2010) allows the dissection of these individual cell types, based on averaged expression patterns (par. 1.2.2). In order to compare the results of my analysis with data across species, I enriched the lab dataset with genes involved in circadian processes (cfr. table 6.1) or transcription factors expressed in the vertebrate pineal-SCN system (table 7.1 and appendix D). This, together with similar efforts ongoing in the lab, provided a dataset of 180 genes for the analysis; of these, 49 were differentially expressed in the *hiomt+* region.

To identify individual cell types, I have taken advantage of the presence of many

Table 7.1: Transcription factors of the vertebrate pineal, retina and SCN/anterior hypothalamus analysed in *Platynereis*.

vertebrate gene ID	<i>Platynereis</i> ortholog	expression in vertebrates
<i>brn1, brn2 and brn4</i>	<i>brn1/2/4</i>	habenula, hypothalamus
<i>brn3</i>	<i>brn3</i>	specific marker of habenula and retinal ganglion cells
<i>bsx</i>	<i>bsx</i>	pineal, arcuate nucleus of the hypothalamus
<i>crx/otx5</i>	<i>otx</i>	pineal and retinal PRCs
<i>er81/etv1</i>	<i>er81/erm/pea3</i>	specific marker of habenula
<i>eya genes</i>	<i>eya</i>	mouse pineal (not clearly described in other species)
<i>foxD3</i>	<i>foxD</i>	specific marker of zebrafish pineal
<i>gfi-1</i>	<i>sens</i>	specific marker of parapineal projection neurons and retinal ganglion cells
<i>islet genes</i>	<i>islet</i>	pineal projection neurons and retina
<i>lhx1</i>	<i>lhx1/5</i>	specific marker of SCN
<i>lhx2</i>	<i>lhx2/9</i>	pineal, habenula and SCN
<i>lhx3</i>	<i>lhx3/7</i>	zebrafish pineal projection neurons
<i>neuroD</i>	<i>neuroD</i>	general PRCs marker, expressed also in the habenula, but not in SCN
<i>not/flh</i>	<i>not</i>	pineal and parapineal, both PRCs and projection neurons
<i>nr2e1/tll</i>	<i>tll</i>	nr2e1: broad in nervous system, including hypothalamus and eye field
<i>pax4, pax6</i>	<i>pax6</i>	pineal, not clear if it is also expressed in the habenula
<i>rfx4</i>	<i>rfx4/6</i>	specific marker of SCN
<i>rx genes</i>	<i>rx</i>	hypothalamic precursors, differentiated pineal and retinal PRCs
<i>tbx2, tbx3</i>	<i>tbx2/3</i>	pineal and parapineal, eye field, hypothalamus

Expression of transcription factors in the vertebrate structures involved directly or indirectly in circadian entrainment (additional expression domains are not indicated). An extended version of this table can be found in Appendix D. Abbreviations: PRC=photoreceptor, SCN=suprachiasmatic nucleus of the hypothalamus.

genes with a small expression domain, and I used those to subdivide the *hiomt* expression domain in 15 “non-overlapping minimal synexpression groups”. Here, these synexpression groups are defined “cell types”: in many cases, this definition matches reality since very often I found genes demarcating single cells; otherwise, it refers to groups of adjacent cells that cannot be distinguished further morphologically and molecularly, using the current dataset. The entire set of these minimal synexpression groups is represented in fig. 8.3.

Some of these cell types became of immediate interest because of the expression of key transcription factors, known in vertebrates for being involved in the development of the pineal organ and the SCN.

As shown in Chapter 5, the development of the deep brain **ciliary photoreceptors**

(cPRCs) and the **asymmetric serotonergic cell** (fig. 7.1C-D) requires a functional Rx. However, some other “famous” eye genes, present in both the pineal and the retina, like *otx* and *pax6*, are not expressed in these cells at differentiation stages.

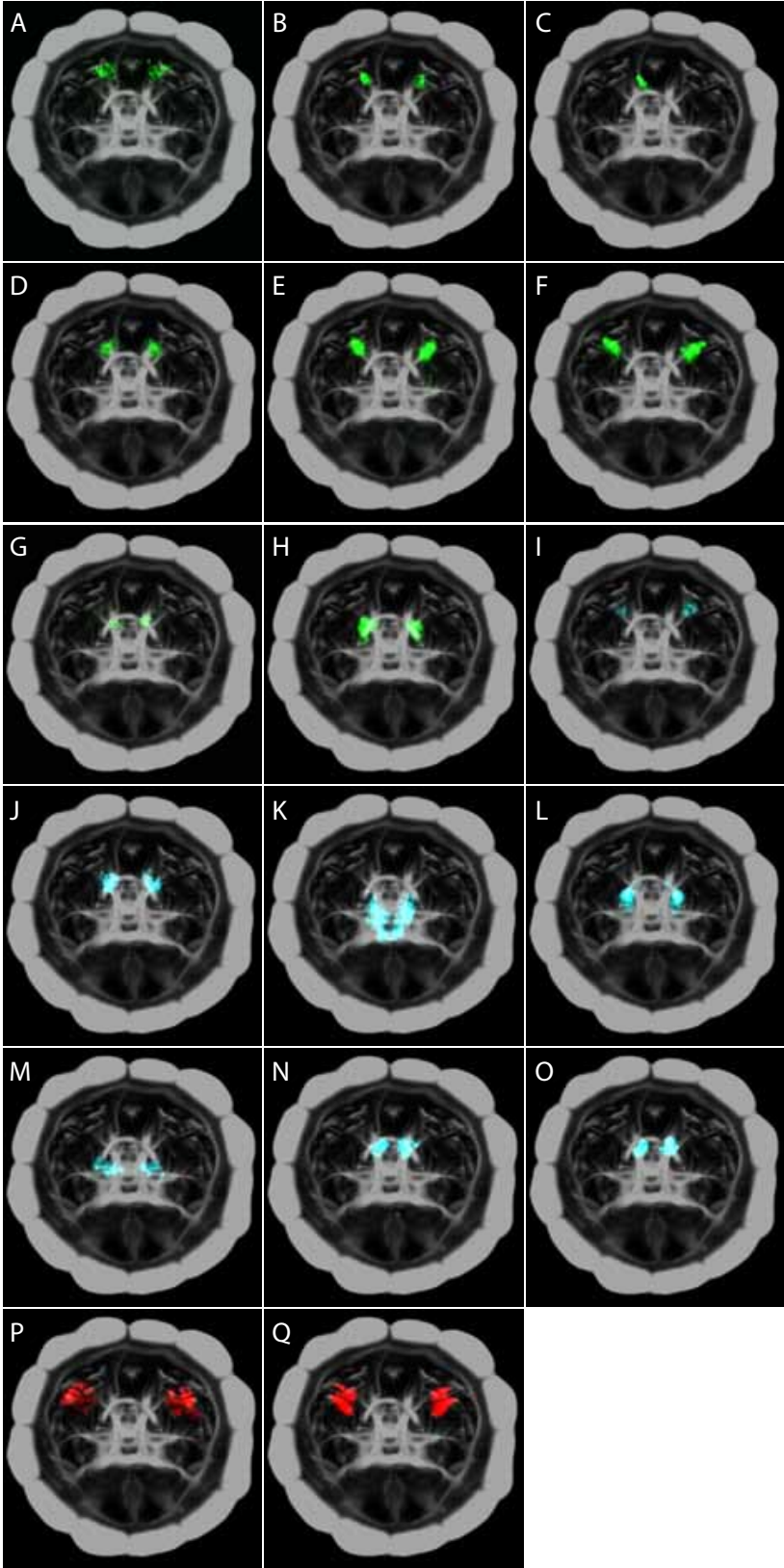
Therefore, I investigated the expression of transcription factors that are specifically expressed in the pineal but not in the retina. One of the most specific pineal markers in the developing vertebrate brain is *not*; however, this transcription factor does not have any role in determining cell fates, but it is required to sustain the proliferation of pineal progenitors and to induce the expression of proneural genes (Masai et al., 1997; Cau, 2003). In *Platynereis*, none of the *c-ops1*+ cells of the dorsal brain expresses *not*, but a small group of *not*+ cells develops adjacent to the cPRCs.

A second transcription factor, *tbx2b*, has been shown to be critical for pineal and parapineal development in zebrafish (Snelson et al., 2008b). In contrast to *not*, this gene has a function in the specification of the photoreceptor fate (Alvarez-Delfin et al., 2009). Consistently, in *Platynereis* *tbx2/3* is expressed in the asymmetric serotonergic cell and in the lineage of the cPRCs (“blue lineage” in par. 3.4).

The transcription factor *bsx* is also known to play a critical role in the final differentiation of pineal photoreceptors (D’Autilia et al., 2010), but is never expressed in the retina. The lineage analysis (par. 3.4) shows that *bsx* expression is very dynamic during development, and one of its early expression sites is the lineage of the asymmetric serotonergic cell. After differentiation, this cell expresses *senseless* (*sens*), a specific marker of retinal ganglion cells and parapineal projection neurons (Dufourcq et al., 2004; Wallis, 2003; Del Bene et al., 2007). In the dorsal brain, *sens* is one of the few transcription factors showing asymmetric expression (Appendix B). *Sens* is a well known specifier of *Drosophila* R8 rhabdomeric photoreceptors (Pepple et al., 2008).

Thus, the asymmetric serotonergic cell has some properties of both photoreceptors (*c-ops1*, *cry1*, *bsx*, *tph*, *hiomt*, *tbx2/3*) and projection neurons (*sens*) of the retina

Figure 7.1 (on the next page): **Subdivision of the *hiomt* expression domain in minimal synexpression groups.** The panel shows the minimal synexpression groups identified for molecular fingerprint analysis. The images are PrImR averages plotted on the average axonal scaffold. None of the minimal synexpression group corresponds to the *complete* expression pattern of one gene; see Methods, par. ?? for details. The color code and the letters correspond to fig. 7.2. A. Dorsal *bsx* cells. B. Lateral DLamide cells. C. Asymmetric 5HT cell. D. cPRCs. E. Lateral *not* cells. F. Lateral *otp* cells. G. *er81-vtn-c-ops1* cells. H. *lhx3/7-sox2* cells. I. Lateral 5HT cells. J. dach deep cells. K. *lhx1/5* cells. L. *six4* cells. M. *pdf* cells. N. deep *rxf4/6* cells. O. *cpa-otp* cells. P. Adult eyes pigment cells (AE-PCs). Q. Adult eyes photoreceptor cells (AE-PRCs).



and pineal. Indeed, as shown before, this cell bears a sensory cilium and at the same time it sends a projection to the brain serotonergic plexus, located underneath the apical organ. In comparison, the cPRCs do not express neither *sens* (they do not have long axons) nor *bsx* and *tph*. The different expression profiles of these two types of *c-ops1+* is correlated to their different clonal origin, and might be also correlated to differences in their functions.

The “not cells” (fig. 7.1E), which are the only cells of the 48hpf brain expressing *not*, are adjacent to the ciliary photoreceptors and located just above the lateral serotonergic cells (see also Appendix B). At 48hpf, there are 3 *not*-expressing cells on each side, and their number increases at later stages. These cells are demarcated also by the expression of *foxD* (compare also Appendix B), the *Platynereis* ortholog of the *foxD3* gene, another very specific marker of the fish pineal cells¹ (Gilmour et al., 2002). The “not cells” express also a third transcription factor, very restricted in both *Platynereis* and vertebrates: *rfx4/6*. However, in vertebrates this gene does not demarcate the pineal but the suprachiasmatic nucleus of the hypothalamus. The coexpression of these specific markers in one cell type of *Platynereis* brain makes it very hard to infer a clear relationship with the cell types of vertebrates.

At 48hpf the gene *bsx* demarcates a specific group of differentiated cells in the *CNGa* domain, here called **dorsal *bsx* cells** (fig. 7.1A). In *Platynereis* *bsx* is not as specific as the other markers described above, since at 48hpf *bsx* expression includes the whole apical region of the episphere, and two expression domains between the larval and the adult eyes. However, the dorsal *bsx* cells are the only ones coexpressing *CNGa* and *cry1*. Like the not cells, these cells express *perops* but not *c-ops1*.

The molecular fingerprint of the **lateral serotonergic cells** is also interesting for evolutionary comparisons. These cells lie immediately adjacent to the ciliary photoreceptors, and are located in a deep position. Considering that they lack apical specializations, they are probably interneurons; consistently, they do not express any opsin. The lateral serotonergic cells are the only cells in the *hiomt* domain to express *rx*, *otx* and *pax6* at differentiation stages; the same genes are present already in their progenitors during development (par. 3.4). There are few cell types in the brain that coexpress these three transcription factors. *Rx* is necessary for *pax6*

¹It needs to be said that the *foxD* expression is less interesting than other genes, like *not*, since the *Platynereis foxD* gene is the ortholog of all the vertebrate *foxD* genes, including *foxD1*, which is expressed in the hypothalamus. This is a clear example where the absence of a 1:1 correspondence of ortholog genes makes the molecular fingerprint comparison more difficult.

expression in these cells, and might be able to induce or maintain *otx* expression (Chapter 5). Obviously, the presence of *rx*, *otx* and *pax6* is reminiscent of the retina and the pineal, but this is certainly not enough to infer homology of cell types. However, exactly for this reason it will be very interesting in the future to find out what is the role of these cells in the brain, and how they better compare with cell types in other organisms.

Finally, many *hiomt* expressing cells are present in a more ventral position, underneath the so called “crescent cell” of the apical organ. Many of these cells are sensory and release neuropeptides, like DLamide (Conzelmann et al., 2011), and project directly to the prototroch. Among these, there are also cells expressing *c-ops1* but not the *CNGa* channel, which have been described previously (Tessmar-Raible et al., 2007). Additional cells expressing *hiomt* at lower levels “wrap” around the apical organ; however, since these cells do not express *CNGa*, they have not been investigated in big detail.

7.2. Hierarchical clustering identifies two major subgroups of *hiomt*+ cells

As discussed above, looking at “marker genes” in distantly related species sometimes is not enough to identify clear cases of cell type homology. Paradoxically, the availability of expression data for many genes, with a single cell resolution, makes it even more difficult to draw convincing conclusions. Clearly one major mistake is to restrict the analysis to 1:1 comparisons, which cannot take into account the more complex evolutionary paths underlying cell type evolution (par. 1.3.3).

For these reasons, I used clustering methods to study the relationships between these cell types. Clustering methods are widely used to compare cells or tissues according to their expression profiles. Based on a defined “distance” measure between the cells or tissues to be compared, hierarchical clustering algorithms use a “bottom-up” approach to iteratively join the “closest” cells or groups of cells, and to construct a dendrogram from this “hierarchy”. By definition, hierarchical clustering methods are more precise at the “bottom” of the dendrogram, i.e. are more efficient in identifying the closest relatives in the dataset.

Hierarchical clustering methods are not unique, since different choices are possible for the calculation of the distance matrix and for linking adjacent cells or clusters. For these reasons, several methods have been explored here, in order to get a “consensus” picture of the clusters between the *hiomt*+ cells. The molecular fingerprints of the pigment cells and the rhabdomeric photoreceptors (Guy, 2009) have been used

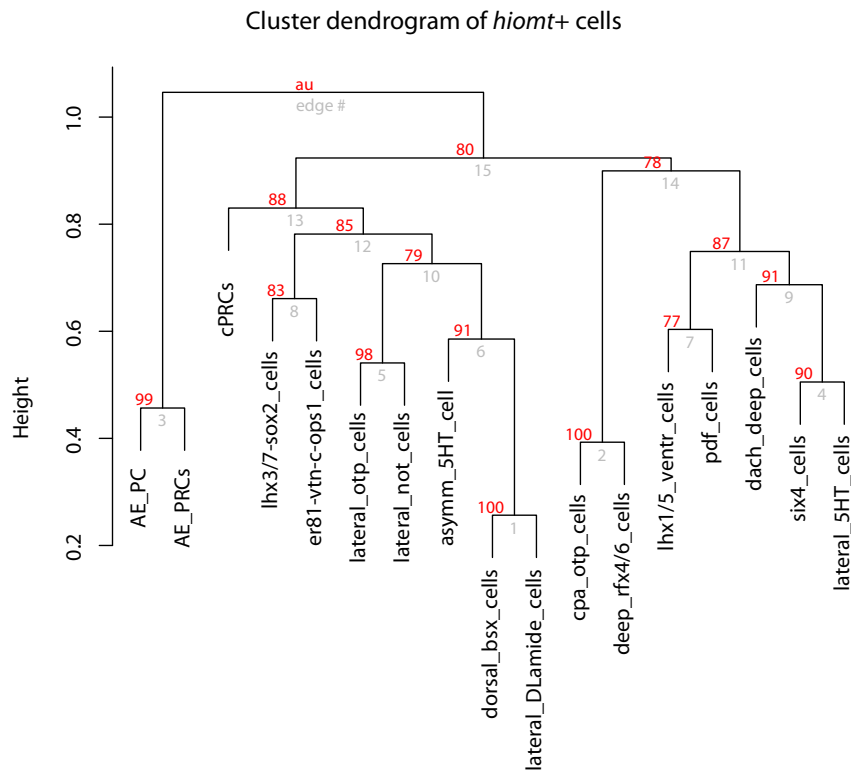


Figure 7.3: **Hierarchical clustering of *Platynereis hiomt* expressing cells.** Bootstrap values (red) associated to the hierarchical clustering of data in fig.7.2. The cluster analysis was performed with the R package *pvcust* using Pearson’s correlation and average linkage.

as an outgroup for the clustering analysis.

As shown in fig. 7.3, the *hiomt+* cells can be subdivided into two major clusters. The first group comprises cells located in the dorsal brain; most of them share the expression of *CNGa* and *cry1* and have the morphology of sensory cells. The second group includes the ventral cells surrounding the apical organ. Interestingly, the cells of the two groups segregate not only spatially (dorsal vs ventral), but also according to their functional properties: the cells of the dorsal group are the only ones expressing *CNGa* and opsins like *c-ops1* and *perops*; some opsins-expressing cells are present in the ventral cluster also, but they probably do not have the full phototransduction cascade, since *CNGa* is absent.

To assess the significance of these clusters, I performed a bootstrap analysis (fig. 7.3, see part IV for details). As expected, this shows that the most supported nodes of the cluster are the lower ones, i.e. the nodes joining pairs of cells, like the “adult eye photoreceptors” (AE-PRCs) and “adult eye pigment cells” (AE-PC), or the “dorsal

bsx cells” and the “lateral DLamide cells”. Indeed, different hierarchical clustering parameters join the “cpa otp cells” and the “deep rfx4/6 cells” to the *CNGa*-dominated dorsal cluster (not shown); this is reflected by the lower support of the higher node, but it is also a consequence of the paucity of the dataset.

An alternative way to represent the diversity of the *hiomt* expressing cells is to use methods from multivariate statistics, like non-metric multidimensional scaling (MDS, Everitt and Hothorn 2011). Given m cell types, the MDS is a method to obtain a graphical representation of these cell types in a low-dimension space, like 2D or 3D. The quality of this representation is given by the *stress* index (Everitt and Hothorn, 2011).

The MDS starts from a distance matrix of the samples (in this case, the cell types). To compute this distance matrix, I used the expression data for n genes, where every cell type is represented by a vector of n coordinates, and each coordinate is 1 or 0, according to the presence or absence of the corresponding gene.

For the cell types, I chose to use the Jaccard distance, which is an asymmetrix index that does not take in account the absence/absence case. In other words, the absence of a certain gene in two cell types does not contribute to the distance measure (does not make the cell types “closer” to each other)². From this distance matrix, I used MDS to calculate a projection in the 3-dimensional space, which is plotted in two different views in fig. 7.4. The MDS shows that the cells of the three clusters described above (the *hiomt+* clusters and the adult eye) segregate well in the 3D space, consistent with the clustering data. Moreover, the cells with more ambiguous location in the clustering (the “cpa otp cells” and the “deep rfx4/6 cells”, indicated by letters N and O in fig. 7.4A-B) are more distant from the other cells of the same cluster (the blue cells in fig. 7.4A-B). Finally, it can be noted that the presence or absence of *hiomt* does not correlate with the overall similarity of the cells analysed (compare fig. 7.4A-B and 7.4C-D). This indicates either that the expression of *hiomt* was lost independently during the evolution of these cell types in the annelid lineage, or that our current dataset is not broad enough to represent the real similarities between these cell types.

²The Jaccard distance is calculated from the Jaccard similarity index with the formula $d = \sqrt{1 - s}$, where s is the sum of intersections divided by the sum of union. For example, if the cell X expresses the genes a , b and c , and the cell Y expresses the genes a , b and d , the Jaccard similarity index is given by $s = (a + b) / (a + b + c + d)$. This suits gene expression data, because the presence of a gene in a certain cell type is more informative than its absence. See the Methods section for further details.

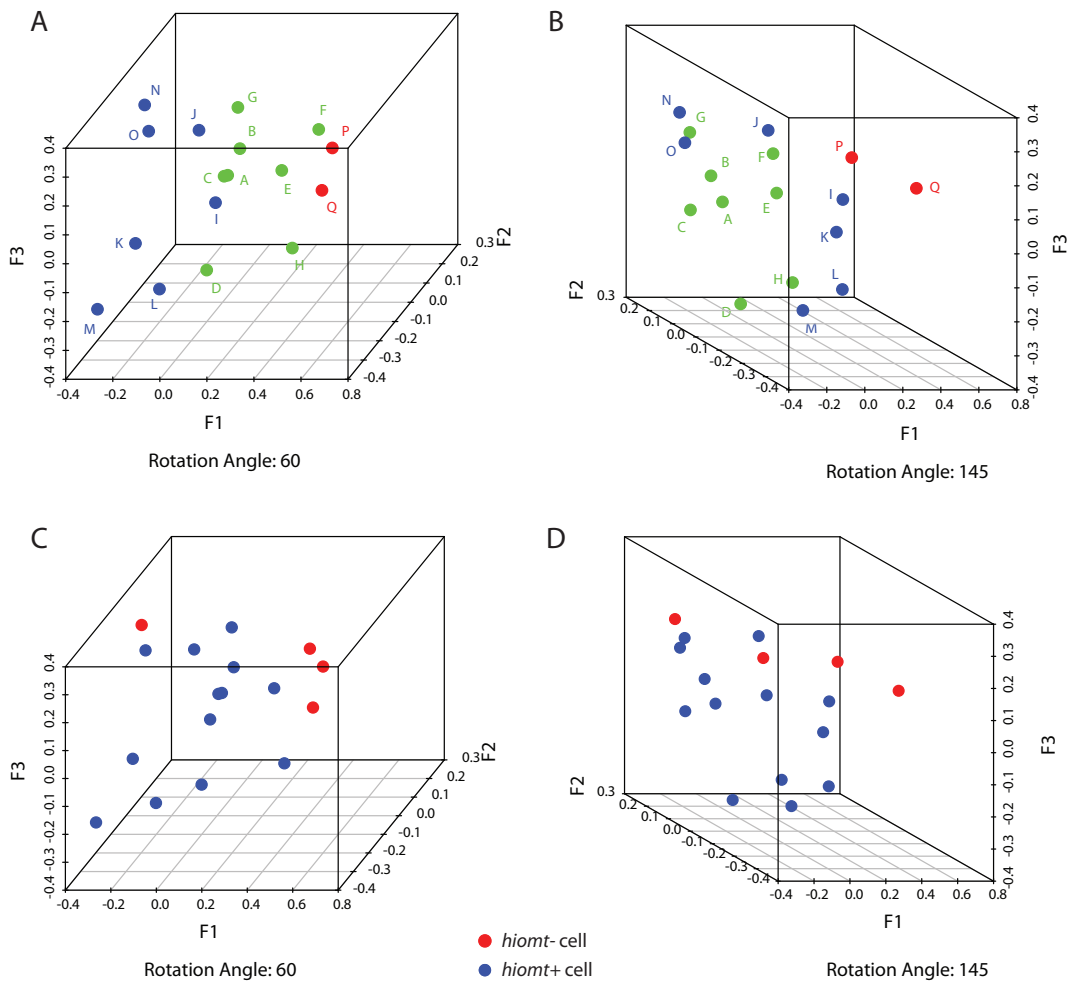


Figure 7.4: MDS visualizes the relationships of the *Platynereis hiomt* expressing cells. A. and B. Alternative views of the 3D plot of a non-metric MDS based on Jaccard distance, from the data in 7.2. The colors and the letters demarcating the points represent the individual cell types according to their cluster affiliation, as indicated in 7.2. C. and D. Alternative views corresponding to A. and B., where the colors indicate the presence or absence of *hiomt* in the cell. *Stress* of the MDS = 10.02.

The disadvantage of the MDS method is that it does not visualize how the distribution of cell types correlates with presence or absence of certain genes. This can be achieved using principal component analysis (PCA, Everitt and Hothorn 2011). The PCA provides a representation of the dataset according to the variables that contribute more significantly to the variance, and ignores the less significant ones, like those that are linearly dependent on each other, that have low variance, or that contribute noise. Geometrically, the $m \times n$ matrix (cell types \times genes) is linearly transformed in the n -dimensional space (intuitively, it is “rotated” and “stretched”) to find new orthogonal axes, which capture better the variance of the dataset. With this new representation, each new axis (called *principal component*) is a linear combination of the starting variables (in this case, the genes). The axes are ordered according to decreasing importance or “weight” (*eigenvalue*), reflecting the amount of variance represented by each axis; thus it is possible to ignore the less important components without losing too much information. Genes that contribute significantly to the same principal component will be highly correlated.

Fig. 7.5 shows the results of a PCA analysis of the *hiomt* cells (and the adult eyes). The cell types analysed distribute differently along the two main principal components (respectively, x and y axes in fig. 7.5A), although the two first principal components represent only 28.33% of the total variability of the dataset. This is an intrinsic limitation of using a binary dataset (presence/absence of the gene) for this analysis. However, the segregation of these cell types along the first two principal components is consistent with the clusters identified previously. If we analyse the contribution of the individual genes to the principal components (fig. 7.5B) it emerges that the first principal component (x axis) segregates the markers of visual eyes (*six1/2*, *otx*, *dach*, *enzA*, *mitf*) and circadian centers (*tbx2/3*, *cry1*, *otp*, *hiomt*). The second principal component segregates the cell types according to their spatial localization in the brain: dorsal cells (*foxD*, *not*, *er81*, *islet*, *eya*, *dll*) and more ventral cells (*brn1/2/4*, *dbx*, *sox2*, *neuroD*).

In summary, this analysis shows that the *hiomt* expression domain comprises several subtypes of cells, which can be distinguished between each other by the presence of restricted markers, both at the level of the regulatory signature (transcription factors, like *not* and *rfx4/6*) and differentiation signature (like neuropeptides). The existence of this diversity, illustrated by the MDS and PCA analyses, implies that in annelids melatonin synthesis is not restricted to individual cell types or tissues, but it can occur in many classes of neurons. However, it is possible to distinguish

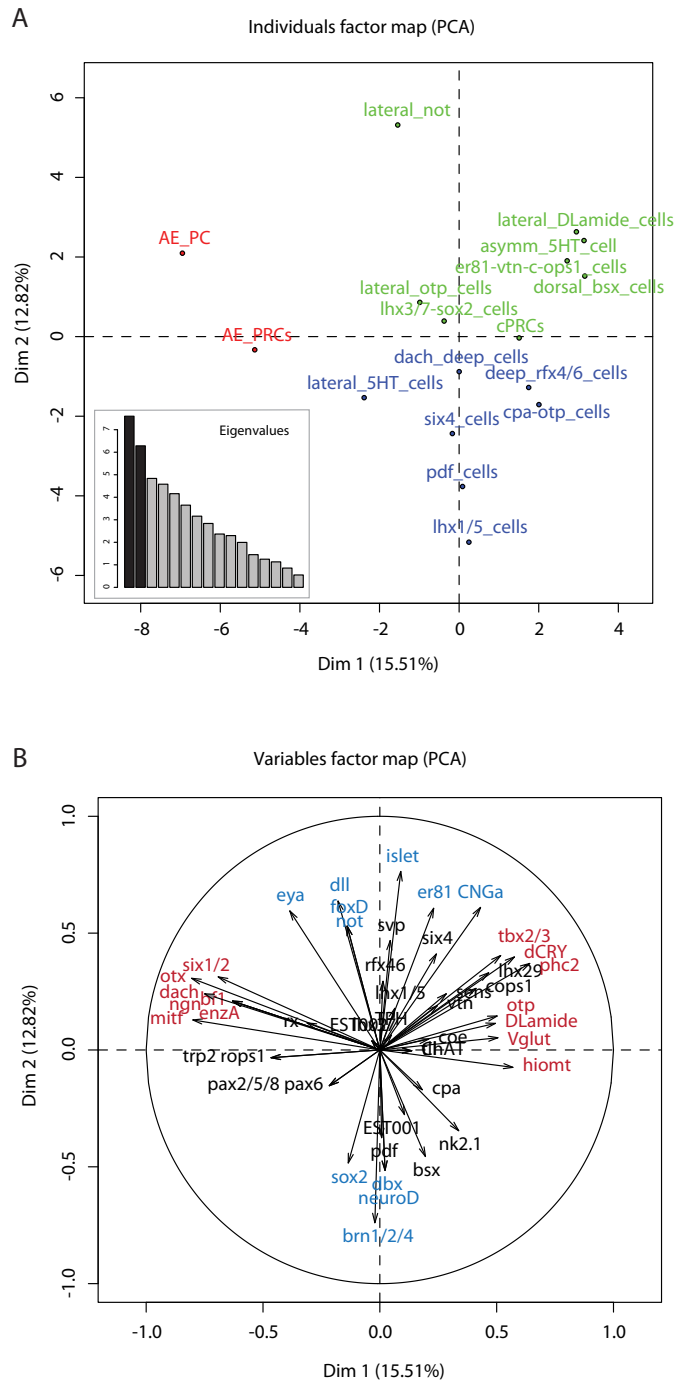


Figure 7.5: PCA of *hiomt* expressing cells. A. Distribution of the cell types according to the first and second principal components (x and y axes, respectively). The color coding corresponds to the cluster affiliation, according to fig.7.2. The inset shows the eigenvalues. B. Variables factor map, showing the correlation of the genes with the first two principal components. Red and cyan indicate the genes that are significantly correlated with the first and the second principal component, respectively ($p < 0.05$).

two major clusters of *hiomt+* cells, with distinct spatial distribution and different differentiation genes. These clusters probably correspond to two different “functional groups” of neurons, sensory neurons vs putative interneurons, showing that the activity of melatonin signalling in annelids is not restricted to photosensory cells.

7.3. A comparison of molecular fingerprints of melatonin producing cells between annelids and vertebrates

The molecular fingerprint data of the melatonin producing cells of *Platynereis* allow some comparisons with the melatonin system of vertebrates, the only group where *hiomt* expressing cells have been identified and characterized. Melatonin synthesis has been demonstrated in the pineal gland (where it is produced in high amounts and released in the blood stream) and the retinal photoreceptors (where it has a paracrine role). However, recent studies indicate that other parts of the brain might be involved in melatonin synthesis, including the SCN, the habenular nuclei, and the ependymal cells of the 3rd ventricle, where the deep brain photoreceptors are located (Hamada et al., 1999; Stefulj et al., 2001; Yu et al., 2002; Isorna et al., 2006). The identification of a sensory and a (putative) non-sensory cluster of *hiomt+* cells in *Platynereis* suggests that these different *Platynereis* cell groups might be related to vertebrate photosensitive and non-photosensitive melatonin synthesis sites, respectively. An alternative hypothesis is that the pineal-hypothalamic axis arose after a division of labour event and functional segregation (Arendt et al., 2008) from ancestral sensory-clock cells. In this case, the *Platynereis* non-photosensitive *hiomt+* cells might have evolved in annelids, or ancestral non-photosensitive melatonin producing cells might have been lost in vertebrates.

For *Platynereis*, the homology of the deep brain ciliary photoreceptors to vertebrate retinal and pineal photoreceptors has been previously proposed (Arendt et al., 2004); moreover, *c-ops1+* cells in the more ventral *otp* region have been compared to deep brain photoreceptors of the hypothalamus (Tessmar-Raible et al., 2007). Both these cell types express *hiomt*, as shown previously. However, the existence of other cell types with interesting molecular fingerprints, like the “not cells” and the asymmetric serotonergic cell, requires to refine the comparisons across species.

A plethora of microarray and ish data is available for vertebrates, especially for the mouse. However, these datasets do not satisfy the needs for single cell resolution. Moreover, the melatonin system evolved greatly from lampreys to mammals, where morphological changes were paralleled by changes in gene expression (Falcón

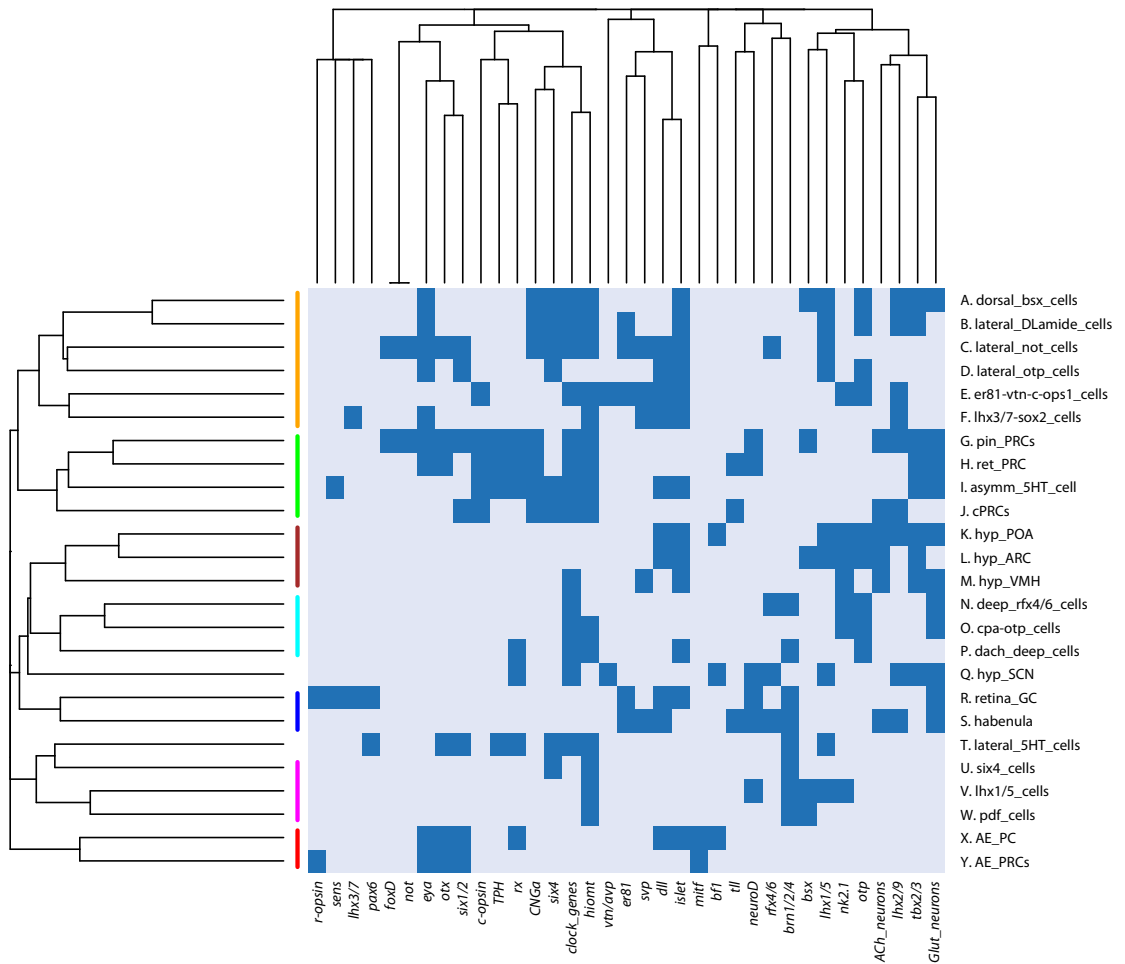


Figure 7.6: **Hierarchical clustering of *Platynereis* and vertebrate cell types involved in the melatonin system.** The figure shows an heatmap where cell types were clustered according to their molecular fingerprints. The dark blue indicates expression. The hierarchical clustering was based on a Jaccard distance matrix and complete linkage method. The vertical bars on the left indicate the groups appearing consistently after running the clustering with different parameters.

et al., 2009). Nevertheless, I used the knowledge available in the literature to deduce an “ur-vertebrate” gene expression table (Appendix D), and use this for molecular fingerprint comparisons with the *Platynereis* dataset. Besides the pineal and retinal photoreceptors (pin-PRCs and ret-PRCs) and the hypothalamic SCN (hyp-SCN), I included also few representative hypothalamic nuclei (hyp-POA, hyp-ARC and hyp-VMH), but also the habenula and the retinal ganglion cells, the latter possibly as an outgroup. For the hypothalamic and the habenular datasets, the only data available came from mouse studies.

Hierarchical clustering using six different methods³ produced consistent “sub-clusters” between these cell types (indicated by the color bars in fig. 7.6). The properties of these subclusters turn out to be very interesting. Indeed, the majority of them includes only *Platynereis* or vertebrate cells. Significantly, the only subcluster that consistently joins *Platynereis* and vertebrate cells is formed by the vertebrate pineal and retina photoreceptors, and the *Platynereis* ciliary photoreceptors and the asymmetric serotonergic cell (fig. 7.6). These cells share the expression of differentiation markers associated to three distinct functional tasks: phototransduction (*c-opsins*, *CNG*), circadian clock and melatonin synthesis (*tph*, *hiomt*). This cluster is linked together also by the expression of some transcription factors: *tbx2/3*, *lhx2/9* and *rx*. In *Platynereis*, the expression of *lhx2/9* in the dorsal brain follows very closely the *CNGa-cry1* patterns (Tomer et al., 2010), while *tbx2/3* and *rx* are expressed in the lineage giving rise to most of the clock region (“blue” lineage in par. 3.4). However, this analysis highlights significant differences in the transcription factor profile of these photoreceptor cells. For example, *otx* genes are expressed only in the vertebrate but not in the *Platynereis c-ops1+* cells, while *six4* is present in the *Platynereis c-ops1+* cells but is not related at all to photoreceptors in vertebrates.

This implies either that the genes that maintain the expression of the conserved differentiation markers (the “terminal selector genes”) are different between annelids and vertebrates, or that the most relevant transcription factors are not included in this clustering. It would be extremely interesting to investigate in *Platynereis* the expression of less “popular” transcription factors which have been recently shown in vertebrates to keep the differentiated state of photoreceptors, without being necessarily involved in the first steps of eye development (Swaroop et al., 2010; de Melo et al., 2011).

³Distance matrix: Pearson’s correlation, uncentered correlation or Jaccard distance; linkage methods: average or complete.

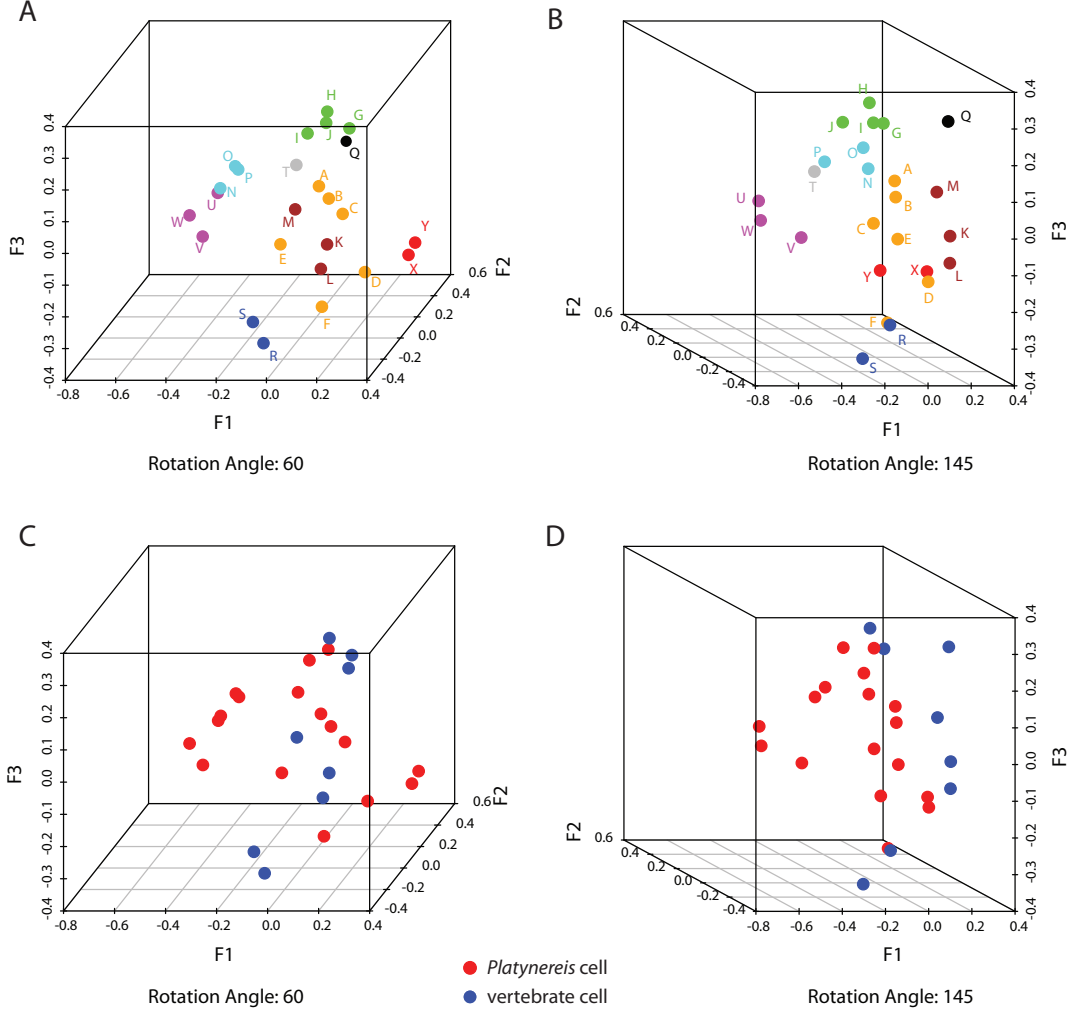


Figure 7.7: MDS of *Platynereis* and vertebrate cell types. A. and B. Alternative views of the 3D plot of a non-metric MDS based on Jaccard distance, from the data in 7.6. The colors and the letters demarcating the points represent the individual cell types according to their cluster affiliation, as indicated in 7.6. C. and D. Alternative views corresponding to A. and B., where the colors indicate if the corresponding cell type belongs to *Platynereis* or vertebrates. Stress of the MDS = 14.53.

In addition to the clustering, the MDS in fig. 7.7 helps to understand better the higher-level relationships between these cell types. The vertebrate/*Platynereis* photoreceptors group (which forms an highly compact cloud in the MDS, green points in fig. 7.7A-B) is more closely related to a group of *Platynereis*-only cells (orange cloud), represented by cells immediately surrounding the cPRCs region, which are the same that cluster together with the cPRCs and the asymmetric serotonergic cell in the analysis with *Platynereis*-only cells (cfr. fig. 7.2). Some of these cell types probably result from protostome or annelid-specific diversification from an ancestral photoreceptor-related cell type (most of them still express *perops* and *CNGa1*); although it cannot be excluded that these cells might compare to some cryptic cell types of the vertebrate brain, given the lack of vertebrate single-cell resolution data.

Some cells of the same group are also particularly similar to the hypothalamic structures analysed here (orange and brown clouds in fig. 7.7A-B; indeed these two subclusters are joined together after running the hierarchical clustering with parameters different from fig. 7.6). Intriguingly, one of these cell types (“er81-vtn-c-ops1 cell”, indicated with “E” in the figure) has been previously compared to cell types of the vertebrate hypothalamus (Tessmar-Raible et al., 2007). This new analysis extends the conclusions from Tessmar-Raible et al. (2007), showing that including more genes and more cell types can improve the general picture and indicate new candidates for further studies.

Another interesting conclusion from this analysis is that the vertebrate suprachiasmatic nucleus (“hyp-SCN”) is not much similar to any other cell type analysed, including the other nuclei of the hypothalamus compared here (which all cluster together). This confirms that the SCN is a special molecular territory within the mammalian CNS. For the comparison with the annelid cell type repertoire, it would be extremely interesting to use single-cell gene expression data from a non-mammalian vertebrate (like a fish), where the SCN is considered functionally different from its mouse anatomical counterpart.

A final observation is that the cells chosen as outgroups, the *Platynereis* adult eyes and the vertebrate habenula and retinal ganglion cells, are indeed well separated from the rest of the cells analysed. The significance of the clustering of the habenula with the retinal ganglion cells needs further investigations, since this dataset has not been designed to analyse specifically these cell types.

In conclusion, this analysis extends the previous molecular comparisons and high-

lights the power of statistical methods to detect relatedness of molecular fingerprints. Methods like this are best suited for more in depth comparative analyses under more realistic evolutionary models, where the 1:1 comparisons are extended to comparisons between groups of cells, consistent with convergent division of labour scenarios. The resolution of this comparison can be dramatically improved in the future by extending the number of cells to compare, extending the number of genes (beyond the candidate gene approach), and generating data from other organisms with single-cell resolution.

DISCUSSION

8.1. The effects of light on *Platynereis* locomotor behaviour

Previous studies showed that *Platynereis* larvae develop different sets of rhabdomeric and ciliary photoreceptors to respond to light (Arendt et al., 2002, 2004; Tessmar-Raible et al., 2007). In particular, Jékely et al. (2008) demonstrated a direct link between light sensitivity and larval locomotion: the rhabdomeric larval eyes sense the direction of the light, and steer the larvae towards the light source for positive phototaxis. This involves a monosynaptic pathway, where each larval eye innervates only one prototroch cell and changes its ciliary beating frequency (CBF).

In this work I found that *Platynereis* larvae have a circadian rhythm of CBF, where CBF is higher during the daytime, and decreases at night. This means that non-directional light affects larval locomotion on a different level, by modulating the ciliary beating frequency of all the prototroch cells, without any directional response.

This photic control of locomotion takes place in the circadian center of the dorsal brain, where three distinct light receptors - *perops*, *c-ops1* and *cry1* - are coexpressed. These neurons (or a significant subset of them) project to the prototroch directly, and express the melatonin synthesis gene *hiomt*; consistently, a melatonin receptor is expressed in the prototroch cells. The coupling of melatonin release to photic input is indicated by the tight coexpression of *hiomt* with the brain opsins and *cry1*. Moreover, preliminary qPCR experiments show an increase of *hiomt* expression in the second half of the subjective night (not shown). And finally, the application of melatonin to *Platynereis* larvae during the subjective day is able to induce a decrease of ciliary beating frequency (CBF) in the prototroch cells (mimicking night conditions). These results support the hypothesis that melatonin is the output of the circadian system and modulates locomotor activity.

8.1.1. The photic control of melatonin synthesis

In the majority of the vertebrate species investigated so far, melatonin release is controlled by the circadian clock and by light directly (par. 2.3.1).

Our data suggest that this dual control of melatonin release might exist also in *Platynereis* larvae: exposing the animals to light during the subjective night induces a strong increase of CBF, and the same effect is produced by blocking the phototransduction with a CNG channel inhibitor. This is consistent with the hypothesis that light induces an OFF-response, which closes the CNG channels and suppresses melatonin release; however, it cannot be excluded that other neurotransmitter systems are involved in this response. The CNG-dependent OFF-response is necessarily triggered by the activation of an opsin; and considering that *hiomt* and *perops* are largely coexpressed (while *c-ops1* comprises only few cells of the *hiomt*-*CNGa* domain), the hypothesis would be that peropsin is the OFF-responding photopigment that controls melatonin synthesis at night.

Accordingly, peropsin would be necessarily coupled with the inhibitory G_i alpha subunit¹, which triggers a cascade terminating with the decrease of cAMP, the closure of CNG channels and the decrease of intracellular Ca²⁺ concentration. Although the coupling of peropsins has never been studied in other species, members of the related neuropsin family have been shown to use G_i for phototransduction (Yamashita et al., 2010; Kojima et al., 2011).

A second pathway, via the putative light-sensitive cry1, would contribute specifically to the entrainment of the clock, and to the clock-dependent melatonin rhythm. In *Drosophila* dCRY (the homolog of Cry1) is indeed the receptor expressed in the clock neurons of the brain, and responsible of the clock entrainment. It would be interesting to test if the transcriptional activity of *Platynereis* Cry1, like all the other “insect type 1 cryptochromes”, is regulated directly by light, and if Cry1 or Period bind directly to the *hiomt* promoter.

8.1.2. The role of the *c-ops1*+ cells

The model proposed above doesn't assign a direct role to the *c-ops1*+ cells in the regulation of melatonin synthesis and CBF rhythms. The *c-ops1*+ cells of *Platynereis* brain are heterogeneous themselves: the more medial *c-ops1*+ *vtn*+ cells do not express *CNGa*, and probably use photic information to control hormonal release (Tessmar-Raible et al., 2007). The deep brain “canonical” cPRCs (Arendt et al., 2004)

¹All the other G proteins that exist in invertebrates would be excitatory.

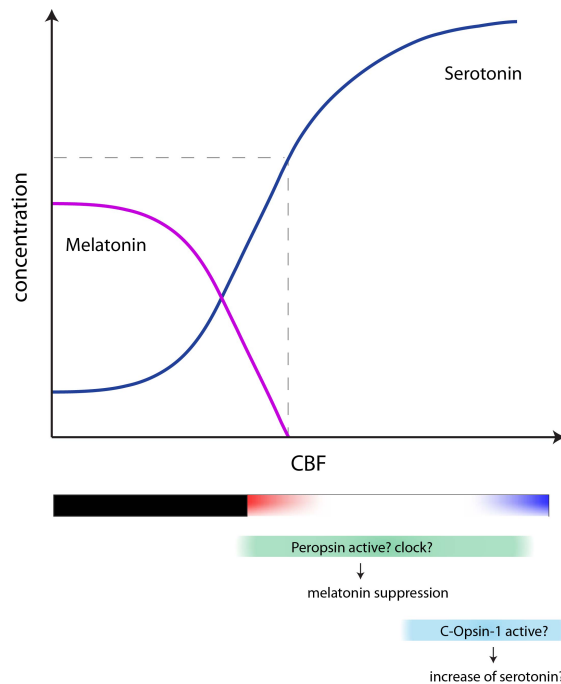


Figure 8.1: **A model for the antagonism of serotonin and melatonin in *Platynereis*.** Gradients of serotonin and melatonin have opposite effect on the ciliary beating frequency. At night, the melatonin concentration reaches the maximum values, pushing the CBF values to the minimum. During daytime, melatonin suppressing signals like the clock and light OFF-response (from Peropsin?) contribute to the decrease of melatonin concentration, the increase of serotonin concentration, and the increase of CBF. Serotonin concentration can be increased above stationary levels by additional stimuli. According to the “chromatic discrimination” model for the *c-ops1* cells, the enrichment of light spectrum with short-wavelength illumination at twilight activates the c-Opsin1, thus contributing to the increase of serotonin transmission.

remain still enigmatic: the current data don’t provide any evidence for direct projections to the prototroch. They might be involved in the entrainment of the clock: they express all the clock markers, and might signal locally to provide photic information to neighboring cells, like the lateral serotonergic cells.

The current data raise some specific hypotheses for the role of the *c-ops1+* asymmetric serotonergic cells. These hypotheses are purely speculative and will need to be tested experimentally.

The immunostainings show that the axon of this cell joins an extensive serotonergic plexus underneath the apical organ, which then innervates the prototroch. Thus it is likely that the asymmetric *c-ops1+* serotonergic cell contributes a photic input to the release of serotonin at the prototroch level.

Like in nearly all the species investigated so far, serotonin increases CBF in

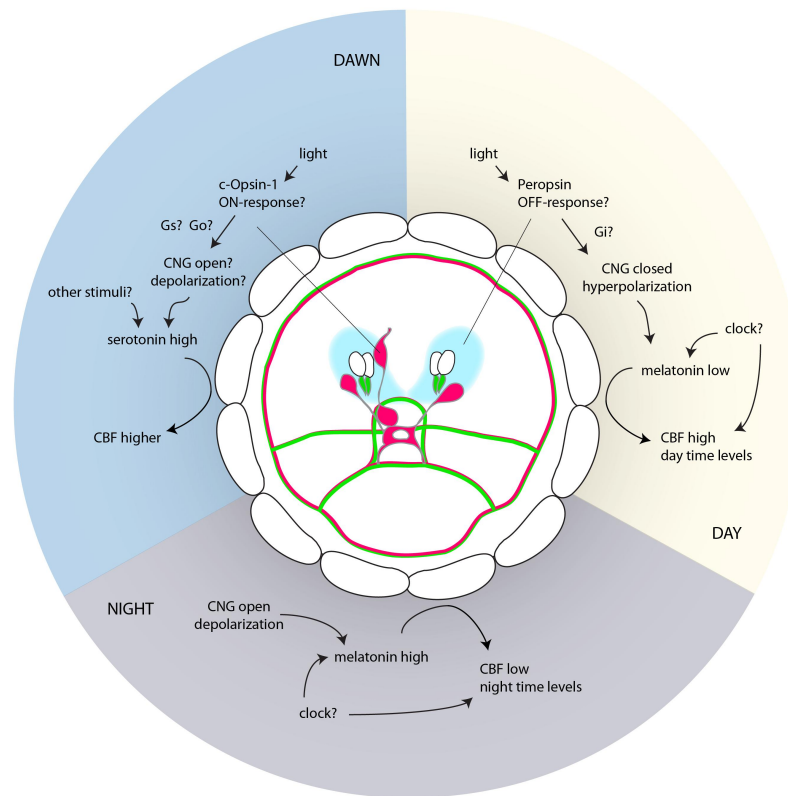


Figure 8.2: **The organization of *Platynereis* photic control of ciliary beating.** The model proposes three alternative states at daytime, nighttime and twilight. During the day, a light OFF-response (probably mediated by Peropsin) closes the CNG channels and decreases the membrane potential of the clock cells. This, together with the circadian clock, suppresses melatonin synthesis. As a result, CBF is higher than night. At night, the absence of light allows the opening of CNG channels, the depolarization of *hiomt+* cells and, together with the clock, melatonin synthesis. Melatonin slows down CBF to night time levels. At twilight (dawn and dusk), the incident light is enriched in short-wavelengths. Melatonin is suppressed as during daytime. In the *c-ops1+ perops+* cells, the *c-Ops1* has an ON-response to light, which increases the serotonin release, and brings CBF to the highest levels in the light-dark cycle.

Platynereis larvae, and tonic serotonin release is necessary to sustain ciliary beating of the prototroch cells (Dr. G. Jekely, personal communication). Thus serotonin and melatonin have antagonistic effects on ciliary beating and locomotion. However, melatonin is synthesized from serotonin, and for this reason in several species a serotonin diurnal rhythm is present in antiphase with the melatonin rhythm (Falcón et al., 2009). Thus in a simple scenario several inputs, including light, can act at different levels to change the serotonin-melatonin ratio, and then the locomotor activity (CBF, fig. 8.1). It remains to be understood how the three different light receptors affect the serotonin-melatonin ratio in the larval brain during the light-dark cycle.

An interesting scenario for the possible function of the *c-ops1+* asymmetric serotonergic cell comes from the observation that this cell coexpresses two opsins, *c-ops1* and *perops*. The expression of two opsins in the same cell is considered the basis for the “chromatic response”, registered in the pineal complex of several species, and described with molecular details in the lizard parietal eye (Su et al., 2008; Ekström and Meissl, 2010). In these examples, the photoreceptors express two opsins, which respond to two different wavelengths, and act antagonistically (via different G proteins) on the concentration of cyclic nucleotides and the gating of CNG channels. In the lizard case described by Su et al. (2008), the blue-sensitive pinopsin induces an OFF-response (hyperpolarization), while the green-sensitive parietopsin triggers an ON-response (depolarization). Thus the final electrical activity of these cells depends on the spectral composition of the incident light, i.e. the ratio between the two wavelengths detected by the two opsins.

It is reasonable to assume that the *c-ops1+ perops+* cells do not use these opsins redundantly (i.e. to sense the same wavelength or to produce the same kind of response). The *c-ops1* would then be coupled to an excitatory G protein, probably G_o or G_s , and elicit an ON-response with the opening of CNG channels. An indication that this could be the case for the *Platynereis c-ops1+* photoreceptors comes from the calcium imaging experiments, where the constant illumination of the episphere elicits an ON-response in a limited number of cells of the dorsal brain, which by position could correspond to the *c-ops1+* cells.

This “chromatic discrimination” mechanism would be perfectly suited to discriminate the twilight (dusk and dawn) and/or the moonlight, since in these cases the spectrum of the light penetrating the sea is enriched in short or long-wavelengths, respectively (McFarland, 1986; Ragni and Ribera D’Alcalà, 2004; Sweeney et al., 2011). With this simple mechanism, the young larva could reliably detect the light-dark

transitions, because these neurons would fire only at dusk and dawn (at night, the c-Ops1 is not active, while at noon, the c-Ops1 ON-response is counteracted by the Perops OFF-response). “Morning” and “evening” information are crucial to fine-tune the daily behaviour in several species; the collective behaviour of marine zooplankton indicates that this must be the case also in marine species (see section 8.5). Here, the chromatic discrimination would be achieved not after integration processing in a complex circuit, but simply with the intracellular response of a small group of sensory-motor neurons (fig. 8.2).

Further experiments are needed to test this hypothesis and elucidate the detailed physiological roles of the asymmetric serotonergic cell and the larval serotonergic system in general.

8.2. Tracing the evolution of brain photoreceptors and circadian centers in Bilateria

The mechanisms described here, underlying photic control of behaviour in *Platynereis* larvae, might be valid for the larvae of other marine invertebrates.

An hint for the conservation of a dorsal brain clock region within annelids comes from the miRNAs study from Christodoulou et al. (2010). The authors identified two conserved miRNAs expressed in the so called *Platynereis* “neurosecretory region” (i.e. the *CNGa-cry1-perops* cells): miR-7 and miR-137. Similarly, a big cluster of miR-7+ miR-137+ cells was found in the posterior brain of another annelid, *Capitella teleta*. Moreover, serotonergic cells closely associated to extra-ocular photoreceptors develop in the same region of *Capitella* brain (Kaller, 2011). Finally, the other genes involved in the *Platynereis* melatonin system, like *hiomt* and *cry1*, are present in the *Capitella* genome. These data indicate that many cell types homologous to those described here in *Platynereis* might exist in *Capitella*, an annelid of the Sederentaria clade. More detailed molecular studies in *Capitella* would help to reconstruct the cell type repertoire of the melatonin system in ancestral annelids.

To establish which components of the annelid circadian-melatonin system are conserved across phylogeny, a similar molecular study should be performed in selected marine species. The presence of melatonin has been demonstrated in several invertebrates (Vivien-Roels and Pévet, 1993; Tilden et al., 1997; Mechawar and Anctil, 1997; Finocchiaro et al., 1988; Itoh et al., 1999; Bembenek et al., 2005; Tanaka et al., 2007; Pape et al., 2008; Muñoz et al., 2011), but this study is the first characterization of the *hiomt* expressing cells in a protostome. Unfortunately, only few other marker genes

have been investigated in other marine larvae, including the opsins, which would be very useful to compare photoreceptor cell types. The data currently available allow anyway to draw some conclusions.

First, the genome data from basal metazoans indicate that the opsins evolved in the last common ancestor of Cnidaria and Bilateria (eumetazoan ancestor). On the other end, the cryptochromes are phylogenetically much older, thus the presence of light-sensitive cryptochromes is likely to explain the simple photic behaviour of species which lack opsins, like the sponges (Leys and Degnan, 2001; Müller et al., 2010). Light-sensitive cryptochromes have been demonstrated in two cnidarians, the sea anemone *Nematostella vectensis* and the coral *Acropora millepora* (Levy et al., 2007; Reitzel et al., 2010). The evolution of opsins in eumetazoans probably conferred the possibility to expand the complexity of responses to light. First of all, opsins can evolve to detect different spectra, while cryptochromes are restricted to blue-light photoreception. Second, opsins are coupled with G-protein transduction cascades, which produce signal amplification, but also flexibility in the kind of response (ON- or OFF-response). The model proposed above for the *Platynereis* asymmetric serotonergic cell shows how these properties alone might be sufficient to evolve complex responses to light.

Lophotrochozoan representatives, including *Platynereis*, have members of several opsin families. Besides the c-opsins, the r-opsins and the G_o-opsins, which have been classically described in the eyes of different species, members of the peropsin and the neuropsin families are present in Bilateria. The latter two opsin types are certainly involved in light signalling, since they retained all the residues involved in signal transduction. Moreover, it is very unlikely that invertebrate peropsins are photoisomerases, because all the invertebrate opsins are bistable (they don't need a photoisomerase to reconstitute the 11-*cis*-retinal). From these considerations, it is clear that the role of these two opsins in metazoans needs to be investigated in more detail. Our data in *Platynereis*, together with the recent characterization of neuropsin expression in brain photoreceptors (Yamashita et al., 2010; Nakane et al., 2010; Kojima et al., 2011), point to an important role of peropsins and neuropsins in animal non-visual photoreception.

Notably, a recent report showed the broad expression of a ciliary-opsin related gene in the apical plate of a lophotrochozoan larva, the brachiopod *Terabratalia transversa* (Passamanek et al., 2011). The phylogenetic position of this opsin is ambiguous, but its expression pattern resembles very closely the *Platynereis perops* rather than the *c-ops1* pattern (Marlow et al., 2012). This confirms that the expres-

sion of opsins in the apical ganglia of marine invertebrates is a common theme, and more data are needed to establish if these brachiopod brain photoreceptors control melatonin release, like in *Platynereis*.

Phototransduction in non-rhabdomeric opsins is coupled to CNG channels. This is the case not only for c-opsins, but also for the G_o -opsins, which are expressed in cells with a ciliary-type morphology. Our data suggests that peropsin might use the same cascade. We can speculate that the split between photoreceptors with ciliary and rhabdomeric morphologies was concomitant to the evolution of two signalling modalities: the cyclic nucleotide-CNG cascade and the phosphoinositides-TRP cascade, respectively (Arendt, 2003). Cnidarian photoreceptors use a CNG channel for phototransduction (Plachetzki et al., 2010), suggesting that this signalling modality was already present in the eumetazoan ancestor.

It is also reasonable to assume that the last common ancestor of protostomes was using brain photoreceptors for the entrainment of the circadian clock. Homologs of c-opsins, called pteropsins, have been identified in the brain of the honeybee (Velarde et al., 2005); several pteropsins are present in the genome of *Daphnia* (Colbourne et al., 2011). Pteropsins do not exist in *Drosophila*, where the clock neurons (located in the protocerebrum) are entrained by the dCRY (the homolog of *Platynereis* cry1) and by the input coming from the eyes (par. 2.2 and Nitabach and Taghert 2008). Anyway, the circadian organization of *Drosophila* is probably derived in many respects. One important aspect is the loss of the mammalian-type cryptochrome (cry2, see fig. C.1), which in mammals binds to Period to control Clock/Bmal activity. In *Drosophila*, the mammalian-type cryptochrome is replaced by Timeless. Interestingly, other insects like the honeybee and the butterflies have all the mammalian-like clock components (Rubin et al., 2006), which have also been identified in cnidarians (Vize, 2009; Reitzel et al., 2010). This is consistent with the hypothesis that the circadian clock at the base of Bilateria had a “mammalian-like” structure, and that the *Drosophila* clock circuits evolved after gene losses and recruitment of genetic elements in the clock oscillator.

As a clock output, this study indicates that melatonin was present already in the last common ancestor of Bilateria. It is possible that melatonin signalling was associated with photoreceptors even earlier in evolution, since *hiomt* genes exist in Cnidaria, and the presence of rhythmic melatonin in neurons has been documented (Mechawar and Anctil, 1997). Moreover, melatonin and serotonin have opposite effects on the spawning of the sea pansy (Anctil et al., 1991).

In protostomes, the circadian clock has a second molecular output, the neuropeptide PDF. The current genomic data available indicate that this neuropeptide evolved specifically in the last common ancestor of protostomes (Anctil, 2009; Veenstra, 2010, 2011). The association of PDF with the clock in lophotrochozoans needs to be demonstrated, but it is likely, considering that in *Platynereis* few *pdf*⁺ cells are present in the dorsal brain; at later stages, a conspicuous cluster of PDF cells develops in the adult eye region (not shown). In vertebrates, PDF is not present and newly evolved peptides (like VIP and PACAP) have roles in the circadian system comparable to the insect PDF peptides (Helfrich-Förster, 2004; Mertens et al., 2007).

In summary, comparative data from *Platynereis* and other species provide a first picture on the organization of brain photoreceptors and circadian centers in the urbilaterian ancestor. More data are needed, especially to elucidate the eumetazoan organization, and to understand how brain photoreceptors and circadian centers evolved in different lineages.

8.3. Serotonergic photoreceptors in other invertebrates?

From a comparative perspective, the most interesting cell type identified in the *Platynereis hiomt* region is the asymmetric serotonergic *c-ops*⁺ cell. Indeed, while the molecular expression data in marine larvae are generally scarce, there is a plethora of studies showing the distribution of serotonergic neurons in several animal phyla (Hay-Schmidt, 2000). Serotonin immunostainings are classically used as a “marker” for studying the apical organ of invertebrate larvae. Recent molecular data from Marlow et al. (2012) show that the same sequence of transcription factors and the same signalling pathways are used to pattern the nervous systems in protostomes and deuterostome larvae. Consequently, the apical organs of these animals can be considered homologous. The detailed homologies at the level of individual cell types within the apical organs will need further molecular data; however, several lines of evidence indicate that the association of serotonin with photoreception might be an ancestral trait conserved throughout evolution.

In all the larvae investigated so far, the apical serotonergic cells innervate the ciliated cells responsible of locomotion, and serotonin increases the frequency of ciliary beating (Doran et al., 2004; Katow et al., 2007; Yaguchi and Katow, 2003a; Kuang et al., 2002).

Spiralians (like annelids, molluscs and some other groups within Lophotrochozoa)

have usually a limited number of apical serotonergic neurons (3-5 cells), including at least one pair of symmetric neurons that project directly to the prototroch (like the *Platynereis* lateral serotonergic cells). The presence of one median (or asymmetric) serotonergic cell has been described in representatives of several groups: in the annelids *Polygordius lacteus* and *Phyllodoce maculata* (Hay-Schmidt, 2000; Voronezhskaya et al., 2003), in the majority of the mollusc species investigated (Page and Parries, 2000), and in entoproct trochophores (Hay-Schmidt, 2000).

The non-spiralian protostomes (phoronids and brachiopods) have bigger clusters of serotonergic cells associated with the apical ganglion (see Hay-Schmidt (2000) and references therein), where an individual “asymmetric cell” cannot be recognized. In the brachiopod *Terebratalia transversa*, the serotonergic cells are located in proximity to the apical tuft (Altenburger et al., 2011), where also the *Ttr-c-ops* is expressed (Passamaneck et al., 2011); although the colocalization of serotonin and *c-ops+* will need to be tested in detail, this indicates already that serotonergic signalling and photoreception are closely interconnected also in this group.

In deuterostomes, serotonergic cells have been described in the apical organ region of sea urchin and hemichordate larvae, in the amphioxus frontal eye, and in the tunicate sensory vesicle.

The sea urchin serotonergic cells express *rx* (Yaguchi and Katow, 2003b; Wei et al., 2009). Recently, the expression of encephalopsin has been documented in the larvae of the sea urchin *Hemicentrotus pulcherrimus*: at early larval stages, the encephalopsin+ cells are scattered throughout the whole ectoderm but more concentrated around the apical organ (Ooka et al., 2010).

A similar connection is suggested by data from hemichordates, which have photoreceptors and eye spots at the apical pole (Brown et al., 2008), where also the serotonergic cells are located (Nakajima et al., 2004).

In ascidians, the brain serotonergic cells are closely associated to the sensory vesicle (including ciliary photoreceptors of the ocellus) and project posteriorly to the motor centers; this led Stach (2005) to suggest that serotonin has “an integral function in chordate locomotion”.

In amphioxus, serotonin immunostaining has been reported in the so-called “row 2” cells of the frontal eye. These cells have the morphology of ciliary photoreceptors, and project posteriorly to the tectal cells, which contact the primary locomotor center (Holland and Holland, 1993; Moret et al., 2004; Lacalli, 1996). A recent miRNA study (Candiani et al., 2011) showed expression of miR-7 in the frontal eye; the

same miRNA is expressed in the *Platynereis* asymmetric serotonergic cell and in the whole clock region (Christodoulou et al., 2010).

The kinship of these serotonergic cells is indicated not only by their position and molecular identity, but also by their function. In all the species tested, serotonin is a modulator of locomotor activity, and it has the specific property of increasing the ciliary beating frequency, or generally of enhancing locomotion (Braubach et al., 2006; Yaguchi and Katow, 2003b; Hardaker et al., 2001; Angstadt et al., 2005; Doran et al., 2004). This effect is the opposite of melatonin, which reduces locomotor activity and induces sleep-like states in several invertebrate and vertebrate species (Zhdanova et al., 2001; Tanaka et al., 2007). Similarly, in *Platynereis* melatonin decreases and serotonin increases ciliary beating frequency (Gaspar Jekely, personal communication), implying that serotonin and melatonin have specular effects on the activity of the prototroch cells. In *Platynereis*, the regulation of serotonin and melatonin by light takes place in the same cells, in the dorsal part of the brain. So the non-visual light input modulates directly the locomotor behaviour with the adjustment of the serotonin-melatonin ratio.

8.4. Ancient links between light receptors and indoleamines

Indoleamines (serotonin and its derivative, melatonin) are older than opsins, and are present in plants, fungi and protists. The presence of indoleamines in almost any living organism is linked to their antioxidant properties. Melatonin, serotonin and their metabolites are very efficient scavengers of free radicals, which are produced in high amounts during oxidation processes, including photosynthesis and photoreception (Pandi-Perumal et al., 2006; Reiter et al., 2010). It has been proposed that this function facilitated the early evolution of the serotonin and melatonin biosynthetic pathway from tryptophan (Azmitia, 2007).

The role of melatonin as a “dark message” might have evolved even before photoreceptors, as a consequence of its chemical properties. Several studies showed that melatonin is extremely unstable in light conditions, since it is photooxidized. Melatonin photooxidation takes place only in cellular extracts, and not in pure solutions (Hardeland et al., 1995). This property might have favored the evolution of melatonin as a signal of darkness. In dinoflagellates, a circadian rhythm of melatonin content, with a peak during the night, has been observed (Hardeland, 1993).

It is then plausible that, with the evolution of opsins, the serotonin-melatonin system was potentiated in photoreceptors for the antioxidative defense (Siu et al., 2006).

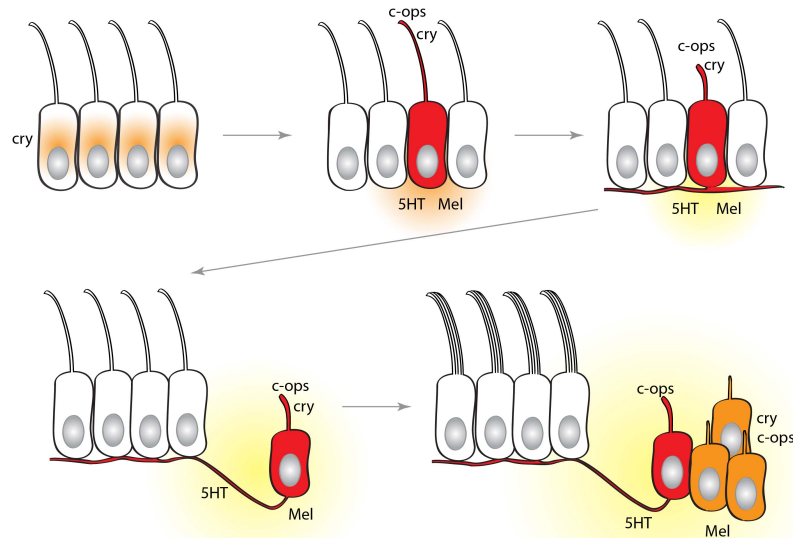


Figure 8.3: **A scenario for the early evolution of metazoan serotonergic and melatonin systems.** According to this scenario, serotonin and melatonin were already present in the earliest metazoans, before the evolution of opsins, where melatonin might have been already used as a “darkness signal” under the control of circadian clocks. With the evolution of opsins, ciliary photoreceptors coopt serotonin and melatonin to signal light and darkness. These photoreceptors specialize as clock cells, and use the indoleamines to regulate the ciliary beating of neighboring cells. Later, these ciliary photoreceptors abandon the epithelium and concentrate in the apical ganglion. More photoreceptors and clock neurons diversify; some of them lose their direct contact with the locomotor ciliated cells (multiciliated in spiralian larvae), but still use the diffusible melatonin as an output of the clock.

The serotonin-melatonin ratio was naturally coupled to light-dark cycles, because of melatonin photooxidation in the light. Since cryptochromes and circadian clocks evolved before opsins, it cannot be excluded that rhythmic melatonin synthesis was already in place in the earliest metazoans.

The presence of melatonin in photoreceptors might have been fixed by a second chemical property of indoleamines. Arylalkylamines, the decarboxylation products of several aminoacids, can react spontaneously with retinal. This reaction depletes the cell of retinal, the opsin cofactor essential to sense light. Moreover, the reaction product is highly toxic. The acetylation of arylalkylamines by Aanat would have prevented the formation of these dangerous arylalkylamines-retinal adducts (Klein, 2004).

According to this model, the evolving opsin-based photoreceptors used indoleamines first for their roles in cellular physiology, and later as neurotransmitters

and neurohormones. Serotonin and melatonin, released with opposing rhythms, became the signals of presence or absence of light, and the modulators of ciliary locomotion. In a division of labour interpretation (fig. 8.3), this modulation was first paracrine, and then neural and paracrine, after the evolution of specialized photoreceptor cells from epithelial sensory locomotor cells.

In the earliest clock centers of bilaterian brains, serotonin was used only for neurotransmission, while melatonin became a systemic signal for darkness, again because of its chemical properties: it is a lipophilic molecule that diffuses easily through the cell membranes. For this reason, more kinds of sensory cells might have specialized in the release of melatonin, without keeping a direct contact with the ciliated locomotor cells. A similar scenario would explain the evolution of the melatonin system as it is found in *Platynereis* larvae.

8.5. The dawn of circadian clocks from an ecological perspective

Rhythmic locomotor behaviours have been described in many species of marine invertebrates. The most widespread rhythmic behaviour is the diel vertical migration (DVM) in the pelagic phase: the day-night change in swimming depth of marine zooplankton, within amplitudes from a few to 100 meters, where normally the zooplankton swimming depth is higher during the nighttime, and viceversa (Kampa and Boden, 1954; Ringelberg, 2010).

Despite some authors believe that the DVM of zooplankton has a purely adaptive role for predator avoidance, several studies showed that the DVM behaviour depends on photoresponses (Sweatt and Forward, 1985), is influenced by the daylength (Hansson et al., 2007a), and specifically by an UV-avoidance behaviour in *Daphnia* (Rhode et al., 2001; Leech et al., 2005; Hansson et al., 2007b). Following these evidences, it has been proposed that circadian rhythms and UV/blue-light photoreceptors evolved for the first time to avoid UV radiation and for feeding, to follow the daily migration of phytoplankton. This corresponded to the evolution of DVM, which was adapted later to predator avoidance (Gehring and Rosbash, 2003; Nilsson, 2009; Ringelberg, 2010).

Studying DVM in the laboratory is very challenging, since it is very hard to reproduce gradients of light, temperature and pressure in a test tube. Recently, Conzelmann et al. (2011) showed for the first time the relationship between ciliary activity and DVM. The authors demonstrated that the position of *Platynereis* larvae in the water column is correlated to the CBF and to ciliary arrests: slowing down the ac-

tivity of prototroch cells leads to a lower swimming depth, and viceversa.

The present study adds an important observation: most of the peptides exerting positive effects on the CBF (increase of CBF) are expressed in the sensory cells of the *cry1-perops* region. For the first time, we can link photosensitivity and regulation of locomotor rhythms, which is the core of DVM. The coupling of circadian clocks and locomotor rhythms takes place in the dorsal brain, where at least three different molecules - *cry1*, *perops* and *c-ops* - can sense light, and potentially respond to different wavelengths. The presence of multiple photopigments might provide some basis to fine-tune the clock entrainment. Indeed, it has been shown that the spectral composition of light in the sea changes with the time of the day and depth (red light penetrates less in the sea, and viceversa), and the amount of these changes, especially in the blue-green part of the spectrum, could be used to estimate the time of the day and the depth in the water column (McFarland, 1986; Ragni and Ribera D'Alcalà, 2004). So we can hypothesize that the three photopigments of *Platynereis* larval clock can be used to discriminate between dawn, midday and dusk. This would be necessary to develop anticipatory behaviours, and in the case of DVM, to start the upward migration at dusk and the downward migration at dawn.

It is evident that the current dataset cannot establish a complete correspondence of rhythmic, melatonin-dependent behaviour and DVM, which was anyway beyond the scopes of this thesis. First, a complete timecourse of the CBF at different circadian timepoints would be necessary to determine how exactly CBF changes between day and nighttime. Second, the spectral dependence of CBF should be assayed. And finally, the quantification of melatonin at different circadian timepoints can indicate exactly when melatonin plays a physiological role in modulating ciliary beating. Preliminary qPRC data indicate that *hiomt* and *melatonin receptor* expression levels increase only in the second half of the night and decrease after dawn; significantly, these daily changes are abolished by application of a melatonin receptor antagonist (not shown). This would suggest that in an ecological context, the melatonin-dependent decrease of CBF is used at the end of the night phase to facilitate the downward movement of the larvae.

9.1. Conserved functions of melatonin in annelids and vertebrates

Light-dependent rhythms of locomotor activity and general arousal states exist in all the vertebrate species investigated so far (Drapeau et al., 2002). The neural pathways that control these rhythms are complex, and involve centers in the hypothalamus, the thalamus and the brainstem. Melatonin is one element of this neuromodulatory system: it is released by the pineal gland, and has a conserved function in inducing sleep-like states and a general decrease of responsiveness to sensory stimulation.

The behavioural data presented here indicate similarities of melatonin function in annelids and vertebrates. These similarities are based on two observations. First, melatonin slows down locomotion in *Platynereis*, through its effect on ciliary beating; in vertebrates, melatonin can efficiently suppress locomotor activity and induce sleep (Zhdanova et al., 2001; Appelbaum et al., 2009). Second, incubation of *Platynereis* nectochaete larvae with melatonin strongly reduces phototaxis, indicating that melatonin decreases the responsiveness to sensory stimulation; the increase of arousal threshold after sensory stimulation (and especially visual stimulation) is one of the defining features of sleep (Emran et al., 2010).

Despite these functional similarities, obvious differences exist between the organization of the melatonin system in annelids and vertebrates. These differences are a consequence of the diversity in neuronal architectures. In the annelid trochophore larvae, melatonin controls directly the ciliated cells that drive locomotion, while in vertebrates the control of locomotor activity is more complex and hierarchical, hence melatonin acts on several brain nuclei. For this reason, looking for the “pineal homolog” in an annelid is not the correct way to address the question of homology. Still, a common origin of the structures that modulate locomotor behaviour in annelids and vertebrate is possible, and can be investigated looking at homologies not

at the organ level, but at the level of cell types.

The molecular data available in *Platynereis* make possible, for the first time, to test how far these functional homologies correspond to non-related neuronal circuits, or can be traced back to deep homologies of cell types.

9.2. The origin of vertebrate photoreceptors: a view from serotonin and melatonin

In his extensive comparison of serotonergic nervous systems across Bilateria, Hay-Schmidt (2000) proposed that the apical ganglion serotonergic cells of invertebrate larvae correspond to the hindbrain raphe nuclei of vertebrates. More recent molecular data showed that the *otx-gbx* boundary, which defines the midbrain-hindbrain boundary in vertebrates, is conserved in protostomes, but it corresponds to the post-trochal region of annelid larvae, posterior to the *six3+* episphere (fig. 1.3, Irimia et al. 2010; Steinmetz et al. 2010, 2011). This implies that the apical ganglion serotonergic cells cannot be compared to hindbrain cell populations, but they would rather be related to cells located in the *six3+* forebrain of vertebrates (fig. 9.1).

The most prominent populations of serotonergic cells of the vertebrate forebrain are located in the hypothalamus and in the pineal complex. These cell populations are conserved in all non-mammalian vertebrates, but are more conspicuous in amniotes (Parent, 1984). And interestingly, they are all related to photoreception and melatonin release.

In *Platynereis*, only a subset of the *hiomt+* cells shows serotonin immunoreactivity. Similarly, serotonin immunoreactive photoreceptors has been documented in the pineal complex (pineal and parapineal) of several species, where serotonin negative cells also exist (for example in lamprey, Pombal et al. 1999). Serotonergic photoreceptors have been recently identified also in the hypothalamus (Yamashita et al., 2010), which harbours an unsuspected diversity of photoreceptors and melatonin-producing cell types (see Introduction, 2.3.2); the majority of them are CSF-contacting neurons.

Serotonin is the substrate of Aanat, thus is necessary for melatonin synthesis; however, such high levels of serotonin could never be shown in retinal photoreceptors, where melatonin synthesis also takes place for paracrine signalling (Tosini et al., 2008). The high levels of serotonin reported in the pineal complex could be explained either because the pineal supplies melatonin for the whole body, hence the amount of melatonin produced is significantly higher, or because serotonin itself

plays some role as a neural output of the pineal complex.

The photoreceptors of the pineal and the parapineal have variable morphologies; some photoreceptors have been found to project directly to the brain (Rüdeberg, 1969; Ekström, 1987; van Veen, 1982; Pombal et al., 1999; Yáñez et al., 1999). Within vertebrates, the cell types of the pineal and the parapineal are considered all evolutionary related, since they represent a “morphological series” with progressive regression and loss of the photoreceptive function (Ekström and Meissl, 2003). If this scenario is true, the most ancestral cell types are the photoreceptors and the ciliated CSF-contacting neurons that project directly to the brain (which indeed exist only in lampreys and fishes).

Unfortunately, the paucity of molecular data available doesn't allow to propose more detailed hypotheses on the evolutionary relationships between the pineal and the hypothalamic photoreceptors. Certainly, separate cell types existed in the last common ancestor of vertebrates. But how old is this diversification? Was this already in place in the chordate ancestor? Or in the Urbilateria?

In the cephalochordate amphioxus, two morphologically distinct ciliary photoreceptor cell types have been described (Lacalli, 1996). The lamellar body is formed by putative photoreceptors with branching cilia and huge surface extension. The cells of the frontal eye, organized into two “rows” and in close association to pigment cells, have a flask-shape, extend one long motor cilium, and project posteriorly to the locomotor centers. Markers expressed in the *Platynereis* clock region, like *tbx2/3* and miR-7, are also present in the anterior cerebral vesicle, where the frontal eye is located (Horton et al., 2008; Candiani et al., 2011). Interestingly, the “row 2” photoreceptors are serotonergic, suggesting that the row1 and row2 cells are distinct photoreceptor cell types, as also indicated by their ultrastructure (Lacalli, 1996). In summary, amphioxus has at least three different ciliary photoreceptor cell types, and it is still possible that other photoreceptors without surface extensions exist, and will be revealed by molecular data.

The differences in molecular fingerprints of pineal and hypothalamic photoreceptors can be attributed, at least partially, to the different tissue distribution of these cells, and a basic subdivision of visual/semivisual (retina and pineal complex) vs neuroendocrine (hypothalamus) functions. The pineal complex is not a simple illuminance detector, but can discriminate the direction and in some cases the spectral composition of light. This semivisual task of the pineal complex has been lost in mammals, but it is still present in other vertebrates (for instance, the shadow responses of fish and *Xenopus*). Moreover, the presence of pigments and expression

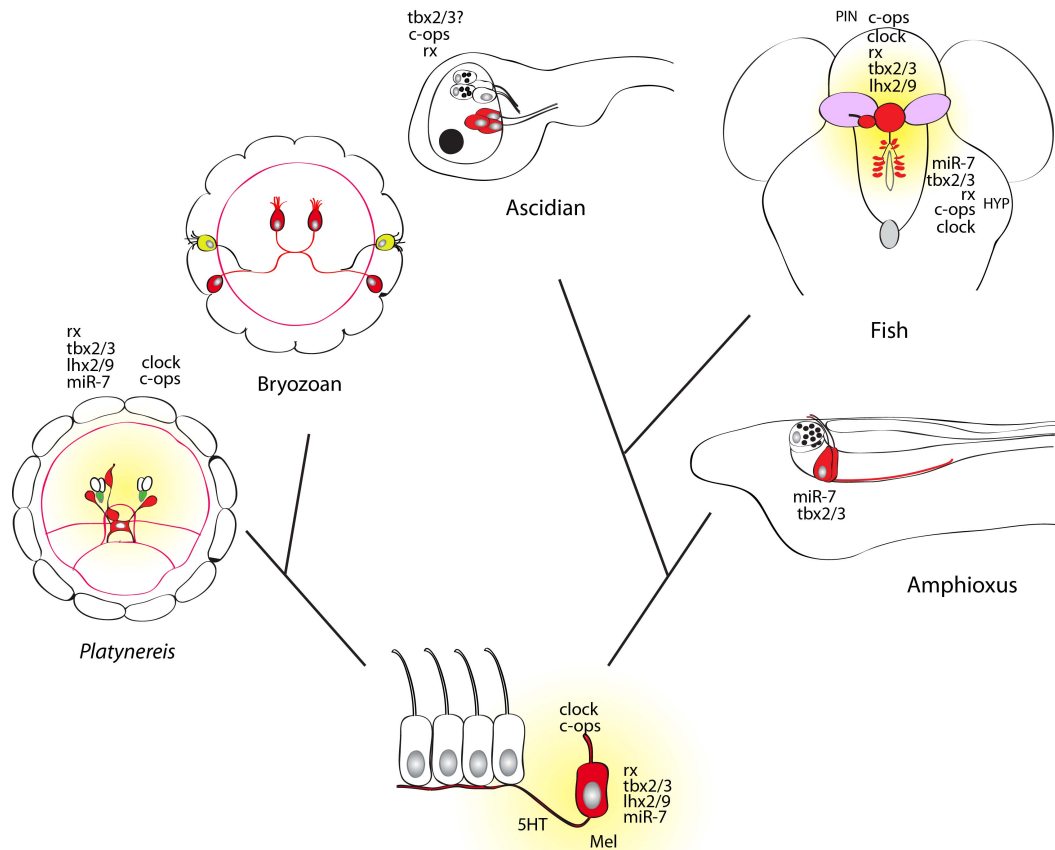


Figure 9.1: **Evolution of serotonin and melatonin photoreceptors in Bilateria.** In the urbilaterian ancestor, ciliary photoreceptors control ciliary locomotion through serotonin and melatonin release. In protostome larvae, serotonergic cells (red) and ciliary photoreceptors (yellow) control locomotion sending projections to the prototroch cells. In the majority of lophotrochozoan larvae, these cells are located in the apical ganglion. In *Platynereis*, a serotonergic *c-ops1+ tbx2/3+ miR-7+* cell exists. The *Platynereis* dorsal brain cells come from *rx+* progenitors and release melatonin, which acts on the prototroch cells. In bryozoan larvae, ciliary photoreceptors and serotonergic cells have a subtrochal localization (Gruhl, 2009). In deuterostomes, the row2 photoreceptors of the amphioxus frontal eye are serotonergic, express *tbx2/3* and *miR-7*, and send projections posteriorly to the locomotor system (discussed in the text). In ascidians, *rx+* ciliary photoreceptors contact serotonergic cells, which send posterior projections to the locomotor center. In vertebrates, melatonin is produced by *rx+ tbx2/3+* photoreceptors in the hypothalamus (*miR-7+*, red cells), the pineal complex (red) and the retina. The pineal complex is connected to the locomotor system through several pathways: the projection of the parapineal to the left habenula (pink) and the IPN (gray) is the most conserved within vertebrates.

of the pigment gene marker *mitf* (Kumasaka et al., 2004; Bailey et al., 2009) can be interpreted as a reminiscence of this ancient function. In line with this, pineal and retinal but not hypothalamic photoreceptors express *otx* transcription factors, which are crucial for eye development.

It is intriguing that in *Platynereis* hierarchical clustering of cell types subdivides the *Platynereis hiomt+* cells into two groups, a “dorsal” and a “ventral” cluster, distinguished by the expression of several transcription factors and differentiation genes. Cells in the dorsal cluster express genes involved in the specification of sensory neurons, like *six1/2*, *six4* and *eya*; consistently, they also express the *CNGa* channel, and they show sensory specialization (flask-shape, apical dendrites), indicating that they are functional sensory cells. Viceversa, the ventral cluster includes cells with a deeper location in the episphere and without sensory specializations, suggesting that they are interneurons.

It would be tempting to compare these sensory and interneuron groups with retinal pineal and hypothalamic cells, respectively. But the current data do not support this conclusion, as shown by hierarchical clustering of molecular fingerprints of *Platynereis* and vertebrate cell types (fig. 7.6). This clustering shows that the *Platynereis* ciliary photoreceptors and asymmetric serotonergic cell are the most closely related to the vertebrate pineal and retina photoreceptors, but cell type resolution data is not available for the hypothalamic brain photoreceptors, which are also likely to be very similar to the other ciliary photoreceptor cell types. All the other cell types are fragmented in vertebrate-only or *Platynereis*-only subclusters, because of the paucity of the dataset.

9.3. Partial conservation of regulatory interaction explains the similarities between annelids and vertebrate cell types

As summarized above, functional similarities support the relatedness of the *Platynereis* photosensory cells of the *hiomt* region and the cells of the pineal complex and hypothalamus of vertebrates. The molecular and developmental data present a more complex picture, which overall doesn't indicate the presence of 1:1 homologies between annelids and vertebrates. Moving away from the vertebrate dogma “melatonin equals pineal” helps to decipher the evolutionary relationships of the annelid and vertebrate *hiomt* expressing cells. Looking at the function of selected transcription factors during development can help to understand how the changes in regulatory interactions between transcription factors might drive changes of cell

types during evolution.

The transcription factor *rx* (*rax* in mammals) is one of the very few genes expressed in retina, pineal and deep brain photoreceptors (Casarosa et al., 1997; Deschet et al., 1999), although species-specific differences exist (like the lack of *rx* expression in the fish pineal).

A question that has not been addressed yet in any vertebrate species is how the early pineal anlage, at the border of the neural plate, is established. At very early stages, this anlage expresses several genes that label also the eye field, like *rx*, *otx* genes and *tbx2/3*. Indeed, fate map studies in *Xenopus* at the neurula stage showed that the pineal precursors lie in continuity with the more medial eye field (Eagleson and Harris, 1990; Rubenstein et al., 1998). So it is possible that the same patterning mechanisms establish very early the diencephalic domain that gives rise to photoreceptive structures.

A model for the establishment of the eye field has been proposed for *Xenopus* (Zuber et al., 2003), and it is likely to be valid in general for vertebrates. The earliest events involve the induction of *otx2* expression in the anterior neural plate by neural induction signals, like *noggin*. Genes of the *tbx2/3* family are subsequently activated; these genes contribute to induction of *rx* and *pax6* expression.

Since the transcription factors *otx*, *rx* and *tbx2/3* are also expressed in the early anlage of the pineal complex, it is likely that the segregation of the pineal and retinal fields takes place after this point. The pineal anlage is distinguished from the retina by the expression of some transcription factors. One of them, *not* (or *flh*), is never present in the eye, and plays an important role in the maintenance and proliferation of the pineal (but not parapineal) progenitors (Masai et al., 1997; Snelson et al., 2008a). Later, other pineal-specific genes, like *bsx* and *foxD3*, are found in the differentiating pineal cells (D'Autilia et al., 2010). Additionally, *sens* is expressed specifically in the zebrafish parapineal neurons, which loose *not* expression after migrating away from the midline (Dufourcq et al., 2004; Snelson et al., 2008a).

In *Platynereis*, the same genes are expressed dynamically in the dorsal brain during development, and in different combinations in the differentiated *hiomt* cells. However, none of the *Platynereis* cell types expresses the combination of all these transcription factors at any point during development.

From the analysis of the early development with time lapse movies and in situ hybridization, three interesting photoreceptor lineages, with a medio-lateral arrangement, can be identified.

The lineage producing the cPRCs and most of the *hiomt+* *CNGa+* cells (“blue lineage” in fig. 3.6) is tracked from two *otx+* NSCs (one on each side of the dorsal episphere) at 12hpf. At 15hpf, the same NSCs turn off *otx* expression and start to express *tbx2/3*, and later *rx*. This is reminiscent of the vertebrate eye field situation, where at onset of *rx* expression *otx2* is downregulated, both in *Xenopus* and zebrafish (Andreazzoli et al., 1999; Chuang and Raymond, 2001).

This lineage has very dynamic division patterns, which are paralleled by dynamic changes of gene expression in neural progenitors. The initial *otx+* NSC starts with some asymmetric cell divisions, producing differentiating neurons, but then divides symmetrically to produce new NSCs. From the comparison of WMISH and time lapse movies it seems likely that the onset of *rx* expression correlates with this symmetric cell division. Mapping the expression of *rx* and *otx* in this lineage with an higher resolution will be especially insightful and clarify how the changes of the NSCs behaviour correlate with gene expression.

The functional studies indicate that in this lineage Rx plays some role in the maintenance of neural progenitors. Knock down of Rx produces loss of cPRCs and *tll* expression, despite *rx* is neither expressed in immediate progenitors of the cPRCs, nor later during their differentiation. This means that Rx cannot have a role in the terminal differentiation and maintenance of the cPRCs phenotype, but it must maintain the proliferative capacity of the NSCs where they come from. A similar role for Rx has been proposed in vertebrates, during the early stages of eye development (Casarosa et al., 2003; Andreazzoli et al., 2003; Zhang et al., 2000; Loosli et al., 2001). Consistently, in *Platynereis* a smaller number of cells, and a decrease of EdU incorporation in the brain have been observed in *rx* morphants (not shown). Moreover, the expression of the proneural marker *ngn* is severely affected in *rx* morphants. Also the expression of *tbx2/3* is strongly reduced (but it does not disappear completely) in morpholino-injected larvae. These results can be interpreted either as an indirect consequence of the reduced mitotic capacity of the *rx+* NSCs, or as a requirement of a functional Rx to sustain *tbx2/3* expression. In medaka, *rx3* was shown to be upstream of *tbx2* in the retina, but not in the hypothalamus (Loosli et al., 2001). It will be definitely of great interest to study in more detail the regulatory relationships between *rx* and *tbx2/3* in *Platynereis*.

Later in development, more cell types populate the “clock area”, so they are likely to be generated by the same lineage, although the time lapse movies do not last enough to cover later stages. These cells are all distinct, as shown by their molecular fingerprint analysis (described in Chapter 7). Among them, the “lateral not cells”

express an interesting combination of markers: *not*, *foxD* and *otx*, which are pineal markers, and *rfx4/6*, a gene that labels specifically the SCN within the nervous system. The function of these cells is currently unknown: they express *perops* and *hiomt*, indicating that they participate to the melatonin system.

The asymmetric serotonergic cell comes from a different lineage, which is also expressing *tbx2/3*, but neither *rx* nor *otx*. At 15-16hpf, *bsx* is found in some cells of the left side of the *tbx2/3+* region; only one of them turns on the expression of *sens* and differentiates into the asymmetric serotonergic cell. Despite *rx* is not expressed in this lineage at 15hpf, the expression of *c-ops1* in the asymmetric serotonergic cell requires a functional Rx. Thus, this requirement might be non-cell autonomous and needs to be investigated further. Interestingly, the presence of serotonin, *c-ops1*, *tbx2/3* and *sens* in this cell is highly reminiscent of the molecular fingerprint of the parapineal cells (it remains to be shown if *bsx* is expressed also in the parapineal, besides its pineal expression).

Finally, a third cell population might be extremely interesting for evolutionary comparisons with vertebrate cell types. This small cell population starts from a very lateral position in the episphere, and is demarcated by the coexpression of *rx*, *otx* and *pax6*; *tbx2/3* is excluded from this region. Later in development, these cells acquire a more medial position; two of them become the two lateral serotonergic cells, which retain *rx* expression after differentiation. Overexpression of Rx induces an increase of the number of lateral serotonergic cells, together with the expansion of the lateral *otx* expression domain. This is consistent with a role of Rx, upstream Otx, in the development of cells of the lateral episphere.

Despite their expression profile is so similar to pineal and retinal progenitors, these *rx+* *otx+* *pax6+* cells were not found to express *c-ops1*. However, another *c-opsin* gene (*c-ops2*) exists in *Platynereis* and is transcribed at larval stages (RT-PCR), but unfortunately it was not possible yet to localize its expression. Thus the expression pattern of *c-ops2* might reveal new cell types, more interesting for evolutionary comparisons.

In *Xenopus*, a cocktail of transcription factors - *otx2*, *tbx3*, *pax6*, *six3*, *rx1*, *tll*, *optx2* - is completely sufficient to induce ectopic eyes *outside the nervous system* (Zuber et al., 2003). All the orthologs of these genes in *Platynereis*¹, except *pax6*, are expressed at some point in the lineage producing the cPRCs and most of the *perops+* *cry1+* *CNGa+*

¹*Platynereis six3* is the ortholog of the vertebrate genes *six3* and *optx2/six6*.

cells. Perturbation analysis shows that *Platynereis* Rx affects the expression of *tbx2/3* and *tll*, but not *otx*, in this lineage, consistent with the different onset of expression of these transcription factors during development. The hypothesis of homology of vertebrate retinal photoreceptors and annelid cPRCs proposed by Arendt et al. (2004) was based on the expression of two differentiation markers, *c-ops1* and *bmal*. These new developmental data add a new level to the comparison, indicating that the same players (transcription factors) are involved in the development of ciliary photoreceptors within different anatomical contexts.

9.4. Differences in the organization and development of annelid and vertebrate brains indicate how complex nervous systems evolved

Some obvious differences exist and need to be taken in account, in order to understand how vertebrates and annelids could evolve different structures from the same last common ancestor.

The first is the expansion of paralogs in the vertebrate lineage, after the whole genome duplication. This expansion was certainly the cause of the rearrangement of GRNs, the establishment of new regulatory interactions and probably the evolution of new cell types. This makes also more difficult to compare cell types and GRNs with invertebrate species. One clear example is the role of *otx* genes in the development of ciliary photoreceptors. In mammals, two *otx* genes, *otx2* and *otx5/crx*, act sequentially to start the entire cascade of photoreceptor differentiation (Hsiau et al., 2007). Moreover, the transcription of opsins and phototransduction genes is directly controlled by *crx*. In the *Platynereis* cPRCs lineage, *otx* is expressed only very early (like the vertebrate *otx2*); in contrast, *otx* expression persists in the rhabdomeric photoreceptors of the adult eyes. Similarly, the vertebrate *rx* genes have a double function in maintaining the proliferative capacity of retinal progenitors early, and controlling the expression of opsins and phototransduction genes in differentiated photoreceptors; this last function is not present in *Platynereis* ciliary photoreceptors.

A second important difference is in the mode of development. Annelid larval brain is formed by few cells, and their development is highly stereotypical, very fast, and with fixed lineages. In each lineage, asymmetric cell divisions produce differentiated neurons from very early stages, and new neurons are produced subsequently. The generation of cell diversity might be mostly based on a developmental sequence of transcription factors expressed in each lineage, like as been shown in the *Drosophila* nervous system (Isshiki et al., 2001). In contrast, vertebrates don't

have fixed lineages, and cell differentiation is preceded by a long proliferative phase, where the number of neural progenitors is massively expanded. During this proliferative phase the different brain compartments are defined. Later, the specification of cell fates depends on the combination of intrinsic mechanisms and extracellular signals. In the retina, the generation of different cell types from multipotent progenitors, and following a stereotypic differentiation schedule was considered as a “lineage” dependent mechanism, but it is now clear that feedback inhibition from the earliest born neurons affect the cell fate of the later born neurons, in order to ensure the right proportions between the different cell types (Cayouette et al., 2006).

These differences are probably at the base of the different organization of annelid and vertebrate nervous systems. In vertebrates, gene duplication together with the expansion of brain size (number of cells) were the substrate for the evolution of new cell types, the establishment of different brain compartments, the segregation of functions and the gain of higher integrative capacities. In contrast, the annelid nervous system retains a simple brain architecture.

In the context of the circadian system, vertebrate elaborated complex circuits, where the photic information entrains a central clock in the hypothalamus (the SCN), which then controls the activity of several other brain nuclei in the hypothalamus and in the brainstem. In contrast, the *Platynereis* “clock” cells in the dorsal brain are primary sensory neurons, which send their axons directly to the prototroch. At later stages, more sensory neurons develop in the posterior brain, but they all send their projections directly in the medial brain, where there are interneurons that project to the ventral nerve cord. This indicates that the sensory information is processed in the medial brain and controls the muscular activity in the trunk. In other words, there are no sharp boundaries between sensory organs and the “brain” proper. Molecularily, this is reflected by the expression of placodal markers, like *six1/2* and *dach*, in the episphere (Tomer et al., 2010). A similar organization exists in the cephalochordate amphioxus, where the sensory cells of the cerebral vesicle, including the frontal eye, send projections to the locomotor system (Lacalli, 1996).

9.5. Making the vertebrate eye from brain photoreceptors

The discussion above brings to the conclusion that genome duplication and expansion of brain size were prerequisites for the evolution of the vertebrate visual system from brain non visual photoreceptors. It is still unknown why in the evolutionary line to vertebrates ciliary-type photoreceptors replaced rhabdomeric photoreceptors

for visual tasks. It has been proposed that the adaptation of vertebrate ancestors to higher depth in the sea favored the more sensitive ciliary-opsins, which replaced the less sensitive rhabdomeric opsins (Lamb, 2009).

If this was the case, it is necessary then to explain how ancestral ciliary opsins gained an higher sensitivity. The opsins currently found in the retinal photoreceptors are indeed highly sensitive, but they are also very different from ancestral ciliary opsins. As shown by recent biochemical studies, the most ancient ciliary opsins use a different counterion to bind the chromophore (the retinal), and are bistable, which means that they can regenerate the chromophore after the first light-induced isomerization. The loss of bistability was coupled to the evolution of a system for the regeneration of 11-*cis*-retinal, which involves several enzymes and transporter proteins, and evolved after genome duplication either at the base of tunicates and vertebrates) or even at the base of vertebrates (Albalat, 2011). In vertebrates, all the ancient bistable opsins have still non visual functions, and are expressed in the hypothalamus, in the pineal and sometimes in several cell types of the retina.

Clearly, vertebrate rods and cones evolved new characteristics and became specialized for vision. It is generally accepted that cones evolved before rods, based on the absence of true rods in lampreys (Ebrey and Koutalos, 2001), although the classification of rods and cones has been questioned (Adler and Raymond, 2008). A bleaching pigment and the visual cycle are only two examples of the new features acquired by these “new” visual photoreceptors. Dramatic changes happened in the phototransduction cascade, with the evolution of the new G-protein alpha subunit G_t (transducin), which replaced a $G_{i/o}$ based cascade, and of the α -arrestin. Moreover, rods and cones have mechanisms of light adaptation, which allow them to respond to relative changes of light, instead of absolute luminance (exactly the opposite of luminance detectors!); light adaptation needs proteins like recoverin, which also don't exist in protostomes. Finally, these cells acquired highly specialized synaptic terminals (the synaptic ribbons) for the tonic release of neurotransmitters, based on proteins (like ribeye) absent in invertebrates.

The new rods and cones used also new transcription factors for their differentiation. Several studies in mouse showed that the zinc finger transcription factor *Nrl* orchestrates the development of rods and suppresses the cone fate (Mears et al., 2001; Hsiau et al., 2007). One of the targets of *Nrl* is the nuclear hormone receptor *nr2e3*, which controls directly the expression of rhodopsin and other phototransduction genes (Haider et al., 2000; Chen et al., 2005). The *nrl* gene doesn't exist outside vertebrates, while *Nr2e3* was probably coopted in the rod GRN. Indeed, in vertebrates

nr2e3 is expressed exclusively in the developing photoreceptors of the retina and the pineal, but not in the hypothalamus (Martinez-De Luna and El-Hodiri, 2007), while in *Platynereis* and in *Drosophila* this gene has a broad expression domain (see Appendix B); the *Drosophila nr2e3* has been implicated in axonal guidance (Lin et al., 2009).

These observations show that rods and cones are the most “derived” ciliary photoreceptors present in vertebrates. The ancestral role of ciliary photoreceptors was non visual, like the homolog cell types of *Platynereis*. Then the reconstruction of the “typogenetic tree” (Arendt, 2008) for ciliary photoreceptors will require more molecular data for the vertebrate brain photoreceptors. The analysis of the *Platynereis* repertoire is compatible with the hypothesis that more than one ciliary photoreceptor cell type existed at the base of Bilateria. The existence of different ciliary photoreceptors in amphioxus is also consistent with this hypothesis. However, only the comparison of molecular data in several species will allow to distinguish between ancestral cell types and lineage-specific cell type diversification events.

9.6. Concluding remarks

The detection of environmental illuminance has a fundamental role in entrainment of animal rhythmic processes. The non-visual “sense” of light appeared very early in animal evolution, and was based on cryptochromes first, and later on ciliary photoreceptors. In annelid larvae, several types of non-visual photoreceptors are located in the brain, where they belong to an area expressing circadian markers. These cells are molecularly heterogeneous, indicating specialized functions within the circadian system. Some of them are serotonergic, and all of them express *hiomt*, a marker for melatonin synthesis.

In vertebrates, serotonin and melatonin are produced by ciliary photoreceptors in the hypothalamus, the pineal complex and the retina. In these animals, melatonin has conserved roles as the “hormone of darkness”: it decreases the locomotor activity and increases the arousal threshold for sensory stimulation. Moreover, the neural output of the pineal complex controls directly the locomotor system for escape responses. Similarly, in *Platynereis* melatonin decreases locomotor activity, being potentially part of the mechanism that regulates the circadian changes of ciliary beating frequency.

The conservation of functions is paralleled by strong similarities of the processes behind the development of these photoreceptor types. Several markers of the retina

and pineal are expressed during the development of the *c-ops1+* cells, as showed by the lineage analysis of these cell types. Moreover, the transcription factor Rx, expressed in all the vertebrate ciliary photoreceptors, is essential to the development of the *Platynereis* brain photoreceptors.

It is likely that early urbilaterians had a circadian system to regulate ciliary locomotion. This early circadian system used the photic input from brain ciliary photoreceptors to entrain the clock, and melatonin as a systemic output. These centers shared the expression of several genes, like *rx*, *tbx2/3*, *lhx2/9* and *miR-7*. In the vertebrate line, some of these ciliary photoreceptors maintained their original location in the brain, while others acquired new characters and gradually replaced the rhabdomic photoreceptors for vision, first with the evolution of directional illuminance detectors (the pineal complex), and later with the elaboration of complex circuits for visual processing (retina).

9.7. Open questions and future outlook

The molecular, developmental and functional characterization of the circadian center of *Platynereis* larvae provides strong evidence for a common ancestry of circadian centers in Bilateria; yet, many questions open up on different fronts, mostly related to the problem of how evolutionary forces change the shapes and the functions of nervous systems.

One unexpected finding was the presence of molecular heterogeneity not only in the *Platynereis hiont* region, but also within the *c-ops1+* cells themselves. This heterogeneity might underlie functional specializations or differences in connectivity, like in the vertebrate hypothalamus, retina and pineal. However, the comparison of the vertebrate and the *Platynereis* repertoires doesn't show clear correspondences between cell "subtypes". It is likely that independent cell type diversification events happened in the annelid and the vertebrate lineages, and that the urbilaterian photoreceptor repertoire was more simple, restricted to fewer cells. The alternative possibility is that different subtypes of ciliary photoreceptor existed already in the last common ancestor of annelids and vertebrates, but the molecular data currently available are not sufficient to recognize them.

Then, a future challenge will be to define the photoreceptor repertoire that was present at the base of Bilateria. This will require to investigate the molecular fingerprint of ciliary photoreceptors in other invertebrate species in key phylogenetic positions, like some other lophotrochozoans, amphioxus and hemichordates. A more de-

tailed analysis of the development and molecular fingerprint of the lamprey and/or fish deep brain photoreceptors would also be extremely valuable for this purpose.

A second challenge will be to define how the cell type developmental history must be taken into account for comparative purposes. Or in other words, to understand how changes in regulatory interactions (GRNs) contribute differentially to the developmental processes that provide spatio-temporal coordinates for cellular differentiation, and to the definition of the cell identity itself. It is possible that these two aspects are not completely separable. In that case, a transcription factor initially involved only in the early commitment might acquire control over the expression of differentiation markers, or viceversa. How would this impact on the comparative efforts over large phylogenetic distances? The case of *rx* genes represents one example: in *Platynereis*, *rx* is necessary to the development of ciliary photoreceptors but not expressed in these cells after differentiation, while in vertebrates *rx* genes are involved in both early commitment and later maintenance of photoreceptor identity.

The answers to these questions will come from comparative studies of GRNs, and the identification of “kernels” for the development of conserved brain regions or cell types. The work discussed here represents a good ground for future investigations. Different methods are now available to interfere with gene expression in the developing *Platynereis* embryo. Moreover, for early stages it is also possible to map gene expression patterns on developmental lineages. This will allow to understand how cell fate is linked to the neuron birthdate within each lineage, and how this is regulated by changes of gene expression at the level of progenitor cells.

In comparing invertebrates and annelids, an obvious question is how to take in account the rise in brain complexity and integrative capacity of the vertebrate evolutionary line. If nervous system evolution started from multifunctional cells, the division of labour model can explain this rise in complexity. But then, how to compare a simple, multifunctional cell, like the sensory-motor neurons of *Platynereis* brain, to complex circuits in the vertebrate?

While there is no obvious answer to this question, it is clear that a possible effort could be to integrate the cell type data in the general perspective of evolution of “brain architecture”. The striking conservation of brain regionalization along the AP and DV axes might underlie some conserved aspects of brain functional organization. These similarities cannot be uncovered only with a morphology-based view of brain organization, since the size, shape and numbers of brain nuclei were incredibly elaborated in different evolutionary lines. A shift from a morphology-based to

a function-based understanding of brain organization could help to recognize conserved aspects of brain architecture over large evolutionary distances. One example is the conserved role of serotonin and melatonin in mediating light-dependent modulation of locomotion in vertebrates and annelids. The reconstruction of the functional organization of the annelid brain will be an important contribution to the comparison of brain architecture across Bilateria.

MATERIALS AND METHODS

10.1. *Platynereis dumerilii* animal culture

Platynereis dumerilii larvae were obtained from an established breeding culture at EMBL, Heidelberg, following Dorresteijn et al. (1993). Adult *Platynereis* worms are maintained with an artificial moon cycle (1 week moonlight and 3 weeks darkness) to synchronize sexual maturation. After fertilization, *Platynereis* embryos were raised in Zentis cups, in natural sea water (NSW), in an incubator at the temperature of 18 °C, with a 16L:8D light cycle (Type KB53, Binder, Tuttlingen, Germany).

10.2. Equipment

Centrifuges:

Eppendorf centrifuges 5417C and 5430, Thermo scientific centrifuge “Multifuge” 3SR+, Thermo scientific Sorvall RC6T

PCR machines:

Peltier Thermal Cycler PTC-200 (BioRad). ABI7500 Light cycler (Applied Biosystems) with 96-well blocks for qPCR (EMBL GeneCore).

Microscopes:

Zeiss Stemi2000 stereomicroscope for observation of the animals and mounting.

Zeiss Axiovert 40C for injection of *Platynereis* zygotes, equipped with a UMMJ-3FC micromanipulator (Narishige) and an Eppendorf FemtoJet express.

Leica SPE with a 40x oil-immersion objective for confocal microscopy.

Zeiss Axiophot with a DMK 21BF04 camera (The Imaging Source) for recording of ciliary beating. The same microscope with a Zeiss AxioCam HRc and DIC optics for bright field imaging.

Leica MZ16 microscope with a Sanyo VCB-3524P camera for phototaxis assays. Zeiss LSM 780 with a 32-Ch GaAsP detector and a 2photon source (Chameleon, Coherent), used with a 40x oli-immersion objective, for GCaMP3 imaging.

Others:

Eppendorf Thermomixer compact

Nanodrop ND-1000 (Thermo scientific)

GenePulser Xcell (BIO RAD) for electroporation of bacterial cells.

10.3. Reagents and solutions most commonly used for molecular biology and WMISH

All the chemicals were purchased from Sigma-Aldrich and Merck, unless indicated otherwise.

Routinely used solutions were prepared after Sambrook and Russell (2001).

Oligonucleotides Oligonucleotides for PCR were purchased from Invitrogen.

Agarose For routine nuclei acids separation, and for the preparation of the injection stage. Sigma, cat. n. A9539.

Low melting agarose For mounting *Platynereis* larvae for live imaging. ultraPURE LMP-Agarose (Gibco).

MetaPhor agarose For fine separation of small size DNA fragments. Lonza, cat. n. 50180.

Mineral Oil Sigma, cat. n. M5904.

10x DNA agarose gel loading buffer 50% Glycerol, 100mM EDTA pH 7.5, 1.5mM Bromophenolblue, 1.9mM Xylenecyanol

10xTBE 890 mM Tris, 890 mM boric acid, 20 mM EDTA pH 8.0. Dilute to 1x for running and preparing agarose gels.

16% PFA Paraformaldehyde, for fixation (Electron Microscopy Sciences, 15710).

10x PBS 70g NaCl; 62,4g Na₂HPO₄.2H₂O; 3,4g KH₂PO₄, pH 7.4.

PTW 1x PBS pH 7.4 + 0.1% Tween-20, sterile filtered.

20x SSC For WMISH. 3M NaCl (175.32g/l) and 0.3M Dinatrium citrate (88.23g/l)

SSCT For WMISH. SSC + 0.1% Tween-20

NBT mix For probe preparation. 15.4mM ATP, 15.4mM CTP, 15.4 GTP, 10mM UTP (Boehringer Ingelheim)

Hyb-mix For WMISH. 50% formamide (Fluka, ultra pure), 5xSSC, 50 µg/ml heparin, 0.1%Tween20, 5 mg/ml torula yeast RNA (Sigma), store at -20°C .

Staining Buffer pH 7.5 without MgCl₂ For WMISH. 100 mM TrisCl pH 7.5, 100 mM NaCl, 0,1%Tween20

Staining Buffer pH 7.5 with MgCl₂ For WMISH. 100 mM TrisCl pH 7.5, 50 mM MgCl₂, 100 mM NaCl, 0,1%Tween20

Staining Buffer pH 9.5 For WMISH. 100 mM TrisCl pH 9.5 (precise), 50 mM MgCl₂, 100 mM NaCl, 0,1%Tween20

10.4. Antibodies

Primary antibodies

Mouse anti-acetylated tubulin	Sigma T6793	1:500
Mouse anti-tyrosinated tubulin	Sigma T9028	1:250
Rabbit anti-serotonin	ImmunoStar 20080	1:500
Mouse anti-synapsin	Dev. studies hybridoma bank, 3C11	1:250
Anti-DIG Fab fragment	Roche, 11093274910	1:5000

Secondary antibodies

DyLight 488 anti-mouse	Jackson Laboratories,	1:500
DyLight 549 anti-rabbit	Jackson Laboratories,	1:500

10.5. Software

DNA sequences were analysed using the plasmid editor ApE (<http://biologylabs.utah.edu/jorgensen/wayned/ape/>). Multiple sequence alignments were generated with MUSCLE and ClustalW (<http://www.ebi.ac.uk/Tools/msa/>).

The software R (<http://www.r-project.org/>) was used for statistics.

Image processing was performed in Fiji (<http://fiji.sc/wiki/index.php/Fiji>) and Imaris (Bitplane). In fluorescence images, brightness and contrast were adjusted equally on all images. Figures and artwork were created using Adobe Photoshop and Adobe Illustrator.

11.1. Immunostaining of *Platynereis* larvae

11.1.1. Fixation of *Platynereis* larvae for immunostaining

- Collect the larvae with custom-made nets (100 μm mesh size, NITEX, Gebr. Stallmann) which fit into individual wells of 6 well plates.
- Relax the muscles of nectochaete larvae by transferring the net to a well containing a solution of 50% MgCl_2 and 50% NSW.
- Transfer the net with the larvae in another well containing a solution of 4% PFA in PTW.
- Incubate for 30min-2hrs at room temperature, or for 4-6hrs at 4 °C.
- Rinse twice with PTW, then transfer the larvae in Eppendorf tubes.
- For short term storage: store at 4 °C for maximum one week.
- For long term storage: wash twice in 100% MetOH, and store at -20°C . The MetOH storage can destroy the epitope, so for each antibody it needs to be tested if it works also in MetOH treated specimens.

11.1.2. Immunostaining protocol

Rehydration The rehydration is necessary only if larvae were kept in MetOH. Larvae kept in PTW can be processed directly with proteinase K (see below).

- Incubate 5min in 75% MetOH-25%PTW
- Incubate 5min in 50% MetOH-50%PTW
- Incubate 5min in 25% MetOH-75%PTW
- Rinse 2x5min in PTW

Proteinase K digestion and postfixation

- Digest with Proteinase K (100 $\mu\text{g}/\text{ml}$ in PTW) without shaking. The length of digestion depends on the developmental stage: 30sec for <24hpf, 1 min for 24-48hpf, 2 min for 48-72hpf, 3 min for >72hpf.
- Stop the digestion with 2x2min washes in 2 mg/ml glycine/PTW.
- Rinse 2x2min in PTW
- Fix for 20min in 4% PFA/PTW
- Rinse 5x5min in PTW

Blocking and primary antibody incubation

- Transfer the larvae in Eppendorf tubes, and block in 5% sheep serum/PTW, for 1hr at RT, while shaking on a thermomixer at 450rpm.
- Remove the blocking solution, and add 50-200 μl of primary antibody, diluted in 5% sheep serum/PTW. Incubate for one night at 4 °C, while shaking on a thermomixer at 450rpm.

Washes and secondary antibody incubation

- Remove the antibody solution, and was 5x5min in PTW, at RT, shaking on a thermomixer at 450rpm.
- Block in 5% sheep serum/PTW, for 30min-1hr at RT, while shaking on a thermomixer at 450rpm.
- Remove the blocking solution, and add 50-200 μl of secondary antibody, diluted in 5% sheep serum/PTW. At this step, add also DAPI to a final concentration of 1 $\mu\text{g}/\text{ml}$. Incubate for one night at 4 °C, while shaking on a thermomixer at 450rpm. The secondary antibody incubation can be also done at RT for 2hrs.
- Remove the antibody solution, and was 5x5min in PTW, at RT, shaking on a thermomixer at 450 rpm.

Mounting

- Transfer the larvae in DABCO/glycerol (2.5 mg/ml DABCO in 87% glycerol), shake for 1 hr at 450 rpm. The larvae can be stored in glycerol at 4 °C.
- For imaging, mount the larvae between a slide and a coverslip, with a spacer made by several layers of tape. For <24hpf larvae, use 2 layers of tape on each side. For 48hpf-5dpf (dorsal or ventral view) larvae, use 3 layers of tape.

11.2. Clones of *Platynereis* genes

11.2.1. Extraction of RNA from *Platynereis* larvae

Protocol from Christodoulou (2009) and Kegel (2008), with minor modifications. Different versions of this protocol were used according to the amount of starting material, as detailed below. Regular amounts of starting material refer to minimum 300 larvae (or at least half batch after fertilization), or one adult worm. The extraction of RNA from a smaller number of larvae (from a minimum of 25) requires specific adaptations.

- Collect *Platynereis* larvae in an Eppendorf tube. Spin for 30sec at 4000 rpm to accumulate them in the bottom of the tube, and quickly remove all the NSW.
- Quickly freeze in liquid nitrogen.
- Add 1ml of Trizol (TriFast, Peqlab) and lyse by pipetting up and down for 3 min. For small amounts of material, use only 500 μ l of Trizol.
- Incubate 5 min at RT.
- Spin 10 min at 12000 rpm at 4 °C.
- Transfer the supernatant in a fresh tube.
- Add 200 μ l of chloroform per 1 ml of Trizol.
- Shake vigorously by hand for 15 sec.
- Incubate 2-5 min at RT, then spin 15 min at 12000 rpm at 4 °C.
- Transfer the supernatant in another tube. Add one volume of phenol:chloroform:isoamylalcohol 25:24:1, vortex 30 sec and spin at 14000 rpm for 5 min at RT.
- Transfer the aqueous phase in another tube. Extract by adding the same volume of chloroform. Vortex 30 sec and spin at 14000 rpm for 5 min at RT. Transfer the aqueous phase in a fresh tube
- For small amounts of starting material: transfer the aqueous phase in another tube, and repeat the chloroform extraction.
- For small amounts of starting material: transfer the aqueous phase in another tube, and centrifuge again at 14000 rpm for 5 min at RT.

- For small amounts of starting material: transfer the aqueous phase in a fresh tube. Add 0.5 μ l of Linear Acrylamide (Ambion, AM9520) for 500 μ l of starting Trizol. Mix.
- Add 500 μ l of ice-cold isopropanol for 1 ml of starting Trizol. Vortex and incubate at -20°C for 1 hr. For small amounts of starting material, incubate overnight.
- Centrifuge at 4°C for 15 min at maximum speed (>14000 rpm). For small amounts of starting material, centrifuge for 1 hr.
- Remove the supernatant, without losing the RNA pellet. Add 1 ml of 70% EtOH (stored at -20°C), invert the tube and centrifuge at 4°C for 5 min at maximum speed (>14000 rpm).
- Remove the supernatant, and repeat the EtOH wash as above.
- Remove the supernatant without disturbing the pellet. Dry the pellet for about 10 min.
- Add 11-31 μ l of nuclease-free water. To resuspend, agitate at 30°C for 15 min.
- Measure the RNA concentration with the nanodrop. Store the RNA at -80°C .

11.2.2. Preparation of cDNA libraries, and PCR

cDNA libraries were prepared from RNA of mixed larval stages using the Superscript III Reverse Transcription kit from Invitrogen, according to manufacturer's instructions.

Gene specific primers were always designed with Primer3, with a T_m of 70 – 72 $^{\circ}\text{C}$. The DNA polymerases Phusion High-Fidelity DNA Polymerase (NEB, cat. n. M0530) or HotStarTaq DNA Polymerase (Qiagen, cat. n. 203205) were used for amplification, according to manufacturer's instructions.

PCR reaction with Phusion:

Template (cDNA library)	0.2 μ l
dNTPs 5mM	0.4 μ l
primer F 5 μ M	1 μ l
primer R 5 μ M	1 μ l
5x Phusion Buffer	2 μ l
Phusion High-Fidelity DNA Polymerase (NEB)	0.1 μ l
water	up to 10 μ l

Cycling program with Phusion (primer $T_m \geq 70^\circ\text{C}$):

1x	98 °C	30 sec
35x	98 °C	7 sec
	72 °C	1 min
1x	72 °C	10 min

11.2.3. Preparation of RACE libraries, and RACE PCR

RACE libraries were prepared from RNA of mixed larval stages using the GeneRacer Advanced RACE Kit (Invitrogen, cat. n. L1502-01), according to manufacturer's instructions. For RACE PCR, 5' and 3'RACE primers were designed with a $T_m \geq 70^\circ\text{C}$.

RACE PCR reaction:

Template (RACE library)	0.4 μ l
dNTPs 5mM	0.4 μ l
Gene Specific Primer 5 μ M	1.2 μ l
GeneRacer Oligo 10 μ M	1.8 μ l
10x HotStarTaq Buffer	2 μ l
HotStarTaq DNA Polymerase (Qiagen)	0.2 μ l
water	to 20 μ l

Nested RACE PCR reaction:

Template (RACE PCR product)	1 μ l
dNTPs 5mM	2 μ l
Gene Specific Primer 5 μ M	2 μ l
GeneRacer Nested Oligo 10 μ M	1 μ l
10x HotStarTaq Buffer	5 μ l
HotStarTaq DNA Polymerase (Qiagen)	0.5 μ l
water	to 50 μ l

Cycling program (touchdown):

1x	95 °C	15 min
5x	94 °C	30 sec
	72 °C	1 min 30 sec
	94 °C	30 sec
5x	70 °C	10 sec
	72 °C	1 min 30 sec
	94 °C	30 sec
20x	65 °C	30 sec
	72 °C	1 min 30 sec
1x	72 °C	10 min

11.2.4. Cloning of PCR products

PCR products were analysed with gel electrophoresis, according to standard protocols (Sambrook and Russell, 2001). For amplification with gene specific primers, fragments of the expected size were excised from the gel. For RACE PCRs, all the possible nested PCR amplicons were analysed.

DNA fragments were purified from gel using the QIAquick Gel Extraction Kit (Qiagen, cat. n. 28704), and cloned in the pCRII-TOPO vector with the TOPO TA Cloning Kit Dual Promoter (Invitrogen, K4660-01), following manufacturer's instructions. Electrocompetent or chemocompetent cells were transformed according

to standard protocols (Sambrook and Russell, 2001), and plated on LB agar plates with X-Gal, for blue-white colony screen.

White colonies were inoculated in 5ml of LB medium. DNA extractions from small bacterial cultures (minipreps) were performed according to Sambrook and Russell (2001). DNA was analysed with the restriction endonuclease EcoRI, which excises the insert in pCRII-TOPO. Positive clones were further confirmed with sequencing (GATC Biotech, Konstanz). The pCRII-TOPO vector has T7 and SP6 RNA polymerase binding sites in opposite directions; sequencing was necessary to find out which RNA polymerase had to be used for antisense transcription.

11.2.5. Sources of *Platynereis* clones used as template for probe synthesis

During my PhD, I could use the growing sequence information coming from the genome project and several transcriptome initiatives (Arendt lab and Jekely lab, unpublished). Sequence fragments of the genes of interest were first identified using tblastn searches in the *Platynereis* resources website: <http://4dx.embl.de/platy/>.

Sequence fragments with high similarity to the query sequence were then compared and assembled, either manually or using contig assembly algorithms like CAP3 (Huang and Madan, 1999). This work resulted in three typical situations:

1. After the assembly, the shorter fragment were all completely overlapping to one longer sequence, usually an EST. This EST was long enough to produce an in situ probe. In this case, the longer EST clone was used directly for the preparation of the template for the probe synthesis. Sometimes, when the physical clone was not available, specific primers were designed on the EST sequence to amplify the gene of interest from a cDNA library.
2. The longest sequence fragment was insufficient to generate a probe for WMISH. This sequence fragment was extended with 5' and/or 3' RACE-PCR.
3. Two different assemblies were found, with high similarity to two different parts of the gene of interest. Specific PCR primers were designed to clone the full length from a cDNA library.

Many other probes for WMISH were produced from clones already present in the lab. The following list reports all the unpublished genes investigated by WMISH in this thesis, and the sources of the corresponding clones. For the PCR primers, F indicates Forward, R indicates Reverse, 3R-F1 and 3R-F2 are the 3' RACE PCR

primers (F2 is the nested oligo), and 5R-R1 and 5R-R2 are the 5'RACE PCR primers (R2 is the nested oligo).

aanat RACE PCR primers designed on the Solexa reads HWI-EAS225:1:59:1281:567#0/1, HWI-EAS225:1:73:929:79#0/1 and HWI-EAS225:1:52:1383:213#0/1.

aanat-5R-R1: ACAAACCTGGAATCCGGCTTTTGAATAA

aanat-5R-R2: TGGAATCCGGCTTTTGAATAAAGTGGAA

aanat-3R-F1: GCACATGAACCAGATGGAGAATCTGTGTG

aanat-3R-F2: TCTGTGTGCATCCATTCAGTGTGTGTTGA

bsx RACE PCR primers designed on the EST If06P0045M18_F.ab1

bsx-5R-R1: TCGTCCTCTCCGTCATCCCCCTTCTTC

bsx-5R-R2: GTTCCCTGGGGCATCATGCTGGAATA

bsx-3R-F1: GCGACCAACAACCTGAACGGGTTGGAAA

bsx-3R-F2: AGGGGGATGACGGAGAGGACGA

c-ops2 Coding sequence predicted from the BAC DNA sequence CT030681 (NCBI), amplified with gene specific primers and extended with RACE PCR.

c-ops2-F: CCTGTGTATAGTGGGAGTGATTGGGACACT

c-ops2-R: AGGGAAGGAAGGACCTCAGCGTAGATG

c-ops2-5R-R1: AGGTTGCCAACGTCAAATGGTCTGACA

c-ops2-5R-R2: GAAGAGGTTTCATCTCGGATGCCAGACC

c-ops2-3R-F1: ACTGCAGGCAAGGCTGAGAAGTCCATC

c-ops2-3R-F2: CCCATCTACGCTGAGGTCCTTCCTCC

CNGa EST IB0AAD16YI23CM1. Expression pattern originally investigated by Dr. G. Jekely.

cpa EST 48-1-11-D

cry1 EST If06P0038L01_F.ab1

foxD Probe courtesy of A. Lauri.

hiomt RACE PCR primers designed on the Solexa read HWI-EAS225:1:16:1174:550#0/1. Several rounds of RACE PCR were necessary to find the entire coding region. Gene specific primers were used at the end to confirm the assemblies of RACE PCR products, and to generate a longer amplicon for WMISH probe synthesis.

hiomt-5R-R0: TTGGAGCATAAATGATTGGGCTGATGG

hiomt-5R-R1/2: AAGGTGGCGATATTCCTTCCCTGAACG

hiomt-5R-R1/2-2: ATGCCTCCACCAGGTTGATTTTCTCA

hiomt-5R-R1: GCTCAGCAGGTAGAGGTCGGCTTCA

hiomt-5R-R2: TGATGAAGAAGTCCCCGGGCAAA

hiomt-3R-F1: TGCATGAGAGATACAGGGCCTTCGACA

hiomt-3R-F2: AGTGCTGTGATTTAGGAGCTGGCACA

hiomt-F: CAGGGGAAGGACGGAAAGCACAATTAC

hiomt-R1: CACCAAACTTTGTGCACATATCACCTCA

lhx3/7 Probe from Dr. K. Tessmar-Raible (Tessmar-Raible, 2004).

melatonin rec. A From the assembly of KN-1127-B-93_O24_SP6.abi and contig_31138419_length_997_cvg_17.3. Amplified with:

melrecA-F: TGAGCACAGACATTTACCAGTGGGATGG

melrecA-R: TGCTGTTCATGCTGGAATTGGCAAAG

melatonin rec. B EST IB0AAA39CB08EM1

mitf RACE primers designed from the assembly of: NODE_55133_length_128_cov_2.648438, HWI-EAS225:1:50:158:155#0/1-RC, HWI-EAS225:1:94:1209:1675#0/1

mitf-3R-F1: ACGAGGCACGCTCCTGGGCCAAA

mitf-3R-F2: TCCTGGGCCAAAGAGAGGCAGAAGAAG

mitf-5R-R1: CCTCCATCTGTCTCTGTCTGTCTTCCA

mitf-5R-R2: TGACGCCTTCAGAATTGTGCCTTTGTT

neurops EST clone KN-1127-B-08_P16_SP6.abi, amplified with:

neurops-F: TTCCCGGGATCCTGTTACCCAGTTAGG

neurops-R: GAGGGCTCTGACCGACTCTTGTGTGA

not Original clone from Prof. D. Arendt. Coding sequence extended with RACE PCR. Gene specific primers were used at the end to confirm the assemblies of RACE PCR products, and to generate a longer amplicon for WMISH probe and mRNA synthesis.

not-5R-R1: GGGTGGCAGTCCATATAACGGATGCAG

not-5R-R2: AGACTCgtGGGGTCCATAGGCCTCAGT

not-3R-F1: GACGCCATCTTAGGCTCCCAACATCCT

not-3R-F3: GGGCAAAGCAAAGAGGGTTAGGACGAT

not-F: CCACTCATCACAGGCATACGAACTGGAA

not-R: TCCATGGGCACtACAATATGTCCTGTCA

nr2e3 EST clone KN-1127-B-129_C21_SP6.abi, amplified with:

nr2e3-F: CCAGCGATTGTTCAAGACTGACTTTGATT

nr2e3-R: CGAACAACATCTTTGTTTCATGCCCATC

pdf EST clone IB0AAD11YI23CM1. Expression pattern originally investigated by Dr. G. Jekely.

per RACE primers designed from the assembly of the Solexa reads HWI-EAS225:2:23:1575:205#0/1 and HWI-EAS225:2:29:1218:784#0/1

per-3R-F1: ACGGCGATACCGTTGCTCGGGTACTT

per-3R-F2: TCGGGTACTTGCCCCAAGATATGATCG

per-5R-R1: AAAACATCAGGATTCATCGGCCCTGT

per-5R-R2: CGTAATCACCGTCTTCGCCCTCATTC

perops Sequence identified after the assembly of several ESTs. Amplified with the primers:

perops-F: TGGTGATGTGCCACTGCTAGTCAGCAT

perops-R: GCAAACCTGCATAAACCAGAGGGACACCTG

For the phylogenetic and genomic analyses, a larger contig was generated by comparing this EST with genome data.

rfx4/6 Probe courtesy of A. Lauri.

sens Specific primers designed on the EST sequence KN-1127_B-30_L13_SP6.abi:

sens-F: GGAAGCGATTGAAAAGTTGCGTAGAGA

sens-R: CGAACTTGGAGACACACTTCTTGAGGA

six4 Clone from Prof. D. Arendt.

tbx2/3 The *tbx2/3* sequence was retrieved by comparing a *Nereis arenaceodentata* *tbx2/3* sequence (Winchell et al., 2010) with *Platynereis* genomic fragments. The following gene specific primers were used:

tbx2/3-F: CTTCCACCTTACAAAGTGCGGCTCTC

tbx2/3-R: TCAACATCCAAATGGTGATGGTGTCCTCA

11.2.6. Phylogenetic analysis

For phylogenetic analysis, sequence data were retrieved from the JGI genome portal webserver, from NCBI and ENSEMBL. Multiple sequence alignments of protein sequences were generated with MUSCLE (<http://www.ebi.ac.uk/Tools/msa/muscle/>), inspected and corrected by eye in Jalview (Waterhouse et al., 2009), and finally trimmed using Gblocks (Castresana, 2000). Phylogenetic trees with the maximum likelihood method were computed with PhyML 3.0 (Guindon et al., 2010), with 1000x bootstrap, using the server <http://www.atgc-montpellier.fr/phyml/>. Phylogenetic trees were plotted with FigTree.

11.3. Whole mount in situ hybridization

11.3.1. Fixation of *Platynereis* larvae for WMISH

For WMISH of 48hpf-5dpf larvae, the fixation protocol described in par. 11.1.1 was used (2 hrs of fixation minimum, and MetOH washes).

For early stage *Platynereis* larvae, and for genes with lower expression levels, the following fixation protocol has been used (contributed by Dr. H. Marlow):

- Collect the larvae with custom-made nets which fit into individual wells of 6 well plates.
- Transfer the net with the larvae in another well containing a solution of 4% PFA, 0.1M MOPS, 2mM EGTA, 1 μ M MgSO₄ and 0.1% Tween-20.
- Incubate for 4-2hrs at 4 °C.
- Rinse twice with PTW. Transfer in Eppendorf tubes.
- Rinse quickly in distilled water.

- Wash twice in ice-cold 100% MetOH, and keep at -20°C .

11.3.2. Probe synthesis

Preparation of the template for *in vitro* transcription

DIG-labeled probes for WMISH were synthesized with *in vitro* transcription, using linearized DNA or PCR products as templates. The template contained a phage polymerase (T7 or SP6) for the transcription of antisense RNA probes.

Plasmid templates were linearized with restriction digestion using a 5'-overhang restriction enzyme. Usually, 10 μg of plasmid DNA were digested overnight. The linearized plasmid was purified with the QIAquick Nucleotide Removal kit (Qiagen, 28304), following manufacturer instructions, and eluted in water.

Preparation of the DIG probe

DIG labeled probes for WMISH were synthesised according to the following protocol.

- Assemble the *in vitro* transcription as follows:

Linearized DNA template	1 μg
DTT 100mM	2 μl
NTPs	1.3 μl
DIG-UTP 10mM	0.7 μl
transcription buffer 10x	2 μl
RiboGuard RNase Inhibitor (Epicentre)	0.5 μl
RNA polymerase (Roche)	1 μl
nuclease free water	up to 20 μl

- Incubate the reaction for 2-4 hrs at 37°C .
- Add 1 μl of DNaseI and incubate 15-30 min at 37°C .
- Purify the RNA probe with the RNeasy Mini kit (Qiagen, 74104), and elute in 50 μl of nuclease-free water.
- Check the concentration and the quality of the RNA probe with gel electrophoresis.
- Dilute the probe to a final concentration of 50 ng/ μl with Hyb-mix (see par. 10.3 for the recipe).

11.3.3. Standard *Platynereis* WMISH protocol

Rehydration

- Incubate 5min in 75% MetOH-25%PTW
- Incubate 5min in 50% MetOH-50%PTW
- Incubate 5min in 25% MetOH-75%PTW
- Rinse 2x5min in PTW

Proteinase K digestion and postfixation

- Digest with Proteinase K (100 $\mu\text{g}/\text{ml}$ in PTW) without shaking. The length of digestion depends on the developmental stage: 30sec for <24hpf, 1 min for 24-48hpf, 2 min for 48-72hpf, 3 min for >72hpf.
- Stop the digestion with 2x2min washes in 2 mg/ml glycine/PTW.
- Rinse 2x2min in PTW
- Fix for 20min in 4% PFA/PTW
- Rinse 5x5min in PTW. Transfer the larvae into Eppendorf tubes.

Probe hybridization

- Prehybridization: remove all the PTW from the tubes, and add 500 μl of Hyb-mix. Incubate at 65 °C for 1-2hrs.
- At the end of prehybridization, start preparing the probes. Dilute the probe stocks to a final concentration of 1-2ng/ μl , in a final volume of 100 μl of Hyb-mix for each tube. Denature the probes at 90 °C for 10 min. Transfer immediately on ice.
- Remove the prehybridization solution and add quickly the probes. Hybridize ON at 65 °C.

Washes

- Warm up the solutions that will be used for the 65 °C washes.
- Remove the probes, and store at -20 °C. Probes can be reused up to 5 times, and usually reused probes give stainings with better signal-to-noise ratio.
- Wash the embryos 15 min in Hyb-mix at 65 °C.
- Wash the embryos 2x30 min in 50% formamide-50% 2x SSCT at 65 °C.

- Wash the embryos 15 min in 2x SSCT at 65 °C.
- Wash the embryos 2x30 min in 0.2x SSCT at 65 °C.
- Remove the 0.2x SSCT solution and add PTW.

Blocking and primary antibody incubation

- Block in 5% sheep serum/PTW, for 1hr at RT, while shaking on a thermomixer at 450rpm.
- Remove the blocking solution, and add 50-100 μ l of primary antibody solution, prepared in 5% sheep serum/PTW. Use the anti-DIG Fab fragments with a 1:5000 dilution, and the anti-acetylated tubulin antibody with a 1:500 dilution. Incubate for one night at 4 °C, while shaking on a thermomixer at 450rpm.

NBT/BCIP staining

- Remove the antibody solution, and was 6x5min in PTW, at RT, shaking on a thermomixer at 450rpm. For a better signal-to-noise ratio, the last PTW wash can be done overnight at 4 °C.
- Equilibrate the larvae 5 min in staining buffer, pH 7.5, without MgCl₂, while shaking.
- Equilibrate the larvae 5 min in staining buffer, pH 7.5, with MgCl₂, while shaking.
- Equilibrate the larvae 2x5 min in staining buffer, pH 9.5 (precise), with MgCl₂, while shaking. Transfer the larvae in 24-well plates.
- Prepare the staining solution using 4.5 μ l NBT (Roche, final concentration 337.5 μ g/ml) and 3.5 μ l BCIP (Roche, final concentration 175 μ g/ml) per ml of staining buffer pH 9.5. Develop the staining in the darkness.
- Change the staining solution every day. Staining can take up to 4-5 days. With this protocol, unspecific background comes up around this time.
- Stop the staining by washing 5 min in staining buffer pH 7.5. Transfer the larvae again in Eppendorf tubes.

Secondary antibody, mounting and imaging

- Wash 2x5min in PTW, at RT, shaking on a thermomixer at 450rpm.
- Remove the PTW and block in 5% sheep serum/PTW, for 30min-1hr.

- Remove the blocking solution, and add 50-100ul an anti-mouse secondary antibody, diluted to a final concentration of 1:500, in 5% sheep serum/PTW.
- Incubate 1-2 nights at 4 °C, while shaking on a thermomixer at 450rpm.
- Remove the antibody solution, and was 6x5min in PTW, at RT, shaking on a thermomixer at 450 rpm.
- Transfer the larvae in DABCO/glycerol (2.5 mg/ml DABCO in 87% glycerol), shake for 1 hr at 450 rpm. The larvae can be stored in glycerol at 4 °C.
- For imaging, mount the larvae between a slide and a coverslip, with a spacer made by several layers of tape. For <24hpf larvae, use 2 layers of tape on each side. For 48hpf-5dpf (dorsal or ventral view) larvae, use 3 layers of tape. For reflection microscopy (Jékely and Arendt, 2007), use a confocal microscope and illuminate the sample with a 635 nm laser. Set up the detection window around the same wavelength, to detect the light reflected by the NBT/BCIP precipitates.

11.3.4. Modified *Platynereis* WMISH protocol

A modified version of the *Platynereis* WMISH protocol was used for early stage in situ (≤ 24 hpf) and for genes with low signal-to-noise ratio. Essentially, in this protocol the tissue is acetylated before hybridization with the probe. Tissue acetylation blocks unspecific binding of the probe, reducing the background noise; in this way, the larvae can be stained for longer times to obtain the specific signal.

As a consequence of acetylation, also the tubulin contained in each cell is acetylated. For this reason, the staining with acetylated tubulin antibody doesn't show nicely the axonal scaffold, but only the outline of the cells on the surface. For this reason, this protocol is combined with a anti-tyrosinated-tubulin antibody. Tyrosination is another tubulin modification taking place in stabilized microtubules. The anti-tyrosinated-tubulin antibody stains the axonal scaffold, but with an efficiency lower than the anti-acetylated tubulin antibody.

The tissue acetylation is performed after the proteinase K step, and before the postfixation. The protocol for tissue acetylation was kindly contributed by Dr. H. Marlow.

Acetylation

- After the proteinase K digestion and the glycine washes, wash 2x5 min in PTW.

- Wash the larvae 5 min in 1% triethanolamine (TEA)/PTW (freshly prepared).
- Wash the larvae 5 min in 1% triethanolamine (TEA)/PTW with 3 μ l/ml acetic anhydride (freshly prepared).
- Wash the larvae 5 min in 1% triethanolamine (TEA)/PTW with 6 μ l/ml acetic anhydride (freshly prepared).
- Wash 2x5min in PTW. Proceed with the postfixation.

11.4. EdU incorporation studies

11.4.1. Incubation of larvae with EdU

For cell proliferation studies, the EdU-based Click-iT EdU Imaging Kit (Invitrogen, C10340) was used. EdU was preferred to BrdU because it can be combined more easily with antibody stainings and WMISH. BrdU detection, based on an anti-BrdU antibody, requires the treatment of the tissue with HCl, to permeabilize the cells and denature the DNA. After HCl treatment, many epitopes are destroyed and cannot be recognized by their antibodies. In contrast, EdU is detected with a simple copper-catalyzed reaction between an alkyne moiety (coupled to the EdU) and an azide (coupled to an Alexa Fluor fluorescent dye).

10mM EdU stock concentrations were prepared resuspending EdU in NSW. During pilot experiments, different concentrations of EdU were tested, to identify the minimal concentration of EdU sufficient to label the dividing cells.

In all the experiments, *Platynereis* larvae were incubated for 2 hrs in 10 μ M EdU. After the incubation, larvae were rinsed in NSW and then either fixed, or raised to the 48hpf stage for the birthdating studies.

11.4.2. Detection of EdU after immunostaining and WMISH

EdU treated larvae were processed normally for immunostaining and WMISH.

The EdU detection reaction was performed after washing away the excess of secondary antibody, following the manufacturer instructions.

The PTW was removed from the Eppendorf tubes, and the larvae were incubated in the dark for 30 min with 25 μ l of Click-iT reaction cocktail:

1x Click-iT reaction buffer	430 μ l
CuSO ₄	20 μ l
Alexa Fluor azide 647 nm	1.2 μ l
Reaction buffer additive	50 μ l
total volume	500 μ l

After the incubation, the Click-iT reaction cocktail was removed, and the larvae were rinsed 2x5 min in PTW, shaking at 450 rpm. Afterwards, larvae were incubated in DAPI/PTW for 30 min, and finally washed 4x5 min in PTW.

11.5. Analysis of molecular fingerprints

11.5.1. Comparison of expression patterns with PrImR

Generation of PrImR average expression patterns

Average expression patterns were generated as described in Tomer et al. (2010).

Briefly, WMISH of the genes of interest were performed with properly staged 48hpf larvae. Gene expression patterns of the larval brains were acquired with confocal microscopy (reflection microscopy, Jékely and Arendt 2007) together with the acetylated (or tyrosinated) tubulin staining. Each confocal stack was registered on the reference axonal scaffold, using an ImageJ macro developed by Dr. R. Tomer according to Tomer et al. (2010). Afterwards, the registered axonal scaffold was compared to the reference scaffold for a quality check. Only the confocal stacks with a good registration of the scaffold were kept for the subsequent steps.

The gene expression patterns of the properly registered larvae were used to create an average expression pattern. For each gene, a minimum of 3 stacks were used to generate the average. This step of the process was performed by Dr. R. Tomer.

The list below reports the sources of the averages used for the analysis of molecular fingerprints (Chapter 7).

bf1 R. Tomer, see Tomer et al. (2010)	c-ops1 R. Tomer, and this work
brn1/2/4 R. Tomer, see Tomer et al. (2010)	cpa this work
bsx this work	cry1 this work
ChAT R. Tomer, see Tomer et al. (2010)	dach R. Tomer, see Tomer et al. (2010)
CNGa this work	dbx R. Tomer, see Tomer et al. (2010)
coe R. Tomer, see Tomer et al. (2010)	DLamide G. Jékely, see Conzelmann et al. (2011)

dll R. Tomer, see Tomer et al. (2010)	pax2/5/8 R. Tomer, see Tomer et al. (2010)
enzA K. Guy, see Guy (2009)	pax6 R. Tomer, see Tomer et al. (2010)
er81 R. Tomer, see Tomer et al. (2010)	pdf this work
eya R. Tomer	phc2 R. Tomer, see Tomer et al. (2010)
foxD R. Tomer	rfx4/6 this work
hiomt this work	r-ops1 R. Tomer, see Tomer et al. (2010)
islet R. Tomer, see Tomer et al. (2010)	rx R. Tomer, see Tomer et al. (2010)
lhx1/5 R. Tomer, see Tomer et al. (2010)	sens this work
lhx2/9 R. Tomer, see Tomer et al. (2010)	six1/2 R. Tomer, see Tomer et al. (2010)
lhx3/7 R. Tomer	six4 this work
mitf this work	sox2 R. Tomer, see Tomer et al. (2010)
neuroD R. Tomer	svp R. Tomer, see Tomer et al. (2010)
ngn R. Tomer, see Tomer et al. (2010)	tbx2/3 this work
nk2.1 R. Tomer, see Tomer et al. (2010)	tll R. Tomer, see Tomer et al. (2010)
not N. Kegel, R. Tomer and this work	tph R. Tomer, see Tomer et al. (2010)
otp R. Tomer, see Tomer et al. (2010)	trp2 K. Guy, see Guy (2009)
otx R. Tomer, see Tomer et al. (2010)	Vglut R. Tomer, see Tomer et al. (2010)

Analysis of minimal synexpression groups

The analysis of minimal synexpression groups was performed using the averaged PrImR expression patterns.

The first step was the identification of all the genes coexpressed with *hiomt*. For this, I used an ImageJ macro developed from R. Tomer, which takes as an input a Z range of the average expression pattern of interest, and compares it with all the others using the “Colocalization Highlighter” plugin of ImageJ. This macro gives as an output coexpression panels, with Z projections of the coexpressions of the gene of interest with all the other genes of the dataset.

Since Z projections can sometimes show false positive results, colocalizations were verified manually looking at the entire stacks (“Synchronize Windows” and “Colocalization Highlighter” in ImageJ).

Some expression patterns showed very restricted expression within the *hiomt* region, while others had broader expression domains in the brain but with discrete expression sites within the the *hiomt* territory (i.e. cells that could be easily sorted out from all the others). These genes were considered to partition the *hiomt* region in minimal synexpression groups. Their overlap was tested with the generation of

coexpression panels, until the minimal set of synexpression groups in the *hiomt* region was identified. The set of minimal synexpression groups is shown in fig. 7.1. Their names are purely indicative, and in the cases the name includes a gene, this gene is usually not uniquely expressed in those cells, but the synexpression group is identifiable within the general expression domain of that gene. These synexpression groups are defined as follows:

dorsal bsx cells An isolated group of *bsx*⁺ cells in the dorsal brain.

lateral-DLamide-cells Isolated *DLamide*⁺ cells in the dorsal brain (the more lateral of all the *DLamide*⁺ cells).

asymmetric 5HT cell The isolated asymmetric cell expressing the serotonergic marker *tph*.

cPRCs Coexpression of *ChAT* and *tll*, calculated with the “Image Calculator” function of ImageJ. The expression of *ChAT* and *tll* in the cPRCs was verified experimentally.

lateral-not-cells Isolated *not*⁺ cells in the dorsal brain (called lateral because a more medial *not*⁺ cell exists).

lateral-otp-cells Isolated *otp*⁺ cells in the dorsal brain (the more lateral of all the *otp*⁺ cells).

er81-vtn-c-ops1-cells Coexpression of *c-ops1*, *er81* and *otp*, calculated with the “Image Calculator” function of ImageJ. These are the *vtn*⁺ photoreceptors described by Tessmar-Raible et al. (2007).

lhx3-sox2-cells Coexpression of *lhx3* and *sox2*, calculated with the “Image Calculator” function of ImageJ.

lateral-5HT-cells Coexpression of *tph* and *syt* (*synaptotagmin*), calculated with the “Image Calculator” function of ImageJ. The lateral *tph* expression domain comprises few cells, while only one serotonergic cells is present on each side. The additional *tph*⁺ cells are probably the future serotonin-immunoreactive cells, which become visible in the dorsal brain after 48hpf (Fischer et al., 2010). For this reason, *syt* coexpression was used to identify only the differentiated cells within the *tph* expression domain.

dach-deep-cells An isolated group of *dach*⁺ cells, located in a deep position within the brain.

lhx1/5-cells The ventral, isolated part of the *lhx1/5* and *hiomt* coexpression, calculated with the “Image Calculator” function of ImageJ. More dorsal *lhx1/5* and *hiomt* coexpressing cells exist, but they are better described within other synexpression groups.

six4-cells Isolated *six4*⁺ cells in the medial brain. Other *six4-hiomt* coexpressing cells exist, but they are better described within other synexpression groups.

pdf-cells Isolated *pdf*⁺ cells in the medial brain. Other *pdf-hiomt* coexpressing cells exist, but they are better described within other synexpression groups.

deep-rfx4/6-cells Isolated *rfx4/6*⁺ cells deep in the medial brain.

cpa-otp-cells Coexpression of *cpa* and *otp*, calculated with the “Image Calculator” function of ImageJ.

AE-PCs (Adult eyes pigment cells) Coexpression of the pigment cell markers *enza* and *mitf*, calculated with the “Image Calculator” function of ImageJ.

AE-PRCs (Adult eyes photoreceptor cells) Expression of *r-ops1* in the adult eyes (larval eyes are not included).

11.5.2. Comparison of molecular fingerprints

Collection of the vertebrate expression data

The vertebrate expression data matrix (see Appendix D) used for the hierarchical clustering in fig. 7.6 was assembled from several resources. The data matrix refers to gene expression in postmitotic and/or differentiated cells/tissues. Whenever possible, the expression of genes within the structures of interest was verified using high resolution expression data resources, like high resolution WMISH screens or microarray studies. The main references were Blackshaw et al. (2004); Mu et al. (2008); Siegert et al. (2012) for the retina, Shimogori et al. (2010); VanDunk et al. (2011) for the hypothalamus, Bailey et al. (2009); Toyama et al. (2009) for the pineal and Quina et al. (2009) for the habenula. The Zfin and the Allen Brain Atlas expression databases were also used. If the expression of the gene of interest was not reported in these sources, published literature was consulted.

To establish the “ur-vertebrate” consensus matrix for the pineal, the loss of photosensitivity in the mammalian pineal was taken in account. For this reason, whenever expression data from anamniotes were in contrast with mouse data, the fish and/or *Xenopus* data were used.

Statistical analysis

All the statistical analysis of molecular fingerprints was performed with R <http://www.r-project.org/> and the package “made4” (Culhane et al., 2005).

Hierarchical clustering was performed with the bottom-up approach, using three different methods for the calculation of the distance matrix (Pearson’s correlation, uncentered correlation and Jaccard distance) and two methods for linkage (average or complete linkage). Bootstrap analysis for hierarchical clustering was computed with the package “pvclust” (Suzuki and Shimodaira, 2006). The MDS (multidimensional scaling) analysis was performed using the isoMDS function of the package MASS (Venables and Ripley, 2002). The PCA (principal component analysis) was performed with the “FactoMineR” package (Husson et al., 2010).

12.1. Analysis of *rx* gene structure and SNPs

12.1.1. Identification of *rx* introns with TAIL-PCR

A first intron in the *rx* gene was identified by N. Kegel, after the alignment of *rx* genes; this intron has a conserved position in the homeodomain (fig. 4.1). In *rx* genes, another intron is normally present before this conserved intron.

I used thermal interlaced PCR (TAIL-PCR, Liu and Whittier 1995) to investigate the first intron that interrupts the *Platynereis-rx* coding sequence. TAIL PCR is used to amplify genomic regions adjacent to a known sequence. Gene specific primers with high T_m (72 °C) are combined with degenerate primers with low T_m , in three seminested PCR reactions where the annealing temperature in the PCR program alternates between high and low values, to facilitate the binding of the two primers sets. The gene specific primers for *rx* were designed around the start codon, to identify genomic fragments immediately downstream. Eight independent sets of TAIL PCR were run with the eight degenerate primers. The products of the eight sets of reactions were analysed by gel electrophoresis. The longest product was purified from gel, cloned in pCRII-TOPO and sequenced. This amplicon spanned the entire exon 1 and the beginning of the first intron. Later genome assembly confirmed the results of this analysis.

Primers:

rx-tail-F1: TGGTGT CAGGGAAAAGGGGTTGCTTCT

rx-tail-F2: CAAGCTGCCTGGTTCTGTTCTGGCTGT

rx-tail-F3: TCGATGCCATTTTGGGGCTGAAAACTGCAAT

rx-tail-R1: CTCTGACTTCGGGCAGGTTGATCTTAA

rx-tail-R2: GTTCCTCTCTGCTGTAGACATCCGGGT

rx-tail-R3: GCAGTCTGAATGAGTCGCGACATCTCC

deg-primer-1: NGTCGASWGANAWGTT

deg-primer-2: GTNCGASWCANAWGTT

deg-primer-3: WGTGNAGWANCANAGA

deg-primer-4: NGTCGASWGANAWCTT

deg-primer-5: GTNCGASWCANAWCAA

deg-primer-6: WGTGNAGWANCANTCT

deg-primer-7: NGTCGASWGANAWAGA

deg-primer-8: NGTCGASWGANAWGTT

First TAIL PCR reaction

<i>Platynereis</i> genomic DNA	150 ng
dNTPs 5mM	2 μ l
First Gene Specific Primer 5 μ M	0.8 μ l
deg. primers 1-8 100 μ M	1 μ l
MgCl ₂ 25 mM	2 μ l
10x LA Taq Buffer (TaKaRa)	2 μ l
LA Taq Polymerase (TaKaRa)	0.1 μ l
water	to 20 μ l

Cycling program:

98 °C-30s; 94 °C-1min; 95 °C-1min; 5 cycles of {94 °C-1min; 65 °C-1min; 68 °C-30s};
 94 °C-1min; 25 °C-3min; 68 °C-3min; 15 cycles of {94 °C-30s; 64 °C-1min; 68 °C-3min};
 94 °C-30s; 64 °C-1min; 68 °C-3min; 94 °C-30s; 44 °C-1min; 68 °C-3min}; 68 °C-5min,
 10 °C ∞ .

Second TAIL PCR reaction

1:50 dilution of the 1st TAIL reaction	1 μ l
dNTPs 5mM	2 μ l
Second Gene Specific Primer 5 μ M	0.8 μ l
deg. primers 1-8 100 μ M	1 μ l
MgCl ₂ 25 mM	2 μ l
10x LA Taq Buffer (TaKaRa)	2 μ l
LA Taq Polymerase (TaKaRa)	0.1 μ l
water	to 20 μ l

Cycling program:

98 °C-30s; 14 cycles of {94 °C-30s; 64 °C-1min; 68 °C-3min; 94 °C-30s; 64 °C-1min; 68 °C-3min; 94 °C-30s; 44 °C-1min; 68 °C-3min}; 68 °C-5min; 10 °C ∞.

Third TAIL PCR reaction

1:50 dilution of the 2nd TAIL reaction	2.5 μ l
dNTPs 5mM	5 μ l
Third Gene Specific Primer 5 μ M	2 μ l
deg. primers 1-8 100 μ M	2.5 μ l
MgCl ₂ 25 mM	5 μ l
10x LA Taq Buffer (TaKaRa)	5 μ l
LA Taq Polymerase (TaKaRa)	0.25 μ l
water	to 50 μ l

Cycling program:

98 °C-30s; 12 cycles of {94 °C-30s; 64 °C-1min; 68 °C-3min; 94 °C-30s; 64 °C-1min; 68 °C-3min; 94 °C-30s; 44 °C-1min; 68 °C-3min}; 68 °C-5min; 10 °C ∞.

12.1.2. SNP analysis

After the identification of the first intron in *rx* coding region, an analysis of SNPs was performed before morpholino design. Genomic DNA was extracted from 10 different *Platynereis* adults, coming from different fertilizations, using the NucleoSpin Tissue Kit (Macherey-Nagel, cat. n. 740952), according to manufacturer's instructions.

For SNP analysis, the entire 5'UTR, the first exon and the exon1-intron1 boundary (about 800bp) were amplified with forward oligos designed in the 5'UTR and reverse oligos designed in the first intron. Another set of PCRs was done to amplify the intron1-exon2 boundary.

The first primer pairs tested was not able to amplify this region from all the genomic DNA samples, most likely for the presence of SNPs. For this reason, different primer pairs were assayed in order to amplify this genomic region from all the individuals. The PCRs were performed with the HotStarTaq DNA Polymerase (Qiagen), with methods similar to those described in par. 11.2. The primer pairs used are the following:

rx-5UTR-F2: CCAGTCTTGCACTGTTCTCGCCTGA and
rx-intron1-left-R2: TCGGGACATCCGAGGCCAAGA for 5'utr-ex1-in1

rx-intron1-right-L2: ACCTCAAATCGGGACTTTACTGTTGT and
rx-tail-R1: CTCTGACTTCGGGCAGGTTGATCTTAA

rx-intron1-right-L1: CTGTGTTGTATACCTCAAATCGGGACT and
rx-tail-R1: CTCTGACTTCGGGCAGGTTGATCTTAA

The PCR products were purified with the QIAquick PCR Purification Kit (Qiagen, 28104) and cloned in pCRII-TOPO, as described previously in par. 11.2. Ligations were transformed in competent cells, and a minimum of three colonies for each PCR reaction (i.e. for each worm) was picked for minipreps and sequencing. The sequences were aligned with ClustalW (<http://www.ebi.ac.uk/Tools/msa/clustalw2/>) for the identification of polymorphic positions.

12.2. Injection of *Platynereis* zygotes

The *Platynereis* injection method was developed by N. Kegel and B. Backfish, under the supervision of Dr. R. Tomer, and optimized with some modifications from myself and Dr. M. Handberg-Thorsager.

12.2.1. Preparation of injection solutions

All the injection solutions were freshly prepared before each experiment. The water and the solutions used to prepare all the injection samples were sterile filtered with 0.22 μm filters (Millipore). After mixing all the components, the injection solutions were centrifuged at full speed for 5 min.

For the morpholino and ZFNs injections, the fluorescent tracer TRITC-dextran (Invitrogen, lysine fixable, D1818) was added, normally with a ratio of 2 vol dextran solution: 3 vol morpholino/RNA solution. The dextran stock is prepared by resuspending the powder with 200mM KCl (sterile filtered) to a final concentration of 830 ng/ μl . After resuspension, the stock is filtered with 0.22 μm filters (Millipore), aliquoted and stored at -20°C .

Dextran was not used in the injections with H2A-RFP mRNA.

Morpholinos

Morpholino antisense oligonucleotides were ordered from GeneTools. Morpholino stocks were prepared by resuspending the lyophilized morpholinos with sterile filtered water, to a final concentration of 1.5-2mM. The GeneTools standard control MO (*stctrl* MO) targets the human β -globin pre-mRNA, it doesn't have hits on the *Platynereis* genome, and the injection of this MO in *Platynereis* zygotes with concentrations up to 1.2mM doesn't cause any toxic effect.

The sequences of the morpholinos mentioned in this study are the following:

***rx-in1ex2* MO** 5'-CTGTCCTCTGCAAAATACCCCAAAA-3'

This morpholino targets the intron1-exon2 junction of the *rx* pre-mRNA; injected at a final concentration of 800nM

***rx-stcod2* MO** 5'-ACCAATGTAATGGTGTAAGTTATTA-3'

This morpholino targets the 5'-UTR of the *rx* mRNA; injected at a final concentration of 500nM.

***st-ctrl* MO** 5'-CCTCTTACCTCAGTTACAATTTATA-3'

This morpholino targets was injected at the same concentration of the *rx* MOs used in the same experiment.

***rx-ex2in2* MO** 5'-AGGTATCATCAACATACCTGAACTC-3'

This morpholino was designed by N. Kegel; it targets the exon2-intron2 splice site.

***rx-in2ex3* MO** 5'-CACACCTGAAACGAGAATGAACGAG-3'

This morpholino was designed by N. Kegel; it targets the intron2-exon3 splice site.

In vitro transcription of capped mRNAs

Capped mRNAs for injection was produced with *in vitro* transcription from linearized templates. The template DNA was prepared like the templates for the transcription of DIG-labeled probes (par. 11.3.2), from the following plasmids:

***rx* mRNA** *rx* mRNA was prepared from a pCS2-*rx* construct. This construct was made by subcloning the full *rx* coding region between the XhoI-XbaI sites of the pCS2+ vector. The template DNA was linearized with NotI, and the SP6 RNA polymerase was used for transcription. The *rx* mRNA was injected at a final concentration of 312.5 ng/ μ l.

EGFP mRNA *EGFP* mRNA was prepared from a pCS2-EGFP plasmid, linearized with Asp718. The SP6 RNA polymerase was used for transcription.

not mRNA *not* mRNA was prepared from a pCS2-not construct. The full *not* coding region was found with 5' and 3'-RACE PCR (see par. 11.2.5). This construct was made by subcloning the full *not* coding region in pCS2+ (StuI opened). The template DNA was linearized with NotI, and the SP6 RNA polymerase was used for transcription.

mYFP mRNA The *mYFP* mRNA was prepared from a pCS2-mYFP construct. This construct was made by subcloning the *mYFP* coding region (courtesy of Prof. J. Wittbrodt) in pCS2+. The template DNA was linearized with NotI, and the SP6 RNA polymerase was used for transcription. The *mYFP* mRNA was kindly provided by S. Rohr and Dr. M. Handberg-Thorsager.

H2A-RFP mRNA The *H2A-RFP* mRNA was kindly provided by S. Rohr and Dr. M. Handberg-Thorsager. It was transcribed from a construct courtesy of Dr. D. Gilmour.

GCaMP3 mRNA *GCaMP3* mRNA was prepared from a pCS2-GCaMP3 construct. This construct was made by subcloning the full *GCaMP3* coding region (courtesy of Dr. K. Svoboda) in the EcoRI and ZbaI sites of the pCS2+ vector. The template DNA was linearized with NotI, and the SP6 RNA polymerase was used for transcription.

mRNA for *rx* ZFNs The mRNA for *rx* ZFNs was provided by Sigma, and injected at a final concentration of 320 ng/ μ l.

From these templates, capped mRNAs were synthesised using the mMessage mMachine High Yield Capped RNA Transcription Kits (Ambion), with the following protocol.

- Assemble the *in vitro* transcription at room temperature as follows:

nuclease free water	up to 20 μ l
2x NTP/CAP	10 μ l
10x reaction buffer	2 μ l
linear DNA template	1 μ g
enzyme mix	2 μ l

- Incubate the reaction at 37 °C for 2-4 hrs.
- Add 1 μ l of TURBO Dnase, and incubate for additional 15min at 37 °C.
- Stop the reaction by adding 30 μ l of nuclease-free water and 30 μ l of LiCl precipitation solution.
- Mix and precipitate for a minimum of 30 min, better overnight, at -20 °C.
- Centrifuge at 4 °C for 15 min at maximum speed.
- Remove the supernatant. Wash the pellet with 70% ice-cold EtOH, centrifuge again at 4 °C for 5 min at maximum speed.
- Remove the supernatant, dry the pellet, and resuspend in 30 μ l of 0.22 μ m filtered nuclease-free water.
- Measure the concentration with the nanodrop, and adjust the final concentration to the desired value. Store the mRNA in single use aliquots at -80 °C.

12.2.2. *Platynereis* injection protocol

Preparation of the zygotes

- Set up some crosses with *Platynereis* sexually mature males and females. Control the quality of the fertilization by watching how the animals reproduce. A successful fertilization usually takes place when the animals spawn within few seconds-half minute after being placed together in the same Zentis cup.
- After 5-10 min, observe the eggs under a stereomicroscope. The sign of fertilization is the disappearance of the egg cortex, and the release of the cortical granules, which are composed of mucopolysaccharides and form a gelatinous mass (jelly) around the zygotes (Fischer et al., 1996). Hence, the fertilized eggs will float in the Zentis cup, and will be arranged in a very regular mosaic pattern.

Then, select the best fertilized embryonic batch. The quality of the zygotes can be evaluated looking at: the shape of the zygote (it must be spherical, oval or flattened zygotes are not good), the distribution of the yolk granules (normally they accumulate at the edges of the cell), the surface of the cell (it must look smooth; if it is wrinkly, the zygote is going to die) and the color (darker zygotes are normally of bad quality). Keep the favourite batch in the 18 °C incubator until 50 min post fertilization.

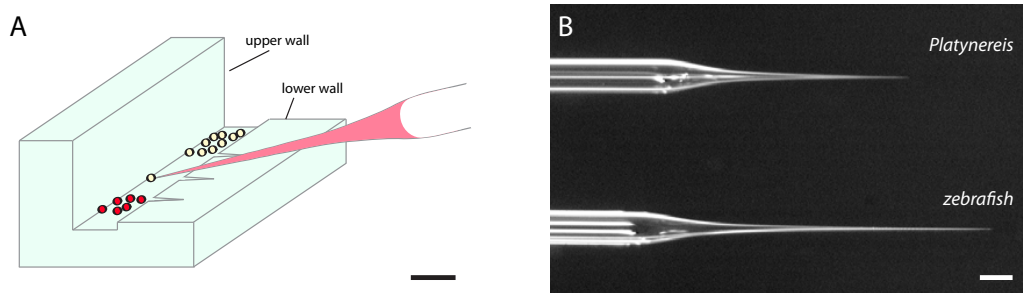


Figure 12.1: *Platynereis* injection stage and needles. A. Agarose stage used for *Platynereis* injections (drawing in scale). B. Comparison of *Platynereis* and zebrafish needles. Scale bar=1mm.

- Dejelly the zygotes 50 min after fertilization, by rinsing them thoroughly with 0.22 μm filtered NSW, using a Zentis cup and one custom-made sieve (made from 50 ml Falcon tubes and a nylon mesh with 100 μm mesh size, NITEX, Gebr. Stallmann). This step will require approximately 600 ml of NSW.
- Digest the zygotes with a 1 min incubation in a solution of 46.7 $\mu\text{g}/\text{ml}$ of proteinase K in NSW.
- Rinse the zygotes thoroughly in NSW (approximately 200 ml). They are ready for injection.

Preparation of the setup and injection

The injection setup is constituted by a Zeiss Axiovert 40C inverted microscope, equipped with a micromanipulator and a microinjector (in this case, FemtoJet from Eppendorf).

The zygotes are accommodated in a stage, prepared from a custom mold that leaves a 1mm wide groove between an high wall and a low wall of agarose (fig. 12.1A). The stage is prepared with 2% agarose in NSW. The low wall has the same height as the zygote diameter. A fine siringe needle is used to prepare scratches in the low wall, as shown in fig. 12.1A.

The needles used for *Platynereis* are pooled from glass capillaries (1mm diameter, with filament, Harvard apparatus) using a Sutter needle pooler. As shown in fig. 12.1B, the tip of the *Platynereis* needle is shorter and wider, compared to the zebrafish needles. With this shape, the needle has enough strength to puncture the zygote (longer tips tend to bend).

Injections are performed under a 10x magnification. For injection, the zygotes are pushed with the tip of the needle against the high wall. After the delivery of the

injection solution, the needle is released by passing through one of the scratches of the low wall. The zygote would normally follow the needle, but in this way it remains trapped by the low wall.

After injection, the embryos are transferred in a 6-well plate, and sorted under a fluorescence stereomicroscope, to eliminate the embryos not injected, and the ones that do not develop correctly.

12.3. Analysis of morpholino and mRNA injected larvae

12.3.1. Analysis of splicing after *rxin1ex2* MO injection

cDNA synthesis

To analyse the splicing variants after *rxin1ex2* MO injection, the same number of *rxin1ex2* MO and *stctrl* MO injected larvae was used to extract RNA, according to the protocol in par. 11.2.1. RNA was resuspended in 11 μ l of water, and the concentration was measured with the nanodrop.

For cDNA synthesis, the QuantiTect Reverse Transcription Kit (Qiagen) was used, with the following protocol.

- Assemble the genomic DNA elimination reaction as follows:

gDNA wipeout buffer 7x	2 μ l
template RNA	>200 ng
nuclease-free water	up to 14 μ l

- Incubate the reaction at 42 °C for 2 min, then place immediately on ice.

- Assemble the reverse transcription reaction as follows:

genomic DNA elimination reaction	14 μ l
Quantiscript Reverse Transcriptase	1 μ l
Quantiscript RT Buffer, 5x	4 μ l
RT Primer Mix	1 μ l

- Incubate at 42 °C for 30 min.
- Incubate at 95 °C for 3 min, to inactivate the reverse transcriptase.

- Dilute the reaction product 1:15 with water (if the starting amount of RNA was $>1\mu\text{g}$, dilute 1:20). This cDNA can be stored at -20°C and used as a qPCR template.

PCR detection of aberrant splicing

cDNAs prepared from *rxin1ex2* MO and *stctrl* MO injected larvae was used as template for the amplification of *rx* cDNA. The primers used were:

rx-start-L2 TGTCAGGGAAAAGGGGTTGCTTCTA
 rx-stop-R1 CATAGCAGTGAGGATCATGGAACACAAG

PCR reaction:

cDNA	10 μl
water	3.1 μl
rx-start-L2 5 μM	2.2 μl
rx-stop-R1 5 μM	2.2 μl
Hot Start buffer 10x (Qiagen)	2.2 μl
dNTP mix 25mM	1.1 μl
HotStarTaq DNA Polymerase (Qiagen)	0.22 μl

Cycling program:

1x	95 $^{\circ}\text{C}$	15 min
	94 $^{\circ}\text{C}$	30 sec
35x	68 $^{\circ}\text{C}$	45 sec
	72 $^{\circ}\text{C}$	2 min
1x	72 $^{\circ}\text{C}$	10 min

qPCR measurement of aberrant splicing

To quantify the efficiency of *rx* knock down, the normal and aberrant splice variants were quantified with qPCR, using SYBR Green labeling and an ABI 7500 thermocycler (EMBL GeneCore). A primer pair spanning the exon1-exon2 boundary

was used to quantify the normally spliced *rx* RNA. A second primer pair in exon3 was used to quantify the total amount of *rx* RNA. The relative expression values in *rxin1ex2* MO injected larvae and *stctrl* MO were calculated using the software REST (Pfaffl et al., 2002). The expression level of the housekeeping gene *cdc5* was used for normalization (Dray et al., 2010).

Primers:

<i>rx_1st_exon2_qPCR_fwd</i>	CTCTCACCACAGAAATCACCTC	ex.1-ex.2
<i>rx_1st_exon2_qPCR_rev</i>	GACGTAGCATTCAAGGAGTCTG	ex.1-ex.2
<i>rx_3rd_exon2_qPCR_fwd</i>	CCCTCGTAGCACTAGTATTGTTTCACT	exon3
<i>rx_3rd_exon2_qPCR_rev</i>	AAATGTCTTCCCATGCTTTCCA	exon3
<i>cdc5-fwd</i>	TGCAGAGGGCTGAAGAATAATAAA	<i>cdc5</i>
<i>cdc5-rev</i>	TGCCCCAGAGTGGGATTATG	<i>cdc5</i>

Reaction setup:

cDNA	5 μ l
water	4 μ l
primer F 10 μ M	0.5 μ l
primer R 10 μ M	0.5 μ l
SYBR Green mix (Applied Biosystems)	10 μ l

Cycling program:

1x	95 °C	10 min
40x	95 °C	15 sec
	60 °C	1min

12.4. Identification of mutations in ZFNs injected larvae

12.4.1. Extraction of genomic DNA

Different genomic DNA extraction methods were used for genotyping in ZFNs experiments.

Extraction of genomic DNA from injected larvae

For genotyping ZFNs injected larvae after 1-2 days of development, the QIAamp DNA Mini kit was used (Qiagen). This kit allows the extraction of high-quality genomic DNA from small tissue samples.

- Collect the injected larvae (>24 hpf) in an Eppendorf tube, remove all the NSW.
- Add 180 μ l of buffer ATL, and 20 μ l of Proteinase K Solution.
- Vortex 15 sec.
- Incubate in a shaker ON at 56 °C.
- Add 200 μ l of buffer AL, vortex 15 sec.
- Add 200 μ l of EtOH. Vortex.
- Incubate 20 min at room temperature.
- Transfer the sample in the column, and centrifuge at 8000 rpm for 1 min. Discard the flowthrough.
- Add 500 μ l of AW1 wash buffer. Centrifuge at 8000 rpm for 1 min. Discard the flowthrough.
- Add 500 μ l of AW2 wash buffer. Centrifuge at 8000 rpm for 1 min. Discard the flowthrough.
- Centrifuge 3 min at full speed.
- Place the column in a fresh tube. Add 40 μ l of buffer AE. Centrifuge at full speed for 1 min.

Extraction of genomic DNA from F0 worms

For genotyping ZFNs founders, the bodies were collected immediately after fertilization and stored at -80°C .

Genomic DNA extraction was performed with the classical phenol-chloroform method described in Sambrook and Russell (2001).

Extraction of genomic DNA from F1 tail clipping and cirri

ZFNs F1 worms were genotyped from tissue fragments, coming from the tail or the cirri. These structures regenerate, so this methods allows to genotype each worm without sacrificing it.

Briefly, the worms were anesthetised in 50% MgCl₂/50% NSW. Then, the cirri or the tail were cutted with a blade under a dissecting scope. The worms were immediately transferred to a well of a 6 well plate. An unique identifier was assigned to each worm. The corresponding tissue fragment was transferred into an Eppendorf tube, and the genomic DNA was prepared with the KAPA Express Extract kit (Kapa Biosystems). This method has a slightly lower quality, compared to the column extraction, but is very fast and can be scaled up to many samples.

- Remove all the NSW. Add:

KAPA Express Extract 10x buffer	2 μ l
KAPA Express Mix	0.8 μ l
water	17.2 μ l

- Incubate 30 min at 75 °C, shaking at maximum speed (1200 rpm in an Eppendorf thermomixer).
- Inactivate the enzymes 10 min at 95 °C.
- Spin down at full speed for 5 min.
- Transfer the supernatant in a fresh tube. Use 2 μ l of this extract for PCR. Store everything else at –20 °C.

12.4.2. PCR, restriction analysis and sequencing

Several primer pairs were used for genotyping ZFNs worms. Optimization was required to identify the best primer pairs, since in some cases several primers were failing amplification, probably for the presence of SNPs. The distribution of SNPs in the *rx* genomic region was taken in account during oligo design.

The PCR assay used for the large screening of F1 worms was based on a first semimultiplex reaction (optimized by A. Lauri). The advantage of this approach is that the presence of two alternative forward primers allows, in the large majority of the cases, to amplify the *rx* locus. This PCR is followed by a nested PCR, to produce a 292bp amplicon. Finally, this amplicon is used for restriction analysis of the amplicon with the AgsI enzyme (see also par. 4.4.2).

Primers:

rx-genoty-F4 CCGTCTGAGCATCAATTACTGGACATT
 rx-genoty-F5 CCGTCTGAGCATCAATTACTGGACATT
 rx-genoty-R2 GTGCATCCCTCTGCCCCTTTG
 rx-genoty-F3 AAGCGTTCACAACATCATCATTAATAA
 rx-genoty-R0 ACCTTGATAGAGGTGATTTCTGTGGTG

PCR reaction (semimultiplex):

template DNA	1-4 μ l
rx-genoty-F4 5 μ M	1 μ l
rx-genoty-F5 5 μ M	1 μ l
rx-genoty-R2 5 μ M	1 μ l
dNTP mix 25mM	0.4 μ l
DMSO 2.5%	0.25 μ l
Advantage 2 buffer 10x (Clontech)	1 μ l
Advantage 2 Polymerase (Clontech)	0.22 μ l
water	up to 10 μ l

Cycling program (semimultiplex):

1x	94 °C	1 min
	94 °C	30 sec
5x	60 °C	40 sec
	72 °C	2 min
	94 °C	30 sec
5x	58 °C	40 sec
	72 °C	2 min
	94 °C	30 sec
25x	56 °C	40 sec
	72 °C	2 min
1x	72 °C	10 min

The nested PCR was done with a similar reaction setup (1.5 μl of each primer) and with the same program. 1.5 μl of PCR product was digested with 0.4 μl of AgsI (SibEnzyme), 0.01 μl of BSA, 1 μl of AgsI 10x buffer in a total volume of 10 μl . The digestion was incubated ON at 37°C; the enzyme was inactivated at 95°C for 15 min. Digestion products were run on a 3% Metaphor Agarose gel (Lonza), prepared according to manufacturer's instructions. AgsI resistant bands (putative ZFNs mutant alleles) were cloned in pCRII-TOPO and sequenced, to identify the mutations.

12.5. Time lapse movies of developing *Platynereis* embryos

12.5.1. Mounting and imaging

For time lapse imaging of developing *Platynereis* embryos, zygotes were injected with H2A-RFP and mYFP mRNAs at final concentrations of 250 ng/ μl and 300 ng/ μl , respectively. TRITC-dextran was not included in the injection mix. Larvae were raised to the desired stage at 18°C. For time lapse imaging, larvae with a normal morphology and a strong fluorescence were selected, and mounted between a slide (with two layers of tape) and a coverslip in 0.8% LMP-Agarose (Gibco)/NSW. After the polymerization of the agarose, NSW was added on the side to fill up the entire space between the slide and the coverslip. The slide was finally sealed with Mineral Oil (Sigma), to prevent the evaporation of water.

For imaging, a Leica SPE confocal microscope was used, with a 40x oil-immersion objective. The 488 nm and 532 nm lasers were used, respectively, to excite the mYFP and H2A-RFP. Images were acquired with a 512 x 512 pixel resolution; stacks had a Z axis resolution of 1.5 μm between consecutive focal planes. Stacks were acquired every 12 min 30 sec, or every 15 min.

12.5.2. Analysis of the movies

Images were analysed with Fiji (image processing package based on ImageJ). Brightness and contrast were adjusted equally on all images. Dividing cells were tracked manually on the original 4D dataset using the MTrackJ plugin (Meijering et al., 2012). Lineages in fig. 3.7 were drawn manually on Adobe Illustrator following the cell divisions in the movies.

13.1. Imaging of calcium in *Platynereis* larvae

13.1.1. Preparation of the larvae, mounting and imaging

For calcium imaging, *Platynereis* zygotes were injected with GCaMP3 and H2A-RFP mRNAs at the final concentrations of 200 ng/ μ l and 300 ng/ μ l, respectively. TRITC-dextran was not included in the injection mix. Larvae were raised to the desired stage at 18 °C. For imaging, larvae with a normal morphology and a strong H2A-RFP fluorescence were selected, and mounted between a slide (with two layers of tape) and a coverslip in 0.8% LMP-Agarose (Gibco)/NSW. After the polymerization of the agarose, NSW was added on the side to fill up the entire space between the slide and the coverslip. The slide was finally sealed with Mineral Oil (Sigma), to prevent the evaporation of water.

For imaging, a Zeiss LSM 780 microscope was used, equipped with a two-photon Chameleon laser (Coherent) and controlled by the Zeiss ZEN 2011 software. Larvae were imaged under a 40x oil-immersion objective. The H2A-RFP signal was used to identify the approximate location of the clock cells in the brain.

The two-photon laser was tuned to 910 nm to excite GCaMP3 and H2A-RFP at the same time; the emission of the two fluorophores was separated using appropriate filter sets and separate photomultiplier tubes. Images (single focal planes) were acquired with a 512 x 512 pixel resolution; consecutive frames were acquired every 200-800 ms. Light stimuli were delivered using the “bleaching” function, combining the 488nm+561nm lasers or the 458nm+514nm+594nm lasers.

13.1.2. Analysis of the GCaMP3 movies

Images were analysed in Fiji, directly from raw data, without any adjustment. The images in fig. 6.5A-B were obtained with the “Fire” LUT in Fiji.

The sum of the pixel intensities over a selected ROI (i.e. cell) was obtained in Fiji. For each cell, GCaMP3 responses are expressed as normalized increments calculated with the formula $\Delta F/F_0 = (F - F_0)/F_0$, where F_0 is the average fluorescence of the same cell in the 10 sec before stimulation. Data were plotted in R.

13.2. Measurements of ciliary beating frequency (CBF)

Platynereis larvae with normal development were selected for the measurement of CBF. Larvae were raised at 18 °C in 16L:8D cycles, using two incubators with shifted light-dark cycles to obtain larvae at the desired zeitgeber time (ZT). CBF was always measured between 48-50hpf, in a room with a temperature of 18 – 20 °C. Larvae were adapted to the temperature of the room for 30 min before the experiment.

Larvae were mounted in 30 μ l of NSW, between a slide and a coverslip, separated by three layers of tape. The NSW was surrounded by Mineral Oil (Sigma) to avoid the evaporation of water. For the recordings in the darkness, mounting was done quickly under a dim red light. The position of the larvae was adjusted to a perfect apical view, and the two prototroch cells at the ventral edge of the animal were always chosen for imaging.

A Zeiss Axiophot with a 20x objective and connected to a DMK 21BF04 camera (The Imaging Source) was used for imaging. In darkness conditions, a 750 nm long-pass filter was placed between the light source and the animal. Ciliary beating was imaged for 10 sec with a frame rate of 60 frames/sec.

For the CNG channel inhibition experiments, *L-cis*-diltiazem (Enzo Life Sciences, BML-CA207) was used at a final concentration of 100 μ M. 100mM *L-cis*-diltiazem stocks were prepared in NSW and stored in aliquots at –20 °C. Larvae were treated with *L-cis*-diltiazem for one hour before the assay.

For melatonin treatments, melatonin (Sigma, M5250) was used with a final concentration of 1 mM (development was not affected after incubations in 1 mM melatonin for more than one day). Melatonin powder (stored at –20 °C) was freshly dissolved in NSW before the assay. Larvae were incubated in melatonin for 1 hour before the assay.

CBF was measured on good quality movies, which were inspected manually. Data were analysed with R. All the experiments were repeated at least twice with animals from different batches; for each treatment, a representative experiment is shown in the text.

13.3. Phototaxis

Phototaxis assays were performed with the setup described in Jékely et al. (2008). Larvae were incubated in 500 μM melatonin for 30 min before the assay.

A Leica MZ16 microscope with a Sanyo VCB-3524P camera was used to image light responses. The position of the larvae before and after directional illumination is plotted as bins along the X axis (the direction of illumination).

APPENDIX

A

THE APICAL ORGAN CELL TYPES

In *Platynereis*, the apical organ cells are the first differentiated cells of the larval episphere (fig. A.1A). The apical organ comprises different kinds of sensory cells, which can be recognized from their morphological specializations. The *ampullary cells* (fig. A.1B) have a typical “ampullary” cell morphology, consisting of basket-shaped intracellular tubulin support structures. These cells form the apical tuft. Dorsal to the ampullary cells, the half-moon shaped *crescent cells* develop later (fig. A.1C). More ventrally, it is possible to recognize the flask-shaped neurosecretory peptidergic cells (fig. A.1D, Tessmar-Raible et al. 2007) and a deep serotonergic interneuron (fig. A.1C). Ventral to these cells, two cells bearing short modified sensory cilia, resembling mechanosensory receptors, are present (fig. A.1E).

The investigation of molecular fingerprints using PrImR (Tomer et al., 2010) revealed a clear distinction between these cell types. This distinction is suggested by the mutually exclusive expression of some markers, like *otx* and *otp* (fig. A.1F), or miR-7 and the “cilia miRNAs” (Christodoulou et al., 2010), like miR-29 (fig. A.1G).

Hierarchical clustering of molecular fingerprints confirmed the existence of two distinct groups of apical organ cells (fig. A.1I).

The first group includes the flask-shaped neuropeptidergic cells and the serotonergic cell, which share the expression of *otp*, miR-7 and the neuropeptide-processing enzymes *phc2* and *carboxypeptidase-E (cpe)*. These cells are probably chemosensory, as suggested by their morphology. The presence of unique markers in this group of cells (fig. A.1H) suggests the existence of further specializations.

The second group included the multiciliated cells and the putative mechanosensory cells. These cells share the expression of regulators of ciliogenesis, like *foxJ*, and of structural cilia genes, including *tektin-2* and *tubby*. Moreover, these cells express a *trp* channel, indicating that they can sense physical environmental stimuli.

The molecular analysis of the apical organ cell types suggests that the apical organ

cells are specialized for different sensory modalities. Cells with similar morphologies exist in the apical organs of several marine larvae. It will be of great interest to find out if the same molecular dichotomy exists in other species, or in other words if the distinction between chemosensory and putative mechanosensory cells is ancient.

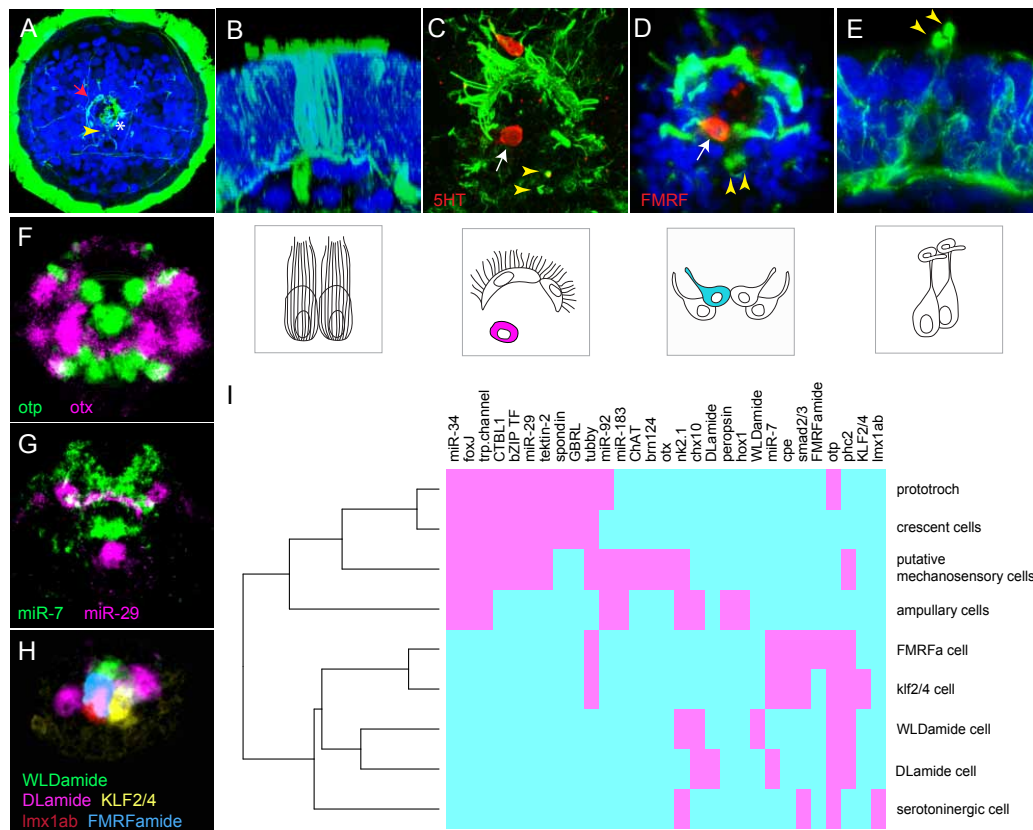


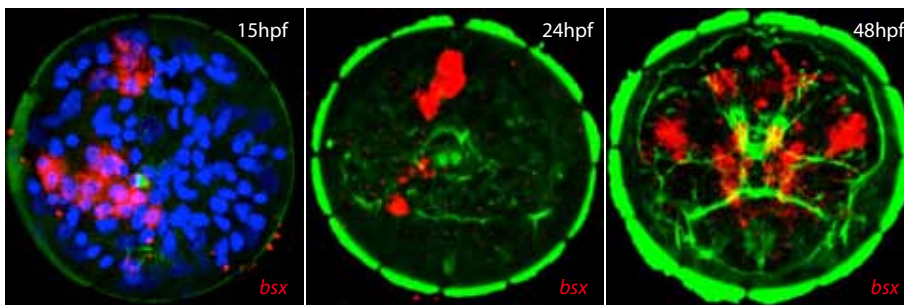
Figure A.1: **The apical organ cell types.** Figure modified from Marlow et al. (2012). A. Episphere at 30hpf stained with anti-acetylated tubulin. The crescent cells (arrow) are dorsal to the ampullary/tuft cells (asterisk). Ventrally, the two short curly cilia of the putative mechanosensory cells are visible (arrowhead). B. Ampullary cells at 30hpf, lateral view. C. Serotonergic cell of the apical organ (arrow, anti-5HT antibody staining) at 48hpf. The putative mechanosensory cells are also visible (arrowheads). D. One of the peptidergic flask-shaped cells, stained with FMRFamide antibody (arrow), 48hpf. E. Lateral view of the putative mechanosensory cells, 48hpf (arrowheads: stiff curly tips of the sensory cilium). F. *otp* (green) and *otx* (magenta) expression patterns at 48hpf (23um Z projection of PrImR averages). G. *miR-7* (green) and *miR-29* (magenta) expression patterns at 48hpf (23um Z projection of PrImR averages). H. Distinct cell types in the *otp*+ domain. The image shows non-overlapping expression of markers of each cell as deduced from PrImR, 11um Z projection of average expression patterns. I. Hierarchical clustering of the molecular fingerprint of individual cell types identified within the apical organ. The molecular fingerprint of the prototroch is included for comparison. Expression in magenta.

B

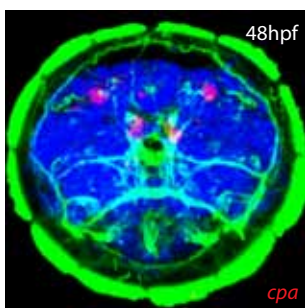
ADDITIONAL GENE EXPRESSION PATTERNS

This appendix includes the gene expression patterns mentioned but not shown in the main text. All the images are apical views, where gene expression is red, tubulin is green and DAPI is blue.

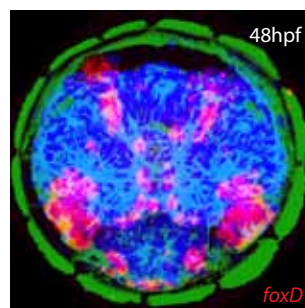
bsx



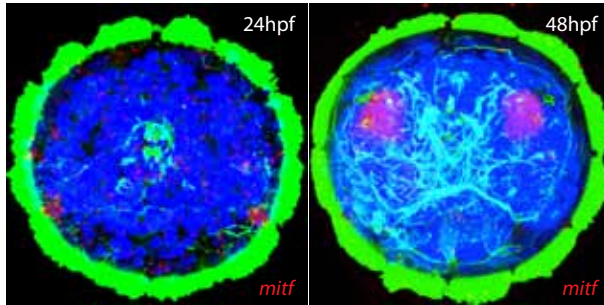
cpa (carboxypeptidase A)



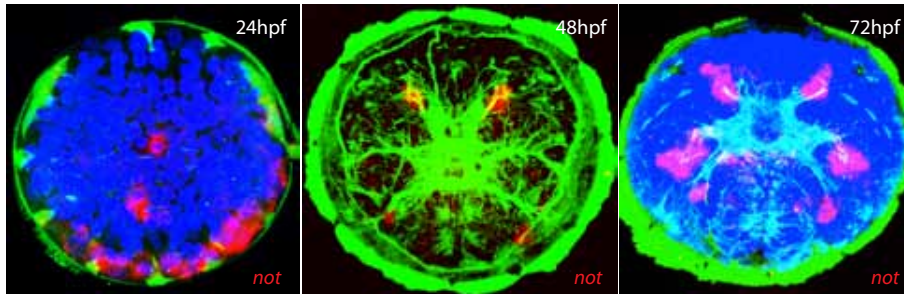
foxD



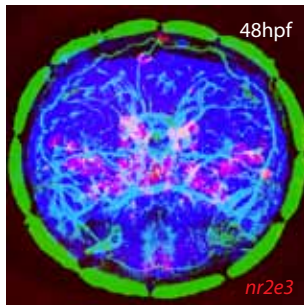
mitf



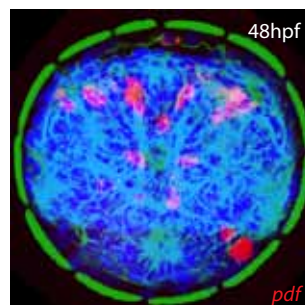
not



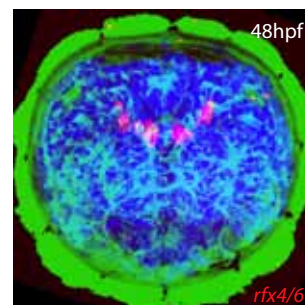
nr2e3



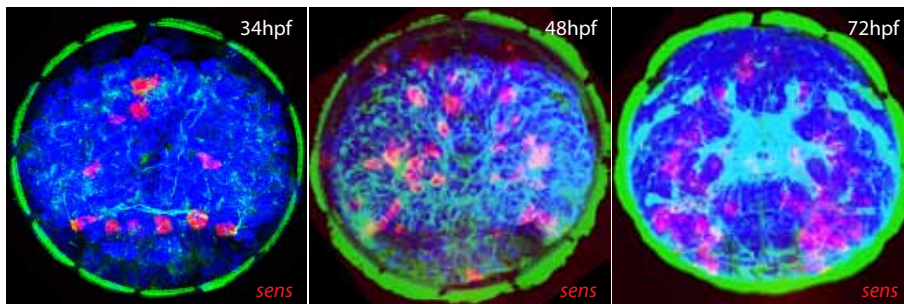
pdf



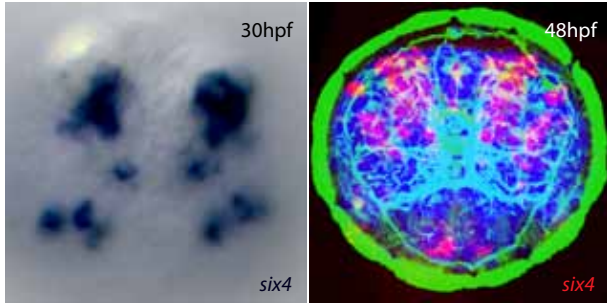
rfx4/6



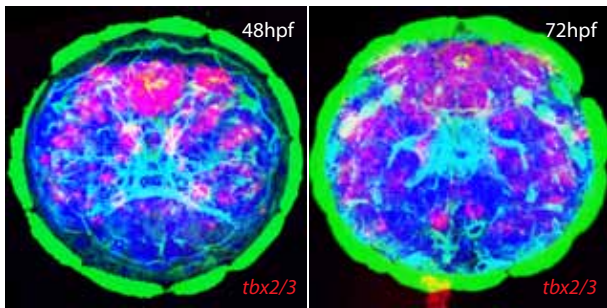
sens



six4



tbx2/3



C

PHYLOGENETIC TREES

Cryptochrome phylogenetic tree

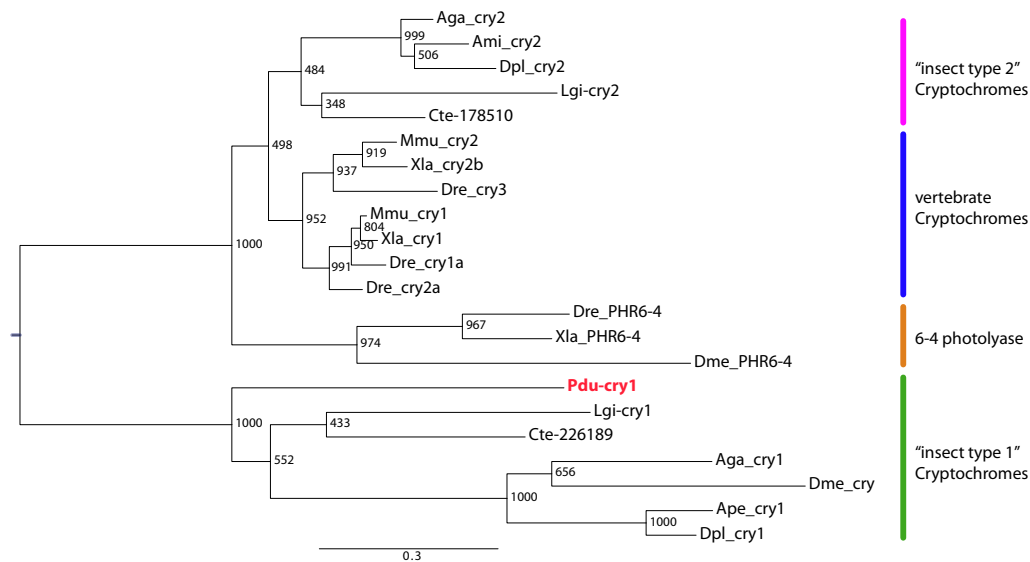


Figure C.1: **Cryptochrome phylogenetic tree.** phylogenetic tree of members of the photolyase/cryptochrome families has been obtained from alignment of the following sequences (GeneBank accession numbers, unless specified otherwise): *Anopheles gambiae* (*Aga*) CRY1 (DQ219482), CRY2 (DQ219483); *Apis mellifera* (*Ame*) CRY2 (XP_393680); *Antheraea pernyi* (*Ape*) CRY1 (AAK11644); *Capitella teleta* (*Cte*) CRY1 (JGI:226189), CRY2 (JGI:178510); *Danaus plexippus* (*Dpl*) CRY1 (AY860425), CRY2 (DQ184682); *Danio rerio* (*Dre*) CRY1a (BAA96846), CRY2a (BAA96848), CRY3 (BAA96850), PHR6-4 (NP_571863); *Drosophila melanogaster* (*Dme*) CRY (AAC83828), PHR6-4 (BAA12067); *Lottia gigantea* (*Lgi*) CRY1 (JGI: 143285), CRY2 (JGI:131547); *Mus musculus* (*Mmu*) CRY1 (NP_031797), CRY2 (AAD46561); *Xenopus laevis* (*Xla*) CRY1 (AAK94665), CRY2a (AAK94666), CRY2b (AAK94667), PHR6-4 (BA97126).

Aanat phylogenetic tree

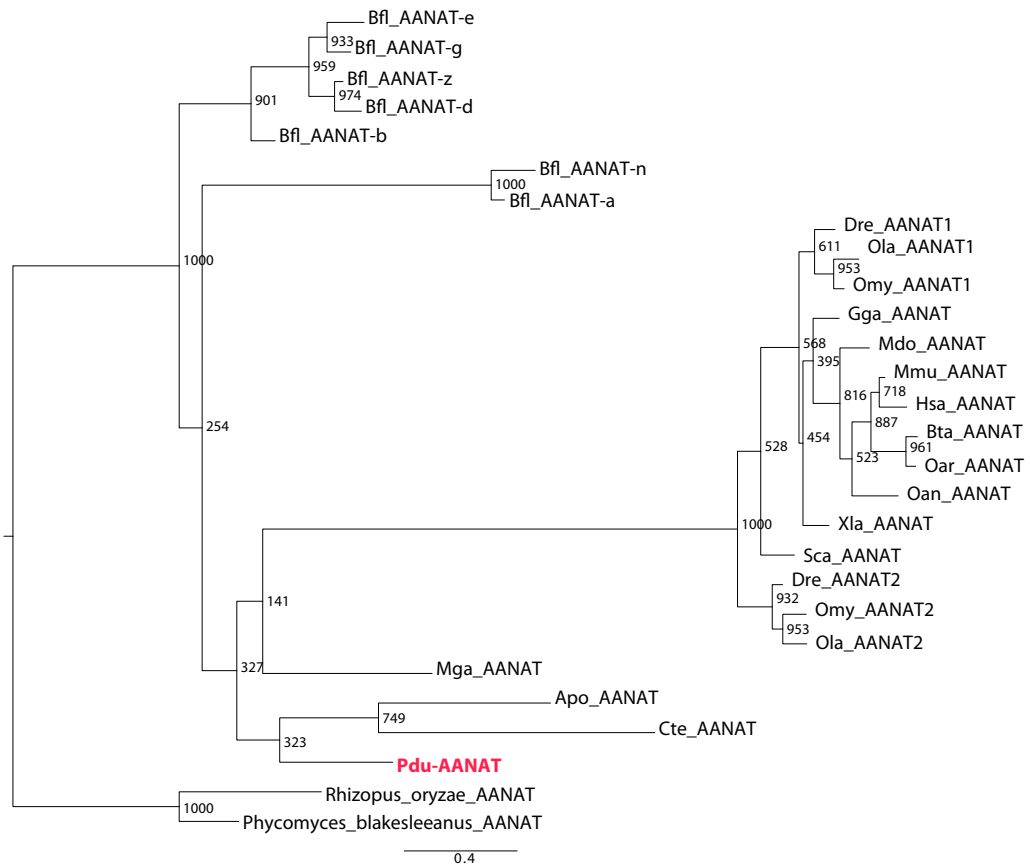


Figure C.2: **Aanat phylogenetic tree.** ML-phylogenetic tree showing the position of *Platynereis* Aanat in comparison with other Aanat genes from other animals. The basal fungi *Rhizopus oryzae* and *Phycomyces blakesleeanus* Aanat sequences were used as outgroups. Sequences from Pavlicek et al. (2010). Apo: *Alvinella pompejana*, Bfl: *Branchiostoma floridae*, Bta: *Bos taurus*, Cte: *Capitella teleta*, Dre: *Danio rerio*, Gga: *Gallus gallus*, Hsa: *Homo sapiens*, Mdo: *Monodelphis domestica*, Mga: *Mytilus galloprovincialis*, Mmu: *Mus musculus*, Oan: *Ornithorhynchus anatinus*, Oar: *Ovis aries*, Ola: *Oryzias latipes*, Omy: *Oncorhynchus mykiss*, Sca: *Scyliorhinus canicula*, Xla: *Xenopus laevis*.

Hiomt phylogenetic tree

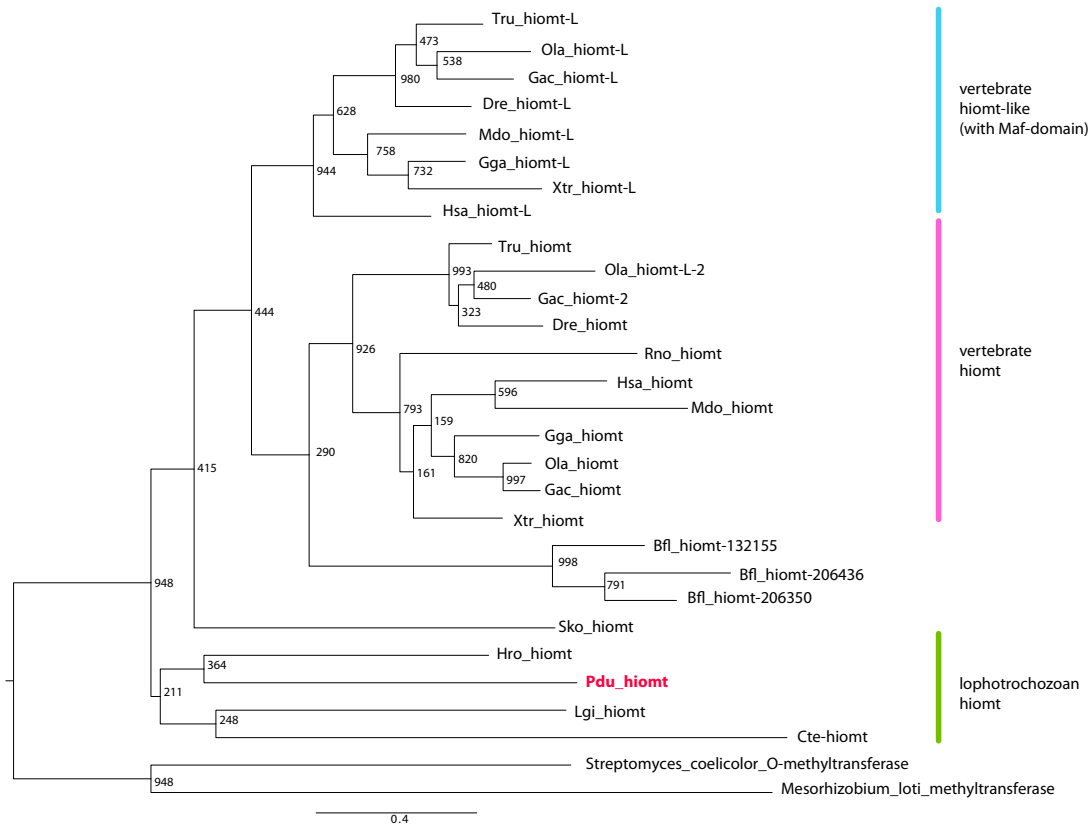
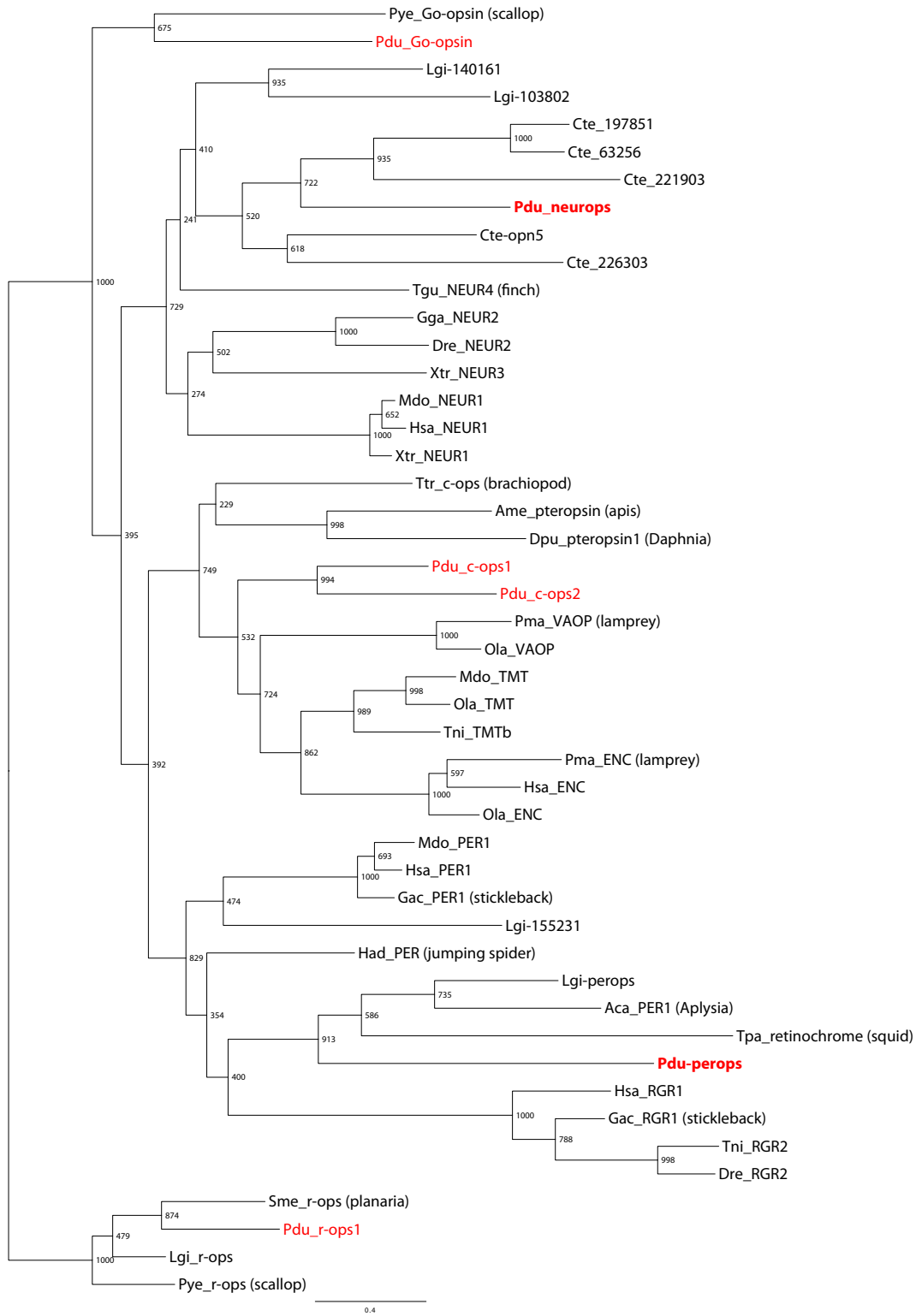


Figure C.3: **Hiomt phylogenetic tree.** ML-phylogenetic tree showing the position of *Platynereis* Hiomt in comparison with other Hiomt genes in Bilateria. The sequences of O-methyltransferases from the bacteria *Streptomyces coelicolor* and *Mesorhizobium loti* were used as outgroups. The tree was assembled from the following sequences (Ensembl IDs, if not specified otherwise): *Bfl* (*Branchiostoma floridae*) hiomt (JGI:132155, 206350, 206436); *Cte* (*Capitella teleta*) hiomt (JGI: 173689); *Dre* (*Danio rerio*) hiomt-L (ENSDARP00000007743), hiomt (ENSDARP000000081319); *Gac* (*Gasterosteus aculeatus*) hiomt-L (ENSGACP00000002589), hiomt-2 (ENSGACP00000006056), hiomt (ENSGACP00000008761); *Gga* (*Galus gallus*) hiomt-L (ENSGALP00000026877), hiomt (ENSGALP00000026872); *Hro* (*Helobdella robusta*) hiomt (JGI: 192339); *Hsa* (*Homo sapiens*) hiomt-L (ENSP00000344560), hiomt (ENSP00000370639); *Lgi* (*Lottia gigantea*) hiomt (JGI: 173251); *Mdo* (*Monodelphis domestica*) hiomt-L (ENSMODP00000000099), hiomt (ENSMODP00000037748); *Ola* (*Oryzias latipes*) hiomt-L (ENSORLPP00000013668) hiomt-L-2 (ENSORLPP00000022484), hiomt (ENSORLPP00000019958); *Rno* (*Rattus norvegicus*) hiomt (ENSRNOP00000001791); *Sko* (*Saccoglossus kowalevskii*) hiomt (GenBank: XP_002736611.1) *Tru* (*Takifugu rubripes*) hiomt-L (JGI: 616542), hiomt (JGI: 585217); *Xtr* (*Xenopus tropicalis*) hiomt-L (JGI: 451002), hiomt (JGI: 147922).

Opsin phylogenetic tree

Figure C.4 (on the next page): **Opsin phylogenetic tree.** ML-phylogenetic tree showing the position of *Platynereis* Opsins. The tree was assembled from the following sequences: *Aca* (*Aplysia californica*) peropsin1 (GenBank EB338056); *Ame* (*Apis mellifera*) pteropsin (NCBI NM_001039968); *Cte* (*Capitella teleta*) opsins (JGI 197851, 221903, 63256, 219000048, 226303); *Dpu* (*Daphnia pulex*) pteropsin 1 (NCBI EFX86931); *Dre* (*Danio rerio*) neuropsin 2 (NCBI NP_001038457), RGR2 (NCBI NM_001024436); *Gac* (*Gasterosteus aculeatus*) peropsin1 (GenBank: DW609002), RGR1 (GenBank: CD495430); *Gga* (*Gallus gallus*) neuropsin 2 (GenBank AB368181); *Hda* (*Hasarius adansoni*) peropsin (GenBank AB525082); *Hsa* (*Homo sapiens*) neuropsin 1 (NCBI NM_181744), encephalopsin (NCBI NM_014322), peropsin1 (NCBI NM_006583), RGR1 (NCBI NM_001012720); *Lgi* (*Lottia gigantea*) opsins (JGI 140161, 103802, 155231), peropsin (JGI 154374) and r-opsin (GenBank: FC774055.1); *Mdo* (*Monodelphis domestica*) neuropsin 1 (NCBI XP_001369202), TMT-opsin (NCBI XM_001372110), peropsin1 (NCBI XP_003341466); *Ola* (*Oryzias latipes*) VA-opsin (GenBank DK020629), TMT-opsin (GenBank DK170580); *Pma* (*Petromyzon marinus*) VA-opsin (GenBank U90667); *Pye* (*Patinopecten yessoensis*) G_o-opsin (GenBank AB006455) and r-opsin (GenBank AB006454); *Sme* (*Schmidtea mediterranea*) r-opsin (GenBank AF112361); *Tgu* (*Takifugu rubripes*) neuropsin4 (NCBI XP_002193730.1); *Tni* (*Tetraodon nigroviridis*) TMT-opsin-b (NCBI CAG05457), RGR2 (NCBI CR692169); *Tpa* (*Todarodes pacificus*) retinochrome (GenBank: X57143); *Ttr* (*Terebratalia transversa*) c-opsin (GenBank HQ679623); *Xtr* (*Xenopus tropicalis*) neuropsin 3 (NCBI XP_002933633), neuropsin 1 (NCBI XP_002936036).



D

VERTEBRATE MOLECULAR FINGERPRINT TABLE

The following table summarizes the expression of transcription factors in selected tissues and cells types of vertebrate model organisms.

References

1 Colombo et al Gene Expr Patterns. 2006	23 Moreno et al Neuroscience 2008
2 Cremona et al Gene Expr Patterns 2004	24 Shi et al Biochem Biophys Res Comm 2009
3 D'Autilia et al PNAS 2011	25 http://publications.ki.se/jspui/handle/10616/40580
4 A Kawahara et al 2002	26 Retaux et al J Neurosci 1999
5 Aamar Dawid Int J Dev Biol 2008	27 Swanhart et al Int J Dev Biol 2010
6 Taira et al Dev Biol 2003	28 Kobayashi et al Mech Dev 2000
7 Masai et al Neuron 1997	29 Klesert et al Nat Genet 2000
8 Bailey et al 2009 9 Dufourcq et al.,2004	30 Ozaki et al Mol Cell Biol 2001
10 Snelson et al Dev Dyn 2008	31 Shimogori et al Nat Neurosci 2010
11 Takabatake et al Mech Dev 2000	32 Fedtsova et al Mech Dev 2001
12 Swanhart et al Int J Dev Biol 2010	33 Wang et al J Neurosci 2010
13 Moreno et al J Comp Neurol 2004	34 Chen et al Mech Dev 1999
14 Bachy et al J Neurosci 2001	35 Münchberg et al Mech Dev 1999
15 Ghanbari et al Mech Dev 2001	36 Roussigné et al Gene Expr Patt 2006
16 Von Dassow et al Genes Dev 1993	37 David et al Mech Dev 2001
17 Mueller et al Brain Res Bull 2002	38 Kriebel et al Dev Dyn 2007
18 Wullimann et al J Comp Neurol 2005	39 Sahly et al Dev Genes Evol 1999
19 Lin et al Dev Biol 2004	40 Xu et al Dev 1997
20 Muñoz et al J Neurochem 2007	41 Toyama et al Dev Dyn 2009
21 Concha et al Neuron 2000	42 Alvarez-Bolado et al J Comp Neurol 1995
22 Quina et al J Neurosci 2009	43 Schonemann et al Genes Dev 1995
	44 Hauptmann et al Dev Dyn 2000

gene ID	Pdu.ortholog	teleost fish			amphibians			mammals			notes	main references
		pinealpp	ha	sc/anterior r/hyp.	pineal	ha	sc/anterior or/hyp.	pineal	ha	scn		
brn1/2/4	brn124	n	y?	n	n.a.	n?	n.a.	y	n	n	43: brn4 is the only one that might expand to the SCN. 44: fish POUIII genes in rostral and ventral diencephalon	42, 43, 44, 45
brn3	brn3	n	y	n	n	y	n	y	n	n		32, 83
bsx	bsx	n.a.	n.a.	n	n	n	n	n	n	n		2,3
crx/ctx6	ctx	y	n	n	n	n	n	n	n	n		8, 31
emx	emx	y	n	n?	n	n?	n	y	n	n	only transient in the perspective pineal; emx2 KO have defects in the pineal; 49: wide expression in diencephalon; dogfish pineal expression	4, 31, 41, 46, 47, 49, zfin, allen
erf1, etv1, erm e81	erm e81	n	y	n	n	y?	n	n	y	n	the xenopus paper shows two spots called "forebrain" in chick eye genes are also restricted to placodes - allen and kriebel show something in the ventricular zone of hypoth	22, 33, 34, 35, 36, allen
eya genes	eya	n	n	n	n	n	n	y	n	n		8, 37, 38, 39, 40, allen
foxD3	foxD	y	n	n.a.	n.a.	n	n	y	n	n		8, 31, allen, zfin
gfi-1	senis	y	n	n	n.a.	n.a.	n	n?	n?	n	in fish, only parapineal ganglion cells. In mouse retinal ganglion cells	9, 72
islet genes	islet	y	n	n.a.	y	n	n	y	n	n		8, 21, 24, 31, 50
lhx1	lhx1/5	n	n	y	n	n	n	n	y	n	lost in mamm. Pineal - because it is not photosensitive?; fish habenula not annotated but seems + in 52; moreover, 53 reports strong lhx5 expr in medaka hab	12, 13, 14, 25, 27
lhx2	lhx2/9	y	y	n.a.	y	y	y	y	y	y	xenopus papers wo lhx3 - in retina, INL cells; 54: fish pineal, subset of prog neurons, also in chick pineal	13, 14, 26
lhx3	lhx3/7	y	n	n/n.a.	n/n.a.	n/n.a.	y	n	n	n		6, 13, 14, 55, 56
neuroD	neuroD	y	y	n	y	y	y	y	y	n		zfin, 17, 18, 19, 20
not	not	y	n	n	y	n	n	n	n	n	chick Gho1 is also in pineal, only mouse has lost it!	16, 57
nr2e1	til	n	y?	n	n	n?	n	y?	y	n	59: dorsal thalamus...	58, 59, 90
pax4, pax6	pax6	y	y	n	n	y?	n	y	n	n	pax6 in developing pineal (mouse, fish) and in diff prog neurons (fish); absence in frog is an exception; pax4 in mammalian photoreceptor; in few neurons at the base of fish habenula (62); in developing mouse epithalamus(65); pax4 in adult mouse pineal; pax6 also in chick and shark habenula	7, 8, 61, 62, 63, 64, 65, 66
rx4	rx4/6	n.a.	n.a.	y	n.a.	n.a.	n	n	y	n		88
rx	rx	n?	n	y*	n	y*	n	y	n	y*	developmental only in SCN, it stays in differentiated pineal	66, 90, 91, 92
six1, six2	six1/2	y?	n	n	n	n	n	y	n	n		8, 15
six4	six4	n	n	n	n	n	n	n	n	n		15, 26, 29, 30
tbx2, tbx3	tbx2/3	y	n	y	n	n.a.	n	n	n	y	tbx3 in xenopus and chick pineal; paralog switch in teleosts?; tbx2 and tbx3 in hypothalamic axis; 68 refers to tbx2-3 expr in medaka hypoth	10, 11, 31, 41, 67

- 45 Baltzinger et al Mech Dev 1996
46 Shah et al Int J Dev Biol 2006
47 Simeone et al EMBO J 1992
48 Pannese et al Mech Dev 1998
49 Kawahara et al Gene Exp Patt 2002
50 Dykens et al J Neurosci 2011
51 Miyasaka et al J Neurosci 2009
52 Ando et al Dev Biol 2005
53 Alunni et al Mech Dev 2004
54 Glasgow et al Dev Biol 1997
55 Grigoriou et al Dev 1998
56 Seidah et al DNA Cell Biol 1994
57 Plouhinec et al Gene Expr Patt 2004
58 Monaghan et al Dev 1995
59 Hollemann et al Dev 1998
60 Kitambi et al Gene Expr Patt 2007
61 Hirsch et al J Neurobiol 1997
62 Wullimann et al Dev Brain Res 2001
63 Moreno et al Brain Res 2008
64 Morona et al J Comp Neurol 2011
65 Grindley et al Mech Dev 1997
66 Manousaki et al Evol Dev 2001
67 Chapman et al Dev Dyn 1996
68 Loosli et al Dev 2001
69 Take-uchi et al Dev 2003
70 Liu et al Mech Dev 2001
71 Hallonet et al Dev 1998
72 Wallis et al Dev 2003
73 Kurrash et al J Neurosci 2007
74 Puelles et al Trends Neurosci 2003
75 Nakagawa et al J neurosci 2001
76 González et al Gene Expr Patt 2002
77 Hatini et al J Neurobiol 1994
78 Münchberg et al Mech Dev 1999
79 Laudet et al Oncogene 1999
80 McCabe et al Dev Dyn 2006
81 Cherry et al J Neurosci 2011
82 Cherry et al PNAS 2009
83 Kim et al J Comp Neurol 2008
84 Blackshaw et al PLoS Genet 2001
85 Booij et al PLoS One 2010
86 Strunnikova et al Hum Mol Gen 2010
87 Leung et al IOVS 2007
88 Araki et al J. Biol. Chem. 2004
89 Martinez de Luna et al 2007
90 Casarosa et al Mech. Dev. 1997
91 Mathers et al Nature 1997
92 Deschet et al Mech. Dev. 1999
93 Aizawa et al Curr Biol 2005

REFERENCES

- C. Ackermann, A. Dorrestijn, and A. Fischer. Clonal domains in postlarval *Platynereis dumerilii* (Annelida: Polychaeta). *Journal of morphology*, 266(3):258–80, Dec. 2005.
- R. Adler and P. a. Raymond. Have we achieved a unified model of photoreceptor cell fate specification in vertebrates? *Brain research*, 1192:134–50, Feb. 2008.
- R. Albalat. Evolution of the genetic machinery of the visual cycle: a novelty of the vertebrate eye? *Molecular biology and evolution*, Dec. 2011.
- R. Allada and B. Y. Chung. Circadian organization of behavior and physiology in *Drosophila*. *Annual review of physiology*, 72:605–24, Mar. 2010.
- R. Allada and J. M. Siegel. Unearthing the phylogenetic roots of sleep. *Current biology*, 18(15):R670–R679, Aug. 2008.
- A. Altenburger, P. Martinez, and A. Wanninger. Homeobox gene expression in Brachiopoda: The role of Not and Cdx in bodyplan patterning, neurogenesis, and germ layer specification. *Gene Expression Patterns*, 11(7):427–36, Oct. 2011.
- K. Alvarez-Delfin, A. C. Morris, C. D. Snelson, J. T. Gamse, T. Gupta, F. L. Marlow, M. C. Mullins, H. a. Burgess, M. Granato, and J. M. Fadool. Tbx2b is required for ultraviolet photoreceptor cell specification during zebrafish retinal development. *Proceedings of the National Academy of Sciences of the United States of America*, 106:2023–8, Feb. 2009.
- M. Anctil. Chemical transmission in the sea anemone *Nematostella vectensis*: A genomic perspective. *Comparative biochemistry and physiology. Part D, Genomics & proteomics*, 4(4):268–289, Dec. 2009.
- M. Anctil, A. K. Pani, and M. a. Ali. Modulation of rhythmic contractions by melatonin via cyclic GMP in the coelenterate *Renilla koellikeri*. *Journal of Comparative Physiology B*, 161(6):569–575, Dec. 1991.
- M. Andreazzoli, G. Gestri, D. Angeloni, E. Menna, and G. Barsacchi. Role of Xrx1 in *Xenopus* eye and anterior brain development. *Development*, 126:2451–60, June 1999.
- M. Andreazzoli, G. Gestri, F. Cremisi, S. Casarosa, I. B. Dawid, and G. Barsacchi. Xrx1 controls proliferation and neurogenesis in *Xenopus* anterior neural plate. *Development*, 130(21):5143–54, Nov. 2003.

- L. M. Angerer and R. C. Angerer. Disruption of gene function using antisense morpholinos. *Methods in cell biology*, 74:699–711, Jan. 2004.
- J. D. Angstadt, J. L. Grassmann, K. M. Theriault, and S. M. Levasseur. Mechanisms of postinhibitory rebound and its modulation by serotonin in excitatory swim motor neurons of the medicinal leech. *Journal of comparative physiology. A, Neuroethology, sensory, neural, and behavioral physiology*, 191(8):715–32, Aug. 2005.
- L. Appelbaum, G. X. Wang, G. S. Maro, R. Mori, A. Tovin, W. Marin, T. Yokogawa, K. Kawakami, S. J. Smith, Y. Gothilf, E. Mignot, and P. Mourrain. Sleep-wake regulation and hypocretin-melatonin interaction in zebrafish. *Proceedings of the National Academy of Sciences of the United States of America*, 106(51):21942–7, Dec. 2009.
- D. Arendt. Evolution of eyes and photoreceptor cell types. *The International journal of developmental biology*, 47(7-8):563–571, Jan. 2003.
- D. Arendt. Genes and homology in nervous system evolution: Comparing gene functions, expression patterns, and cell type molecular fingerprints. *Theory in Biosciences*, 124(2):185–197, 2005.
- D. Arendt. The evolution of cell types in animals: emerging principles from molecular studies. *Nature Reviews Genetics*, 9(11):868–82, Nov. 2008.
- D. Arendt and K. Nübler-Jung. Inversion of dorsoventral axis? *Nature*, 371:26, 1994.
- D. Arendt, K. Tessmar, M.-I. M. de Campos-Baptista, A. Dorresteyn, and J. Wittbrodt. Development of pigment-cup eyes in the polychaete *Platynereis dumerilii* and evolutionary conservation of larval eyes in Bilateria. *Development*, 129:1143–54, Mar. 2002.
- D. Arendt, K. Tessmar-Raible, H. Snyman, A. W. Dorresteyn, and J. Wittbrodt. Ciliary photoreceptors with a vertebrate-type opsin in an invertebrate brain. *Science*, 306(5697):869–71, Oct. 2004.
- D. Arendt, A. S. Denes, G. Jékely, and K. Tessmar-Raible. The evolution of nervous system centralization. *Philosophical transactions of the Royal Society of London. Series B, Biological sciences*, 363(1496):1523–8, Apr. 2008.
- D. Arendt, H. Hausen, and G. Purschke. The 'division of labour' model of eye evolution. *Philosophical transactions of the Royal Society of London. Series B, Biological sciences*, 364:2809–17, Oct. 2009.
- C. H. J. Asbreuk, H. S. a. van Schaick, J. J. Cox, M. P. Smidt, and J. P. H. Burbach. Survey for paired-like homeodomain gene expression in the hypothalamus: restricted expression patterns of Rx, Alx4 and gooseoid. *Neuroscience*, 114(4):883–9, Jan. 2002.
- E. C. Azmitia. Serotonin and brain: evolution, neuroplasticity, and homeostasis. *International review of neurobiology*, 77(06):31–56, Jan. 2007.
- M. J. Bailey, S. L. Coon, D. a. Carter, A. Humphries, J.-S. Kim, Q. Shi, P. Gaildrat, F. Morin, S. Ganguly, J. B. Hogenesch, J. L. Weller, M. F. Rath, M. Møller, R. Baler, D. Sugden, Z. G. Rangel, P. J. Munson, and D. C. Klein. Night/day changes in pineal expression of >600 genes: central role of adrenergic/cAMP signaling. *The Journal of biological chemistry*, 284(12):7606–22, Mar. 2009.

- D. G. Baskin. Neurosecretion and the Endocrinology of Nereid Polychaetes. *Integrative and Comparative Biology*, 16(2):107–124, 1976.
- V. Bégay, P. Bois, J. P. Collin, J. Lenfant, and J. Falcón. Calcium and melatonin production in dissociated trout pineal photoreceptor cells in culture. *Cell calcium*, 16(1):37–46, July 1994.
- J. Bembenek, H. Sehadova, N. Ichihara, and M. Takeda. Day/night fluctuations in melatonin content, arylalkylamine N-acetyltransferase activity and NAT mRNA expression in the CNS, peripheral tissues and hemolymph of the cockroach, *Periplaneta americana*. *Comparative biochemistry and physiology. Part B, Biochemistry & molecular biology*, 140(1):27–36, Jan. 2005.
- I. H. Bianco and S. W. Wilson. The habenular nuclei: a conserved asymmetric relay station in the vertebrate brain. *Philosophical transactions of the Royal Society of London. Series B, Biological sciences*, 364(1519):1005–20, Apr. 2009.
- S. Blackshaw, S. Harpavat, J. Trimarchi, L. Cai, H. Huang, W. P. Kuo, G. Weber, K. Lee, R. E. Fraioli, S.-H. Cho, R. Yung, E. Asch, L. Ohno-Machado, W. H. Wong, and C. L. Cepko. Genomic analysis of mouse retinal development. *PLoS biology*, 2(9):E247, Sept. 2004.
- G. S. Boyan and H. Reichert. Mechanisms for complexity in the brain: generating the insect central complex. *Trends in neurosciences*, 34(5):247–57, May 2011.
- J. Bradley, J. Reiser, and S. Frings. Regulation of cyclic nucleotide-gated channels. *Current opinion in neurobiology*, 15(3):343–9, June 2005.
- W. E. Bradshaw and C. M. Holzapfel. Evolution of Animal Photoperiodism. *Annual Review of Ecology, Evolution, and Systematics*, 38(1):1–25, Dec. 2007.
- O. R. Braubach, A. J. G. Dickinson, C. C. E. Evans, and R. P. Croll. Neural control of the velum in larvae of the gastropod, *Ilyanassa obsoleta*. *The Journal of experimental biology*, 209:4676–89, Dec. 2006.
- F. D. Brown, A. Prendergast, and B. J. Swalla. Man is but a worm: chordate origins. *Genesis*, 46(11):605–13, Nov. 2008.
- H. A. Burgess and M. Granato. Modulation of locomotor activity in larval zebrafish during light adaptation. *The Journal of experimental biology*, 210:2526–39, July 2007.
- G. M. Cahill and J. C. Besharse. Circadian clock functions localized in *Xenopus* retinal photoreceptors. *Neuron*, 10(4):573–7, Apr. 1993.
- S. Candiani, L. Moronti, D. De Pietri Tonelli, G. Garbarino, and M. Pestarino. A study of neural-related microRNAs in the developing amphioxus. *EvoDevo*, 2(1):15, Jan. 2011.
- J. a. C. R. Cardoso, F. a. Vieira, A. S. Gomes, and D. M. Power. PACAP, VIP and their receptors in the metazoa: insights about the origin and evolution of the ligand-receptor pair. *Peptides*, 28(9):1902–1919, Sept. 2007.
- S. Casarosa, M. Andreazzoli, A. Simeone, and G. Barsacchi. *Xrx1*, a novel *Xenopus* homeobox gene expressed during eye and pineal gland development. *Mechanisms of development*, 61:187–198, 1997.

- S. Casarosa, M. A. Amato, M. Andreazzoli, G. Gestri, G. Barsacchi, and F. Cremisi. *Rx1* controls proliferation and multipotency of retinal progenitors. *Molecular and Cellular Neuroscience*, 22:25–36, Jan. 2003.
- J. Castresana. Selection of conserved blocks from multiple alignments for their use in phylogenetic analysis. *Molecular biology and evolution*, 17(4):540–52, Apr. 2000.
- E. Cau. *Ash1a* and *Neurogenin1* function downstream of *Floating head* to regulate epiphysial neurogenesis. *Development*, 130(11):2455–2466, June 2003.
- M. Cayouette, L. Poggi, and W. a. Harris. Lineage in the vertebrate retina. *Trends in neurosciences*, 29(10):563–70, Oct. 2006.
- N. Cermakian and P. Sassone-Corsi. Multilevel regulation of the circadian clock. *Nature reviews molecular cell biology*, 1(1):59–67, Oct. 2000.
- J. Chen, A. Rattner, and J. Nathans. The rod photoreceptor-specific nuclear receptor *Nr2e3* represses transcription of multiple cone-specific genes. *The Journal of neuroscience*, 25(1):118–29, Jan. 2005.
- V. S. Chowdhury, K. Yamamoto, T. Ubuka, G. E. Bentley, A. Hattori, and K. Tsutsui. Melatonin stimulates the release of gonadotropin-inhibitory hormone by the avian hypothalamus. *Endocrinology*, 151(1):271–80, Jan. 2010.
- F. Christodoulou. *Animal microRNAs and the evolution of tissue identity*. PhD thesis, University of Crete, Feb. 2009.
- F. Christodoulou, F. Raible, R. Tomer, O. Simakov, K. Trachana, S. Klaus, H. Snyman, G. J. Hannon, P. Bork, and D. Arendt. Ancient animal microRNAs and the evolution of tissue identity. *Nature*, 463(7284):1084–8, Feb. 2010.
- J. C. Chuang and P. a. Raymond. Zebrafish genes *rx1* and *rx2* help define the region of forebrain that gives rise to retina. *Developmental biology*, 231(1):13–30, Mar. 2001.
- J. C. Chuang, P. H. Mathers, and P. A. Raymond. Expression of three *Rx* homeobox genes in embryonic and adult zebrafish. *Mechanisms of Development*, 84:195–198, 1999.
- J. a. Coffman, C. Dickey-Sims, J. S. Haug, J. J. McCarthy, and A. J. Robertson. Evaluation of developmental phenotypes produced by morpholino antisense targeting of a sea urchin *Runx* gene. *BMC biology*, 2:6, Jan. 2004.
- J. K. Colbourne, M. E. Pfrender, D. Gilbert, W. K. Thomas, A. Tucker, T. H. Oakley, S. Tokishita, A. Aerts, G. J. Arnold, M. K. Basu, D. J. Bauer, C. E. Cáceres, L. Carmel, C. Casola, J.-H. Choi, J. C. Detter, Q. Dong, S. Dusheyko, B. D. Eads, T. Fröhlich, K. a. Geiler-Samerotte, D. Gerlach, P. Hatcher, S. Jogdeo, J. Krijgsveld, E. V. Kriventseva, D. Kültz, C. Laforsch, E. Lindquist, J. Lopez, J. R. Manak, J. Muller, J. Pangilinan, R. P. Patwardhan, S. Pitluck, E. J. Pritham, A. Rechtsteiner, M. Rho, I. B. Rogozin, O. Sakarya, A. Salamov, S. Schaack, H. Shapiro, Y. Shiga, C. Skalitzky, Z. Smith, A. Souvorov, W. Sung, Z. Tang, D. Tsuchiya, H. Tu, H. Vos, M. Wang, Y. I. Wolf, H. Yamagata, T. Yamada, Y. Ye, J. R. Shaw, J. Andrews, T. J. Crease, H. Tang, S. M. Lucas, H. M. Robertson, P. Bork, E. V. Koonin, E. M. Zdobnov, I. V. Grigoriev, M. Lynch, and J. L. Boore. The ecoresponsive genome of *Daphnia pulex*. *Science*, 331(6017):555–61, Feb. 2011.

- B. Collins and J. Blau. Even a stopped clock tells the right time twice a day: circadian timekeeping in *Drosophila*. *Pflügers Archiv : European journal of physiology*, 454(5):857–67, Aug. 2007.
- M. L. Concha and S. W. Wilson. Asymmetry in the epithalamus of vertebrates. *Journal of anatomy*, 199 (Pt 1-2):63–84, 2001.
- S. Conway Morris. Darwin’s dilemma: the realities of the Cambrian ‘explosion’. *Philosophical transactions of the Royal Society of London. Series B, Biological sciences*, 361(1470):1069–83, June 2006.
- S. Conway Morris and J. S. Peel. The earliest annelids: Lower Cambrian polychaetes from the Sirius Passet Lagerstätte, Peary Land, North Greenland. *Acta Palaeontologica Polonica*, 53(1):85–87, 2008.
- M. Conzelmann, S.-L. Offenburger, A. Asadulina, T. Keller, T. A. Münch, and G. Jékely. Neuropeptides regulate swimming depth of *Platynereis* larvae. *Proceedings of the National Academy of Sciences of the United States of America*, 2011.
- X. Cui, D. Ji, D. a. Fisher, Y. Wu, D. M. Briner, and E. J. Weinstein. Targeted integration in rat and mouse embryos with zinc-finger nucleases. *Nature biotechnology*, 29(1):64–7, Jan. 2011.
- A. C. Culhane, J. Thioulouse, G. Perrière, and D. G. Higgins. MADE4: an R package for multivariate analysis of gene expression data. *Bioinformatics*, 21(11):2789–90, June 2005.
- S. D’Aniello, E. D’Aniello, A. Locascio, A. Memoli, M. Corrado, M. T. Russo, F. Aniello, L. Fucci, E. R. Brown, and M. Branno. The ascidian homolog of the vertebrate homeobox gene *Rx* is essential for ocellus development and function. *Differentiation*, 74(5):222–34, June 2006.
- S. D’Autilia, V. Broccoli, G. Barsacchi, and M. Andreazzoli. *Xenopus Bsx* links daily cell cycle rhythms and pineal photoreceptor fate. *Proceedings of the National Academy of Sciences of the United States of America*, 107(14):6352–7, Apr. 2010.
- J. de Melo, G.-H. Peng, S. Chen, and S. Blackshaw. The Spalt family transcription factor *Sall3* regulates the development of cone photoreceptors and retinal horizontal interneurons. *Development*, 138(11): 2325–36, June 2011.
- F. Del Bene, L. Ettwiller, D. Skowronska-Krawczyk, H. Baier, J.-M. Matter, E. Birney, and J. Wittbrodt. In vivo validation of a computationally predicted conserved *Ath5* target gene set. *PLoS genetics*, 3 (9):1661–71, Sept. 2007.
- A. S. Denes, G. Jékely, P. R. H. Steinmetz, F. Raible, H. Snyman, B. Prud’homme, D. E. K. Ferrier, G. Balavoine, and D. Arendt. Molecular architecture of annelid nerve cord supports common origin of nervous system centralization in bilateria. *Cell*, 129(2):277–88, Apr. 2007.
- K. Deschet, F. Bourrat, F. Ristoratore, D. Chourrout, and J. S. Joly. Expression of the medaka (*Oryzias latipes*) *Ol-Rx3* paired-like gene in two diencephalic derivatives, the eye and the hypothalamus. *Mechanisms of development*, 83(1-2):179–82, May 1999.
- C. Dibner, U. Schibler, and U. Albrecht. The mammalian circadian timing system: organization and coordination of central and peripheral clocks. *Annual review of physiology*, 72:517–49, Mar. 2010.

- S. A. Doran, R. Koss, C. H. Tran, K. J. Christopher, W. J. Gallin, and J. I. Goldberg. Effect of serotonin on ciliary beating and intracellular calcium concentration in identified populations of embryonic ciliary cells. *Journal of Experimental Biology*, 207(8):1415–1429, Mar. 2004.
- A. W. C. Dorresteijn. Quantitative analysis of cellular differentiation during early embryogenesis of *Platynereis dumerilii*. *Roux's Archives of Developmental Biology*, 199:14–30, 1990.
- A. W. C. Dorresteijn, B. O' Grady, A. Fischer, E. Porchet-Henner, and Y. Boilly-Marer. Molecular specification of cell lines in the embryo of *Platynereis* (Annelida). *Roux's Archives of Developmental Biology*, 202:260–269, 1993.
- Y. Doyon, J. M. McCammon, J. C. Miller, F. Faraji, C. Ngo, G. E. Katibah, R. Amora, T. D. Hocking, L. Zhang, E. J. Rebar, P. D. Gregory, F. D. Urnov, and S. L. Amacher. Heritable targeted gene disruption in zebrafish using designed zinc-finger nucleases. *Nature biotechnology*, 26(6):702–8, June 2008.
- P. Drapeau, L. Saint-Amant, R. R. Buss, M. Chong, J. R. McDearmid, and E. Brustein. Development of the locomotor network in zebrafish. *Progress in neurobiology*, 68:85–111, Oct. 2002.
- N. Dray, K. Tessmar-Raible, M. Le Gouar, L. Vibert, F. Christodoulou, K. Schipany, A. Guillou, J. Zantke, H. Snyman, J. Béhague, M. Vervoort, D. Arendt, and G. Balavoine. Hedgehog signaling regulates segment formation in the annelid *Platynereis*. *Science*, 329(5989):339–42, July 2010.
- R. Dubruille and P. Emery. A plastic clock: how circadian rhythms respond to environmental cues in *Drosophila*. *Molecular neurobiology*, 38(2):129–45, Oct. 2008.
- H. D. Dufour, Z. Chettouh, C. Deyts, R. de Rosa, C. Goridis, J.-S. Joly, and J.-F. Brunet. Precranial origin of cranial motoneurons. *Proceedings of the National Academy of Sciences of the United States of America*, 103(23):8727–32, June 2006.
- P. Dufourcq, S. Rastegar, U. Strähle, and P. Blader. Parapineal specific expression of *gf1* in the zebrafish epithalamus. *Gene Expression Patterns*, 4(1):53–57, Jan. 2004.
- G. W. Eagleson and W. a. Harris. Mapping of the presumptive brain regions in the neural plate of *Xenopus laevis*. *Journal of neurobiology*, 21(3):427–40, Apr. 1990.
- R. M. Eakin. Evolutionary significance of photoreceptors: in retrospect. *American Zoologist*, 19:647–653, 1979.
- T. Ebrey and Y. Koutalos. Vertebrate photoreceptors. *Progress in retinal and eye research*, 20(1):49–94, Jan. 2001.
- J. S. Eisen and J. C. Smith. Controlling morpholino experiments: don't stop making antisense. *Development (Cambridge, England)*, 135(10):1735–43, May 2008.
- P. Ekström. Photoreceptors and CSF-Contacting Neurons in the Pineal Organ of a Teleost Fish Have Direct Axonal Connections with the Brain : An HRP-Electron-Microscopic Study. *Journal of neuroscience*, 7(4):967–995, 1987.

- P. Ekström and H. Meissl. The pineal organ of teleost fishes. *Reviews in Fish Biology and Fisheries*, pages 199–284, 1997.
- P. Ekström and H. Meissl. Evolution of photosensory pineal organs in new light: the fate of neuroendocrine photoreceptors. *Philosophical transactions of the Royal Society of London. Series B, Biological sciences*, 358(1438):1679–700, Oct. 2003.
- P. Ekström and H. Meissl. Pineal photoreception and temporal physiology in fish. In *Biological clock in fish*. Science Publishers, 2010.
- M. E. El Halawani, S. Kang, B. Leclerc, S. Kosonsiriluk, and Y. Chaiseha. Dopamine and melatonin neurons in the avian hypothalamus and their role as photoperiodic clocks. *General and comparative endocrinology*, 163(1-2):123–127, 2009.
- F. Emran, J. Rihel, A. R. Adolph, and J. E. Dowling. Zebrafish larvae lose vision at night. *Proceedings of the National Academy of Sciences of the United States of America*, 107(13):6034–9, Mar. 2010.
- D. H. Erwin and E. H. Davidson. The last common bilaterian ancestor. *Development*, 129(13):3021–32, July 2002.
- B. Everitt and T. Hothorn. *An introduction to Applied Multivariate Analysis with R*. Springer, 2011.
- G. L. Fain, R. Hardie, and S. B. Laughlin. Phototransduction and the evolution of photoreceptors. *Current biology*, 20(3):R114–24, Feb. 2010.
- J. Falcón, L. Besseau, S. Sauzet, and G. Boeuf. Melatonin effects on the hypothalamo-pituitary axis in fish. *Trends in endocrinology and metabolism*, 18(2):81–8, Mar. 2007.
- J. Falcón, L. Besseau, M. Fuentès, S. Sauzet, E. Manganou, and G. Boeuf. Structural and functional evolution of the pineal melatonin system in vertebrates. *Annals of the New York Academy of Sciences*, 1163(ii):101–11, Apr. 2009.
- J. Falcón, L. Besseau, E. Manganou, S. Sauzet, M. Fuentès, and G. Boeuf. The pineal organ of fish. In *Biological clock in fish*. Science Publishers, 2010a.
- J. Falcón, H. Migaud, J. a. Muñoz Cueto, and M. Carrillo. Current knowledge on the melatonin system in teleost fish. *General and comparative endocrinology*, 165(3):469–82, Feb. 2010b.
- J. T. Finn, E. C. Solessio, and K. W. Yau. A cGMP-gated cation channel in depolarizing photoreceptors of the lizard parietal eye. *Nature*, 385:815–819, 1997.
- L. Finocchiaro, J. Callebert, J. M. Launay, and J. M. Jallon. Melatonin biosynthesis in *Drosophila*: its nature and its effects. *Journal of neurochemistry*, 50(2):382–7, Feb. 1988.
- A. Fischer. *Mesoderm formation and muscle development of Platynereis dumerilii (Nereididae, Annelida)*. PhD thesis, Freien Universität Berlin, 2010.
- A. Fischer and A. Dorresteijn. The polychaete *Platynereis dumerilii* (Annelida): a laboratory animal with spiralian cleavage, lifelong segment proliferation and a mixed benthic/pelagic life cycle. *BioEssays*, 26(3):314–25, Mar. 2004.

- a. Fischer, a. W. Dorresteijn, and U. Hoeger. Metabolism of oocyte construction and the generation of histospecificity in the cleaving egg. Lessons from nereid annelids. *The International journal of developmental biology*, 40(1):421–30, Feb. 1996.
- A. H. L. Fischer, T. Henrich, and D. Arendt. The normal development of *Platynereis dumerilii* (Nereididae, Annelida). *Frontiers in zoology*, 7(31), 2010.
- N. Flames and O. Hobert. Gene regulatory logic of dopamine neuron differentiation. *Nature*, 458(7240): 885–9, Apr. 2009.
- R. G. Foster and A. Roberts. The Pineal Eye in *Xenopus laevis* Embryos and Larvae: A Photoreceptor with a Direct Excitatory Effect on Behaviour. *Journal of Comparative Physiology*, 145:413–419, 1982.
- T. Furukawa, C. A. Kozak, and C. L. Cepko. *rax*, a novel paired-type homeobox gene, shows expression in the anterior neural fold and developing retina. *Proceedings of the National Academy of Sciences of the United States of America*, 94:3088–3093, 1997.
- M. Gallego and D. M. Virshup. Post-translational modifications regulate the ticking of the circadian clock. *Nature reviews molecular cell biology*, 8(2):139–48, Mar. 2007.
- B. Galliot and M. Quiquand. A two-step process in the emergence of neurogenesis. *The European journal of neuroscience*, 34(6):847–62, Sept. 2011.
- J. T. Gamse, Y.-C. Shen, C. Thisse, B. Thisse, P. a. Raymond, M. E. Halpern, and J. O. Liang. *Otx5* regulates genes that show circadian expression in the zebrafish pineal complex. *Nature genetics*, 30(1):117–21, Jan. 2002.
- S. Gavrillets. Rapid transition towards the Division of Labor via evolution of developmental plasticity. *PLoS computational biology*, 6(6):e1000805, June 2010.
- W. Gehring and M. Rosbash. The coevolution of blue-light photoreception and circadian rhythms. *Journal of molecular evolution*, 57 Suppl 1:S286–9, Jan. 2003.
- R. W. Gess, M. I. Coates, and B. S. Rubidge. A lamprey from the Devonian period of South Africa. *Nature*, 443(7114):981–4, Oct. 2006.
- D. T. Gilmour, H.-M. Maischein, and C. Nüsslein-Volhard. Migration and function of a glial subtype in the vertebrate peripheral nervous system. *Neuron*, 34(4):577–88, May 2002.
- M. d. P. Gomez and E. Nasi. Calcium-independent, cGMP-mediated light adaptation in invertebrate ciliary photoreceptors. *The Journal of neuroscience*, 25(8):2042–9, Feb. 2005.
- C. B. Green, J. S. Takahashi, and J. Bass. The meter of metabolism. *Cell*, 134(5):728–42, Sept. 2008.
- A. Gruhl. Serotonergic and FMRFamideergic nervous systems in gymnolaemate bryozoan larvae. *Zoomorphology*, 128(2):135–156, Feb. 2009.
- S. Guindon, J.-F. Dufayard, V. Lefort, M. Anisimova, W. Hordijk, and O. Gascuel. New algorithms and methods to estimate maximum-likelihood phylogenies: assessing the performance of PhyML 3.0. *Systematic biology*, 59(3):307–21, May 2010.

- K. Guy. *Development and molecular characterization of adult and larval eyes in Platynereis dumerilii (Polychaeta, Annelida, Lophotrochozoa)*. PhD thesis, Heidelberg University, 2009.
- N. B. Haider, S. G. Jacobson, a. V. Cideciyan, R. Swiderski, L. M. Streb, C. Searby, G. Beck, R. Hockey, D. B. Hanna, S. Gorman, D. Duhl, R. Carmi, J. Bennett, R. G. Weleber, G. a. Fishman, a. F. Wright, E. M. Stone, and V. C. Sheffield. Mutation of a nuclear receptor gene, NR2E3, causes enhanced S cone syndrome, a disorder of retinal cell fate. *Nature genetics*, 24(2):127–31, Feb. 2000.
- T. Hamada, M. Ootomi, K. Horikawa, T. Niki, H. Wakamatu, and N. Ishida. The expression of the melatonin synthesis enzyme: arylalkylamine N-acetyltransferase in the suprachiasmatic nucleus of rat brain. *Biochemical and biophysical research communications*, 258(3):772–7, May 1999.
- L.-a. Hansson, E. Becares, M. Ferna, T. Kairesalo, M. R. Miracle, S. Romo, D. Stephen, K. Vakkilainen, W. V. D. Bund, E. V. Donk, D. Balayla, and B. Moss. Relaxed circadian rhythm in zooplankton along a latitudinal gradient. *Oikos*, 116:585–591, 2007a.
- L.-A. Hansson, S. Hylander, and R. Sommaruga. Escape from UV threats in zooplankton: a cocktail of behavior and protective pigmentation. *Ecology*, 88(8):1932–9, Aug. 2007b.
- L. A. Hardaker, E. Singer, R. Kerr, G. Zhou, and W. R. Schafer. Serotonin Modulates Locomotory Behavior and Coordinates Egg-Laying and Movement in *Caenorhabditis elegans*. *Journal of Neurobiology*, 49(4):303–313, 2001.
- R. Hardeland. The presence and function of melatonin and structurally related indoleamines in a dinoflagellate, and a hypothesis on the evolutionary significance of these tryptophan metabolites in unicellulars. *Experientia*, 49:614–622, 1993.
- R. Hardeland, I. Balzer, B. Poeggeler, B. Fuhrberg, H. Uría, G. Behrmann, R. Wolf, T. J. Meyer, and R. J. Reiter. On the primary functions of melatonin in evolution: mediation of photoperiodic signals in a unicell, photooxidation, and scavenging of free radicals. *Journal of pineal research*, 18(2):104–11, Mar. 1995.
- C. Hasse, N. Rebscher, W. Reiher, K. Sobjinski, E. Moerschel, L. Beck, K. Tessmar-Raible, D. Arendt, and M. Hassel. Three consecutive generations of nephridia occur during development of *Platynereis dumerilii* (Annelida, Polychaeta). *Developmental dynamics*, 239(7):1967–76, July 2010.
- A. Hay-Schmidt. The evolution of the serotonergic nervous system. *Proceedings of the Royal Society of London B*, 267:1071–1079, 2000.
- L. W. Haynes. Block of the cyclic GMP-gated channel of vertebrate rod and cone photoreceptors by l-cis-diltiazem. *The Journal of general physiology*, 100(5):783–801, Nov. 1992.
- A. Hejnol, M. Obst, A. Stamatakis, M. Ott, G. W. Rouse, G. D. Edgecombe, P. Martinez, J. Baguña, X. Bailly, U. Jondelius, M. Wiens, W. E. G. Müller, E. Seaver, W. C. Wheeler, M. Q. Martindale, G. Giribet, and C. W. Dunn. Assessing the root of bilaterian animals with scalable phylogenomic methods. *Proceedings of the Royal Society B: Biological Sciences*, 276(1677):4261–70, Dec. 2009.
- C. Helfrich-Förster. The circadian clock in the brain: a structural and functional comparison between mammals and insects. *Journal of comparative physiology. A, Neuroethology, sensory, neural, and behavioral physiology*, 190(8):601–13, Aug. 2004.

- C. Helfrich-Förster. Neurobiology of the fruit fly's circadian clock. *Genes, brain, and behavior*, 4(2):65–76, Mar. 2005.
- C. Helfrich-Förster, C. Winter, a. Hofbauer, J. C. Hall, and R. Stanewsky. The circadian clock of fruit flies is blind after elimination of all known photoreceptors. *Neuron*, 30(1):249–61, Apr. 2001.
- C. Helfrich-Förster, T. Edwards, K. Yasuyama, B. Wisotzki, S. Schneuwly, R. Stanewsky, I. a. Meintertzhagen, and A. Hofbauer. The extraretinal eyelet of *Drosophila*: development, ultrastructure, and putative circadian function. *The Journal of neuroscience*, 22(21):9255–66, Nov. 2002.
- C. M. Heuer and R. Loesel. Immunofluorescence analysis of the internal brain anatomy of *Nereis diversicolor* (Polychaeta, Annelida). *Cell and tissue research*, 331(3):713–24, Mar. 2008.
- C. M. Heuer, C. H. Müller, C. Todt, and R. Loesel. Comparative neuroanatomy suggests repeated reduction of neuroarchitectural complexity in Annelida. *Frontiers in zoology*, 7:13, Jan. 2010.
- O. Hikosaka. The habenula: from stress evasion to value-based decision-making. *Nature reviews. Neuroscience*, 11(7):503–13, July 2010.
- S. A. Hires, L. Tian, and L. L. Looger. Reporting neural activity with genetically encoded calcium indicators. *Brain cell biology*, 36(1-4):69–86, Aug. 2008.
- F. Hirth. An urbilaterian origin of the tripartite brain: developmental genetic insights from *Drosophila*. *Development*, 130(11):2365–2373, June 2003.
- O. Hobert, I. Carrera, and N. Stefanakis. The molecular and gene regulatory signature of a neuron. *Trends in neurosciences*, 33(10):435–45, Oct. 2010.
- N. D. Holland. Early central nervous system evolution: an era of skin brains? *Nature reviews. Neuroscience*, 4(8):617–27, Aug. 2003.
- N. D. Holland and L. Z. Holland. Serotonin-containing Cells in the Nervous System and Other Tissues During Ontogeny of a Lancelet, *Branchiostoma floridae*. *Acta Zoologica*, 74(3):195–204, 1993.
- S. A. Holley, P. D. Jackson, Y. Sasai, B. Lu, E. M. De Robertis, F. M. Hoffmann, and E. L. Ferguson. A conserved system for dorso-ventral patterning in insects and vertebrates involving *sog* and *chordin*. *Nature*, 376:249–253, 1995.
- A. C. Horton, N. R. Mahadevan, C. Minguillon, K. Osoegawa, D. S. Rokhsar, I. Ruvinsky, P. J. de Jong, M. P. Logan, and J. J. Gibson-Brown. Conservation of linkage and evolution of developmental function within the *Tbx2/3/4/5* subfamily of T-box genes: implications for the origin of vertebrate limbs. *Development genes and evolution*, 218(11-12):613–28, Dec. 2008.
- T. H.-C. Hsiao, C. Diaconu, C. a. Myers, J. Lee, C. L. Cepko, and J. C. Corbo. The cis-regulatory logic of the mammalian photoreceptor transcriptional network. *PLoS one*, 2(7):e643, Jan. 2007.
- X. Huang and a. Madan. CAP3: A DNA sequence assembly program. *Genome research*, 9(9):868–77, Sept. 1999.

- T. Hunt and P. Sassone-Corsi. Riding tandem: circadian clocks and the cell cycle. *Cell*, 129(3):461–4, May 2007.
- F. Husson, S. Lê, and J. Pagès. *Exploratory Multivariate Analysis by Example using R*. Chapman & Hall, 2010.
- M. Irimia, C. Piñeiro, I. Maeso, J. L. Gómez-Skarmeta, F. Casares, and J. Garcia-Fernández. Conserved developmental expression of Fezf in chordates and *Drosophila* and the origin of the Zona Limitans Intrathalamica (ZLI) brain organizer. *EvoDevo*, 1(1):7, Jan. 2010.
- E. Isorna, L. Besseau, G. Boeuf, Y. Desdevises, R. Vuilleumier, A. L. Alonso-g, J. Delgado, and J. Falc. Retinal, pineal and diencephalic expression of frog arylalkylamine N-acetyltransferase-1. *Molecular and Cellular Endocrinology*, 252:11–18, 2006.
- T. Isshiki, B. Pearson, S. Holbrook, and C. Q. Doe. *Drosophila* neuroblasts sequentially express transcription factors which specify the temporal Identity of their neuronal progeny. *Cell*, 106:511–521, 2001.
- M. T. Itoh, T. Shinozawa, and Y. Sumi. Circadian rhythms of melatonin-synthesizing enzyme activities and melatonin levels in planarians. *Brain research*, 830(1):165–73, May 1999.
- L. M. Iyer, L. Aravind, S. L. Coon, D. C. Klein, and E. V. Koonin. Evolution of cell-cell signaling in animals: did late horizontal gene transfer from bacteria have a role? *Trends in genetics : TIG*, 20(7): 292–299, July 2004.
- G. Jägersten. *Evolution of the metazoan life cycle. A comprehensive theory*. Academic Press, New York, 1972.
- D. Jamieson and A. Roberts. A Possible Pathway Connecting the Photosensitive Pineal Eye to the Swimming Central Pattern Generator in Young *Xenopus laevis* Tadpoles. *Brain, behavior and evolution*, 54(6):323–337, Dec. 1999.
- D. Jamieson and a. Roberts. Responses of young *Xenopus laevis* tadpoles to light dimming: possible roles for the pineal eye. *The Journal of experimental biology*, 203(Pt 12):1857–67, June 2000.
- P. Janvier. Modern look for ancient lamprey. *Nature*, 443, 2006.
- G. Jékely. Origin and early evolution of neural circuits for the control of ciliary locomotion. *Proceedings of the Royal Society B: Biological Sciences*, 278:914–22, Mar. 2011.
- G. Jékely and D. Arendt. Cellular resolution expression profiling using confocal detection of NBT/BCIP precipitate by reflection microscopy. *BioTechniques*, 42(6):751–755, June 2007.
- G. Jékely, J. Colombelli, H. Hausen, K. Guy, E. Stelzer, F. Nédélec, and D. Arendt. Mechanism of phototaxis in marine zooplankton. *Nature*, 456(7220):395–9, Nov. 2008.
- H. a. D. Johard, T. Yoishii, H. Dirksen, P. Cusumano, F. Rouyer, C. Helfrich-Förster, and D. R. Nässel. Peptidergic clock neurons in *Drosophila*: ion transport peptide and short neuropeptide F in subsets of dorsal and ventral lateral neurons. *The Journal of comparative neurology*, 516(1):59–73, Sept. 2009.

- J.-S. Joly, J. Osório, A. Alunni, H. Auger, S. Kano, and S. Rétaux. Windows of the brain: towards a developmental biology of circumventricular and other neurohemal organs. *Seminars in cell & developmental biology*, 18(4):512–24, Aug. 2007.
- B. Jones and W. McGinnis. A new *Drosophila* homeobox gene, *bsh*, is expressed in a subset of brain cells during embryogenesis. *Development*, 117(2):793–806, Feb. 1993.
- T. Kaller. *Molekulare und ultrastrukturelle Charakterisierung von Photorezeptorzellen und Augen bei Annelida*. PhD thesis, Freien Universität Berlin, 2011.
- E. M. Kampa and B. P. Boden. Submarine illumination and the twilight movements of a sonic scattering layer. *Nature*, 443:869–871, 1954.
- S. Kang, A. Thayananuphat, T. Bakken, and M. E. El Halawani. Dopamine-melatonin neurons in the avian hypothalamus controlling seasonal reproduction. *Neuroscience*, 150(1):223–233, 2007.
- S. Kang, B. Leclerc, S. Kosonsiriluk, L. Mauro, A. Iwasawa, and M. E. El Halawani. Melanopsin expression in dopamine-melatonin neurons of the premammillary nucleus of the hypothalamus and seasonal reproduction in birds. *Neuroscience*, 170(1):200–213, 2010.
- H. Katow, S. Yaguchi, and K. Kyojuka. Serotonin stimulates $[Ca^{2+}]_i$ elevation in ciliary ectodermal cells of echinoplutei through a serotonin receptor cell network in the blastocoel. *The Journal of experimental biology*, 210(Pt 3):403–12, Feb. 2007.
- N. Kegel. The role of the transcription factor *Pdu-rx* in the marine ragworm *Platynereis Dumerilii*, Diploma thesis, 2008.
- A. Kimura, D. Singh, E. F. Wawrousek, M. Kikuchi, M. Nakamura, and T. Shinohara. Both *PCE-1/RX* and *OTX/CRX* interactions are necessary for photoreceptor-specific gene expression. *The Journal of biological chemistry*, 275(2):1152–60, Jan. 2000.
- D. C. Klein. The 2004 Aschoff/Pittendrigh lecture: Theory of the origin of the pineal gland—a tale of conflict and resolution. *Journal of biological rhythms*, 19(4):264–279, Aug. 2004.
- D. C. Klein, M. J. Bailey, D. A. Carter, J.-S. Kim, Q. Shi, A. Ho, C. Chik, P. Gaildrat, F. Morin, S. Ganguly, M. F. Rath, M. Moller, D. Sugden, Z. G. Rangel, P. J. Munson, J. L. Weller, and S. L. Coon. Pineal Function : Impact of Microarray Analysis. *Molecular and cellular endocrinology*, 314(2):170–183, 2010.
- A. Kohsaka and J. Bass. A sense of time: how molecular clocks organize metabolism. *Trends in endocrinology and metabolism*, 18(1):4–11, 2006.
- D. Kojima, S. Mori, M. Torii, A. Wada, R. Morishita, and Y. Fukada. UV-Sensitive Photoreceptor Protein OPN5 in Humans and Mice. *PLoS ONE*, 6(10):e26388, Oct. 2011.
- P. Kratsios, A. Stolfi, M. Levine, and O. Hobert. Coordinated regulation of cholinergic motor neuron traits through a conserved terminal selector gene. *Nature neuroscience*, 15(2):205–214, Nov. 2011.
- S. Kroeber, H. Meissl, E. Maronde, and H. W. Korf. Analyses of signal transduction cascades reveal an essential role of calcium ions for regulation of melatonin biosynthesis in the light-sensitive pineal organ of the rainbow trout (*Oncorhynchus mykiss*). *Journal of neurochemistry*, 74(6):2478–89, June 2000.

- S. Kuang, S. a. Doran, R. J. a. Wilson, G. G. Goss, and J. I. Goldberg. Serotonergic sensory-motor neurons mediate a behavioral response to hypoxia in pond snail embryos. *Journal of neurobiology*, 52(1):73–83, July 2002.
- M. Kumasaka, H. Sato, S. Sato, I. Yajima, and H. Yamamoto. Isolation and developmental expression of Mitf in *Xenopus laevis*. *Developmental Dynamics*, 230(1):107–13, May 2004.
- C. Kusmic, P. L. Marchiafava, and E. Strettoi. Photoresponses and light adaptation of pineal photoreceptors in the trout. *Proceedings of the Royal Society of London B*, 248(1322):149–157, 1992.
- T. C. Lacalli. Frontal Eye Circuitry, Rostral Sensory Pathways and Brain Organization in Amphioxus Larvae: Evidence from 3D Reconstructions. *Philosophical Transactions of the Royal Society B: Biological Sciences*, 351(1337):243–263, Mar. 1996.
- T. C. Lacalli. Body plans and simple brains. *Nature*, 424:263–264, Aug. 2003.
- T. D. Lamb. Evolution of vertebrate retinal photoreception. *Philosophical transactions of the Royal Society of London. Series B, Biological sciences*, 364(1531):2911–24, Oct. 2009.
- T. D. Lamb, S. P. Collin, and E. N. Pugh. Evolution of the vertebrate eye: opsins, photoreceptors, retina and eye cup. *Nature reviews neuroscience*, 8(12):960–76, Dec. 2007.
- B. Leclerc, S. Kang, L. Mauro, S. Kosonsiriluk, Y. Chaiseha, and M. E. El Halawani. Photoperiodic Modulation of Clock Gene Expression in the Avian Premammillary Nucleus. *Journal of neuroendocrinology*, 11(1):119–128, 2010.
- D. M. Leech, A. Padeletti, and C. E. Williamson. Zooplankton behavioral responses to solar UV radiation vary within and among lakes. *Journal of Plankton Research*, 27(5):461–471, Apr. 2005.
- O. Levy, L. Appelbaum, W. Leggat, Y. Gothlif, D. C. Hayward, D. J. Miller, and O. Hoegh-Guldberg. Light-responsive cryptochromes from a simple multicellular animal, the coral *Acropora millepora*. *Science*, 318(5849):467–70, Oct. 2007.
- S. P. Leys and B. M. Degnan. Cytological basis of photoresponsive behavior in a sponge larva. *The Biological bulletin*, 201(3):323–38, Dec. 2001.
- S. Lin, Y. Huang, and T. Lee. Nuclear receptor unfulfilled regulates axonal guidance and cell identity of *Drosophila* mushroom body neurons. *PloS one*, 4(12):e8392, Jan. 2009.
- J. Liu, A. Ward, J. Gao, Y. Dong, N. Nishio, H. Inada, L. Kang, Y. Yu, D. Ma, T. Xu, I. Mori, Z. Xie, and X. Z. S. Xu. *C. elegans* phototransduction requires a G protein-dependent cGMP pathway and a taste receptor homolog. *Nature neuroscience*, 13(6):715–22, June 2010.
- Y. G. Liu and R. F. Whittier. Thermal asymmetric interlaced PCR: automatable amplification and sequencing of insert end fragments from P1 and YAC clones for chromosome walking. *Genomics*, 25(3):674–81, Feb. 1995.
- A. Lloyd, C. L. Plaisier, D. Carroll, and G. N. Drews. Targeted mutagenesis using zinc-finger nucleases in *Arabidopsis*. *Proceedings of the National Academy of Sciences of the United States of America*, 102(6):2232–7, Feb. 2005.

- F. Loosli, S. Winkler, C. Burgtorf, E. Wurmbach, W. Ansorge, T. Henrich, C. Grabher, D. Arendt, M. Carl, A. Krone, E. Grzebisz, and J. Wittbrodt. Medaka eyeless is the key factor linking retinal determination and eye growth. *Development*, 128(20):4035–44, Oct. 2001.
- F. Loosli, W. Staub, K. C. Finger-Baier, E. a. Ober, H. Verkade, J. Wittbrodt, and H. Baier. Loss of eyes in zebrafish caused by mutation of *chokh/rx3*. *EMBO reports*, 4(9):894–9, Sept. 2003.
- B. Lorente-Cánovas, F. Marín, R. Corral-San-Miguel, M. Hidalgo-Sánchez, J. L. Ferrán, L. Puelles, and P. Aroca. Multiple origins, migratory paths and molecular profiles of cells populating the avian interpeduncular nucleus. *Developmental biology*, 361(1):12–26, Jan. 2012.
- C. J. Lowe, M. Wu, A. Salic, L. Evans, E. Lander, N. Stange-Thomann, C. E. Gruber, J. Gerhart, and M. Kirschner. Anteroposterior patterning in hemichordates and the origins of the chordate nervous system. *Cell*, 113(7):853–65, June 2003.
- G. O. Mackie. Neuroid conduction and the evolution of conducting tissues. *The Quarterly Review of Biology*, 45(4):319–332, 1970.
- S. Malpel, A. Klarsfeld, and F. Rouyer. Larval optic nerve and adult extra-retinal photoreceptors sequentially associate with clock neurons during *Drosophila* brain development. *Development*, 129(6):1443–53, Mar. 2002.
- B. Manavathi, S. Peng, S. K. Rayala, A. H. Talukder, M. H. Wang, R.-A. Wang, S. Balasenthil, N. Agarwal, L. J. Frishman, and R. Kumar. Repression of *Six3* by a corepressor regulates rhodopsin expression. *Proceedings of the National Academy of Sciences of the United States of America*, 104(32):13128–33, Aug. 2007.
- M. Mandado, P. Molist, R. Anadón, and J. Yáñez. A DiI-tracing study of the neural connections of the pineal organ in two elasmobranchs (*Scyliorhinus canicula* and *Raja montagui*) suggests a pineal projection to the midbrain GnRH-immunoreactive nucleus. *Cell and Tissue Research*, 303(3):391–401, Mar. 2001.
- H. Mano and Y. Fukada. A median third eye: pineal gland retraces evolution of vertebrate photoreceptive organs. *Photochemistry and photobiology*, 83(1):11–8, 2007.
- H. Marlow, M. A. Tosches, R. Tomer, P. R. H. Steinmetz, A. Lauri, T. Larsson, and D. Arendt. Larval body patterning and apical organs are conserved in animal evolution. *submitted*, 2012.
- H. Q. Marlow, M. Srivastava, D. Q. Matus, D. Rokhsar, and M. Q. Martindale. Anatomy and development of the nervous system of *Nematostella vectensis*, an anthozoan cnidarian. *Developmental neurobiology*, 69(4):235–54, Mar. 2009.
- R. I. Martinez-De Luna and H. M. El-Hodiri. The *Xenopus* ortholog of the nuclear hormone receptor *Nr2e3* is primarily expressed in developing photoreceptors. *The International journal of developmental biology*, 51(3):235–40, Jan. 2007.
- R. I. Martinez-De Luna, L. E. Kelly, and H. M. El-Hodiri. The Retinal Homeobox (*Rx*) gene is necessary for retinal regeneration. *Developmental biology*, 353(1):10–8, May 2011.

- I. Masai, C. P. Heisenberg, K. a. Barth, R. Macdonald, S. Adamek, and S. W. Wilson. Floating Head and Masterblind Regulate Neuronal Patterning in the Roof of the Forebrain. *Neuron*, 18:43–57, Jan. 1997.
- T. Mashimo, A. Takizawa, B. Voigt, K. Yoshimi, H. Hiai, T. Kuramoto, and T. Serikawa. Generation of knockout rats with X-linked severe combined immunodeficiency (X-SCID) using zinc-finger nucleases. *PloS one*, 5(1):e8870, Jan. 2010.
- P. H. Mathers, a. Grinberg, K. a. Mahon, and M. Jamrich. The Rx homeobox gene is essential for vertebrate eye development. *Nature*, 387(6633):603–7, June 1997.
- K. Matulef and W. N. Zagotta. Cyclic nucleotide-gated ion channels. *Annual review of cell and developmental biology*, 19:23–44, Jan. 2003.
- W. N. McFarland. Light in the Sea - Correlations with Behaviors of Fishes and Invertebrates. *American Zoologist*, 26:389–401, 1986.
- A. J. Mears, M. Kondo, P. K. Swain, Y. Takada, R. a. Bush, T. L. Saunders, P. a. Sieving, and A. Swaroop. Nrl is required for rod photoreceptor development. *Nature genetics*, 29(4):447–52, Dec. 2001.
- N. Mechawar and M. Anctil. Melatonin in a Primitive Metazoan: seasonal changes of levels and immunohistochemical visualization in neurons. *Journal of Comparative Neurology*, 254:243–254, 1997.
- O. Medina-Martinez, F. Amaya-Manzanares, C. Liu, M. Mendoza, R. Shah, L. Zhang, R. R. Behringer, K. a. Mahon, and M. Jamrich. Cell-autonomous requirement for rx function in the mammalian retina and posterior pituitary. *PloS one*, 4(2):e4513, Jan. 2009.
- E. Meijering, O. Dzyubachyk, and I. Smal. *Methods for cell and particle tracking.*, volume 504. Elsevier Inc., 1 edition, Jan. 2012.
- H. Meissl and J. Yáñez. Pineal photosensitivity. A comparison with retinal photoreception. *Acta Neurobiologiae Experimentalis*, 54:19–29, 1994.
- H. Meissl, S. Kroeber, J. Yáñez, and H. W. Korf. Regulation of melatonin production and intracellular calcium concentrations in the trout pineal organ. *Cell and tissue research*, 286(3):315–23, Dec. 1996.
- X. Meng, M. B. Noyes, L. J. Zhu, N. D. Lawson, and S. a. Wolfe. Targeted gene inactivation in zebrafish using engineered zinc-finger nucleases. *Nature biotechnology*, 26(6):695–701, June 2008.
- I. Mertens, S. J. Husson, T. Janssen, M. Lindemans, and L. Schoofs. PACAP and PDF signaling in the regulation of mammalian and insect circadian rhythms. *Peptides*, 28(9):1775–83, Sept. 2007.
- E. J. Meyer, A. Ikmi, and M. C. Gibson. Interkinetic nuclear migration is a broadly conserved feature of cell division in pseudostratified epithelia. *Current biology*, 21(6):485–91, Mar. 2011.
- N. P. Meyer and E. C. Seaver. Neurogenesis in an annelid: characterization of brain neural precursors in the polychaete *Capitella* sp. I. *Developmental biology*, 335(1):237–52, Nov. 2009.
- P. a. Morcos. Achieving targeted and quantifiable alteration of mRNA splicing with Morpholino oligos. *Biochemical and biophysical research communications*, 358(2):521–7, June 2007.

- F. Moret, J.-C. Guillard, S. Coudouel, L. Rochette, and P. Vernier. Distribution of tyrosine hydroxylase, dopamine, and serotonin in the central nervous system of amphioxus (*Branchiostoma lanceolatum*): implications for the evolution of catecholamine systems in vertebrates. *The Journal of comparative neurology*, 468(1):135–50, Jan. 2004.
- P. J. Morgan and D. G. Hazlerigg. Photoperiodic signalling through the melatonin receptor turns full circle. *Journal of neuroendocrinology*, 20(6):820–6, June 2008.
- J. Morton, M. W. Davis, E. M. Jorgensen, and D. Carroll. Induction and repair of zinc-finger nuclease-targeted double-strand breaks in *Caenorhabditis elegans* somatic cells. *Proceedings of the National Academy of Sciences of the United States of America*, 103(44):16370–5, Oct. 2006.
- X. Mu, X. Fu, P. D. Beremand, T. L. Thomas, and W. H. Klein. Gene regulation logic in retinal ganglion cell development: *Isl1* defines a critical branch distinct from but overlapping with *Pou4f2*. *Proceedings of the National Academy of Sciences of the United States of America*, 105(19):6942–7, May 2008.
- J. L. P. Muñoz, M. a. López Patiño, C. Hermosilla, M. Conde-Sieira, J. L. Soengas, F. Rocha, and J. M. Míguez. Melatonin in octopus (*Octopus vulgaris*): tissue distribution, daily changes and relation with serotonin and its acid metabolite. *Journal of comparative physiology. A, Neuroethology, sensory, neural, and behavioral physiology*, 197(8):789–97, Aug. 2011.
- W. A. Müller. Autoradiographische Untersuchungen über die synthetische Aktivität in neurosekretorischer Zellen im Gehirn von *Platynereis dumerilii* während der sexuellen Entwicklung und Regeneration. *Z. Zellforsch.*, 139:487–510, 1973.
- W. E. G. Müller, X. Wang, H. C. Schröder, M. Korzhev, V. a. Grebenjuk, J. S. Markl, K. P. Jochum, D. Pisignano, and M. Wiens. A cryptochrome-based photosensory system in the siliceous sponge *Suberites domuncula* (Demospongiae). *The FEBS journal*, 277(5):1182–201, Mar. 2010.
- T. Nagata, M. Koyanagi, H. Tsukamoto, and A. Terakita. Identification and characterization of a protostome homologue of peropsin from a jumping spider. *Journal of comparative physiology. A, Neuroethology, sensory, neural, and behavioral physiology*, 196(1):51–9, Jan. 2010.
- Y. Nakajima, T. Humphreys, H. Kaneko, and K. Tagawa. Development and neural organization of the tornaria larva of the Hawaiian hemichordate, *Ptychodera flava*. *Zoological science*, 21(1):69–78, Jan. 2004.
- Y. Nakane and T. Yoshimura. Deep brain photoreceptors and a seasonal signal transduction cascade in birds. *Cell and tissue research*, 342(3):341–4, Dec. 2010.
- Y. Nakane, K. Ikegami, H. Ono, N. Yamamoto, S. Yoshida, K. Hirunagi, S. Ebihara, Y. Kubo, and T. Yoshimura. A mammalian neural tissue opsin (Opsin 5) is a deep brain photoreceptor in birds. *Proceedings of the National Academy of Sciences of the United States of America*, 107(34):15264–8, Aug. 2010.
- S. M. Nelson, L. Park, and D. L. Stenkamp. Retinal homeobox 1 is required for retinal neurogenesis and photoreceptor differentiation in embryonic zebrafish. *Developmental biology*, 328(1):24–39, Apr. 2009.

- C. Nielsen. Larval and adult brains. *Evolution & development*, 7(5):483–9, 2005.
- D.-E. Nilsson. Photoreceptor Evolution: Ancient Siblings Serve Different Tasks. *Current biology*, 15(3):R94–6, Feb. 2005.
- D.-E. Nilsson. The evolution of eyes and visually guided behaviour. *Philosophical transactions of the Royal Society of London. Series B, Biological sciences*, 364(1531):2833–47, Oct. 2009.
- M. N. Nitabach and P. H. Taghert. Organization of the Drosophila Circadian Control Circuit. *Current Biology*, 18(2):R84–R93, Jan. 2008.
- M. Nomaksteinsky, E. Röttinger, H. D. Dufour, Z. Chettouh, C. J. Lowe, M. Q. Martindale, and J.-F. Brunet. Centralization of the deuterostome nervous system predates chordates. *Current biology*, 19(15):1264–9, Aug. 2009.
- K. Nübler-Jung and D. Arendt. Is ventral in insects dorsal in vertebrates? *Roux's Archives of Developmental Biology*, 203:357–366, 1994.
- H. Ochiai, K. Fujita, K.-I. Suzuki, M. Nishikawa, T. Shibata, N. Sakamoto, and T. Yamamoto. Targeted mutagenesis in the sea urchin embryo using zinc-finger nucleases. *Genes to cells*, 15(8):875–85, Aug. 2010.
- H. Ohuchi, S. Tomonari, H. Itoh, T. Mikawa, and S. Noji. Identification of chick rax/rx genes with overlapping patterns of expression during early eye and brain development. *Mechanisms of Development*, 85:193–195, 1999.
- H. Ohuchi, T. Yamashita, S. Tomonari, S. Fujita-Yanagibayashi, K. Sakai, S. Noji, and Y. Shichida. A non-Mammalian type opsin 5 functions dually in the photoreceptive and non-photoreceptive organs of birds. *PLoS one*, 7(2):e31534, Jan. 2012.
- S. Ooka, T. Katow, S. Yaguchi, J. Yaguchi, and H. Katow. Spatiotemporal expression pattern of an encephalopsin orthologue of the sea urchin *Hemicentrotus pulcherrimus* during early development, and its potential role in larval vertical migration. *Development, growth & differentiation*, 52(2):195–207, Feb. 2010.
- L. R. Page and S. C. Parries. Comparative study of the apical ganglion in planktotrophic caenogastropod larvae: ultrastructure and immunoreactivity to serotonin. *The Journal of comparative neurology*, 418(4):383–401, Mar. 2000.
- Y. Pan, S. Nekkhalapudi, L. E. Kelly, and H. M. El-Hodiri. The Rx-like homeobox gene (Rx-L) is necessary for normal photoreceptor development. *Investigative ophthalmology & visual science*, 47(10):4245–53, Oct. 2006.
- Y. Pan, R. I. Martinez-De Luna, C.-H. Lou, S. Nekkhalapudi, L. E. Kelly, A. K. Sater, and H. M. El-Hodiri. Regulation of photoreceptor gene expression by the retinal homeobox (Rx) gene product. *Developmental biology*, 339(2):494–506, Mar. 2010.
- S. R. Pandi-Perumal, V. Srinivasan, G. J. M. Maestroni, D. P. Cardinali, B. Poeggeler, and R. Hardeland. Melatonin: Nature's most versatile biological signal? *The FEBS journal*, 273(13):2813–38, July 2006.

- C. Pape, M. Teschke, and B. Meyer. Melatonin and its possible role in mediating seasonal metabolic changes of Antarctic krill, *Euphausia superba*. *Comparative biochemistry and physiology. Part A, Molecular & integrative physiology*, 149(4):426–34, Apr. 2008.
- A. Parent. Functional Anatomy and Evolution of Monoaminergic Systems. *American Zoologist*, 24: 783–790, 1984.
- Y. J. Passamanek, N. Furchheim, A. Hejnl, M. Q. Martindale, and C. Lüter. Ciliary photoreceptors in the cerebral eyes of a protostome larva. *EvoDevo*, 2(1):6, Jan. 2011.
- J. Pavlicek, S. Sauzet, L. Besseau, S. L. Coon, J. L. Weller, G. Boeuf, P. Gaildrat, M. V. Omelchenko, E. V. Koonin, J. Falcón, and D. C. Klein. Evolution of AANAT: expansion of the gene family in the cephalochordate amphioxus. *BMC evolutionary biology*, 10:154, Jan. 2010.
- K. L. Pepple, M. Atkins, K. Venken, K. Wellnitz, M. Harding, B. Frankfort, and G. Mardon. Two-step selection of a single R8 photoreceptor: a bistable loop between senseless and rough locks in R8 fate. *Development (Cambridge, England)*, 135(24):4071–9, Dec. 2008.
- N. Peschel and C. Helfrich-Förster. Setting the clock-by nature: circadian rhythm in the fruitfly *Drosophila melanogaster*. *FEBS letters*, 585(10):1435–42, May 2011.
- M. W. Pfaffl, G. W. Horgan, and L. Dempfle. Relative expression software tool (REST) for group-wise comparison and statistical analysis of relative expression results in real-time PCR. *Nucleic acids research*, 30(9):e36, May 2002.
- C. S. Pittendrigh. Temporal organization: reflections of a Darwinian clock-watcher. *Annual review of physiology*, 55:16–54, 1993.
- D. C. Plachetzki, C. R. Fong, and T. H. Oakley. The evolution of phototransduction from an ancestral cyclic nucleotide gated pathway. *Proceedings of the Royal Society B: Biological Sciences*, 277(1690):1963–9, July 2010.
- M. A. Pombal, J. Yáñez, O. Marín, A. González, and R. Anadón. Cholinergic and GABAergic neuronal elements in the pineal organ of lampreys, and tract-tracing observations of differential connections of pinealofugal neurons. *Cell and tissue research*, 295(2):215–23, Feb. 1999.
- M. H. Porteus and D. Carroll. Gene targeting using zinc finger nucleases. *Nature biotechnology*, 23(8): 967–73, Aug. 2005.
- L. Puelles and J. L. Rubenstein. Forebrain gene expression domains and the evolving prosomeric model. *Trends in Neurosciences*, 26(9):469–476, Sept. 2003.
- L. a. Quina, S. Wang, L. Ng, and E. E. Turner. Brn3a and Nurr1 mediate a gene regulatory pathway for habenula development. *The Journal of neuroscience*, 29(45):14309–22, Nov. 2009.
- M. Ragni and M. Ribera D’Alcalà. Light as an information carrier underwater. *Journal of Plankton Research*, 26(4):433–443, Feb. 2004.

- F. Raible, K. Tessmar-Raible, K. Osoegawa, P. Wincker, C. Jubin, G. Balavoine, D. Ferrier, V. Benes, P. de Jong, J. Weissenbach, P. Bork, and D. Arendt. Vertebrate-type intron-rich genes in the marine annelid *Platynereis dumerilii*. *Science*, 310(5752):1325–6, Nov. 2005.
- S. S. Ranade, D. Yang-Zhou, S. W. Kong, E. C. McDonald, T. a. Cook, and F. Pignoni. Analysis of the Otd-dependent transcriptome supports the evolutionary conservation of CRX/OTX/OTD functions in flies and vertebrates. *Developmental biology*, 315(2):521–34, Mar. 2008.
- R. J. Reiter. The melatonin rhythm: both a clock and a calendar. *Experientia*, 49(8):654–664, Aug. 1993.
- R. J. Reiter, D.-X. Tan, and L. Fuentes-Broto. Melatonin: a multitasking molecule. *Progress in brain research*, 181(08):127–51, Jan. 2010.
- A. M. Reitzel, L. Behrendt, and A. M. Tarrant. Light entrained rhythmic gene expression in the sea anemone *Nematostella vectensis*: the evolution of the animal circadian clock. *PloS one*, 5(9):e12805, Jan. 2010.
- M. Rembold, F. Loosli, R. J. Adams, and J. Wittbrodt. Individual Cell Migration Serves as the Driving Force for Optic Vesicle Evagination. *Science*, 313:1130–1134, 2006.
- B. Rhode. Development and Differentiation of the Eye in *Platynereis dumerilii* (Annelida, Polychaeta). *Journal of morphology*, 212:71–85, 1992.
- S. C. Rhode, M. Pawlowski, and R. Tollrian. The impact of ultraviolet radiation on the vertical distribution of zooplankton of the genus *Daphnia*. *Nature*, 412(6842):69–72, July 2001.
- C. Ribelayga, F. Gauer, C. Calcari, P. Pevet, and V. Simonneaux. Photoneural regulation of rat pineal hydroxyindole-O-methyltransferase (HIOMT) messenger ribonucleic acid expression: an analysis of its complex relationship with HIOMT activity. *Endocrinology*, 140(3):1375–84, Mar. 1999.
- J. Ringelberg. *Diel Vertical Migration of Zooplankton in Lakes and Oceans. Causal Explanations and Adaptive Significances*. Springer, 2010.
- M. E. Robu, J. D. Larson, A. Nasevicius, S. Beiraghi, C. Brenner, S. a. Farber, and S. C. Ekker. P53 Activation By Knockdown Technologies. *PLoS genetics*, 3(5):e78, May 2007.
- K. Rohde, D. C. Klein, M. Mø ller, and M. F. Rath. Rax : developmental and daily expression patterns in the rat pineal gland and retina. *Journal of neurochemistry*, 118(6):999–1007, Sept. 2011.
- J. L. Rubenstein, K. Shimamura, S. Martinez, and L. Puelles. Regionalization of the prosencephalic neural plate. *Annual review of neuroscience*, 21:445–77, Jan. 1998.
- J. L. R. Rubenstein, S. Martinez, K. Shimamura, and L. Puelles. The embryonic vertebrate forebrain: the prosomeric model. *Science*, 266:578–580, 1994.
- E. B. Rubin, Y. Shemesh, M. Cohen, S. Elgavish, H. M. Robertson, and G. Bloch. Molecular and phylogenetic analyses reveal mammalian-like clockwork in the honey bee (*Apis mellifera*) and shed new light on the molecular evolution of the circadian clock. *Genome research*, 16(11):1352–65, Nov. 2006.

- C. Rüdberg. Structure of the parapineal organ of the adult rainbow trout, *Salmo gairdneri* Richardson. *Zeitschrift für Zellforschung*, 93(2):282–304, Jan. 1969.
- C. Rueffler, J. Hermisson, and G. P. Wagner. Evolution of functional specialization and division of labor. *Proceedings of the National Academy of Sciences of the United States of America*, 109(6):E326–335, 2011.
- K. Sakai, Y. Imamoto, C.-Y. Su, H. Tsukamoto, T. Yamashita, A. Terakita, K.-W. Yau, and Y. Shichida. Photochemical Nature of Parietopsin. *Biochemistry*, Jan. 2012.
- J. Sambrook and D. Russell. *Molecular cloning: a laboratory manual*. Cold Spring Harbor Laboratory Press, 2001.
- S. Santagata, C. Resh, A. Hejnal, M. Q. Martindale, and Y. J. Passamaneck. Development of the larval anterior neurogenic domains of *Terebratalia transversa* (Brachiopoda) provides insights into the diversification of larval apical organs and the spiralian nervous system. *EvoDevo*, 3(1):3, Jan. 2012.
- Y. Sasai, B. Lu, H. Steinbeisser, and E. M. De Robertis. Regulation of neural induction by the Chd and Bmp-4 antagonistic patterning signals in *Xenopus*. *Nature*, 376:333–336, 1995.
- K. Sato, T. Yamashita, H. Ohuchi, and Y. Shichida. Vertebrate ancient-long opsin has molecular properties intermediate between those of vertebrate and invertebrate visual pigments. *Biochemistry*, 50:10484–90, Dec. 2011.
- T. F. Schultz and S. a. Kay. Circadian clocks in daily and seasonal control of development. *Science*, 301(5631):326–8, July 2003.
- T. Shimogori, D. a. Lee, A. Miranda-Angulo, Y. Yang, H. Wang, L. Jiang, A. C. Yoshida, A. Kataoka, H. Mashiko, M. Avetisyan, L. Qi, J. Qian, and S. Blackshaw. A genomic atlas of mouse hypothalamic development. *Nature neuroscience*, 13(6):767–75, June 2010.
- S. Siegert, E. Cabuy, B. G. Scherf, H. Kohler, S. Panda, Y.-Z. Le, H. J. Fehling, D. Gaidatzis, M. B. Stadler, and B. Roska. Transcriptional code and disease map for adult retinal cell types. *Nature neuroscience*, page doi:10.1038/nn.3032, Jan. 2012.
- A. W. Siu, M. Maldonado, M. Sanchez-Hidalgo, D.-X. Tan, and R. J. Reiter. Protective effects of melatonin in experimental free radical-related ocular diseases. *Journal of pineal research*, 40(2):101–9, Mar. 2006.
- C. D. Snelson, J. T. Burkart, and J. T. Gamse. Formation of the asymmetric pineal complex in zebrafish requires two independently acting transcription factors. *Developmental Dynamics*, 237:3538–44, Dec. 2008a.
- C. D. Snelson, K. Santhakumar, M. E. Halpern, and J. T. Gamse. *Tbx2b* is required for the development of the parapineal organ. *Development*, 135(9):1693–702, May 2008b.
- T. Stach. Comparison of the serotonergic nervous system among Tunicata: implications for its evolution within Chordata. *Organisms Diversity & Evolution*, 5(1):15–24, Apr. 2005.

- J. Stefulj, M. Hörtnner, M. Ghosh, K. Schauenstein, I. Rinner, a. Wölfler, J. Semmler, and P. M. Liebmann. Gene expression of the key enzymes of melatonin synthesis in extrapineal tissues of the rat. *Journal of pineal research*, 30(4):243–7, May 2001.
- P. R. H. Steinmetz, R. Urbach, N. Posnien, J. Eriksson, R. P. Kostyuchenko, C. Brena, K. Guy, M. Akam, G. Bucher, and D. Arendt. Six3 demarcates the anterior-most developing brain region in bilaterian animals. *EvoDevo*, 1(1):14, Jan. 2010.
- P. R. H. Steinmetz, R. P. Kostyuchenko, A. Fischer, and D. Arendt. The segmental pattern of *otx*, *gbx*, and *Hox* genes in the annelid *Platynereis dumerilii*. *Evolution & development*, 13(1):72–9, 2011.
- M. Stephenson-Jones, O. Floros, B. Robertson, and S. Grillner. Evolutionary conservation of the habenular nuclei and their circuitry controlling the dopamine and 5-hydroxytryptophan (5-HT) systems. *Proceedings of the National Academy of Sciences of the United States of America*, 109(3):E164–E173, 2011.
- C. Stigloher, J. Ninkovic, M. Laplante, A. Geling, B. Tannhäuser, S. Topp, H. Kikuta, T. S. Becker, C. Houart, and L. Bally-Cuif. Segregation of telencephalic and eye-field identities inside the zebrafish forebrain territory is controlled by *Rx3*. *Development*, 133:2925–35, Aug. 2006.
- J. Strauss and H. Dirksen. Circadian clocks in crustaceans: identified neuronal and cellular systems. *Frontiers in bioscience*, 15:1040–74, 2010.
- T. H. Struck, C. Paul, N. Hill, S. Hartmann, C. Hösel, M. Kube, B. Lieb, A. Meyer, R. Tiedemann, G. Purschke, and C. Bleidorn. Phylogenomic analyses unravel annelid evolution. *Nature*, 471(7336):95–8, Mar. 2011.
- C.-Y. Su, D.-G. Luo, A. Terakita, Y. Shichida, H.-W. Liao, M. A. Kazmi, T. P. Sakmar, and K.-W. Yau. Parietal-Eye Phototransduction Components and Their Potential Evolutionary Implications. *Science*, 311(2006):1617–1621, 2008.
- R. Suzuki and H. Shimodaira. Pvcust: an R package for assessing the uncertainty in hierarchical clustering. *Bioinformatics*, 22(12):1540–2, June 2006.
- L. W. Swanson. *Brain architecture. Understanding the basic plan*. Oxford University Press, second edition, 2011.
- A. Swaroop, D. Kim, and D. Forrester. Transcriptional regulation of photoreceptor development and homeostasis in the mammalian retina. *Nature reviews neuroscience*, 11:563–76, Aug. 2010.
- A. J. Sweatt and R. B. Forward. Diel Vertical Migration and Photoresponses of the Chaetognath *Sagitta hispida* Conant. *Biological Bulletin*, 168(1):18, Feb. 1985.
- A. M. Sweeney, C. a. Boch, S. Johnsen, and D. E. Morse. Twilight spectral dynamics and the coral reef invertebrate spawning response. *The Journal of experimental biology*, 214(Pt 5):770–7, Mar. 2011.
- D. Tanaka, K. Furusawa, K. Kameyama, H. Okamoto, and M. Doi. Melatonin signaling regulates locomotion behavior and homeostatic states through distinct receptor pathways in *Caenorhabditis elegans*. *Neuropharmacology*, 53(1):157–68, July 2007.

- E. E. Tarttelin, J. Bellingham, M. W. Hankins, R. G. Foster, and R. J. Lucas. Neuropsin (Opn5): a novel opsin identified in mammalian neural tissue. *FEBS Letters*, 554(3):410–416, Nov. 2003.
- D. Tautz. Chordate evolution in a new light. *Cell*, 113(7):812–3, June 2003.
- K. Tessmar-Raible. *The evolution of sensory and neurosecretory cell types in bilaterian brains*. PhD thesis, Philipps-Universität Marburg, 2004.
- K. Tessmar-Raible and D. Arendt. Emerging systems: between vertebrates and arthropods, the Lophotrochozoa. *Current Opinion in Genetics & Development*, 13(4):331–340, Aug. 2003.
- K. Tessmar-Raible, P. Steinmetz, H. Snyman, M. Hassel, and D. Arendt. Fluorescent two-color whole mount in situ hybridization in *Platynereis dumerilii* (Polychaeta, Annelida), an emerging marine molecular model for evolution and development. *BioTechniques*, 39(4):460–464, Oct. 2005.
- K. Tessmar-Raible, F. Raible, F. Christodoulou, K. Guy, M. Rembold, H. Hausen, and D. Arendt. Conserved sensory-neurosecretory cell types in annelid and fish forebrain: insights into hypothalamus evolution. *Cell*, 129(7):1389–400, June 2007.
- S. Thor and J. B. Thomas. Motor neuron specification in worms, flies and mice: conserved and 'lost' mechanisms. *Current opinion in genetics & development*, 12(5):558–64, Oct. 2002.
- L. Tian, S. A. Hires, T. Mao, D. Huber, M. E. Chiappe, S. H. Chalasani, L. Petreanu, J. Akerboom, S. a. McKinney, E. R. Schreiter, C. I. Bargmann, V. Jayaraman, K. Svoboda, and L. L. Looger. Imaging neural activity in worms, flies and mice with improved GCaMP calcium indicators. *Nature methods*, 6(12):875–81, Dec. 2009.
- a. R. Tilden, P. Rasmussen, R. M. Awantang, S. Furlan, J. Goldstein, M. Palsgrove, and a. Sauer. Melatonin cycle in the fiddler crab *Uca pugilator* and influence of melatonin on limb regeneration. *Journal of pineal research*, 23(3):142–7, Oct. 1997.
- R. Tomer, A. S. Denes, K. Tessmar-raible, and D. Arendt. Profiling by image registration reveals common origin of annelid mushroom bodies and vertebrate pallium. *Cell*, 142(5):800–9, Sept. 2010.
- G. Tosini, N. Pozdeyev, K. Sakamoto, and P. M. Iuvone. The circadian clock system in the mammalian retina. *BioEssays*, 30(7):624–33, July 2008.
- R. Toyama, X. Chen, N. Jhavar, E. Aamar, J. Epstein, N. Reany, S. Alon, Y. Gothilf, D. C. Klein, and I. B. Dawid. Transcriptome analysis of the zebrafish pineal gland. *Developmental Dynamics*, 238(7):1813–26, July 2009.
- E. M. Ullrich-Lüter, S. Dupont, E. Arboleda, H. Hausen, and M. I. Arnone. Unique system of photoreceptors in sea urchin tube feet. *Proceedings of the National Academy of Sciences of the United States of America*, 108(20):8367–72, May 2011.
- T. van Veen. The parapineal and pineal organs of the elver (glass eel), *Anguilla anguilla* L. *Cell and Tissue Research*, 222:433–444, 1982.
- C. VanDunk, L. a. Hunter, and P. a. Gray. Development, maturation, and necessity of transcription factors in the mouse suprachiasmatic nucleus. *The Journal of neuroscience*, 31(17):6457–67, Apr. 2011.

- J. a. Veenstra. Neurohormones and neuropeptides encoded by the genome of *Lottia gigantea*, with reference to other mollusks and insects. *General and comparative endocrinology*, 167(1):86–103, May 2010.
- J. A. Veenstra. Neuropeptide evolution: neurohormones and neuropeptides predicted from the genomes of *Capitella teleta* and *Helobdella robusta*. *General and comparative endocrinology*, 171(2):160–75, Apr. 2011.
- R. A. Velarde, C. D. Sauer, K. K. O. Walden, S. E. Fahrbach, and H. M. Robertson. Pteropsin: a vertebrate-like non-visual opsin expressed in the honey bee brain. *Insect biochemistry and molecular biology*, 35(12):1367–1377, 2005.
- W. N. Venables and B. D. Ripley. *Modern Applied Statistics with S. Fourth Edition*. Springer, New York, 2002.
- B. Vigh and I. Vigh-Teichmann. Actual problems of the cerebrospinal fluid-contacting neurons. *Microscopy research and technique*, 41(1):57–83, Apr. 1998.
- B. Vigh, M. J. Manzano, A. Zádori, C. L. Frank, A. Lukáts, P. Röhlich, A. Szél, and C. Dávid. Nonvisual photoreceptors of the deep brain, pineal organs and retina. *Histology & Histopathology*, 17:555–590, 2002.
- B. Vivien-Roels and P. Pévet. Melatonin: presence and formation in invertebrates. *Experientia*, 49(8):642–647, Aug. 1993.
- P. D. Vize. Transcriptome analysis of the circadian regulatory network in the coral *Acropora millepora*. *The Biological bulletin*, 216(2):131–7, Apr. 2009.
- E. E. Voronezhskaya, E. B. Tsitrin, and L. P. Nezlin. Neuronal development in larval polychaete *Phyllodoce maculata* (Phyllodocidae). *The Journal of comparative neurology*, 455(3):299–309, Jan. 2003.
- W. Wales. Extraretinal control of vertical migration in fish larvae. *Nature*, 253:42–43, 1975.
- D. Wallis. The zinc finger transcription factor *Gfi1*, implicated in lymphomagenesis, is required for inner ear hair cell differentiation and survival. *Development*, 130(1):221–232, Jan. 2003.
- Q.-l. Wang, S. Chen, N. Esumi, P. K. Swain, H. S. Haines, G. Peng, B. M. Melia, I. McIntosh, J. R. Heckenlively, S. G. Jacobson, E. M. Stone, A. Swaroop, and D. J. Zack. QRX, a novel homeobox gene, modulates photoreceptor gene expression. *Human molecular genetics*, 13(10):1025–40, May 2004.
- A. Ward, J. Liu, Z. Feng, and X. Z. S. Xu. Light-sensitive neurons and channels mediate phototaxis in *C. elegans*. *Nature neuroscience*, 11(8):916–22, Aug. 2008.
- A. M. Waterhouse, J. B. Procter, D. M. a. Martin, M. Clamp, and G. J. Barton. Jalview Version 2—a multiple sequence alignment editor and analysis workbench. *Bioinformatics*, 25(9):1189–91, May 2009.
- Z. Wei, J. Yaguchi, S. Yaguchi, R. C. Angerer, and L. M. Angerer. The sea urchin animal pole domain is a Six3-dependent neurogenic patterning center. *Development*, 136(9):1583–1583, Apr. 2009.

- E. B. Wilson. The cell lineage of Nereis. A contribution to the cytogeny of the annelid body. *Journal of morphology*, VI(3):361–478, 1892.
- C. J. Winchell, J. E. Valencia, and D. K. Jacobs. Expression of Distal-less, dachshund, and optomotor blind in *Neanthes arenaceodentata* (Annelida, Nereididae) does not support homology of appendage-forming mechanisms across the Bilateria. *Development genes and evolution*, 220(9-10): 275–95, Dec. 2010.
- H.-Y. Wu, M. Perron, and T. Hollemann. The role of *Xenopus* Rx-L in photoreceptor cell determination. *Developmental biology*, 327(2):352–65, Mar. 2009.
- W. Wurst and L. Bally-Cuif. Neural plate patterning: upstream and downstream of the isthmic organizer. *Nature reviews neuroscience*, 2(2):99–108, Feb. 2001.
- J. Yáñez, M. a. Pombal, and R. Anadón. Afferent and efferent connections of the parapineal organ in lampreys: a tract tracing and immunocytochemical study. *The Journal of comparative neurology*, 403(2):171–89, Jan. 1999.
- J. Yáñez, J. Busch, R. Anadón, and H. Meissl. Pineal projections in the zebrafish (*Danio rerio*): overlap with retinal and cerebellar projections. *Neuroscience*, 164(4):1712–20, Dec. 2009.
- S. Yaguchi and H. Katow. Expression of tryptophan 5-hydroxylase gene during sea urchin neurogenesis and role of serotonergic nervous system in larval behavior. *The Journal of comparative neurology*, 466(2):219–29, Nov. 2003a.
- S. Yaguchi and H. Katow. Expression of tryptophan 5-hydroxylase gene during sea urchin neurogenesis and role of serotonergic nervous system in larval behavior. *The Journal of comparative neurology*, 466(2):219–29, Nov. 2003b.
- T. Yamashita, H. Ohuchi, S. Tomonari, K. Ikeda, K. Sakai, and Y. Shichida. Opn5 is a UV-sensitive bistable pigment that couples with Gi subtype of G protein. *Proceedings of the National Academy of Sciences of the United States of America*, pages 1–6, 2010.
- X. Yang, M. Downes, R. T. Yu, A. L. Bookout, W. He, M. Straume, D. J. Mangelsdorf, and R. M. Evans. Nuclear receptor expression links the circadian clock to metabolism. *Cell*, 126(4):801–10, Aug. 2006.
- K. Yoshida and H. Saiga. Repression of Rx gene on the left side of the sensory vesicle by Nodal signaling is crucial for right-sided formation of the ocellus photoreceptor in the development of *Ciona intestinalis*. *Developmental biology*, 354(1):144–50, June 2011.
- M. Yoshizawa and W. R. Jeffery. Shadow response in the blind cavefish *Astyanax* reveals conservation of a functional pineal eye. *The Journal of experimental biology*, 211(Pt 3):292–9, Feb. 2008.
- M. W. Young and S. A. Kay. Time zones: a comparative genetics of circadian clocks. *Nature Reviews Genetics*, 2(9):702–715, Sept. 2001.
- E. Z. Yu, J. M. Hallenbeck, D. Cai, and R. M. McCarron. Elevated arylalkylamine-N-acetyltransferase (AA-NAT) gene expression in medial habenular and suprachiasmatic nuclei of hibernating ground squirrels. *Brain research. Molecular brain research*, 102(1-2):9–17, June 2002.

- Q. Yuan, F. Lin, X. Zheng, and A. Sehgal. Serotonin modulates circadian entrainment in *Drosophila*. *Neuron*, 47(1):115–27, July 2005.
- L. Zhang, P. H. Mathers, and M. Jamrich. Function of Rx, but not Pax6, is essential for the formation of retinal progenitor cells in mice. *Genesis*, 28(3-4):135–42, 2000.
- X. Zhang and R. H. Cote. cGMP signaling in vertebrate retinal photoreceptor cells. *Frontiers in bioscience*, 10:1191–1204, 2005.
- I. V. Zhdanova, S. Y. Wang, O. U. Leclair, and N. P. Danilova. Melatonin promotes sleep-like state in zebrafish. *Brain research*, 903(1-2):263–8, June 2001.
- L. Ziv, A. Tovin, D. Strasser, and Y. Gothilf. Spectral sensitivity of melatonin suppression in the zebrafish pineal gland. *Experimental eye research*, 84(1):92–99, 2007.
- M. E. Zuber, G. Gestri, A. S. Viczian, G. Barsacchi, and W. A. Harris. Specification of the vertebrate eye by a network of eye field transcription factors. *Development*, 130(21):5155–67, Nov. 2003.